GEORGIA INSTITUTE OF TECHNOLOGY
OFFICE OF CONTRACT ADMINISTRATION

NOTICE OF PROJECT CLOSEOUT

Date 9/11/89

oject No. E-20-G14 Center No. R6231-0A0

oject Director A. P. Georgakakos School/Lab CE

onsor University of Iowa

ntract/Grant No. P. O. T27153 GTRC XX GIT ___

ime Contract No. 14-08-0001-G-1297

tle Optimal Real-Time Forecasting & Control Reservoir Hydrosystems Using Remote and On-site Sensors

fective Completion Date 2/28/89 (Performance) 2/28/89 (Reports)

oseout Actions Required:

___ None
___ Final Invoice or Copy of Last Invoice- Already Submitted
___ Final Report of Inventions and/or Subcontracts
___ Government Property Inventory & Related Certificate
___ Classified Material Certificate
___ Release and Assignment
___ Other ___

cludes Subproject No(s). ___

oproject Under Main Project No. ___

tinues Project No. ___ Continued by Project No. ___

stribution:

___ Project Director
___ Administrative Network
___ Accounting
___ Procurement/GTRI Supply Services
___ Research Property Management
___ Research Security Services
X Reports Coordinator (OCA)
X GTRC
X Project File
2 Contract Support Division (OCA)
___ Other ___

E-20-617

"Optimal Real-Time Forecasting and Control of Reservoir Hydrosystems Using Remote and On-Site Sensors"

Supported by
the U.S. Geological Survey, Department of the Interior
under award number 14 - 08 - 0001 - G1297

Water Resources Research
Act of 1984

Project Starting Date : September 1, 1986
Project Termination date: August 31, 1986

Progress Report for the period
September 1 through November 30, 1986

by

Aris P. Georgakakos, Ph. D.
Professor of Hydrology and Water Resources
School of Civil Engineering
Georgia Institute of Technology
Atlanta, Georgia 30332
Tel.: (404) 894-2240 or -2201

December 12, 1986

PART II

A State-Space Model for River Routing

The contents of this report were developed under a grant from the Department of the Interior, U. S. Geological Survey. However, those contents do not necessarily represent the policy of that agency, and you should not assume endorsement by the Federal Government.

Section CONTENTS Page No.

II.1. INTRODUCTION

An instrumental structural characteristic of the proposed forecast-control model is its state-space form; State-space models allow the application of efficient filtering and control theory techniques and can be easily synthesized to form composite formulations. However, state-space modeling is a fairly new concept in hydrology, and the availability of such models is limited.

In this part, our objective is to develop a state-space model for river routing which can benefit from the extensive past research experience. This model will then be used to model the response of the river segments that link the reservoirs or drain the watersheds.

II.2 HYDROLOGIC ROUTING MODELS

Simplified river routing models have drawn the attention of many researchers over the past 50 years. Fread (1983) presents a unified framework which encompasses most well-known models and helps the understanding of their differences and similarities. His "Unified Coefficient Routing Model" reflects the results of this long research experience and will be the subject of this section.

The Unified Coefficient Routing Model has the following form:

$$O^{t+\Delta t} = C_1 I^t + C_2 I^{t+\Delta t} + C_3 O^t + C \qquad (2.1a)$$

where O is the outflow from a channel reach of length (Δx),

I is the inflow to the reach,

the superscript t denotes the variable evaluated at time t,

the superscript $t+\Delta t$ denotes the variable evaluated at time $(t+\Delta t)$ where

Δt is the time step,

and C_1, C_2, C_3, and C_4 are routing coefficients which are obtained as follows:

$$C_0 = 1 + \Theta\,\tilde{a} - X \tag{2.2a}$$

$$C_1 = [(1-\Theta)\,\tilde{a} + X]/C_0 \tag{2.2b}$$

$$C_2 = (\Theta\,\tilde{a} - X)/C_0 \tag{2.2c}$$

$$C_3 = [1 - (1-\Theta)\,\tilde{a} - X]/C_0 \tag{2.2d}$$

$$C_4 = \bar{q}\,\Delta x\,\tilde{a}/C_0 \tag{2.2e}$$

$$\tilde{a} = c\,\Delta t/\Delta x \tag{2.2f}$$

$$\bar{q} = (q_i^j + q_i^{j+1})/2 \tag{2.2g}$$

$$0 \leq \Theta \leq 1 \tag{2.2h}$$

$$0 \leq X \leq 1 \tag{2.2i}$$

In the above equations, $\bar{q}$ is the lateral inflow or outflow along the reach Δx during the interval Δt, and c is the wave speed. Parameters Θ, X, and $\tilde{a}$ are given by expressions which are specific to each routing model; for instance, the Muskingum-Cunge routing procedure results when

$$\Theta = 1/2, \tag{2.3a}$$

$$X = 1/2\,[1 - q_0/(c\,\Delta x\,S_0)], \text{ and} \tag{2.3b}$$

$$\tilde{a} = c\,\Delta t/\Delta x = \Delta t/K \tag{2.3c}$$

where q_0 is the unit width discharge, K is the travel time through reach Δx, and S_0 is the channel's energy slope.

Equation (2.1a) may be rewritten in the following form:

$$Q_{i+1}^{j+1} = C_1 Q_i^j + C_2 Q_i^{j+1} + C_3 Q_{i+1}^j + C_4 \quad (2.1b)$$

where subscript i denotes the upstream end of the routing reach, subscript i+1 denotes the downstream end of the routing reach, superscript j denotes time t, and superscript j+1 denotes time t+Δt.

Fread (1983) suggests the following procedures for the estimation of the paramater values:

The wave speed is computed from

$$c = \beta V = 1.27 \beta S_0^{0.3} q_0^{0.4}/n^{0.6} \quad (2.4a)$$

where

$$\beta = 1.67 - 0.67 A_0/B_0^2 (dB_0/dy), \quad (2.4b)$$

A_0 is the associated cross-sectional area,

B_0 is the associated channel top width,

(dB_0/dy) is the rate of change of B_0 with depth y,

n is the Manning coefficient and S_0 is the bottom slope.

Parameters q_0, A_0, B_0 and (dB_0/dy) may be assumed constant; they are usually associated with a reference discharge Q_0 which may be some characteristic flow such as the mean of the discharge hydrograph, the peak, or the center of mass.

Parameter K may be computed from $K = \Delta x/c$ where Δx is the routing reach length and c is the wave speed. Alternatively, K can be computed from inflow-outflow discharge observations; it is equivalent to the time interval between the occurrence of the center of mass of inflow and that of the outflow.

The routing interval Δt can be obtained from

$$\Delta t \leq T_r/M \quad (2.5)$$

where T_r is the time of rise of the inflow hydrograph and M is an integer in the range [6,20]. Larger M values are associated with more rapid and nonuniform variation of the inflow hydrograph.

The selection of the reach length Δx must be restricted to a certain range specific to each routing scheme. The Muskingum-Cunge procedure requires that

$$\Delta x \leq 0.5 \, [c\Delta t + q_0/(cS_0)]. \tag{2.6}$$

The channel energy slope S_0 may be approximated by the channel bottom slope and estimated as the longitudinal average over the reach Δx. It may also be computed from Manning's equation as follows:

$$S_0 = Q_0^2 \, B_0^{4/3} \, n/(2.21 \, A_0^{10/3}) \tag{2.7}$$

where Q_0 is the uniform initial flow with associated top width B_0 and cross-sectional area A_0.

In natural channels, the hydraulic characteristics that enter or are computed from the Manning's equation should reflect spatial and temporal averages. For instance, the appropriate depth-discharge relation is given by

$$\tilde{Q} = 1.49 \, S_0^{1/2} \, \tilde{A}^{5/3}/(n \, \tilde{B}^{2/3}) \tag{2.8}$$

where the symbol $\tilde{}$ represents the average of the variable over the time interval Δt and along the reach Δx. A and B must also be known functions of the average depth y.

Fread (1983) suggests two routing methods in relation to the previous model. In the linear form of the Unified Coefficient routing model, the coefficients C_1, C_2, C_3, and C_4 are considered to be constant for each Δx routing reach and throughout the duration of the routing computations. The

various model parameters are evaluated initially from observations or the channel hydraulic characteristics; then, Equation (2.1) is applied recursively along each Δx routing reach and at each time step until the routing is terminated.

In the nonlinear routing form, the coefficients vary with each reach Δx and time step Δt. The computations start by estimating the discharge Q_{i+1}^{j+1} using a linearly extrapolated value:

$$\hat{Q}_{i+1}^{j+1} = Q_{i+1}^{j} + \Delta t^{j}/\Delta t^{j-1} (Q_{i+1}^{j} - Q_{i+1}^{j-1}). \tag{2.9}$$

Then, the average discharge $\tilde{Q}$ is obtained from

$$\tilde{Q} = 0.25 (Q_{i}^{j} + Q_{i}^{j+1} + Q_{i+1}^{j} + \hat{Q}_{i+1}^{j+1}), \tag{2.10}$$

$\tilde{y}$ is obtained from Equation (2.8), and $\tilde{A}$ and $\tilde{B}$ are computed from a tabular function of y. Lastly, parameters q_0, c, X, K, C_1, C_2, C_3, and C_4 are specified as described previously, and Equation (2.1) is invoked to compute Q_{i+1}^{j+1}. The procedure is then advanced to another routing reach or another time step, if there is only one routing reach, whenever the difference $|Q_{i+1}^{j+1} - Q_{i+1}^{j+1}|$ is smaller than a prespecified threshold (see Fread, 1983). If this difference does not fulfil this requirement, $\hat{Q}_{i+1}^{j+1}$ is replaced by Q_{i+1}^{j+1}, and the procedure is repeated.

Concluding this review section, we wish to note that our presentation emphasized the calibration and usage of the Muskingum-Cunge routing procedure because of its diffusion-type nature. Diffusion routing models have the potential for better accuracy in comparison with those of the kinematic wave philosophy.

The next section is concerned with the conversion of the Unified Coefficient Routing model to state-space form. The advantage of this indirect

route to state-space modeling is that it has the benefit of using the previous experience in the calibration of the associated parameters.

II.3 A STATE-SPACE FORMULATION

Consider a river segment which requires N routing reaches. Direct application of the routing equation (2.1) for each reach results in the following set of difference equations:

$$Q_1(t+1) = C_{1,1}\, Q_0(t) + C_{1,2}\, Q_0(t+1) + C_{1,3}\, Q_1(t) + C_{1.4} \qquad (3.1a)$$

$$Q_2(t+1) = C_{2,1}\, Q_1(t) + C_{2,2}\, Q_1(t+1) + C_{2,3}\, Q_2(t) + C_{2,4} \qquad (3.1b)$$

$$Q_i(t+1) + C_{i,1}\, Q_{i-1}(t) + C_{i,2}\, Q_{i-1}(t+1) + C_{i,3}\, Q_i(t) + C_{i,4} \qquad (3.1c)$$

$i = 3,4,\ldots,N.$

A state space formulation requires that quantities at time (t+1) are obtained in terms of their values at time t. The previous equations (3.1) can be converted into such a recursive scheme if the flow $Q_{i-1}(t+1)$ on the right-hand of the routing equation for reach i is substituted by its expression from the routing equation for reach i-1. For instance, substituting Eq. (3.1a) into Eq. (3.1b) and rearranging yields

$$Q_2(t+1) = C_{2,3}\, Q_2(t) + (C_{2,1} + C_{2,2}\, C_{1,3})\, Q_1(t) + C_{2,2}\, C_{1,1}\, Q_0(t) + C_{2,2}\, C_{1,2}\, Q_0(t+1) + C_{2,2}\, C_{1,4} + C_{2.4} \qquad (3.2)$$

Similarly, substitution of this equation into the routing expression for the 3rd reach gives the following result:

$$Q_3(t+1) = C_{3,3}\, Q_3(t) + (C_{3,1} + C_{3,2}\, C_{2,3})\, Q_2(t) +$$

$$+ \ (C_{3,2}\, C_{2,1} + C_{3,2}\, C_{2,2}\, C_{1,3})\, Q_1(t) + C_{3,2}\, C_{2,2}\, C_{1,1}\, Q_0(t)$$

$$+ C_{3,2}\, C_{2,2}\, C_{2,1}\, Q_0(t+1) + C_{3,2}\, C_{2,2}\, C_{1,4} + C_{3,2}\, C_{2,4}$$

$$+ C_{3,4} \qquad (3.3)$$

In general, there holds that

$$Q_i(t+1) = C_{i,3}\, Q_i(t) + (C_{i,1} + C_{i,2}\, C_{i-1,3})\, Q_{i-1}(t)$$

$$+ C_{i,2}\, (C_{i-1,1} + C_{i-1,2}\, C_{i-2,3})\, Q_{i-2}(t)$$

$$+ C_{i,2}\, C_{i-1,2}\, (C_{i-2,1} + C_{i-2,2}\, C_{i-3,3})\, Q_{i-3}(t) + \ldots$$

$$+ C_{i,2}\, C_{i-1,2} \cdots C_{3,2}\, (C_{2,1} + C_{2,2}\, C_{1,3})\, Q_1(t)$$

$$+ C_{i,2}\, C_{i-1,2} \cdots C_{2,2}\, C_{1,2}\, Q_0(t+1)$$

$$+ C_{i,2}\, C_{i-1,2} \cdots C_{2,2}\, C_{1,1}\, Q_0(t) + C_{i,4} + C_{i,2}\, C_{i-1,4}$$

$$+ C_{i,2}\, C_{i-1,2}\, C_{i-2,4} + \cdots + C_{i,2}\, C_{i-1,2} \cdots C_{3,2}\, C_{2,4}$$

$$+ C_{i,2}\, C_{i-1,2} \cdots C_{2,2}\, C_{1,4} \qquad (3.4)$$

where $i = 3,4,\ldots,N$.

Using matrix notation, we can represent all these equations for $i = 1,2,\ldots,N$ in the following equivalent form:

$$\underline{Q}(t+1) = \underline{\underline{A}}\, \underline{Q}(t) + \underline{\underline{B}}\, \underline{U}(t) + \underline{c} \qquad (3.5)$$

(single underscores denote vectors while double underscores indicate matrices) where

$$\underline{Q}(t) = [Q_1(t)\ Q_2(t)\ \ldots\ Q_N(t)]^T,$$

(the superscript T denotes transpose)

$$\underline{v}(t) = [Q_0(t)\ Q_0(t+1)]^T,$$

$$\underline{\underline{A}} = \begin{bmatrix} C_{1,3} & 0 & \cdots & 0 \\ C_{2,1} + C_{2,2}\,C_{1,3} & C_{2,3} & & \\ \vdots & & & \\ C_{N-1,2} \cdots C_{3,2}(C_{2,1} + C_{2,2}\,C_{1,3}) & \cdots & C_{N-1,3} & 0 \\ C_{N,2} \cdots C_{3,2}(C_{2,1} + C_{2,2}\,C_{1,3}) & \cdots & & C_{N,3} \end{bmatrix}$$

(NxN)

$$\underline{\underline{B}} = \begin{bmatrix} C_{1,1} & C_{1,2} \\ C_{2,2}C_{1,1} & C_{2,2}\,C_{1,2} \\ \vdots & \vdots \\ C_{N,2}\,C_{N-1,2} \cdots C_{2,2}\,C_{1,1} & C_{N,2}\,C_{N-1,2} \cdots C_{2,2}\,C_{1,2} \end{bmatrix}$$

(Nx2)

$$\text{and } \underline{c} = \begin{bmatrix} C_{1,4} \\ C_{2,4} + C_{2,2}\,C_{1,4} \\ \vdots \\ C_{N,4} + C_{N,2}\,C_{N-1,4} + \cdots + C_{N,2}\,C_{N-1,2} \cdots C_{2,2}\,C_{1,4} \end{bmatrix} .$$

(Nx1)

Equation (3.5) constitutes the state equation of the routing model with vector $\underline{Q}(t)$ being the system's state and vector $\underline{U}(t)$ its input. Vector $\underline{c}$ is related to the lateral inflow (or outflow), and, in certain cases, it may not be present. However, when this model is used as a part of the rainfall-runoff forecasting scheme, the lateral inflow will also be an input, and Equation (3.5) must be considered as follows:

$$\underline{Q}(t+1) = \underline{A}\,\underline{Q}(t) + \underline{B}\,\underline{U}(t) + \underline{c}\,\underline{q}(t) \qquad (3.6)$$

where $\underline{q}(t) = [\bar{q}_1(t)\ \bar{q}_2(t)\ \ldots\ \bar{q}_N(t)]^T$ and

$$\underset{(NxN)}{\underline{C}} = \begin{bmatrix} d_{1,4} & & & 0 \\ C_{2,2}\,d_{1,4} & & d_{2,4} & \\ \vdots & & & \\ C_{N,2} \cdots C_{2,2}\,d_{1,4} & & C_{N,2} \cdots C_{3,2}\,d_{2,4} \cdots & d_{N,4} \end{bmatrix} \quad \begin{matrix} \\ \\ \\ 0 \end{matrix}$$

with $d_{i,4} = \Delta x_i\ \bar{a}_i / C_{i,0}$ (see Eq. 2.2e).

For the segments originating from reservoirs, the input $\underline{U}(t)$ will represent reservoir releases, while for those emerging from watersheds, predicted streamflows.

The above system will be assumed observable through measurements of the discharge $Q_N(t)$ at the outlet of the last reach Δx_N. Thus, the associated observation equation can be stated as follows:

$$z(t) = \underline{H}^T\,\underline{Q}(t) \qquad (3.7)$$

where $\underline{H} = [0\ 0\ \ldots\ 1]^T$.

Equations (3.5) and (3.7) complete the deterministic state-space formulation of the routing model. Notice that all the elements of the coefficient matrices can be determined from the hydraulic characteristics of the channels. These coefficients will be constants if the linear philosophy of the previous section is adopted; otherwise, they will be time-varying.

II.4 OBSERVABILITY AND CONTROLLABILITY STUDY

Before proceeding with the stochastic aspects of our model, we shall investigate whether or not it is observable, controllable, or both. These two properties play instrumental roles in the design of optimal stochastic filters to be presented next.

A system is observable if and only if a finite series of observations $\{z(t_0), z(t_1), \ldots, z(t_M); M \text{ finite}\}$ is enough to uniquely determine the initial value of the state vector at time t_0. Equivalently, the previous system is observable (Kailath, 1980, Chapter 2) if and only if the matrix

$$\underline{\underline{O}} = \begin{bmatrix} \underline{H}^T \\ - - - - - \\ s\,\underline{\underline{I}} - \underline{\underline{A}} \end{bmatrix} \tag{4.1}$$

has rank N for all s. Substituting $\underline{H}$ and $\underline{\underline{A}}$ from the previous section, we have that

$$\underline{\underline{O}}_{[(N+1)\times N]} = \begin{bmatrix} 0 & \cdots & 0 & 1 \\ s - A_{1,1} & & 0 & 0 \\ -A_{2,1} & & s - A_{2,2} & \\ \vdots & & \vdots & \vdots \\ -A_{N,1} & & -A_{N,2} & \cdots \quad s - A_{N,N} \end{bmatrix} \tag{4.2}$$

where the elements $A_{i,j}$ represent the corresponding entries of the matrix $\underline{\underline{A}}$ defined following Eq. (3.5). The critical values of s for which this matrix may not fulfil the observability requirement are the eigenvalues of $\underline{\underline{A}}$. (If s is not an eigenvalue, the determinant $\det(s\underline{\underline{I}} - \underline{\underline{A}})$ will be nonzero and thereby the matrix $\underline{\underline{O}}$ will have rank N.) Given the structure of the matrix $\underline{\underline{O}}$, the system is observable if we cannot find an NxN submatrix with at least one zero

column or row for any value of s. The critical values of s are now restricted to $A_{1,1}$ and $A_{N,N}$, but one can easily verify that in either case no (NxN) submatrix with at least one zero row or column can be found. Thus, the system is observable.

A system is controllable if and only if, given any initial state vector $\underline{Q}_I(t_0)$ and any terminal state vector $\underline{Q}_T$, there exists a finite time t_M and an input sequence $\{\underline{U}(t_0), \underline{U}(t_1), \ldots, \underline{U}(t_M)\}$ which "drives" the system from $\underline{Q}_I(t_0)$ to $\underline{Q}_T$. Alternatively, the system is controllable if and only if the matrix $(s\underline{\underline{I}} - \underline{\underline{A}} \mid \underline{\underline{B}})$ has rank N for all s. Using arguments similar to those of the observability proof, we can easily show that the system is also controllable. Furthermore, this result applies to the system (3.6) as well.

Systems which are both controllable and observable have two desirable properties: (1) their stochastic filtering design is stable, and (2) their state-space formulation is irreducible (see Kailath, 1980 and Chen, 1970). The first implies that, in the state estimator, the observation errors do not accumulate, while the second guarantees that there does not exist any other state-space model of smaller than N dimension.

II.5 STOCHASTING FILTERING AND PREDICTION

The need to convert a deterministic state-space formulation into a stochastic one stems from the possibility of modeling errors. The stochastic model is obtained by adding random error terms to the state and observation equations:

$$\underline{Q}(t+1) = \underline{\underline{A}}\,\underline{Q}(t) + \underline{\underline{B}}\,\underline{U}(t) + \underline{\underline{C}}\,\underline{q}(t) + \underline{w}(t) \qquad (5.1)$$

$$z(t) = \underline{H}^T\,\underline{Q}(t) + v(t) \qquad (5.2)$$

where $\underline{w}(t)$ and $v(t)$ are time-uncorrelated gaussian random processes with zero means and covariances $\underline{\underline{P}}_w$ and R respectively. These parameters will be assumed known for now; the next section, however, will present a new Maximum Likelihood parameter estimation procedure for their identification.

Given the stochastic nature of this system, the problem is to obtain best estimates of the state vector based on all available observations. The following recursive equations constitute the well-known Kalman Filter and solve this problem optimally.

(i) Update

$$\hat{\underline{Q}}(t/t) = \underline{Q}(t/t-1) + \underline{K}(t)\, v(t) \tag{5.3}$$

$$v(t) = z(t) - \underline{H}^T\, \hat{\underline{Q}}(t/t-1) \tag{5.4}$$

$$\underline{K}(t) = \underline{\underline{\Sigma}}(t/t-1)\, \underline{H}[\underline{H}^T\, \underline{\underline{\Sigma}}(t/t-1)\, \underline{H} + R]^{-1} \tag{5.5}$$

$$\underline{\underline{\Sigma}}(t/t) = [\underline{\underline{I}} - \underline{K}(t)\, \underline{H}^T]\, \underline{\underline{\Sigma}}(t/t-1) \tag{5.6}$$

$t = 0,1,\ldots$

(ii) Prediction

$$\hat{\underline{Q}}(t+1/t) = \underline{\underline{A}}\, \hat{\underline{Q}}(t/t) + \underline{\underline{B}}\, \hat{\underline{U}}(t) + \underline{\underline{C}}\, \hat{\underline{q}}(t) \tag{5.7}$$

$$\underline{\underline{\Sigma}}(t+1/t) = \underline{\underline{A}}\, \underline{\underline{\Sigma}}(t/t)\, \underline{\underline{A}}^T + \underline{\underline{B}}\, \underline{\underline{P}}_U\, \underline{\underline{B}}^T + \underline{\underline{C}}\, \underline{\underline{P}}_q\, \underline{\underline{C}}^T + \underline{\underline{P}}_w \tag{5.8}$$

$t = 0,1,\ldots$

where $\hat{\underline{Q}}(t/t) = E\{\underline{Q}(t)/[z(0),\ldots,z(t)]\}$,

$\hat{\underline{Q}}(t/t-1) = E\{\underline{Q}(t)/[z(0),\ldots,z(t-1)]\}$,

$\underline{\underline{\Sigma}}(t/t) = E\{[\underline{Q}(t) - \hat{\underline{Q}}(t/t)][\underline{Q}(t) - \hat{\underline{Q}}(t/t)]^T\}$,

$\underline{\underline{\Sigma}}(t/t-1) = E\{[\underline{Q}(t) - \underline{Q}(t/t-1)][\underline{Q}(t) - \underline{Q}(t/t-1)]^T\}$,

(the symbol $E\{\cdot\}$ indicates expectation).

$\underline{\underline{P}}_U$ and $\underline{\underline{P}}_q$ are the covariance matrices of the vectors $\underline{U}$ and $\underline{q}$, obtained from the predictions of the rainfall-runoff model. The vector $\underline{K}(t)$ is the Kalman gain vector and $\nu(t)$, the Kalman innovations variable.

Computationally, the most involved part of this algorithm is the update step. However, as it turns out, for the system under consideration the covariance update step simplifies as follows:

$$\hat{Q}_i(t/t) = \hat{Q}_i(t/t-1) + \frac{\Sigma_{iN}(t/t-1)}{\Sigma_{NN}(t/t-1)+R} \quad [z(t) - \hat{Q}_N(t/t-1)] \tag{5.9}$$

$$\Sigma_{ij}(t/t) = \Sigma_{ij}(t/t-1) - \frac{\Sigma_{in}(t/t-1)\ \Sigma_{Nj}(t/t-1)}{\Sigma_{NN}(t/t-1) + R} \tag{5.10}$$

where $\underline{\hat{Q}}_i(t/s)$ and $\underline{\underline{\Sigma}}_{ij}(t/s)$ represent respectively the i^{th} and the ij^{th} elements of the vector $\underline{\hat{Q}}(t/s)$ and the matrix $\underline{\underline{\Sigma}}(t/s)$, s=t, t-1.

These expressions have been obtained by performing the operations indicated in Equations (5.3) through (5.6)

II.6 A NEW MAXIMUM LIKELIHOOD PARAMETER ESTIMATION SCHEME

Usually, the identification of the noise covariance terms $\underline{\underline{P}}_W$ and R of uncertain dynamical systems is accomplished by a trial and error approach where ranges of values are scanned with the hope to identify the ones which validate the hypothesized model structure (i.e., which generate white model residuals). When $\underline{\underline{P}}_W$ is a matrix of substantial size, this approach becomes tedious, expensive, and less accurate. On the other hand, incorrect parameter usage may lead to filter "divergence" where the predicted residual variance is too small and optimistic. Based on comparisons between expected and estimated statistics

of the filter residuals, one can diagnose this suboptimal performance and attempt to correct it (see, for instance, Mehra, 1970, where the correction is based on imposing the whiteness property on the filter residuals). However, we feel that the correction techniques are either heuristic or computationally burdensome and that another approach, based on the maximization of the Maximum Likelihood, is theoretically and practically preferable.

We shall next give a new formulation of the Maximum Likelihood parameter estimation problem which can be solved efficiently, using optimal control techniques. We shall demonstrate the idea for the previously developed system, but the approach is generally applicable.

The filtering form of the Loglikelihood function $\xi(T)$ is given by (see Schweppe, 1973, Chapter 14):

$$\xi(T) = \frac{1}{2} \left[\xi_{bias}(T) + \xi_{obs}(T)\right] \tag{6.1}$$

$$\xi_{bias}(T) = - T \, \ell n(2\pi) - \sum_{t=1}^{T} \ell n(\Sigma_z(t/t-1)) \tag{6.2}$$

$$\xi_{obs}(T) = - \sum_{t=1}^{T} \frac{[z(t) - \underline{H} \, \underline{\hat{Q}}(t/t-1)]^2}{\Sigma_z(t/t-1)} \tag{6.3}$$

where T is the total number of observations and

$$\Sigma_z(t/t-1) = E\{[z(t) - \underline{H} \, \underline{\hat{Q}}(t/t-1)]^2\} \tag{6.4}$$

However, from Eq. (6.4) we also have that

$$\Sigma_z(t/t-1) = R + \underline{H} \, \underline{\Sigma}(t/t-1) \, H^T =$$

$$= R + \underline{H}[\underline{A} \, \underline{\Sigma}(t-1/t-1) \, \underline{A}^T + \underline{B} \, \underline{P}_U(t-1) \, \underline{B}^T + \underline{C} \, P_q(t-1) \, \underline{C}^T +$$

$$+ \underline{\underline{P}}_W] \underline{H}^T \tag{6.5}$$

where the second equality follows from Equation (5.8). Also, $\hat{\underline{Q}}(t/t)$ and $\underline{\underline{\Sigma}}(t/t)$ can be obtained in terms of $\hat{\underline{Q}}(t-1/t-1)$ and $\underline{\underline{\Sigma}}(t-1/t-1)$ by combining the update and prediction steps of the Kalman Filter as follows:

$$\hat{\underline{Q}}(t/t) = \underline{\underline{A}}\, \hat{\underline{Q}}(t-1/t-1) + \underline{\underline{\Sigma}}(t/t-1)\, \underline{H}\, \Sigma_z^{-1}(t/t-1)\, [z(t) - \underline{H}\, \hat{\underline{Q}}(t/t-1)] \tag{6.6}$$

where $\underline{\underline{\Sigma}}(t/t-1)$ is obtained in terms of $\underline{\underline{\Sigma}}(t-1/t-1)$ from Eq. (5.8), $\Sigma_z(t/t-1)$ is obtained in terms of $\underline{\underline{\Sigma}}(t-1/t-1)$ from Eq. (6.5), and $\hat{\underline{Q}}(t/t-1)$ is obtained in terms of $\hat{\underline{Q}}(t-1/t-1)$ from Eq. (5.7).

Also, combining Eq. (5.6), (5.5), and (6.5) we find

$$\underline{\underline{\Sigma}}(t/t) = \underline{\underline{\Sigma}}(t/t-1) - \underline{\underline{\Sigma}}(t/t-1)\, \underline{H}\, \Sigma_z^{-1}(t/t-1)\, \underline{H}^T\, \underline{\underline{\Sigma}}(t/t-1) \tag{6.7}$$

where again $\underline{\underline{\Sigma}}(t/t-1)$ and $\Sigma_z(t/t-1)$ can be expressed in terms of $\underline{\underline{\Sigma}}(t-1/t-1)$ as before.

To facilitate the notation, we shall represent the system of Equations (6.6) and (6.7) in the following form:

$$\underline{x}(t) = \underline{f}_{t-1}(\underline{x}(t-1), \underline{u}) \tag{6.8}$$

where $\underline{x}(t)$ includes all the elements of $\hat{\underline{Q}}(t/t)$ and $\underline{\underline{\Sigma}}(t/t)$, $\underline{u}$ represents R and $\underline{\underline{P}}_W$, and the vector function $\underline{f}_{t-1}(\cdot,\cdot)$ stands for the functional relationships (6.6) and (6.7) among these quantities. Equation (6.8) represents a deterministic dynamical system with state vector $\underline{x}(t)$ and control vector $\underline{u}$.

Next, the critical point is to observe that the Loglikelihood function is additively separable in terms depending on $\hat{\underline{Q}}(t-1/t-1)$, $\underline{\underline{\Sigma}}(t-1/t-1)$, R, and $\underline{\underline{P}}_W$.

This can be readily concluded from Eq. (6.1), (6.2), and (6.3) which amount to the following expression:

$$\xi(t) = -\frac{1}{2}\sum_{t=1}^{T}\left[\ell n(\Sigma_z(t/t-1)) + \frac{z(t) - \underline{H}\,\underline{\bar{Q}}(t/t-1)}{\Sigma_z(t/t-1)}\right]\frac{1}{2}\,T\ell n(2\pi). \quad (6.9)$$

where again Eq. (5.6), (5.5), and (6.5) can be invoked to prove the separable additivity of $\xi(T)$ in terms of $\underline{x}(t)$ and $\underline{u}$.

Let $g_{t-1}\,(\underline{x}(t-1),\,\underline{u})$ represent the summant in Eq. (6.9). Then, the estimation of the parameter vector $\underline{u}$ can be cast as the following optimal control problem:

Find the optimal vector $\underline{u}$ which maximizes the functional

$$J = \sum_{t=1}^{T} g_{t-1}(\underline{x}(t-1),\underline{u}) \quad (6.10)$$

subject to the dynamics

$$\underline{x}(t) = \underline{f}_{t-1}\,(\underline{x}(t-1),\,\underline{u}), \qquad t=1,2,\ldots,T. \quad (6.11)$$

(Being a constant, the term $-\frac{1}{2}\,T\,\ell n(2\pi)$ can be dropped without affecting the maximization of the Loglikelihood.)

The reason why this Maximum Likelihood formulation is preferable to the ordinary ones is because it exploits the dynamical nature of the problem. It also allows the application of efficient control algorithms especially designe for problems with such structure.

The solution of this problem will be obtained from a recently developed algorithm which is called Extended Linear Quadratic Gaussian control or ELQG for short (Georgakakos and Marks, 1986). Apart from its excellent convergence properties, this algorithm also has the ability to compute the Hessian matrix of the objective function with respect to the control vector. This quantity is

of the objective function with respect to the control vector. This quantity is very useful in the characterization of the optimal solution, because in this framework it represents the Information matrix. This matrix (more precisely its diagonal elements) is instrumental in characterizing the identifiability of the unknown parameters.

II.7 CONCLUSION

This report was concerned with the theoretical development of a state-space routing model, compatible to the rainfall-runoff and reservoir system components of the integrated forecast-control scheme. The coefficients of the new model can be readily determined based on the channels' hydraulic properties, or inflow-outflow observations, or both. Its state-space form allows the application of stochastic filtering techniques which use available observations to more accurately predict future state trajectories. The identification of this models' noise covariances will be performed by means of a new Maximum Likelihood estimation procedure. The new model will be tested and evaluated in real world case studies during the following quarter.

REFERENCES

Chen, C.T., "Introduction to Linear Systems Theory," Holt, Rinehart, and Winston, NY, 1970.

Fread, D.L., "A Unified Coefficient Routing Model," NOAA Report, 1983.

Georgakakos, A.P., and Marks, D.H., "A New Method for the Real Time Operation of Reservoir Systems," Water Resources Research, accepted for publication, Sept. 1986.

Kailath, T., "Linear Systems," Prentice-Hall, Englewood Cliffs, N.J., 1980.

Mehra, R.K., "On the Identification of Variances and Adaptive Kalman Filtering," IEEE Trans. on Automatic Control, Vol. AC-15, No. 2, pp. 175-184.

Schweppe, F.C., "Uncertain Dynamic Systems," Prentice-Hall, Englewood Cliffs, N.J., 1973.

"Optimal Real-Time Forecasting and Control of Reservoir Hydrosystems Using Remote and On-Site Sensors"

Supported by
the U.S. Geological Survey, Department of the Interior
under award number 14 - 08 - 0001 - G1297

Water Resources Research
Act of 1984

Project Starting Date : September 1, 1986
Project Termination date: August 31, 1988

Progress Report for the period
December 1, 1986, through February 28 1987

by

Aris P. Georgakakos, Ph. D.
Professor of Hydrology and Water Resources
School of Civil Engineering
Georgia Institute of Technology
Atlanta, Georgia 30332
Tel.: (404) 894-2240 or -2201

March 13, 1987

PART II

A State-Space Model for River Routing

The contents of this report were developed under a grant from the Department of the Interior, U. S. Geological Survey. However, those contents do not necessarily represent the policy of that agency, and you should not assume endorsement by the Federal Government.

Section	CONTENTS	Page No.

II.1 INTRODUCTION AND OVERVIEW

This progress report discusses some implementation aspects of the state-space model for river routing developed and presented over the first quarter of the project.

More specifically, the following tasks were completed over this quarter:

a. The DWOPER river routing computer program was acquired and installed on the Georgia Tech computer system.

b. Several sets of data from the Ohio-Tennessee-Mississippi river system were acquired to be used in case studies.

c. The computer code of the proposed state-space river routing model was developed and tested on the Georgia Tech computer system.

d. A case study and sensitivity analysis were performed.

e. The performance of the proposed state-space river routing model was compared to that of the DWOPER model.

II.2 The DWOPER Model

The DWOPER (Dynamic Wave Operational) model was developed by D.L. Fread (1978) and solves the complete one-dimensional St. Venant equations of unsteady flow using an implicit finite difference integration scheme. This model constitutes the state of the art in dynamic river routing and is applicable to rivers of varying physical features such as irregular geometry, variable roughness parameters, lateral inflows, flow diversions, off-channel storage, local head losses such as bridge contraction-

expansions, lock and dam operations, and wind effects.

The DWOPER model is especially useful where backwater effects and mild bottom slopes are most troublesome to hydrologic routing models.

The proposed state-space model (hereafter referred to as SSRR - State Space River Routing model) is a hydrologic routing model supplied with a state estimator to take advantage of available discharge measurements. This feature (of state feedback) is expected to strengthen its predictive ability and widen its applicability.

In this work, the performance of the SSRR model will be compared with that of the DWOPER model which will be considered as representative of the actual river flows.

II.3 CASE STUDY DATA

The case study to be presented utilizes data from the Ohio river just before it joins the Cumberland river. The branch of the case study has a length of 44.8 miles and mild bottom slope in the proximity of 0.50 ft/mi. Crossectional data were available at three locations: Shawneetown, Fords Ferry, and Golconda. The data consisted of tabulated values providing the area, the top width, and the Manning's roughness coefficient as a function of discharge.

Daily streamflow data were available for the Ohio river at Shawneetown as well as for the Saline and Tradewater rivers. The latter were considered as lateral inflows. The streamflow records

had a length of 84 days.

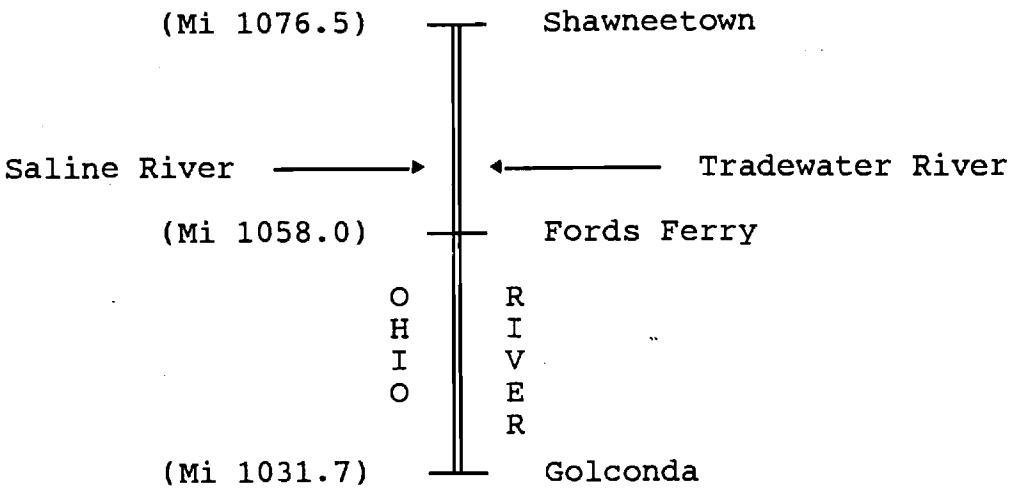

II.4 A CASE STUDY

First the DWOPER model was employed to predict the streamflow discharges at Golconda. The predicted values are shown on Figure 1. They range from 120,000 to 600,000 cubic feet per second approximately.

The SSRR model was implemented in two versions: The first utilized one routing reach (from Shawneetown to Golconda) and the second, two (one from Shawneetown to Fords Ferry and another from Fords Ferry to Golconda). For each version, the Muskingum-Cunge parameters were computed as presented in the first Progress Report (Equations (2.2) through (2.7)) for a reference discharge of 595,000 cubic feet per second.

Parameter	First SSRR Version	Second SSRR Version Two Reaches First	Second
Manning's Coef.	0.0269	0.270	0.268
Slope	0.00229	0.00246	0.0021
Area ($Feet^2$)	169,542.	174,866.	154,274.
Top Width, B_0 (Feet)	7563.	8423.	5475.
dB_0/dy	167.	206.	123.
Reach Length (Feet)	236,544.	97,680.	138,864.
Unit-Width Discharge ($Feet^2/Sec.$)	79.	71.	109.
Routing Interval (Seconds)	86,400.	86,400.	86,400.

Figures 2 and 3 show the results from the two SSRR models, using one and two reaches respectively. (The thicker line corresponds to the results from DWOPER.) Both versions exhibit a bias (Version I overpredicts while Version II underpredicts); however, Version II follows the DWOPER predictions more closely. In both of these runs, the SSRR model was implemented with a value of 0.5 for the coefficient Θ (see previous progress report, Eq. (2.3a)) and a large value for the measurement error variance. As a result of the latter, the model's predictions are exclusively based on its dynamical equations. The measurement equation is virtually inactive.

In an attempt to tune the model's predictive ability, we run several experiments with different Θ values. For Version I, the results appear on Figures 4 through 10; Figures 11 through 17

display the Version II results. To better quantify the model's predictive power, in each of the above experiments we also computed the bias and the standard deviation of the prediction errors. The results are summarized in the following tables:

S S R R V e r s i o n I

Θ	Bias (ft^3/sec)	St. Deviation (ft^3/sec)
0.5	-65,637.9	56,259.1
1.	-65,680.6	54,466.5
5.	-65,544.3	45,903.9
10.	-63,545.4	39,499.9
50.	-38,018.6	29,457.6
100.	-23,333.2	25,829.3
500.	-4,767.3	22,860.1
1000.	-1,843.9	22,749.2

S S R R V e r s i o n II

Θ	Bias (ft^3/sec)	St. Deviation (ft^3/sec)
0.5	68,268.6	30,656.6
1.	39,682.5	21,633.9
5.	14,750.6	21,226.6
10.	11,145.9	22,132.4
50.	5,788.8	22,872.2
100.	3,992.2	22,859.5
500.	1,893.3	22,759.6
1000.	1,576.3	22,785.3

As can be seen from the above figures, between the two versions, the one with the two routing reaches performs the best (it exhibits smaller biases and standard deviations). This result was expected due to the nonuniformity of the channel parameters in the two river segments. Futhermore, the SSRR model can be improved by adjusting Θ (as Θ increases, the prediction bias

becomes smaller while the standard deviation may somewhat increase). This is a significant observation, because it shows that the Muskingum-Cunge formulation is flexible to account for troublesome routing problems such as backwater effects by appropriate tuning of the Θ parameter. With respect to forecasting, the best Θ-value is the one which yields the smallest error standard deviation. To identify this value, another set of SSRR-II experiments was run with finer Θ discretizations. It was found that a value of 2 yields the smallest standard deviation of 20,220.2 ft^3/sec and a bias of 24,415.1 ft^3/sec. This run appears on Figure 18. Figure 19 shows the results from the same model with bias adjustment. It can be seen that the performance of the SSRR model has improved considerably.

The last set of experiments was concerned with the performance of the SSRR model with state feedback. The covariances of the measurement and system errors (in Equations 5.1 and 5.2 of the first progress report) were set approximately equal and the SSRR-II model was run with Θ=2. The results appear on Figure 20. The standard deviation of the prediction error for this run was reduced to 11,729.5 ft^3/sec, and the model's ability to simulate the DWOPER flows was greatly enhanced.

II.5 CONCLUSIONS

The proposed state-space river routing model was implemented and tested in a real world case study. The results indicate that

the model is capable of good quality forecasts even in cases where traditional hydrologic routing models experience difficulties. During the first part of the upcoming quarter, this model will also be tested in several other real world case studies with varying hydrologic characteristics (e.g., steeper bottom slopes). However, it is expected that in the absence of backwater effects, its performance will only further improve.

A P P E N D I X A

CASE STUDY FIGURES

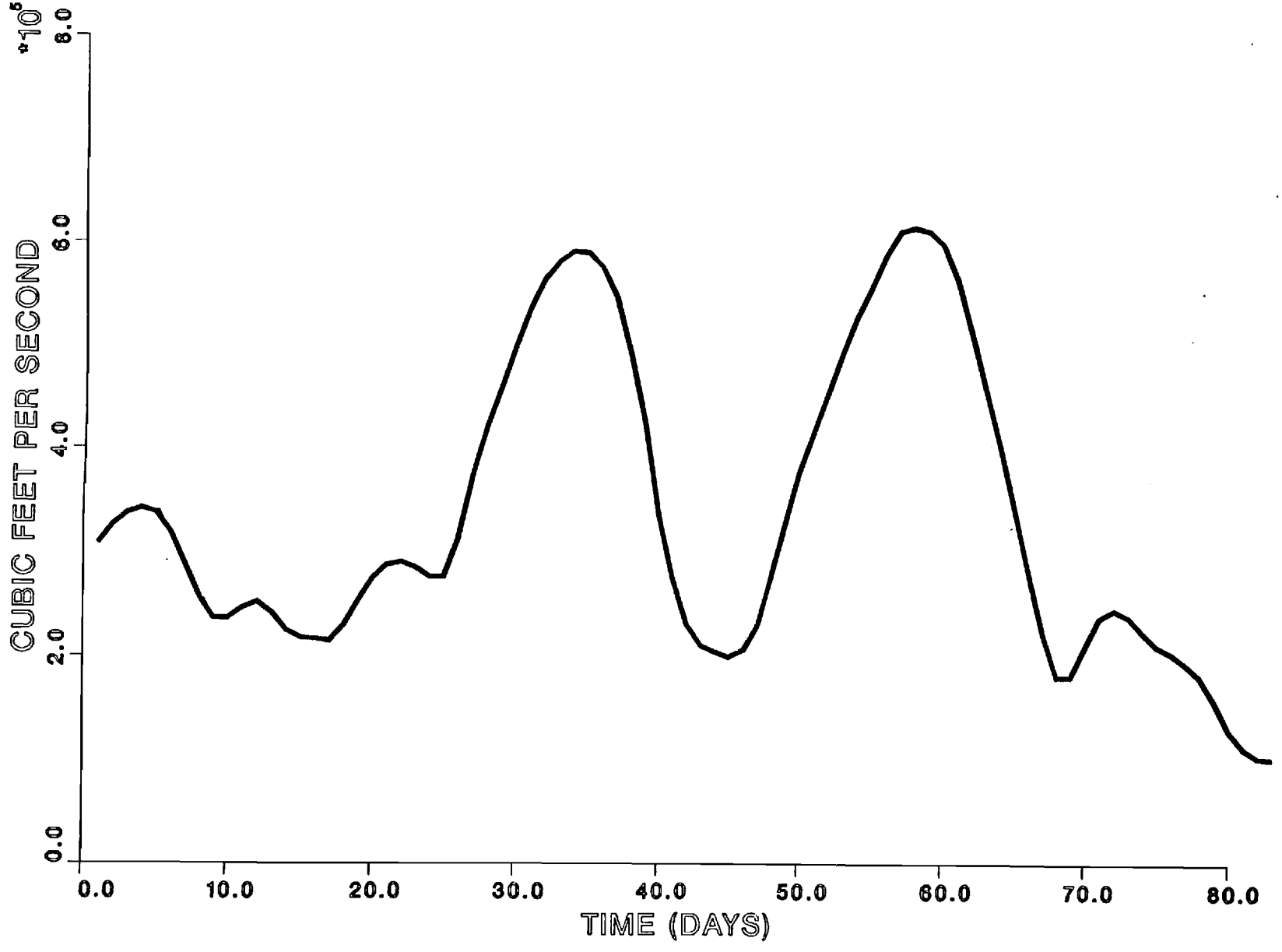

FIGURE 1: DWOPER FLOW PREDICTIONS

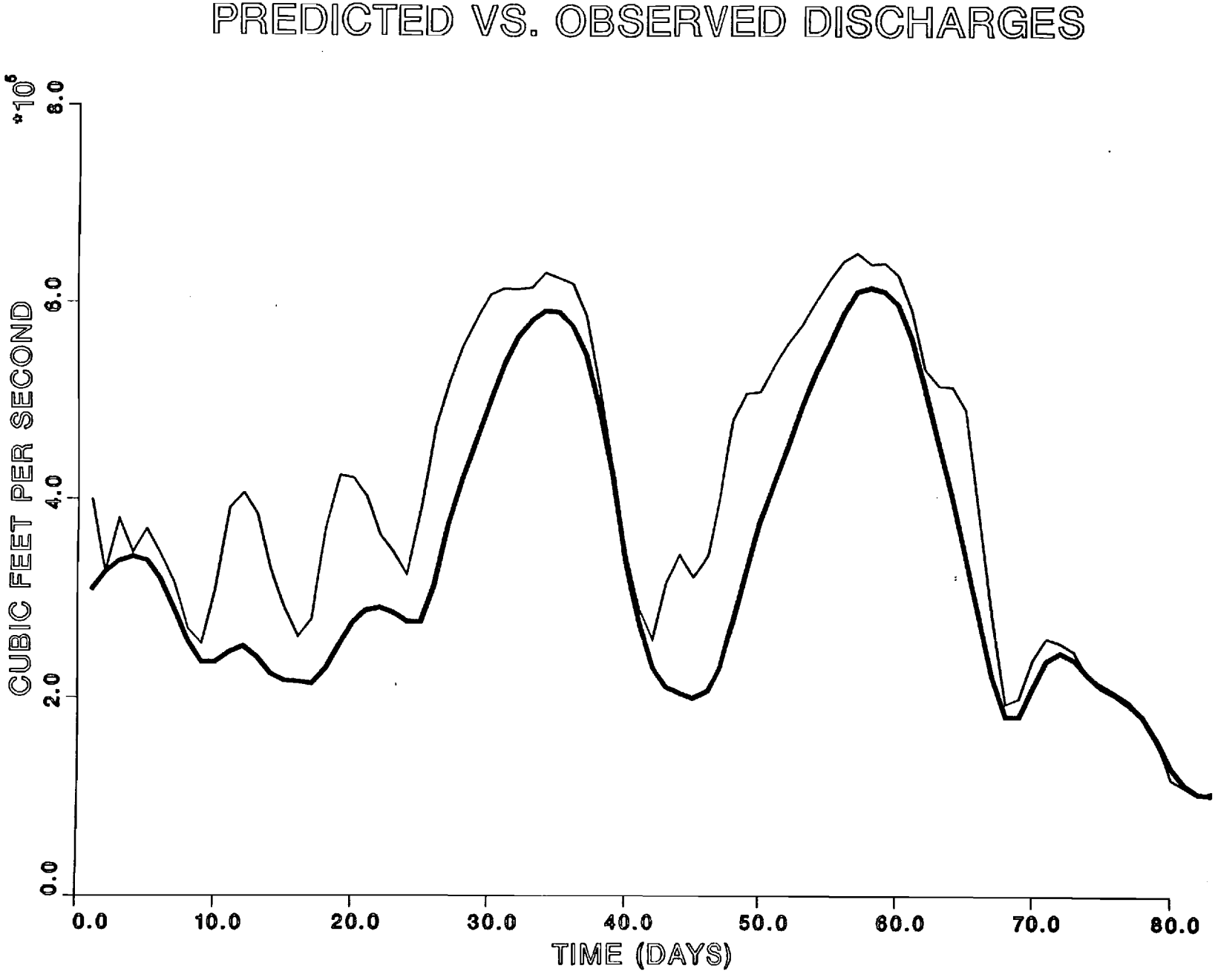

FIGURE 2: SSRR-I, θ=0.5

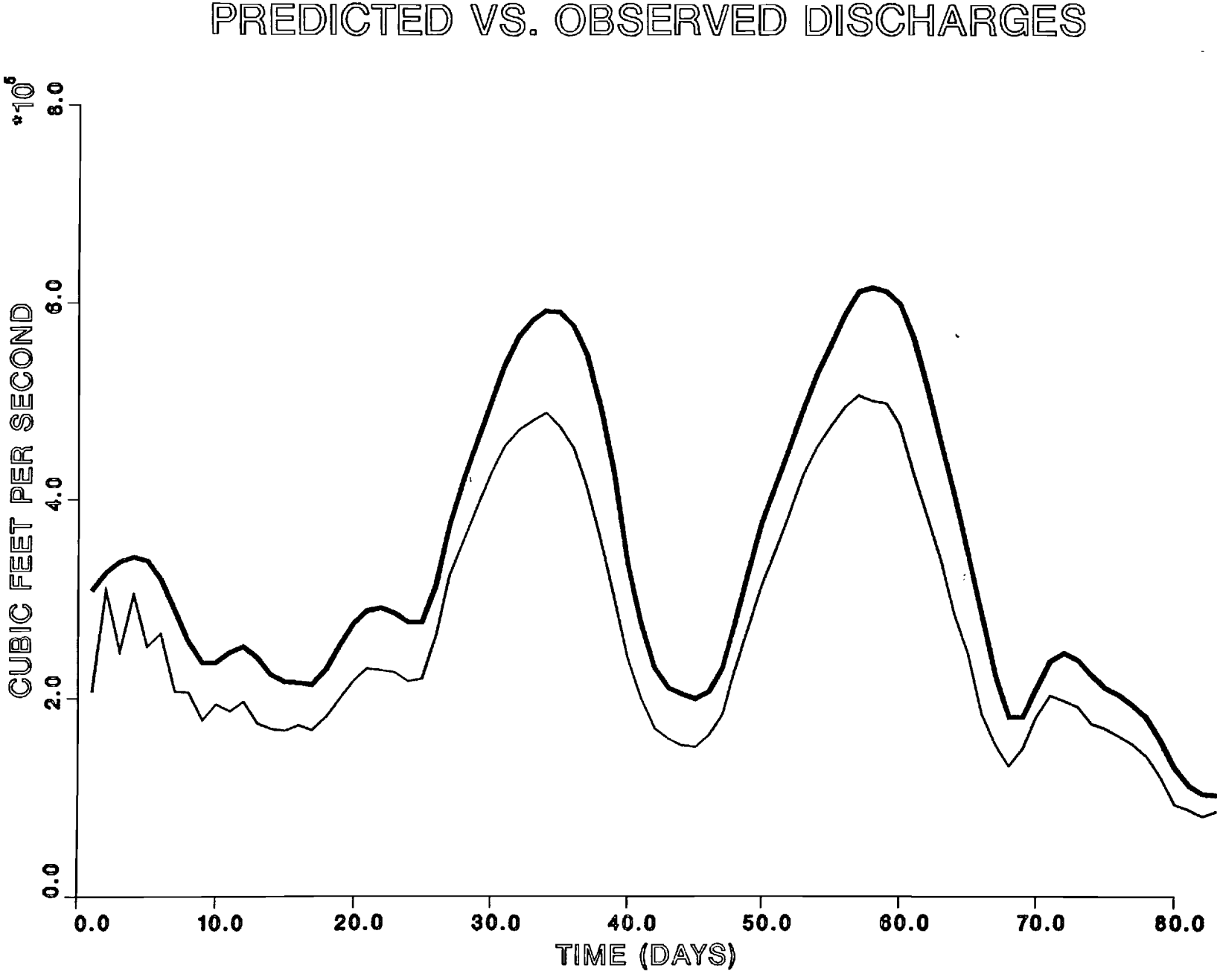

FIGURE 3: SSRR-II, θ=0.5

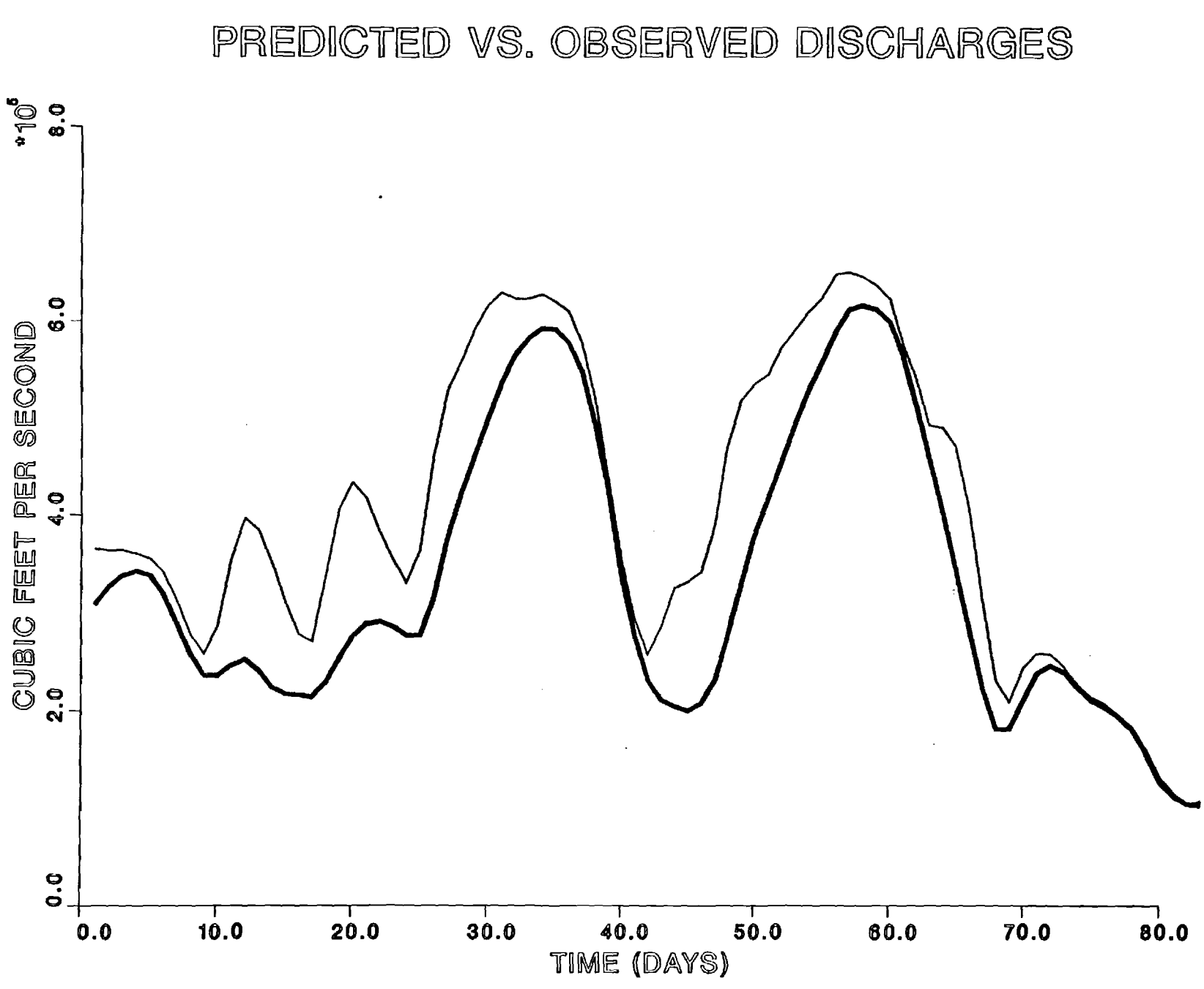

FIGURE 4: SSRR-I, 0=1

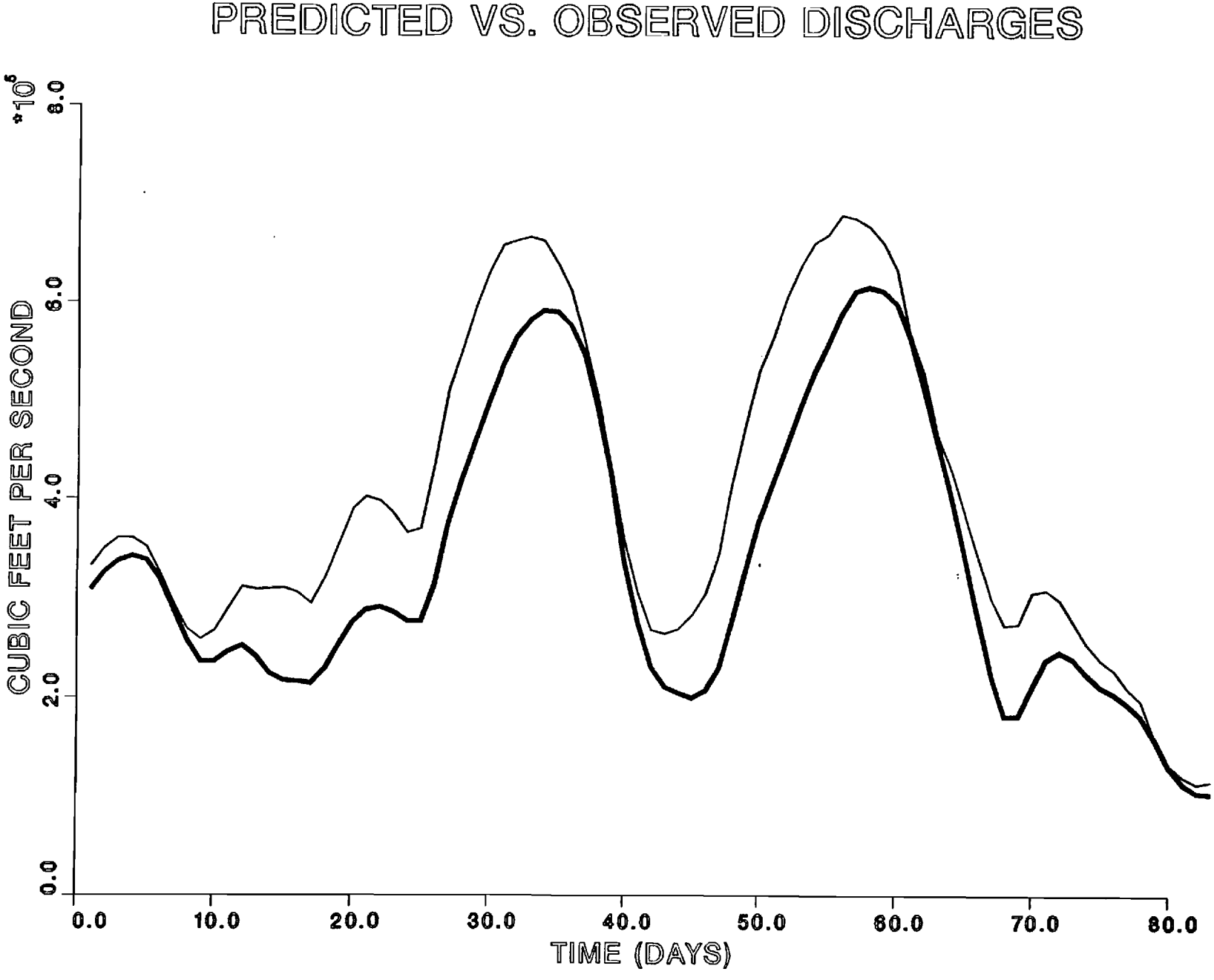

FIGURE 5: SSRR-I, θ=5

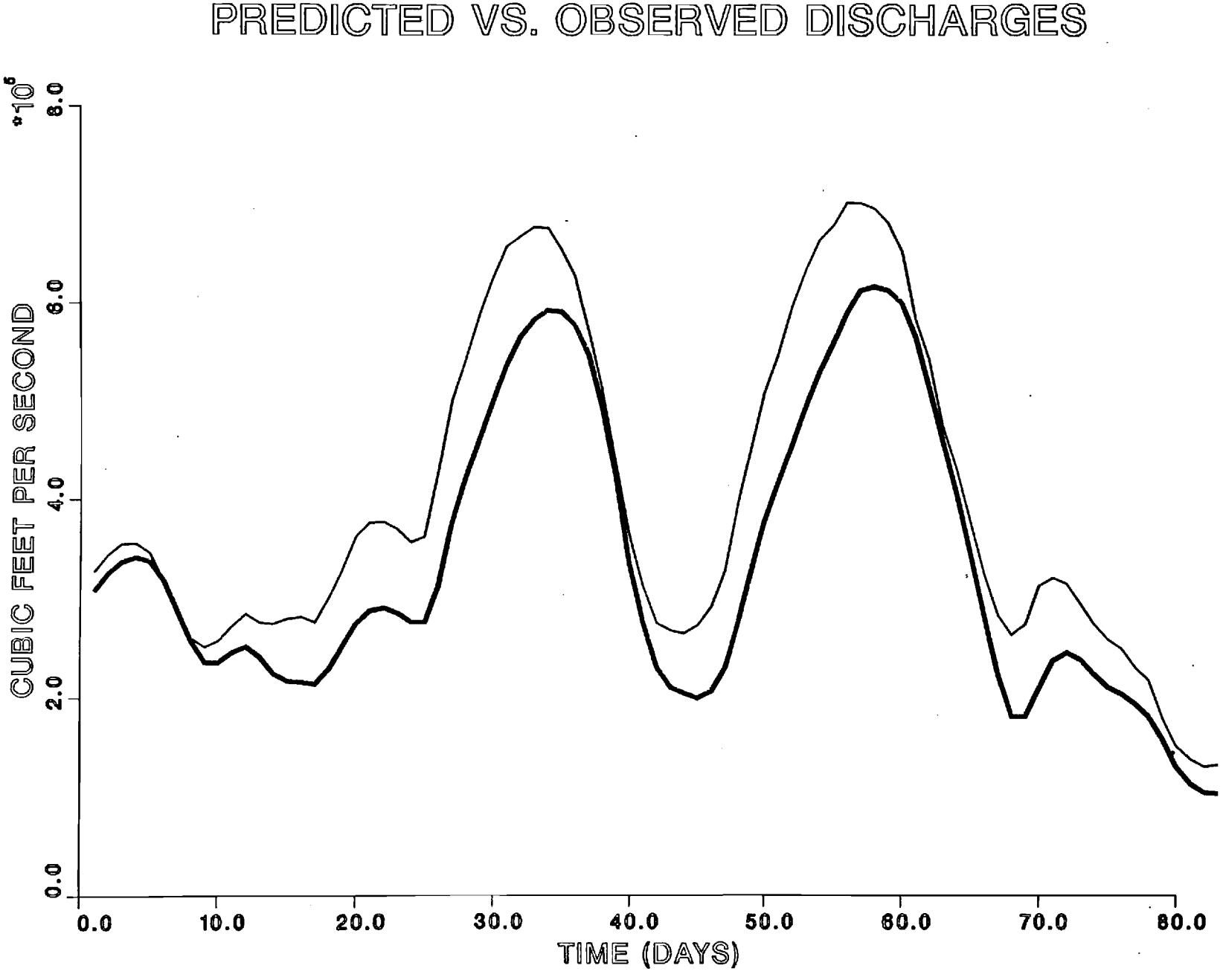

FIGURE 6: SSRR-I, θ=10

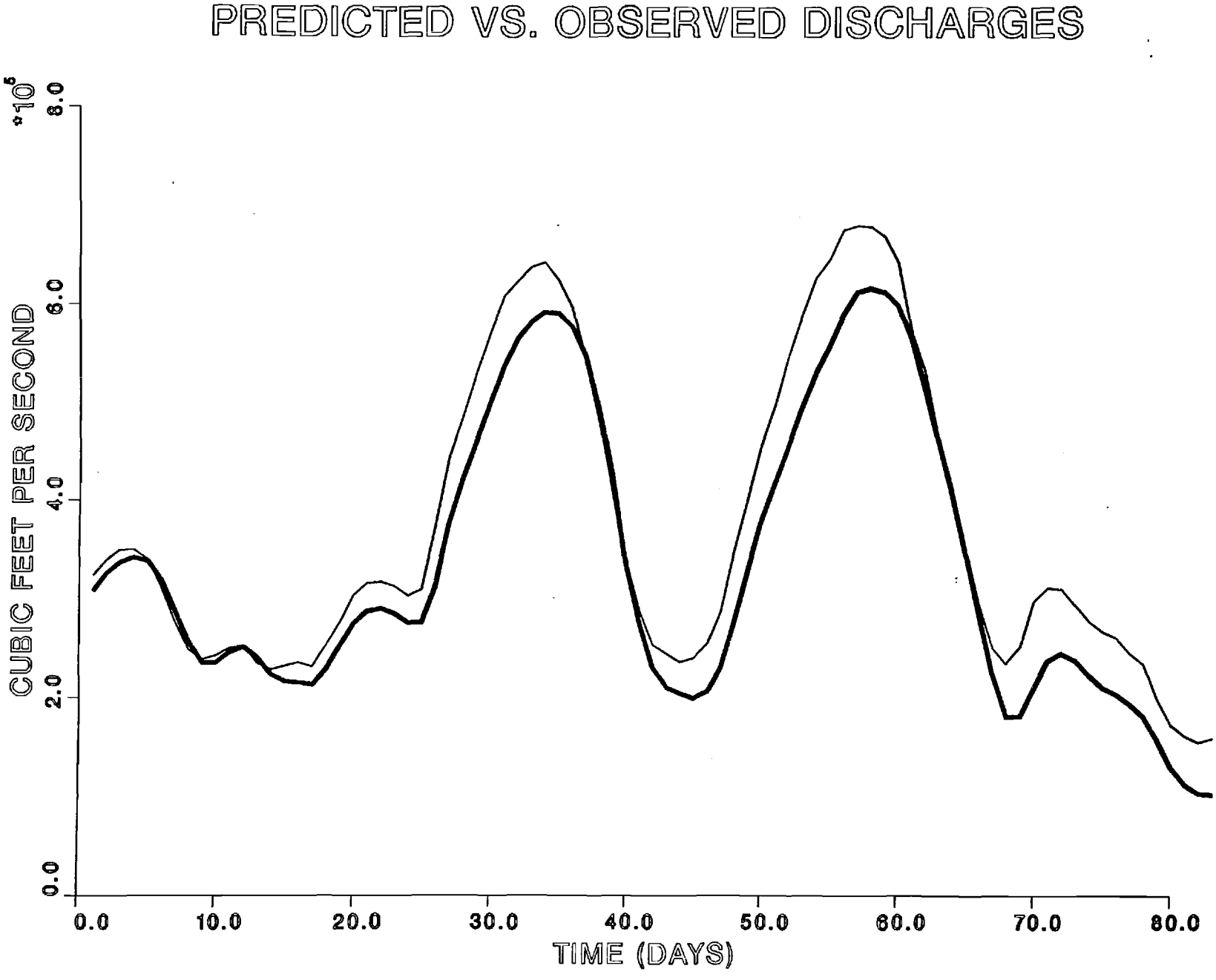

FIGURE 7: SSRR-I, θ=50

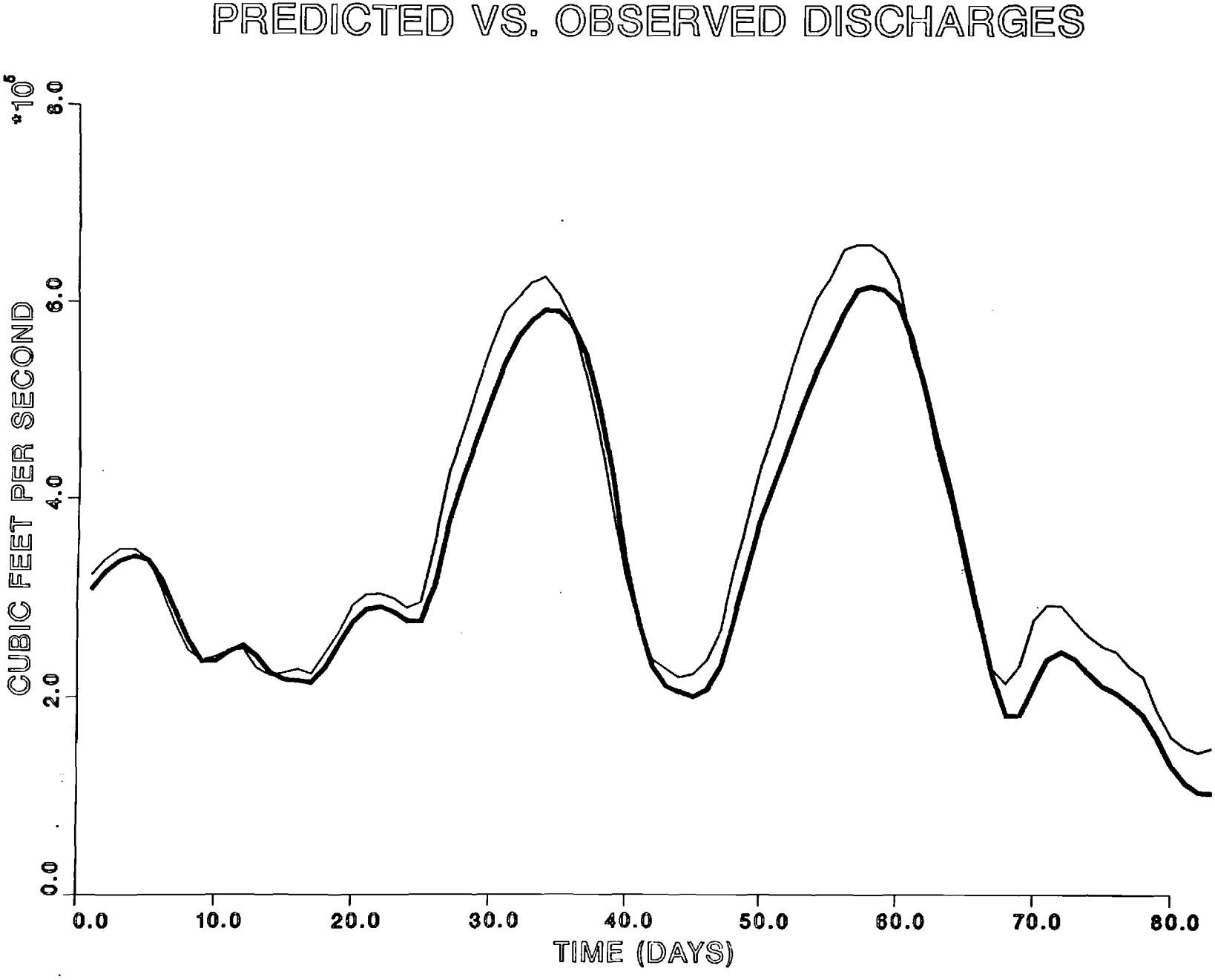

FIGURE 8: SSRR-I, θ=100

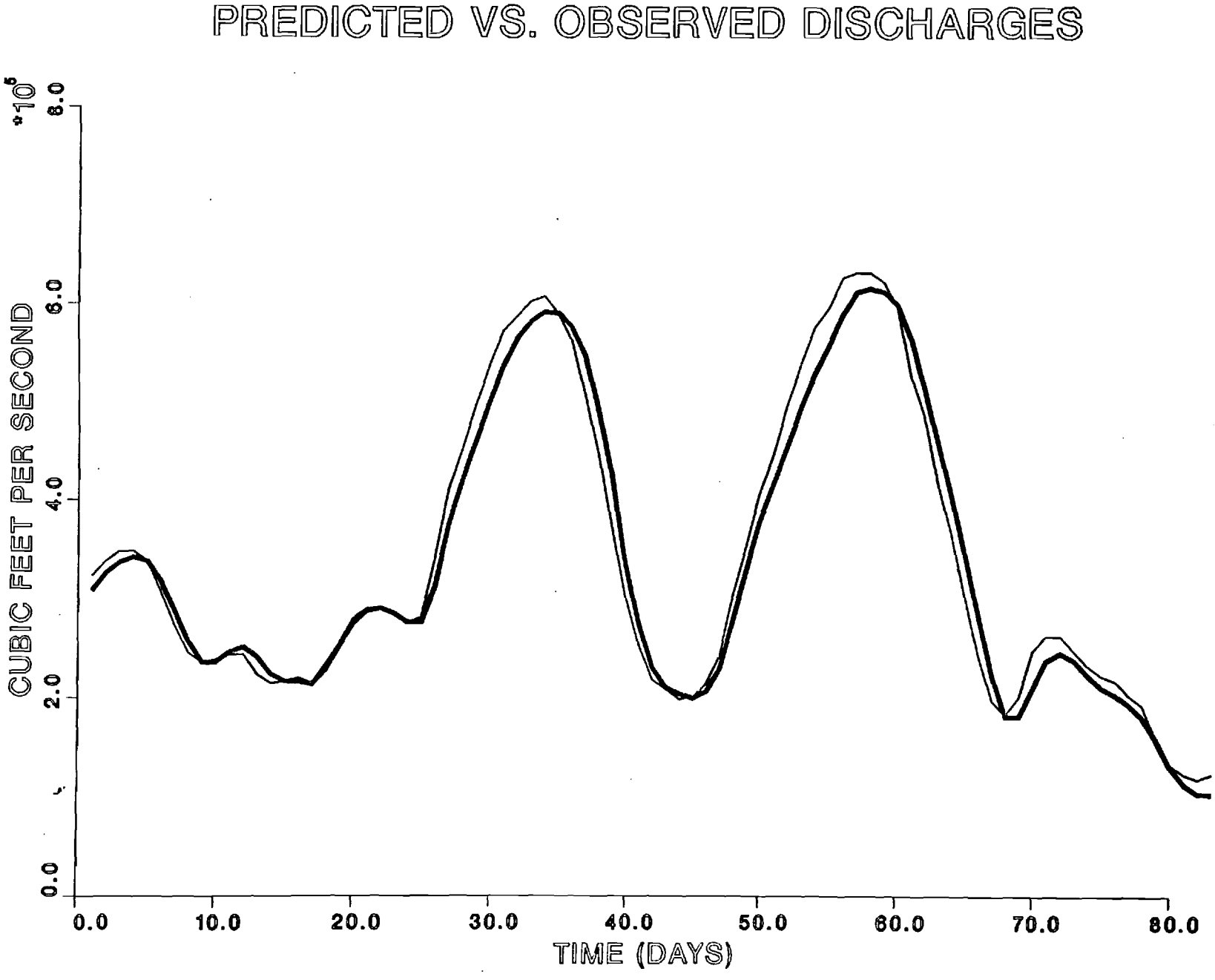

FIGURE 9: SSRR-I, θ=500

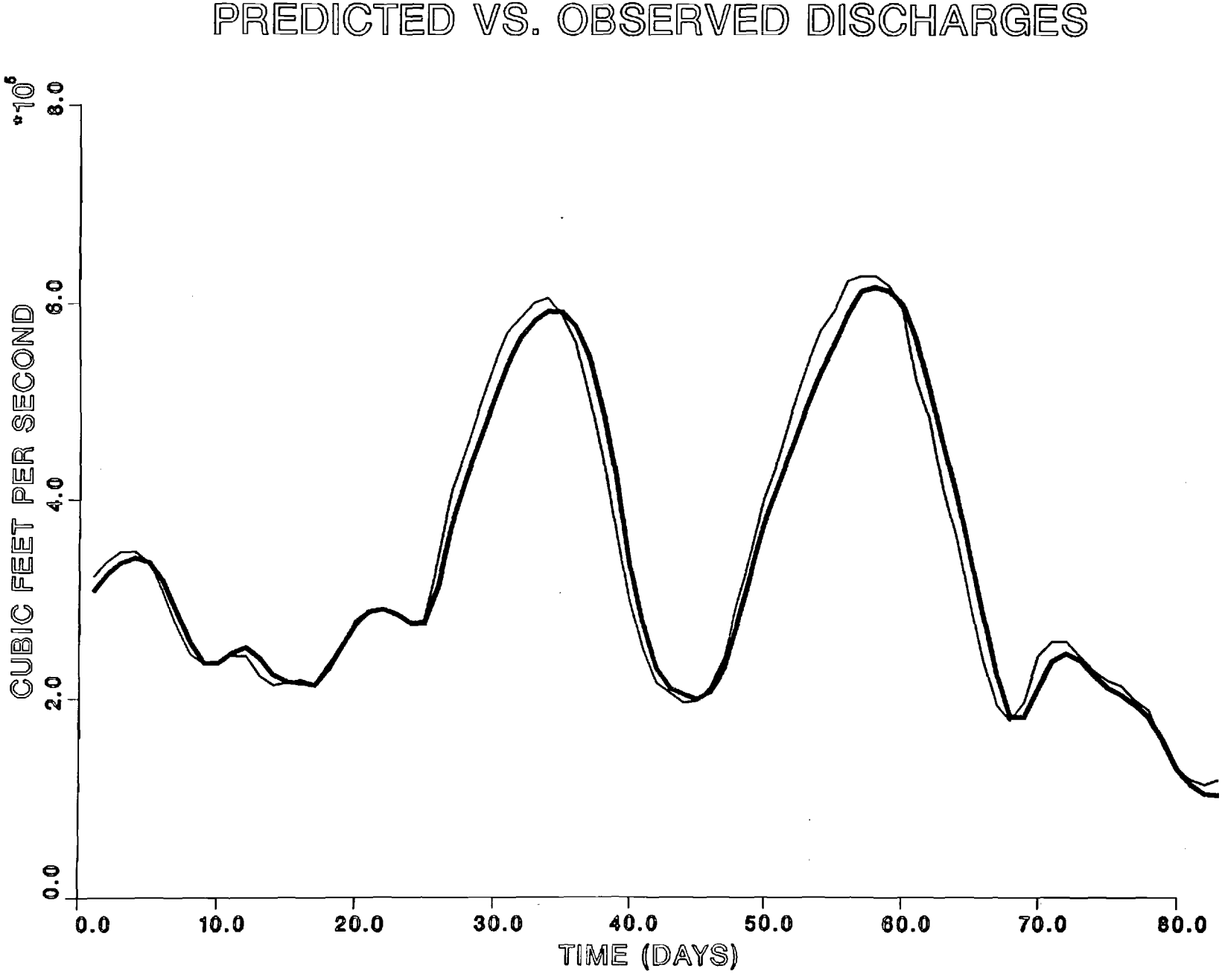

FIGURE 10: SSRR-I, θ=1000

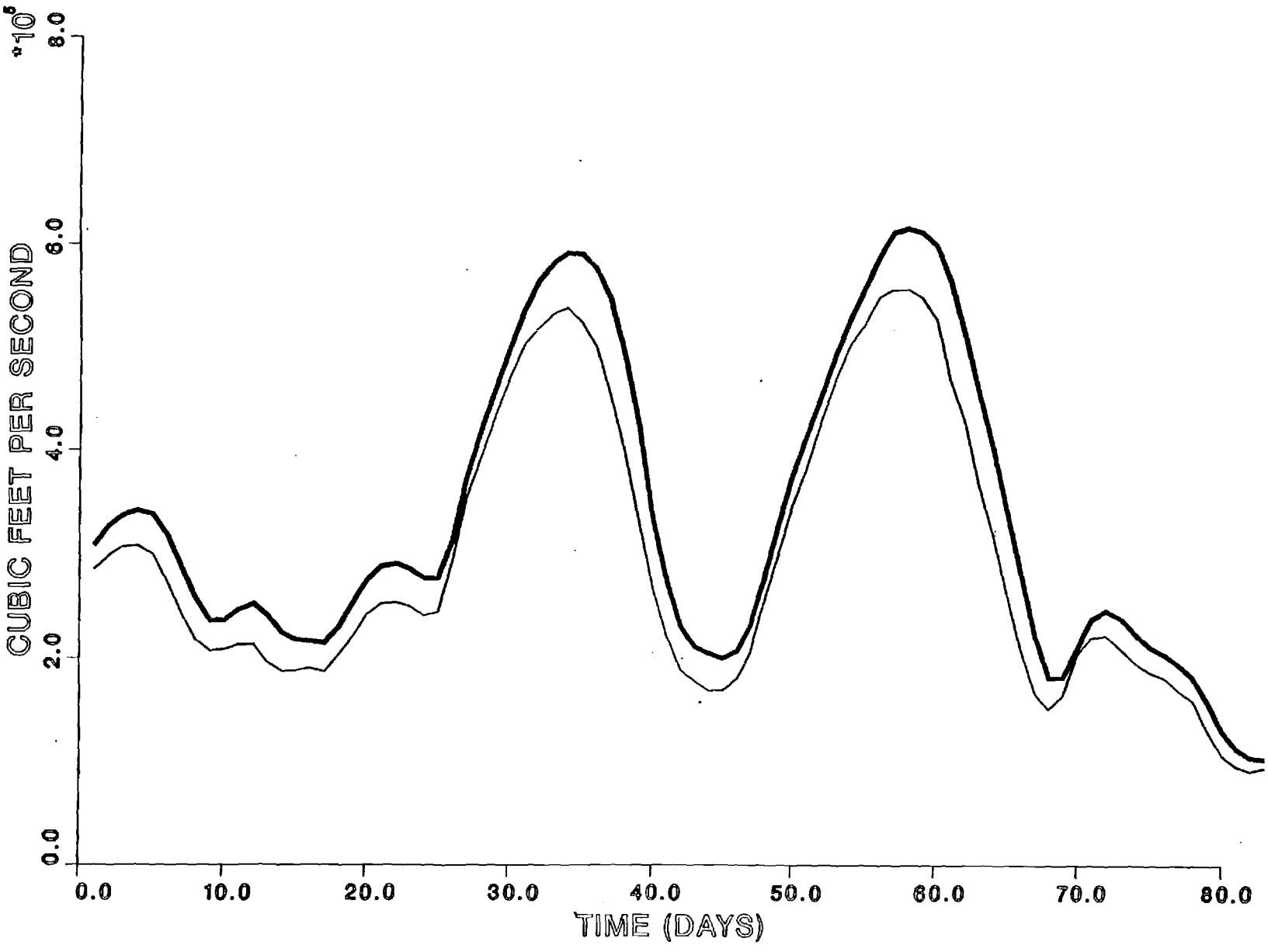

FIGURE 11: SSRR-II, θ=1

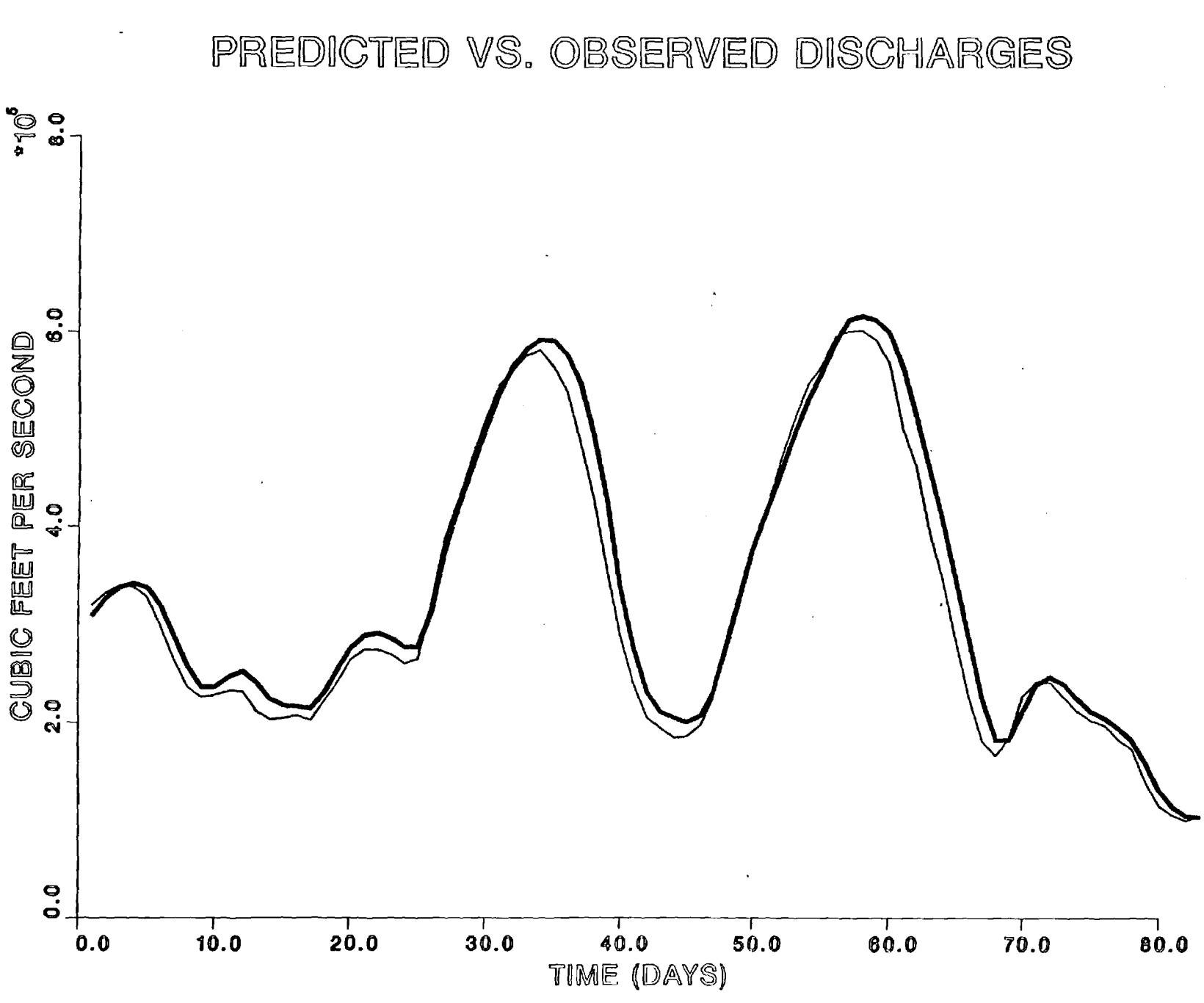

FIGURE 12: SSRR-II, 0=5

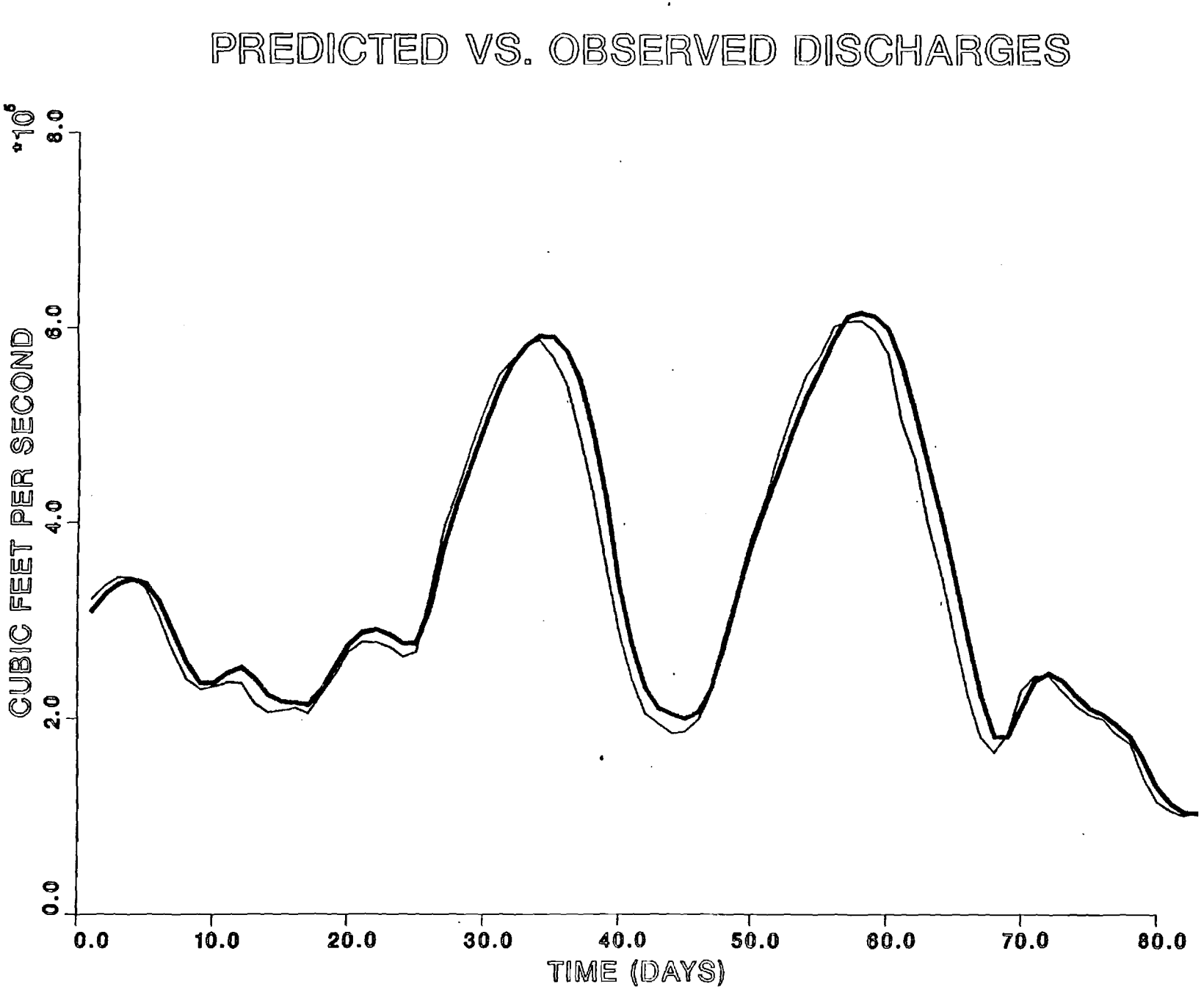

FIGURE 13: SSRR-II, θ=10

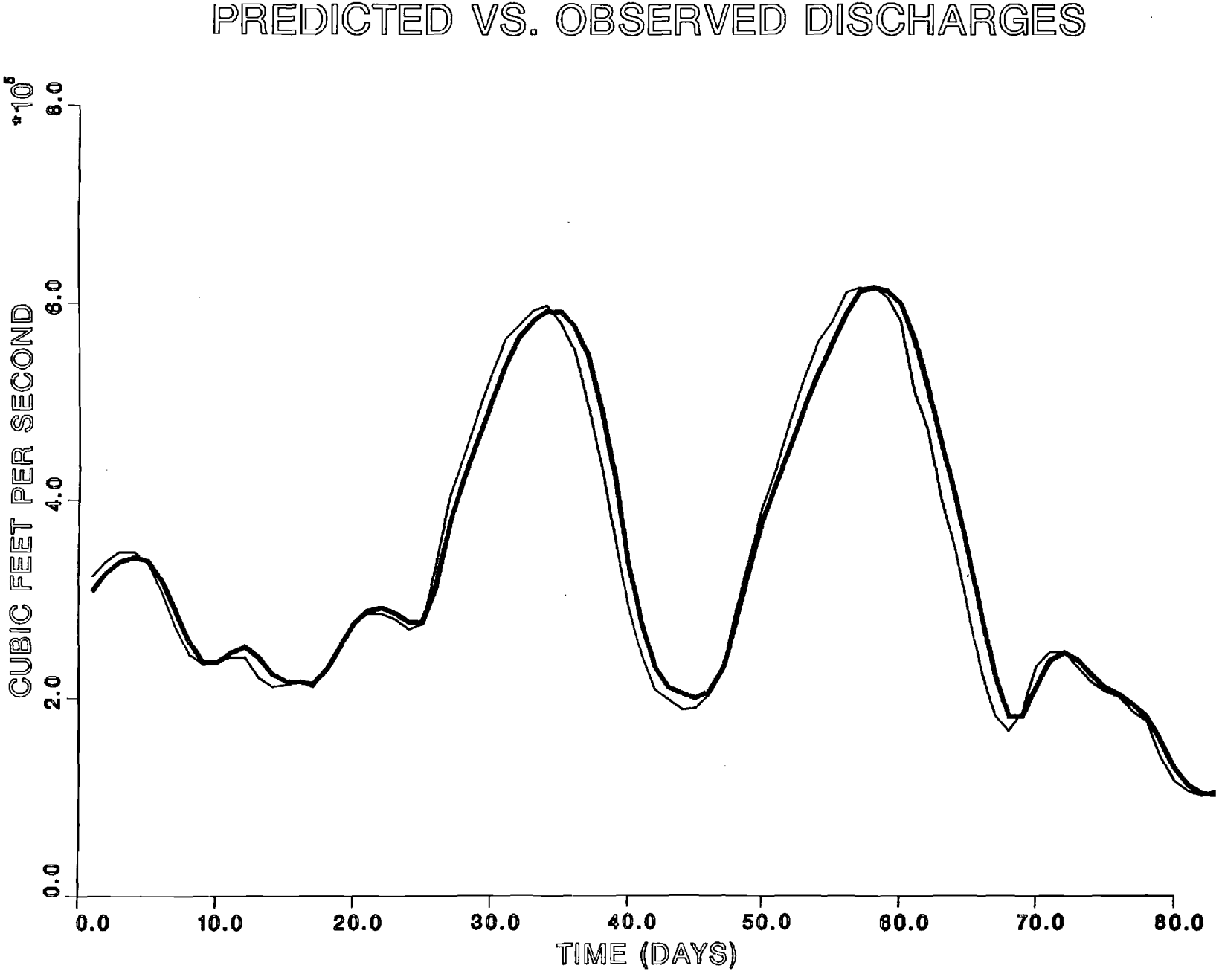

FIGURE 14: SSRR-II, θ=50

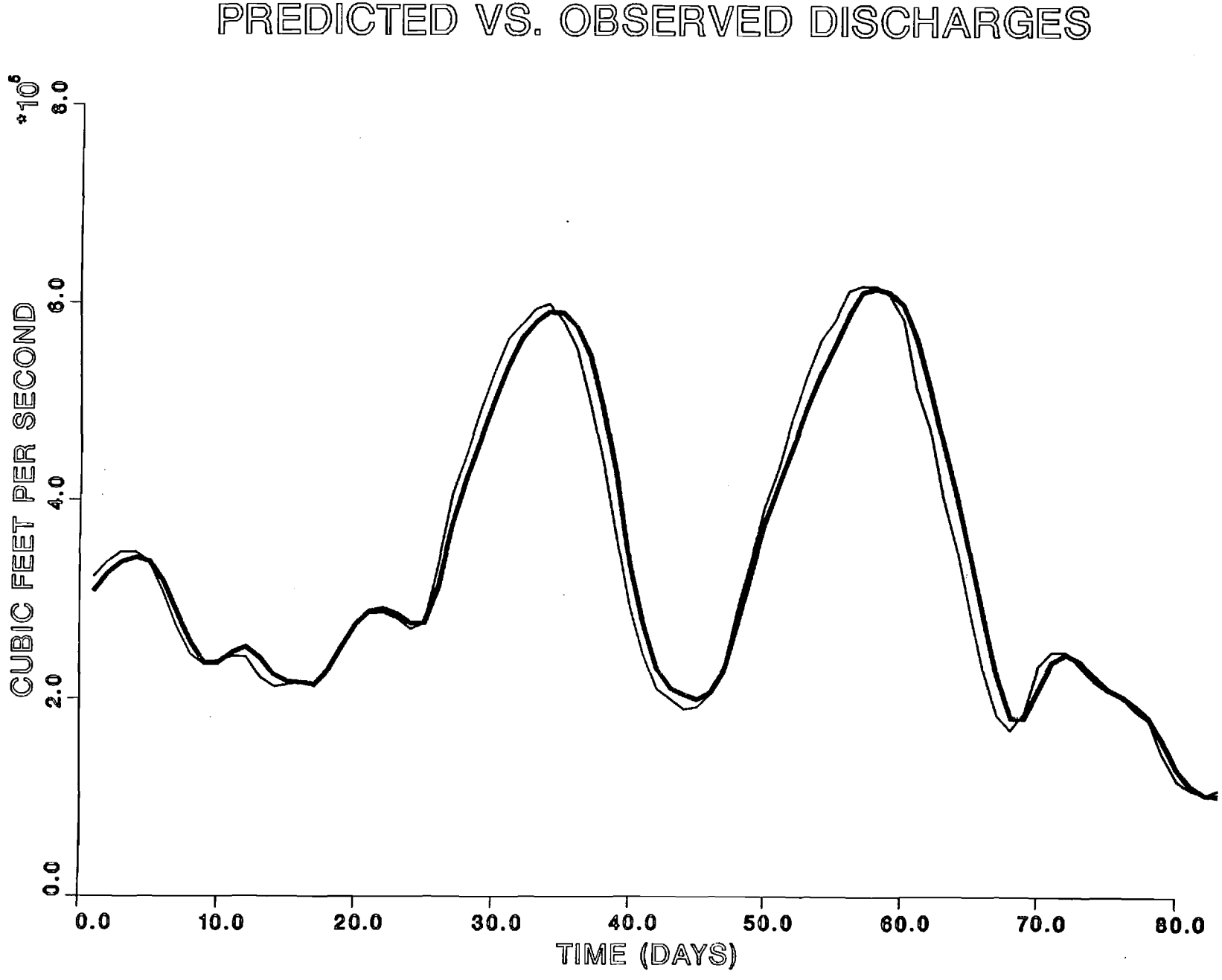

FIGURE 15: SSRR-II, θ=100

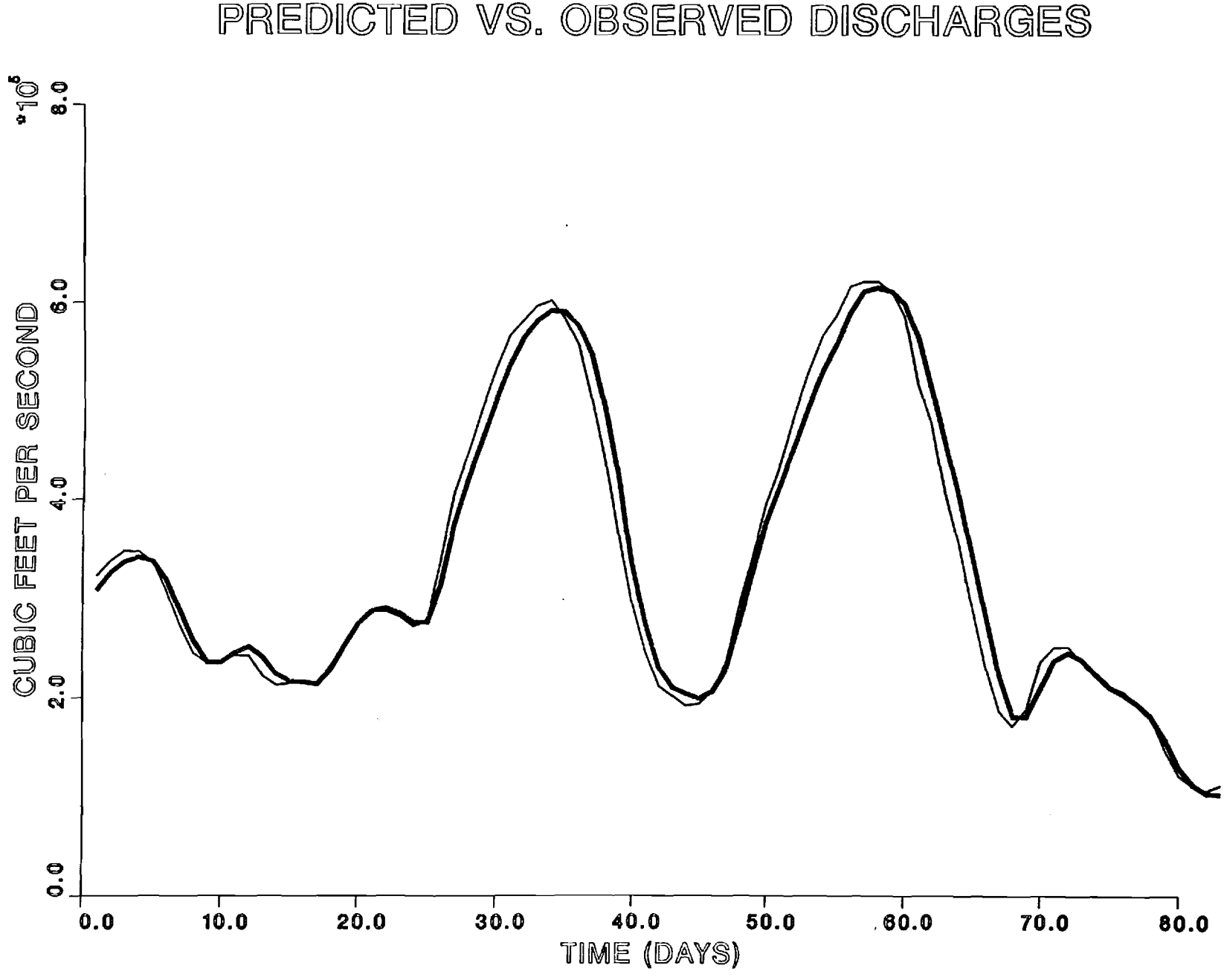

FIGURE 16: SSRR-II, θ=500

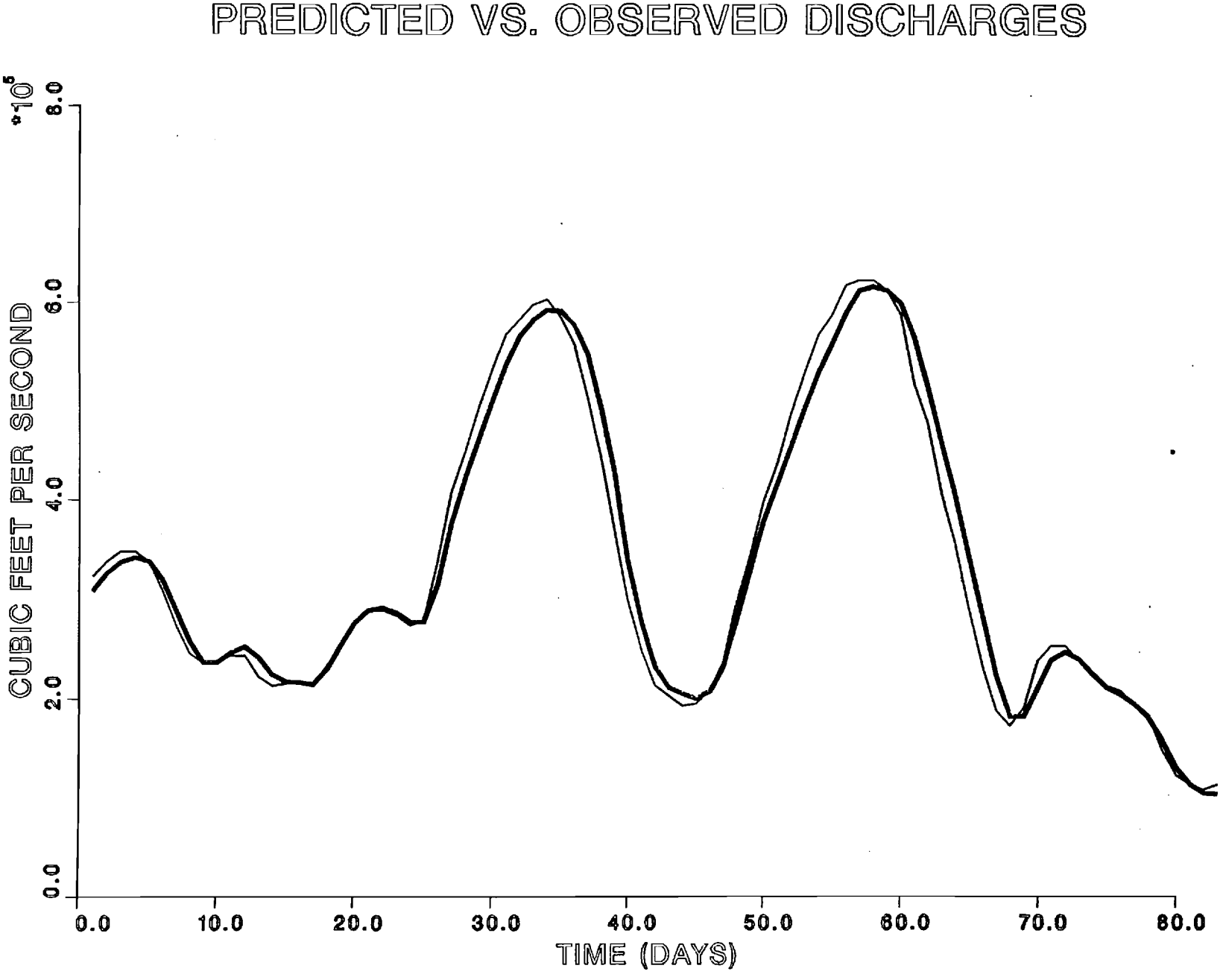

FIGURE 17: SSRR-II, θ=1000

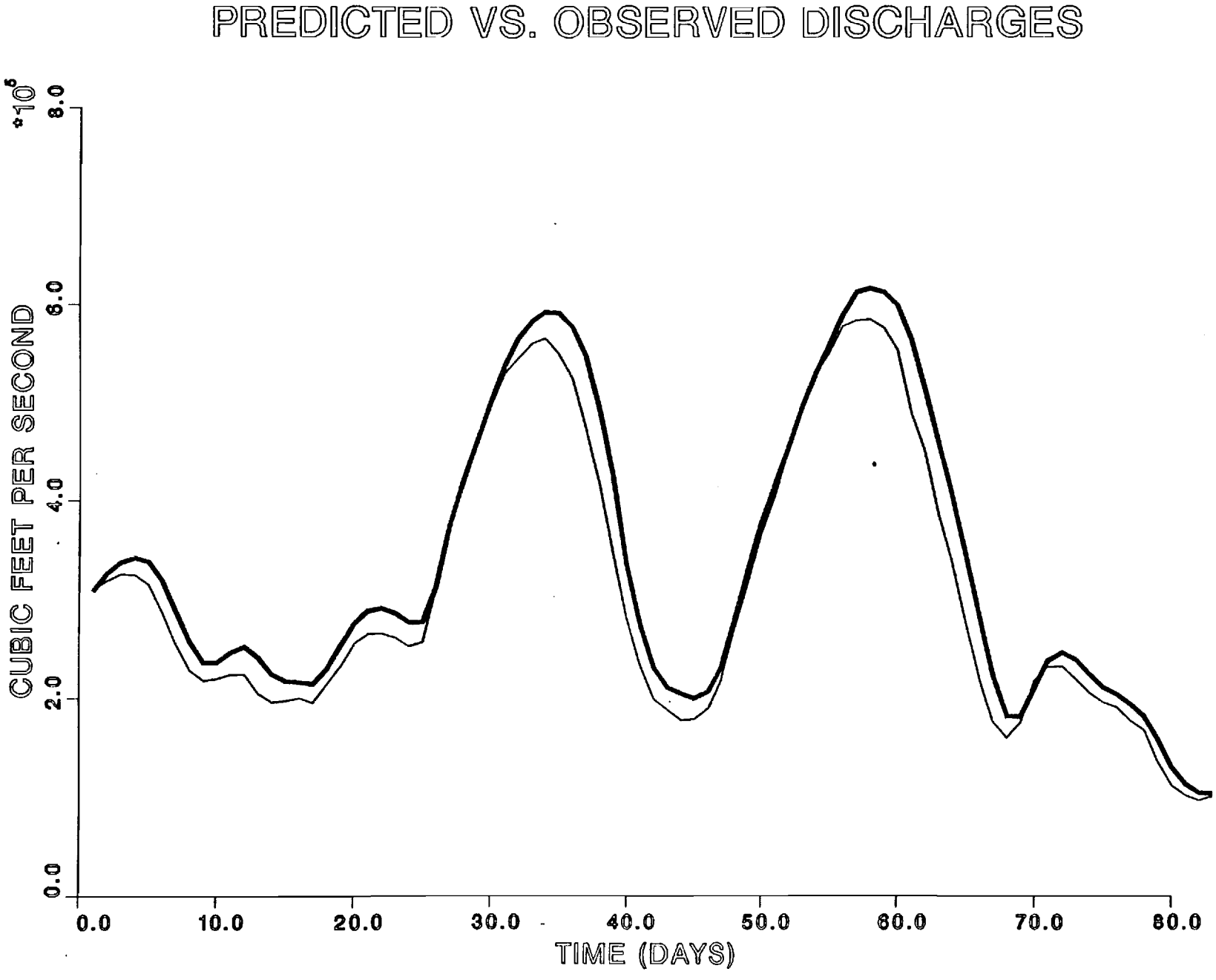

FIGURE 18: SSRR-II, θ=2

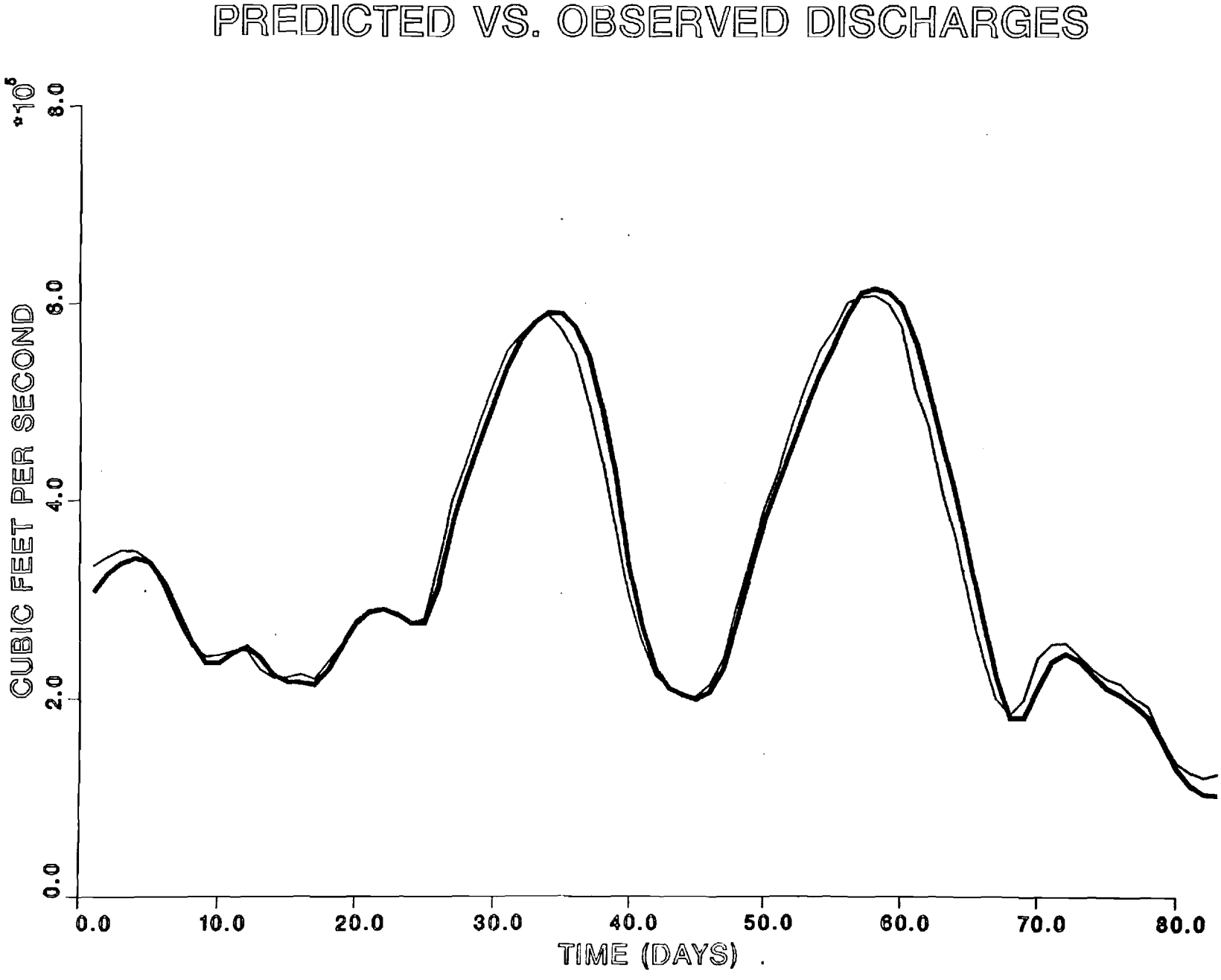

FIGURE 19: SSRR-II, 0=2, BIAS-CORRECTED

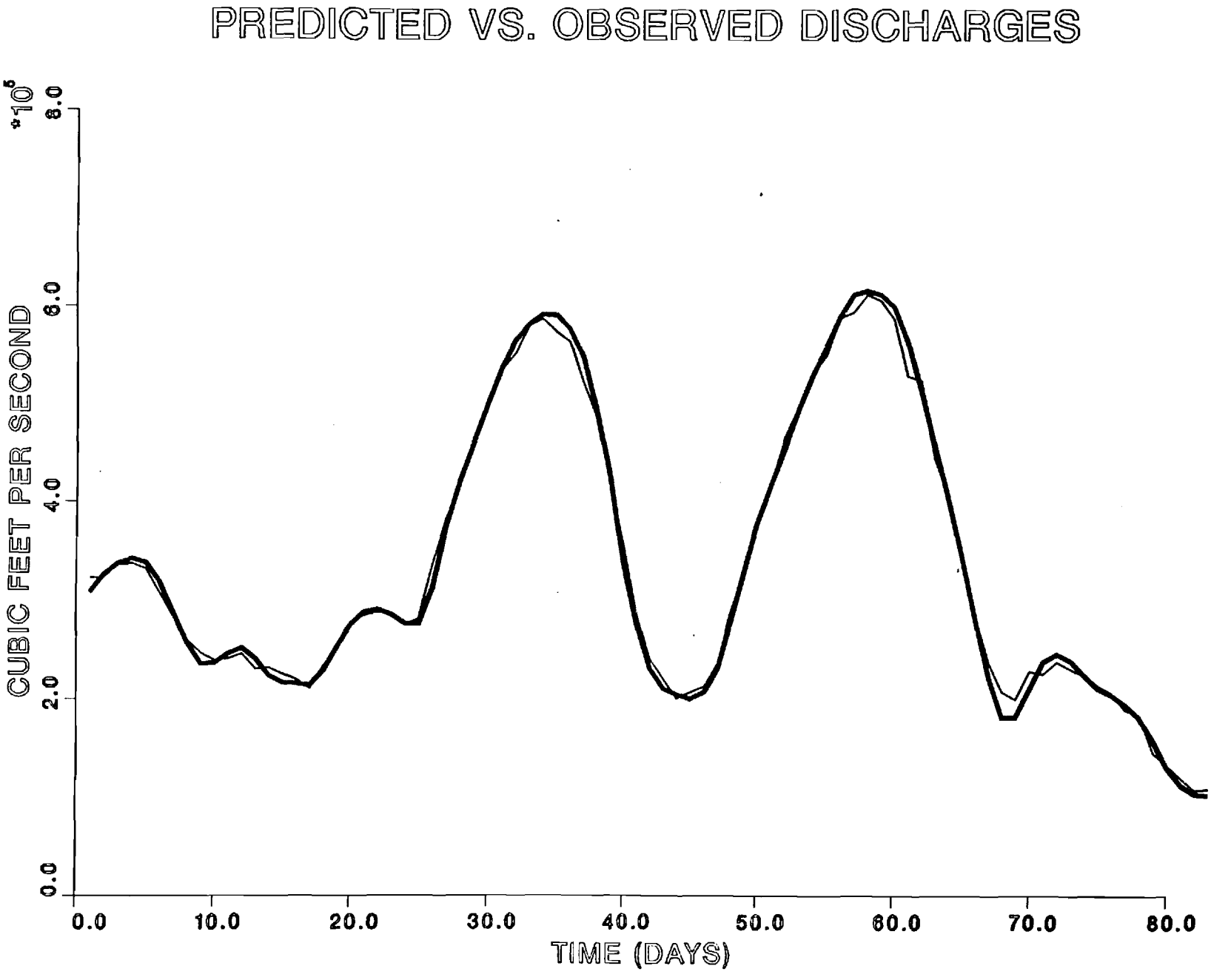

FIGURE 20: SSRR-II, 0=2, STATE FEEDBACK

"Optimal Real-Time Forecasting and Control of Reservoir Hydrosystems Using Remote and On-Site Sensors"

Supported by
the U.S. Geological Survey, Department of the Interior
under award number 14 - 08 - 0001 - G1297

Water Resources Research
Act of 1984

Project Starting Date : September 1, 1986
Project Termination date: August 31, 1988

Progress Report for the period
March 1, 1987, through May 31, 1987

by

Aris P. Georgakakos, Ph. D.
Professor of Hydrology and Water Resources
School of Civil Engineering
Georgia Institute of Technology
Atlanta, Georgia 30332
Tel.: (404) 894-2240 or -2201

June 13, 1987

The contents of this report were developed under a grant from the Department of the Interior, U. S. Geological Survey. However, those contents do not necessarily represent the policy of that agency, and you should not assume endorsement by the Federal Government.

This progress report is a summary of the research tasks completed over the third quarter of the project's tenure: These tasks are as follows:

A. Review of Forecasting models for Municipal and Agricultural water and Power demand.

B. Development of a computationally efficient Maximum Likelihood method for the estimation of parameters of state space models.

C. Reservoir system data gathering and preparation.

The discussion of these tasks is relegated respectively in three appendices (A, B, and C).

APPENDIX A

FORECASTING MODELS: MUNICIPAL WATER DEMAND, AGRICULTURAL WATER DEMAND, AND POWER DEMAND.

TABLE OF CONTENTS

INTRODUCTION

This appendix provides a critical review of several research papers dealing with real time forecasting of water and power demand. The first of its three sections deals with the forecasting of municipal water demand. Three most relevant papers are presented, and an extensive reference list is included, indicating that several models have been developed in this area. The second section deals with the forecasting of agricultural water demand. This aspect of water demand modeling is much more complicated due to the large number of controlling variables. Three papers are discussed, and the conclusion is drawn that forecasting of agricultural water demand has had limited success. The associated referenced literature indicates that more research needs to be performed in this area. The third section deals with the forecasting of power demand. This section includes a critical review of three models which have been shown to perform well. The reference list shows that many effective models are available in this area.

In each of these sections, the techniques used are explained, the associated variables are indicated, the types of application are reported, and the performance of each model is evaluated.

The papers within each section are presented chronologically with the oldest one first. At the conclusion of each section the models are compared and ranked in order of increasing sophistication. The reference list includes all the papers reviewed relevant to the forecasting of water and power demand.

1: Municipal Water Demand Models

1.1 Alternative Models for Estimating the Time Series Components of Water Consumption Data

Authors: Hiroshi Yamuchi
Wen-yuan Huang

Source: Water Resources Bulletin, Vol. 13, No. 3, pages 599-610, June 1977.

This study was conducted in Honolulu Hawaii, with additive and multiplicative models used to analyze trend, cyclical, seasonal, and irregular components. The stepwise regression technique was applied to 187 data points representing daily water consumption within the service area of the Honolulu Board of water supply.

The authors begin with a basic model:

$$Q_t^m = f(T,S,C,I)$$

where:

Q_t^m = Average daily water consumption, month, time t

T = Trend component

C = Cyclical component

S = Seasonal component

I = Irregularities

They then propose that this equation can be either additive, or multiplacative:

$$Q_t^m = T_t + C_t + S_t + I_t$$

$$Q = (T_t)(C_t)(S_t)(I_t)$$

and chose to examine a straight additive model and an exponentially multiplicative one:

$$Q = a_o + \sum_{i=1}^{4} a_i t^i + \sum_{m=1}^{11} B_m X_m + U_t^m$$

$$Q_t^m = \exp(a_o + \sum_{i=1}^{4} a_i t^i + \sum_{m=1}^{11} B_m X_m + U_t^m)$$

where:

Q_t^m = Average daily water consumption

m = Month (Jan=0, Feb=1,...Dec=11)

t = Time interval, Dec 1959 as base 1-12=Jan-Dec 1960,
13-24=Jan-Dec 1961, 180-187=Jan-July 1975

$a + \sum_{i=1}^{4} a_0^i t^i$ = Polynomial representing combined trend and cyclical components

a = Regression coefficients

t = Time interval (months)

$\sum_{m=1}^{11} B_m X_m^m$ = Expression of dummy variables representing seasonal components

B = Regression components

X = 1,0 Dummy variables for month of year with Jan. as base month

U_t^m = Error term representing irregular component

The authors state that the use of dummy variables allow them to study water consumption behavior for any month of the year.

Comparing these two models, the authors found that in the additive model the irregularities tend to increase with time, while in the multiplicative model the irregularities show the opposite trend.

1.1.1 Variables Used

These models do not use any specific climatological variables, but instead rely on seasonal changes on a month to month basis. Due to the consistent nature of the climate in Hawaii, this approach may prove inadequate in places with wide climatic variability.

1.1.2 Types of Application

These models utilize daily water usage data to predict monthly water demand. The authors state that their formulation could be adapted to quarterly forecasts of water demand, but make no mention of daily water demand forecasting.

where:

Q_t^m = Average daily water consumption

m = Month (Jan=0, Feb=1,...Dec=11)

t = Time interval, Dec 1959 as base 1-12=Jan-Dec 1960, 13-24=Jan-Dec 1961, 180-187=Jan-July 1975

$a_o + \sum_{i=1}^{4} a_i t^i$ = Polynomial representing combined trend and cyclical components

a = Regression coefficients

t = Time interval (months)

$\sum_{m=1}^{11} B_m X_m$ = Expression of dummy variables representing seasonal components

B = Regression components

X = 1,0 Dummy variables for month of year with Jan. as base month

U_t^m = Error term representing irregular component

The authors state that the use of dummy variables allow them to study water consumption behavior for any month of the year.

Comparing these two models, the authors found that in the additive model the irregularities tend to increase with time, while in the multiplicative model the irregularities show the opposite trend.

1.1.1 Variables Used

These models do not use any specific climatological variables, but instead rely on seasonal changes on a month to month basis. Due to the consistent nature of the climate in Hawaii, this approach may prove inadequate in places with wide climatic variability.

1.1.2 Types of Application

These models utilize daily water usage data to predict monthly water demand. The authors state that their formulation could be adapted to quarterly forecasts of water demand, but make no mention of daily water demand forecasting.

1.1.3 Performance

Both the multiplicative and additive models seem to effectively predict water demand, with the multiplicative model being slightly better. However, due to their statistical nature, both models produced insufficient estimates of extreme demand values.

1.2 A Monthly Time Series Model of Municipal Water Demand

Authors: Roger D. Hansen
Rangesan Narayanan

Source: Water Resources Bulletin, Vol. 17, No. 4, pages 578-585, August, 1981.

The authors have developed a multivariate time series model which includes price of water, average temperature, total precipitation, and percentage of daylight hours. They have applied their model to Salt Lake City, and have met with favorable results.

The basic equation set up is of the form:

$$Q_t = B_0 + B_1 x_{1t} + B_2 x_{2t} + \ldots U_t$$

where:

Q_t = Average monthly demand (per capita)

x_t = Explanatory variable

B = Regression coefficients

U_t = Error term

In this model water use is expressed as a linear combination of explanatory variables plus an error term. The authors point out that in their study area they needed to separate winter and summer seasons because winter precipitation (snow accumulation) would not affect water use. If this model was used in the Southeast, these seasonal differences would not be as pronounced.

The authors point out that ordinary least squares (OLS) estimates of the regression coefficients present some difficulties. They maintain that this is due to the fact that the error terms might be correlated in some way, and the OLS estimates would not be efficient. They deal with this problem by taking the equation:

$$Q_t = B_o + Bx_t + e_t$$

lagging it by one period and multiplying by ρ. After the new equation is subtracted from the original they obtain:

$$Q_t - \rho Q_{t-1} = B_o(1-\rho) + B(x_t - \rho x_{t-1}) + U_t$$

Since U_t is serially independent, the parameters can be estimated using an OLS procedure.

1.2.1 Variables Used

This model makes use of price, average temperature, total precipitation, and percentage of daylight hours.

1.2.2 Types of Application

This model, too, is designed for monthly water use studies. However, if data was available on a day-to-day basis, it could be used for daily predictions. This model was divided into two sections, winter and summer, with climatological factors replaced by dummy variables during the winter season. In an area like the State of Georgia this division would not be necessary, since snowfall is extremely limited.

1.2.3 Performance

This model was applied to Salt Lake City, Utah, and was used to make an ex post forecast for the years 1975 through 1977. The results were good, although this model had difficulty in predicting water use during a drought period which occurred during the summer of 1977. The authors admit that the model totally failed in 1977, but blame this failure on this drought. The authors mention that, since price is included in their formulation, water use under different pricing schemes can be found by adjusting the price inputs. The authors also point out that their model would have been better had they been able to obtain data on personal income, persons per household, and population density.

1.3 Cascade Model of Monthly Municipal Water Use

Authors: David R. Maidment
Emanuel Parzen

Source: Water Resources Research, Vol. 20, No. 1, pages 15-23, January 1984.

This model, as the title implies, utilizes a series of steps to eliminate components of municipal water demand to eventually end up with just the random component of the time series. These components are removed as follows:

Original Series

↓

Detrending

↓

Deseasonalizing

↓

Autoregression

↓

Climatic Regression

↓

Random Error Series

The process for the removal of each of these components is discussed in the following sections.

(i) Trend: The authors state several ways of removing trend in water use. These include taking logarithms or a power transformation, by dividing water use by population or number of water connections, by fitting a polynomial or power function of time to the data, or by regressing mean annual water use against trend causing variables. The authors have chosen to use the regression technique in their analysis. The trend causing variables chosen are real average effective buying income per household, real marginal water price, number of water connections, and population.

(ii) Deseasonalizing: The authors mention several alternatives for removing seasonality from the series, but have chosen to subtract the Fourier-fitted monthly means.

(iii) Autoregression: The authors state that this portion of the series is a short-memory process, and can be removed by fitting the autoregressive model:

$$W_c(t) = \sum_{j=1}^{P} d_j W_c(t-j) + W_d(t)$$

where the coefficients are found by using the Yule-Walker equations. They state the optimal order of the auto-regressive model can be found by using either Parzen's criterion autoregressive transfer, or the Akaike test.

(iv) Climatic Correlation: The authors fit a multiple time series model using the climatic variables of rainfall, evaporation, and air temperature. The optimal order of the time series is determined by a multivariate form of the CAT criterion.

1.3.1 Variables Used

The information needed to run this model includes monthly values for water use, and the total volume of water supplied to the city's water treatment plants from all sources. The annual values of the socioeconomic variables are also needed, including average effective buying income, water price, population, and the number of water connections. The climatic variables needed include precipitation, maximum air temperature, and pan evaporation.

1.3.2 Types of Application

This model is designed for use in predicting monthly water demand, but it would seem that if the data were available on a daily basis, this model could be adapted for real time forecasting. This model is designed for use in municipal areas, and it use in a rural setting is questionable.

1.3.3 Performance

The authors applied their model to six cities in Texas, and found that they were able to account for about 80-87% of the variability in the water demand. This means that 13-20% of the demand is assumed to be random. They do point out, however, that better results have been found when working with larger cities. They state that perhaps the water demand in larger cities is

inherently more stable.

1.4 Summary of Municipal Water Demand Models

The following is a classification of the previous models in order of increasing sophistication:

1. Additive/Multiplicative Model
2. Monthly Time Series Model
3. Cascade Model

The best of these models is by far the cascade model presented by Maidment and Parzen. Their model takes into consideration the important variables, including buying income, population, temperature, precipitation, and evaporation. Although developed and tested on cities in Texas, this model could easily be used in the Southeast region for predicting water demand.

2. AGRICULTURAL WATER DEMAND MODELS

2.1 Modeling Supplemental Irrigation Water Demand

Author: J. David Dean

Source: ASCE Journal of Irrigation and Drainage Division, Vol. 106, No. IR4, pages 285-297, December 1980.

This paper makes use of several subroutines in the Environmental Protection Agency's Agricultural Runoff Model (ARM). The ARM Model is a computer tool for the evaluation of runoff, snow accumulation and melt, sediment loss, pesticide loss, and nutrient content of runoff from agricultural watersheds. The author used the hydrology subroutine (LANDS) in his study. LANDS accounts for water in the interception storage, upper and lower zone storages, and groundwater by budgeting precipitation and evapo-transpiration input/output and making use of a deep percolation component. Overland flow, infiltration and interflow are simulated during events. The effects of tillage and cultivation practices as well as vegetation are taken into account.

The basic equation is

$$SMP = a\theta^b$$

where:

SMP = The matrix potential

θ = Percent (by volume) water in each zone

a,b = Empirical Coefficients for various soil types

The model calculates the soil matrix potential, and compares this value against an upper threshold. When this value goes above the threshold an irrigation is triggered. Water requirements for each zone are calculated, and the sum of the zonal requirements and a factor for the interception of the crop canopy gives the irrigation requirement for that time.

2.1.1 Variables Used

This model appears to use only the soil properties and crop types to determine irrigation needs. The author states that this paper does not include any stochastic elements, so the stochasticity of the rainfall events is not considered.

2.1.2 Types of Application

This model may be applied to a variety of areas with different soil types. However, the exclusion of the rainfall and evapotranspiration characteristics may be the cause of substantial errors.

2.1.3 Performance

The author performed a test of this model on a watershed in Watkinsville, Georgia from 1973 to 1975. The author states that his results were reasonable. This test used two different levels of irrigation.

2.2 Modeling Water Demands of Irrigation Projects

Authors: David M. Maidment
Paul D. Hutchinson

Source: ASCE Journal of Irrigation and Drainage Division, Vol. 109, No. 4, pages 405-417, December 1983.

This study was made for an agricultural area in New Zealand, an area which relies on both surface water and groundwater for irrigation. The total area under consideration is approximately 1,040 square miles, of which 111,200 acres, composed of many small farms, is irrigated. The methodology used is to consider water demand as a function of five factors; irrigable area, soil type, cropping pattern, irrigation strategy, and weather variation. The authors divide the area into subregions which have the same soil type, cropping pattern, irrigation strategy, and climate. Since In each of these subregions several of these factors are fixed, the equation to predict overall water demand is given by:

$$W(t) = C \sum_{n=1}^{N} \frac{A_n}{n_n} I_n(t)$$

where:

A_n = Irrigated area in sq. kilometers

n_n = Irrigation efficiency

C = A dimensionless scaling factor (based on historical data)

$I_n(t)$ = Irrigation applied to a given crop on a given soil under a given irrigation strategy and weather pattern

Assessment of water demand from each of these regions is then simulated by using the soil moisture balance equation:

$$S(t) = S(t-1) - E(t) + R(t) - D(t) + I(t)$$

where:

S(t),S(t-1) = Average soil moisture levels

E(t) = Evapotranspiration

R(t) = Rainfall

D(t) = Drainage

I(t) = Irrigation

The estimated values for I(t) can be either an amount just enough to return the soil to field capacity, or can be a fixed amount set by the system design. The timing can either be a fixed interval or on demand (water continuously available). For both timing schemes, irrigation takes place when the soil moisture content falls below a certain "trigger level," or minimum soil moisture content. This trigger level can vary with time (water is more critical at certain times in the growing season), and can vary according to crop type.

The water demand for the region is then found by combining the water demand for the subregions, accounting for distribution in time for the various sub-areas.

2.2.1 Variables Used

This model uses soil type, cropping pattern, pan evaporation, rainfall, and drainage characteristics for each subregion. Also, historical data is needed to determine the appropriate scaling factor to be used in the above equation.

2.2.2 Types of Application

This model appears flexible enough for application in various regions as long as the soil and crop types are known and the various subregions can be defined. It does, however, require a great deal of data on agricultural land uses for its calibration.

2.2.3 Performance

This model appears to do quite well in several areas. The first test the authors performed was to compare predicted soil moisture levels with actual field values. They found that the simulation gave a series of moisture levels prior to irrigation having a mean statistically indistinguishable from the 27 measured values (at the 95% confidence level).

The authors then simulated water sales for the period 1967-1978. The results from this comparison were also found to be quite good. The simulate data tracked the actual data very well, with the exception being a difference of three to five days lag in the actual data after a rainfall event. The authors contribute this lag to the farmer's continuing to water for a short time after a rainfall event. A scaling factor of 0.72 was calculated, meaning that for a given fixed amount of irrigation and a fixed cycle time, 72% of the irrigable land was actually irrigated.

This model was also applied to a prospective irrigation scheme for seven different crops under two irrigation strategies and for two soil types; a total of 28 different combinations. This portion of the study was done to determine peak demand times for water, and these peaks were found to occur in early December and in February. The results of this test were used to determine effects on surface and groundwater under these different irrigation schemes.

2.3 Summary of Agricultural Water Demand Models

Of the previous models, the second appears to be the best. That model looks at evaporation, precipitation, crop type, and irrigation plan, and develops good forecast values for water demand. It also appears that it can be used on a real time basis.

In examining the references cited, it appears that there has not been nearly as much work done in the area of irrigation water demand; as a result, there are fewer models from which to choose.

3. POWER DEMAND MODELS

3.1 Short Term Load Forecasting Using Multiple Correlation Models

Authors: K. Srinivasan
R. Pronovost

Source: IEEE Transactions on Power Apparatus and Systems, vol. PAS-94, No. 5, September/October 1975, pp. 1854-1857.

This paper deals with hourly forecasting for the Hydro-Quebec system, and considers historical data only. The authors mention that the next step in their research would be to add weather related variables.

The model presented here is based on the observation that a substantial correlation exists in the energy consumption pattern at certain intervals, namely a day, a week, and a year, in addition to a correlation between two successive hours. The authors propose a linear first order model for each of these intervals. The forecast values and variances for each of the four intervals are optimally combined.

The authors begin with the equation

$$X(k) = A(k-1)X(k-1) + B(k-1) + W(k-1)$$

where:

X(k) = The load at the Kth time period

A(k),B(k) = Non-zero parameters dependent on k

Q(k) = Gaussian random noise.

The parameters A(k), B(k), and Q(k) are then optimally estimated using historical observations of X(k) and X(k-1).

After the model is identified, the authors perform a forecasting case study for historical data from 1969 to 1971. The forecasts were performed as follows: Every Thursday, a forecast was issued for the next 10 days. This forecast assumes no knowledge of the actual loads past Wednesday. At the end of that week the forecasted values are compared to the actual loads.

3.1.1 Variables Used

This model uses only historical data, and has no inputs for weather related variables. The authors state that adding weather related variables would be their next area of research.

3.1.2 Types of Applications

This model was developed for use in Quebec, but it shows that statistically based model seem to be adequate in the prediction of power demand.

3.1.3 Performance

Even with a relatively simple first order linear model, and without any effects of temperature taken into account, this model produced very good results. The authors did not provide any information on confidence bands for their predictions, but the plots of forecast versus actual loads are in very good agreement.

3.2 Weather Sensitive Electric Demand and Energy Analysis on a Large Geographically Diverse Power System-Application to Short Term Hourly Electric Demand Forecasting

Author: Ronald P. Thompson

Source: IEEE Transactions on Power Apparatus and Systems, Vol. PAS-95, No. 1, January/February 1976, pages 285-391.

This paper looks at weather sensitive electric loads and suggests a forecast methodology for short term applications. The author claims that on-line experience has produced results with a forecasting error of approximately 2.0% during the highly weather sensitive summer load period. This model was developed for The Pacific Gas and Electric Company in California.

The development of this model involved the following steps:

I. Identification and collection of variables to be tested for correlation with area load.

II. Development of forecasting methodology based on historical data

A. Peak load forecasting

B. Hourly load forecasting

III. Simulation evaluation of forecasting models

IV. Real-time application and evaluation of forecasting models

This model divides the study area into sub-areas with similar weather and load characteristics. The study then divided the system load into three components:

A. Base Load

B. Weather Sensitive Load

C. Random Load

The base load was computed as the average load which would occur under the given weather characteristics (based on historical data). The variables considered for the weather sensitive load were maximum and minimum temperature, exponential maximum temperature, maximum and minimum humidity, enthalpy, exponential enthalpy, precipitation, sky cover, average wind, and average cooling power. After trying several models with different combinations of these weather variables, the author found that maximum temperature values gave the best results. The random load was considered to be fluctuations within each sub-area, or other non-weather or time associated loads

(up to 300 mw for the PG&E study area).

The author then developed a series of models based on different amounts of historical weather and load data. The models were developed using a stepwise regression analysis. The load data was normalized, and then a stepwise regression algorithm was used to correlate the normalized loads with the corresponding weather data. The resulting regression equation represents the weather sensitive component of the total system load. The system load forecast was then found by adding the weather sensitive component, the mean load, and the random loads.

Having determined the forecasted peak load and daily energy, hourly loads were then derived by modeling the historical relationship of daily and hourly load levels. This model only forecasted the hourly loads when the forecast average load (daily load/24) exceeded the previous weekday load by 100 mw.

3.2.1 Variables Used

Of the many weather variables considered, the author found that maximum temperature provided the best results. In addition to these values, this model used historical load data, including peak load data and average load data.

3.2.2 Types of Application

This model provided excellent results. When run for the summers of 1973 and 1974, the forecast values were with 2% of the actual load.

3.3 Forecasting of Hourly Load by Pattern Recognition - A Deterministic Approach

Authors: Abdolhosein S. Dehdashti
James A. Tudoor
Michael C. Smith

Source: IEEE Transactions on Power Apparatus and Systems, Vol. PAS-101, No. 9, September 1982.

This paper presents a model which is designed to forecast power demand for small geographical areas, and takes into account both climatic variables and recent load information. The authors break each 24 hour period into eight three hour periods. This is due in part to the fact that the National Oceanic and Atmospheric Administration publishes data on three hour intervals. The authors assume that insignificant changes in weather conditions take place during those three hour periods.

The authors selected sixteen weather variables, noting that depending on the circumstances different variables can be excluded. These variables are maximum, minimum and average temperature for that day and for the previous day, average dewpoint for that day and for the previous day, minutes of sunshine for that day and for the previous day, average windspeed for the day, and instantaneous air temperature, wet bulb temperature, dewpoint, humidity, and windspeed.

The authors then used various means to find the most efficient independent variables that explain similar load patterns on an electrical power system. Two types of studies were performed on weather variables:

1. All combination Regression
2. Stepwise Linear Regression Analysis

The authors did a standardizing type of operation on the historical data to eliminate the growth trend. They also performed cluster analysis, to separate historical data into classes with similar characteristics. Any variations within classes was assumed to represent the unknown nature of the load.

3.3.1 Variables Used

There is a possibility of sixteen weather related variables which can be used in this model. These variables are listed above. In addition, a historical base of load data is required.

3.3.2 Types of Applications

This model has enough variables that it could be used for any climate. The authors point out, however, that this model is designed for use in geoegraphically small areas with uniform weather patterns with well defined seasons.

3.3.3 Performance

This model was applied to the city of Columbia, Missouri, a college town with a peak summer demand in 1980 of 123 MW. The summer of 1980 was apparently a very hot summer, so the authors feel that this was a good test.

The results they obtained for the forecast values versus the actual values had a maximum error of 4%, with an average error of 2%. Even when the load was forecasted for the one the hottest days of the summer the results were good.

The authors contend that since the days are broken into 3 hour intervals, the forecasts can react quickly to sudden changes in the weather, or can be updated when sudden changes in the load occur.

SUMMARY OF POWER DEMAND MODELS

Unlike the limited number of models available for irrigation modelling, there appears to be no lack of good models for forecasting power demand. A ranking of increasing sophistication of the previously discussed model follows:

1. Multiple Correlation Model (Linear Model)
2. California Model
3. Deterministic Model

It should be noted that even the simplest of these models, the linear model by Srinivasan and Pronovost (which does not include weather variables), gives very good results. Based on this experience it appears that power demand may be forecasted effectively on a real-time basis.

CONCLUSIONS

Based on the previous discussion and the study of the papers cited, it is evident that there exists considerable research experience with municipal water and power demand modeling. The power demand models are capable of better predictions, but the municipal water demand models appear adequate.

The area of agricultural demand, however, appears to lack effective models. Forecasting agricultural water demand involves the use of weather related variables, differences in soil types, differences in cropping patterns, and differences in irrigation techniques and schemes. The plethora of controlling variables makes agricultural water demand forecasting an involved task.

REFERENCES

Agthe, D.E., and R.B. Billings, "Dynamic Models of Residential Water Demand," Water Resources Research, Vol. 16, No. 3, 1980, pp. 476-480.

Baier, W., and G.W. Robertson, "Estimating Supplemental Irrigation Water Requirements for Climatological Data," Canadian Agricultural Engineering, Jan. 1967.

Baier, W., and G.W. Robertson, "Climatic Estimates of Average and Probable Irrigation Requirements and of Seasonal Drainage in Canada," Journal of Hydrology, Vol. 10, 1970, pp 20-37.

Carver, P.H., and J.J. Boland, "Short and Long-Run Effects of Price on Municipal Water Use," Water Resources Research, Vol. 16, No. 4, 1980, pp. 609-618.

Christiaase, W.R., "Short Term Load Forecasting Using General Exponential Smoothing," IEEE Transactions on Power Apparatus and Systems, Vol. PAS-90, 1971, pp. 900-911.

Corpening, S.L., N.D. Reppen, and R.J. Ringlee, "Experience with Weather Sensitive Load Models for Short and Long-Term Forecasting," IEEE Transactions on Power Apparatus and Systems, Vol. PAS-92, No. 6, 1973.

Danielson, L.E., "An Analysis of Residential Demand for Water Using Micro Time Series Data," Water Resources Research, Vol. 14, No. 4, 1979, pp. 763-767.

Davey, J., J.J. Saaks, G.W. Cunningham, and K.W. Priest, "Practical Application of Weather Sensitive Load Forecasting to System Planning," IEEE Transactions on Power Apparatus and Systems, Vol. PAS-92, 1973, pp. 971-977.

David, W.P., and E.A. Hiler, "Predicting Irrigation Requirements of Crops," Journal of the Irrigation and Drainage Division, ASCE, Vol. 96, No. IR3, Proc. Paper 7507, Sept. 1970, pp. 241-255.

Dean, J.D., "Determination of Irrigation Water Demand in Humid Climates," thesis presented to the University of Georgia, at Athens, GA, in 1979, in partial fulfillment of the requirements for the degree of Master of Science.

Dean, J.D., "Modeling Supplemental Irrigation Water Demand," Journal of Irrigation and Drainage Division, ASCE, Vol. 106, No. IR4, 1980, pp. 285-297.

Domokos, M., J. Weber, and L. Duckstein, "Problems in Forecasting Water Requirements," Water Resources Bulletin, Vol. 12, No. 2, 1976, pp. 253-274.

Dryar, H.A., "The Effect of Weather on System Load," Transactions of American Institute of Engineering, Vol. 63, 1944, pp. 1006-1013.

Foster, H.S., and B.R. Beattie, "A Cross-Sectional Investigation of the Determinants of Urban Residential Water Demand in the United States, 1960 and 1970," Report TR-86, Texas Water Resources Institute, Texas A&M Univ., College Station, Texas, May 1978, 54 p.

Franklin, S.F., and D.R. Maidment, "Forecasting Municipal Water Use During a Drought: A Case Study of Deerfield Beach, Florida," Tech. Rep. CRWR-188, Center Res. Water Resour., Univ. of Texas, Austin, Texas, 1983, 103 p.

Galina, F.D., and F.C. Schwepp, "A Weather Dependent Probabilistic Model for Short Term Load Forecasting," IEEE Conference Paper No. C72/71-2 Winter Power Meeting, Feb. 1972.

Gottleib, M., "Urban Domestic Demand for Water: A Kansas Case Study," Land Economics,Vol. 39, No. 2, 1963, pp. 204-210.

Gupta, P.C., "A Stochastic Approach to Peak Power Demand Forecasting in Electric Utility Systems," IEEE Transactions on Power Apparatus and Systems, Vol. PAS-90, 1971, pp. 824-832.

Gupta, P.C., and K. Yameda, "Adaptive Short Term Load Forecasting of Hourly Load Using Weather Information," IEEE Transactions on Power Apparatus and Systems, Vol. PAS-91, 1972, pp. 2085-2094.

Hansen, R.D., and R. Narayanan, "A Monthly Time Series Model of Municipal Water Demand," Water Resources Research, Vol. 17, No. 4, 1981, pp. 578-585.

Heinemann, G.T., D.A. Norman, and E.C. Plant, "The Relationship Between Summer Weather and Summer Loads - A Regression Analysis," IEEE Transactions on Power Apparatus and Systems, Vol. PAS-85, No. 11, 1966, pp. 1144-1154.

Hershfield, D.M., "Effective Rainfall and Irrigation Water Requirements," Journal of Irrigation and Drainage Division, ASCE, Vol. 90, No. IR2, Proc. Paper 3920, June 1964, pp. 33-38.

Holmes, D.W., R.J. Dawson, H. Gunston, and C.H. Batchelor, "Water Management Study at Kaudulla Irrigation Scheme, Sri Lanka," Report OD 26, Hydraulics Research Station, Wallingford, England, July 1979.

Jensen, M.E., ed., "Consumptive Use of Water and Irrigation Water Requirements," Technical Committee on Irrigation Water Requirements," Irrigation and Drainage Division, ASCE, 1973.

Kibler, D.F., D.D. Fritton, E.L.White, R.J. Trotter, and D.F. Tandy, "Analysis of Water Requirements for Agricultural Irrigation in Pennsylvania," Research Publication No. 99, Institute for Research on Land and Water Resources, Pennsylvania State University, University Park, PA, Sept. 1977.

Liang, J.C., and M.G. Strintzis, "Power System Load Forecasting Based on Autoregressive Moving Average Models," IEEE Control of Power Systems Conference, Oklahoma City, Oklahoma, Feb. 1979.

Lijensen, D.P., and J. Rosing, "Adaptive Forecasting of Hourly Based on Load Measurements and Weather Information," IEEE Transactions on Power Apparatus and Systems, Vol. PAS-90, 1971, pp. 1751-1767.

Maidment, D.R., W.J. Lewthwaite, and S.G. Hamblett, "Rakaia Water Use and Irrigation Development," Water and Soil Estimation Miscellaneous Publication 19, Ministry of Works and Development, Wellington, New Zealand, 1980.

Maidment, D.R., and E. Parzen, "A Cascade Model of Monthly Municipal Water Use," Texas Engineering Experiment Station, College Station, Texas, 1981, 157 p.

Maidment, D.R., and E. Parzen, "Time Patterns of Water Use in Six Texas Cities," Journal of Water Resources Planning Management, Vol. 110, No. 1, 1983.

Matanga, G.B., and M.A. Marino, "Irrigation Planning, 1, Crop Pattern," Water Resources Research, Vol. 15, No. 3, 1979, pp. 672-678.

Mathewman, P.P., and N. Nicholson, "Techniques for Load Prediction in the Electricity-Supply Industry," Proceedings of IEE,Vol. 155, No. 10, 1968, pp. 1451-1457.

Morgan, W.D., "A Time Series Demand for Water Using Micro Data and Binary Variables," Water Resources Bulletin, Vol. 10, No. 4, 1974.

Morgan, W.D., and J.C. Smolen, "Climatic Indicators in the Estimation of Municipal Water Demand," Water Resources Bulletin, Vol. 12, No. 3, 1976, pp. 511-518.

Oh, H.S., and H. Yamauchi, "An Economic Analysis of the Patterns and Trends of Water Consumption with the Service Areas of the Honolulu Board of Water Supply," Report No. 84, Water Resources Research Center, University of Hawaii, Honolulu, Hawaii, 1974, 95 p.

Ritchie, J.T., "Evaluating Irrigation Needs for Southeastern U.S.A.," Contributions of Irrigation and Drainage to the World Food Supply, ASCE, 1975.

Robertson, G.W., and R.M. Holmes, "Estimating Irrigation Water Requirements for Meteorological Data," Publication No. 1054, Canada Department of Agriculture, May, 1959.

Salas-La Cruz, J.D., and V. Yevjevich, "Stochastic Structure of Water Use Time Series," Hydrology Paper No. 52, Colorado State University, Fort Collins, Colorado, 1972, 71 p.

Srinivasan, K., and R. Pronovost, "Short Term Load Forecasting Using Multiple Correlation Models," IEEE Transactions on Power apparatus and Systems, Vol. PAS-94, No. 5, 1975, pp. 1854-1858.

Stanton, K.N., "Medium Range, Weekly and Seasonal Peak Demand Forecasting by Probability Methods," IEEE Transactions on Power Apparatus and Systems, Vol. PAS-90, 1971, pp. 1183-1189.

Stewart, R.G., and I. Metzger, "Industrial Water Forecasts," Journal American Water Works Association, Vol. 63, 1971, pp. 155-157.

Thompson, R.P., "Weather Sensitive Demand and Energy Analysis on a Large Geographically Diverse Power System - Application to Short-term Hourly Electric Demand Forecasting," IEEE Transactions on Power Apparatus and Systems, Vol. PAS-95, No. 1, 1976, pp. 385-393.

Toyoda, J., M. Chen, and Y. Inoue, "An Application of State Estimation to Short Term Load Forecasting," IEEE Transactions on Power Apparatus and Systems, Vol. PAS-89, 1970, pp. 1678-1688.

Vemuri, S., W.L. Huang, and D.J. Nelson, "On-Line Algorithms for Forecasting Hourly Loads of an Electric Utility," Paper No. 81 WM 017-3, IEEE Winter Power Meeting, Atlanta, Feb. 1981.

Vemuri, S., E.F. Hill, and R. Balasubramanian, "Load Forecasting Using Stochastic Models," IEEE Transactions, Paper, PICA-1973, pp. 31-37.

Ware, J.E., and R.M. North, "The Price and Consumption of Water for Residential Use in Georgia," Research Monograph 40, School of Business Administration, Georgia State Univ., Atlanta, Georgia, 1967, 19 p.

Whitford, P.W., "Residential Water Demand Forecasting," Water Resources Research, Vol. 8, No. 4, 1972, pp. 829-839.

Willsie, R.H., and H.L. Pratt, "Water Use Relationships and Projection Corresponding with Regional Growth, Seattle Region," Water Resources Bulletin, Vol. 10, No. 2, 1974, pp. 360-371.

Wiser, E.H., "Irrigation Planning Using Climatological Data," Journal of Irrigation and Drainage Division, ASCE, Vol. 91, No. IR4, Proc. Paper 4551, Dec. 1964, pp. 1-11.

Wolf, E.C., "A Dynamic Model for Evaluating Union Electric's Hourly Demand," EPRI Symposium on Load Forecasting, April 1981.

Wong, S.T., "A Model on Municipal Water Demand: A Case Study of Northeastern Illinois," Land Economics, Vol. No. 48, No. 1, 1972, pp. 34-44.

Yamauchi, H., and W. Huang, "Alternative Methods for Estimating the Time Series Components of Water Consumption Data," Water Resources Bulletin, Vol. 13, No. 3. 1977, pp. 599-610.

APPENDIX B

A NEW MAXIMUM LIKELIHOOD ALGORITHM FOR PARAMETER ESTIMATION

1. Introduction

The successful design of a state estimator depends critically upon the correct specification of the noise covariance, erroneous estimates of which may lead to "filter divergence" and suboptimal performance. Research in parameter estimation has resulted in a variety of heuristic (Jazwinski, 1970) as well as Maximum Likelihood (Maybeck, 1982) procedures. The latter are theoretically preferable, yet they call for solving a mathematically complicated problem and in large scale applications they become numerically insufficient. One objective of our research was to develop a computationally efficient Maximum Likelihood estimation algorithm for the optimal identification of large state space models. This appendix provides some theoretical insight for and offers a case study with the method developed.

2. Organization of the Algorithm

The new M. L. method is based on the formulation of the parameter identification problem in an optimal control setting. Optimal control problems are characterized by a set of difference or differential equations (system dynamics) and an additive performance index. The system dynamics quantify the time evolution of the state vector and depend on an input vector, some or all the elements of which are controllable; The performance index is the function for minimization and comprises of an additive series of terms depending on contemporaneous state and control vectors.

The parameter estimation problem can be converted into the previous setting with the following specifications:

(a) The elements of the updated mean vector and the updated covariance matrix comprise the new state vector.

(b) The unknown parameters make up the control vector.

(c) The combined predictor-corrector equations constitute the system dynamics.

(d) The performance index for optimization is the Loglikelihood function.

The method developed for the solution of this problem is an iterative algorithm each iteration of which proceeds in the following manner:

(1) Start from a nominal control trajectory.

(2) Specify the corresponding state trajectory through the system dynamics.

(3) Find the gradient vector trajectory.

(4) Find the hessian matrix trajectory.

(5) Find the Newton optimization direction or a scaled reduced gradient direction, in the absence of convexity.

(6) Using the Armijo stepsize selection rule and generate the new control sequence improving the Performance Index.

(7) Iterate until no further improvement is possible.

The most important characteristic of the new method is the analytical derivation of the gradient, hessian, and optimization direction sequences. This feature facilitates the computations, while the use of the Armijo rule with the Newton or the Scaled Reduced Gradient direction guarantees fast convergence and reliability. The mathematical details of this method are the subject of a technical paper under preparation; In the following section, we shall present a short case study illustrating the performance of this technique.

3. A Case Study

In this application we seek the optimal identification of the system noise variance of the state space routing model presented in the previous progress report. The routing model is calibrated here for the upper Mississippi river with one routing reach. The data base includes 84 daily flows computed by the DWOPER routing model.

Figure 1 is a plot of the (-Loglikelihood) versus the noise variance. Tables 1 and 2 provide some iteration data from two computational experiments: In the first the process is initiated at

Var[w] = 10^6, in the second at Var[w] = 5 x 10^8. The data reported include the values of the Var[w], the negative Loglikelihood, and the gradient of the negative Loglikelihood with respect to the Var[w].

As can be seen by the results, the method identifies the optimal value within 7 to 8 iterations. These iterations take approximately 1.8 seconds CPU time on a CYBER 180/855 main frame digital computer. Actually, a good approximation of the solution has already been obtained within 4 to 5 iterations, indicating excellent convergence characteristics. Notice, furthermore, that this feature is unaffected by the local concavity or convexity of the performance index; The method is designed to iterate according to the Scaled Reduced Gradient in concave regions (minimization problem) and revert to Newton iterations in convex ones.

Although the previous application concerned the specification of the noise covariance, the method developed is quite general and can be used in the identification of any unknown parameter.

REFERENCES

Jazwinski, A. H., "Stochastic Processes and Filtering Theory," Academic Press, New Work, 1970.

Maybeck, P. S., "Stochastic Models Estimation and Control: Volume 2," Academic Press, New York, 1982.

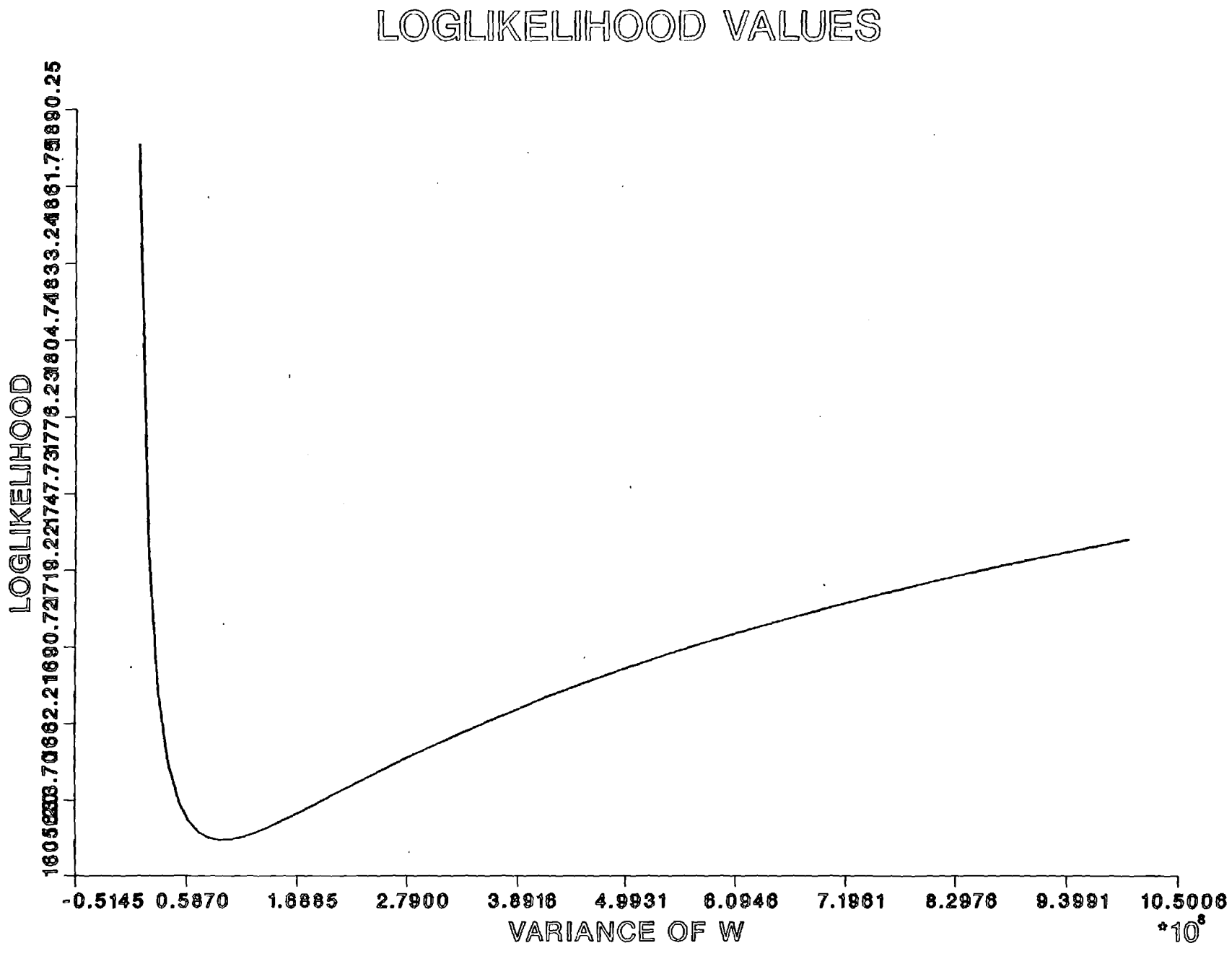
LOGLIKELIHOOD VALUES
LOGLIKELIHOOD
1605233.70662.21690.72719.22747.73776.23804.74833.24861.75890.25
-0.5145 0.5870 1.6885 2.7900 3.8916 4.9931 6.0946 7.1961 8.2976 9.3991 10.5006
VARIANCE OF W
*10^6

Table 1: First Computational Experiment

	Var[w]	-Loglikelihood	Gradient
Initially	0.1000×10^{7}	0.3162×10^{4}	-0.8016×10^{-5}
Iteration #1	0.4212×10^{7}	0.2266×10^{4}	-0.1472×10^{-5}
Iteration #2	0.1062×10^{8}	0.1888×10^{4}	-0.3453×10^{-6}
Iteration #3	0.2136×10^{8}	0.1725×10^{4}	-0.9479×10^{-7}
Iteration #4	0.3741×10^{8}	0.1655×10^{4}	-0.2780×10^{-7}
Iteration #5	0.5850×10^{8}	0.1627×10^{4}	-0.7828×10^{-8}
Iteration #6	0.8056×10^{8}	0.1620×10^{4}	-0.1670×10^{-8}
Iteration #7	0.9388×10^{8}	0.1619×10^{4}	-0.3655×10^{-10}
Iteration #8	0.9438×10^{8}	0.1619×10^{4}	-0.9574×10^{-11}
Iteration #9	0.9428×10^{8}	0.1619×10^{4}	-0.7283×10^{-12}
Iteration #10	0.9428×10^{8}	0.1619×10^{4}	-0.5496×10^{-13}

Table 2: Second Computational Experiment

	Var[w]	-Loglikelihood	Gradient
Initially	0.5000×10^{9}	0.1683×10^{4}	0.1530×10^{-8}
Iteration #1	0.1557×10^{9}	0.1626×10^{4}	0.2180×10^{-9}
Iteration #2	0.6516×10^{8}	0.1624×10^{4}	-0.5232×10^{-8}
Iteration #3	0.8585×10^{8}	0.1619×10^{4}	-0.9123×10^{-9}
Iteration #4	0.9494×10^{8}	0.1619×10^{4}	0.5933×10^{-10}
Iteration #5	0.9409×10^{8}	0.1619×10^{4}	-0.1759×10^{-10}
Iteration #6	0.9433×10^{8}	0.1619×10^{4}	0.4721×10^{-11}
Iteration #7	0.9428×10^{8}	0.1619×10^{4}	-0.3575×10^{-12}
Iteration #8	0.9428×10^{8}	0.1619×10^{4}	-0.2697×10^{-13}

APPENDIX C

RESERVOIR SYSTEM DATA

Following is a list of hydrologic data which have been requested by the Savannah and the Mobile Districts of the U.S. Army Corps of Engineers. These data sets concern the response of the Savannah and Apalachicola river basins.

1. Daily (and weekly) inflow records to the system reservoirs (for 20-25 years).
2. Daily reservoir releases over the period of the inflow record.
3. Mean daily rainfall and evaporation values contemporaneous to the inflows.
4. Elevation vs storage and area vs storage tables or curves for the system reservoirs.
5. Reservoir capacities and dead-storages.
6. Spillway characteristics for the system reservoirs.
7. Power production curves (;namely, curves providing the power vs net hydraulic head and turbine discharge).
8. Tailwater curves for the system reservoirs (; i.e., tailwater level vs discharge curves).
9. Daily or weekly power targets.
10. Maximum and minimum releases for the various system objectives (navigation, pollution abatement, recreation, and others).
11. Flood control storages.
12. Other level constraints for the system reservoirs.
13. Currently employed release rule curves.

The data set of the Savannah river system has already been received and is currently being utilized in the generation of explicit functional relationships between reservoir elevation and storage, tailwater elevation and release , power generation, turbine discharge, and forebay elevation. The identification of these functions is being performed via simple and multiple (nonlinear) regression analysis. The data set of the Apalachicola basin are expected within the upcoming two weeks.

After thorough examination of both data sets, the most suitable (longest and most reliable) one will be selected for our case study.

"Optimal Real-Time Forecasting and Control of Reservoir Hydrosystems Using Remote and On-Site Sensors"

Supported by
the U.S. Geological Survey, Department of the Interior
under award number 14 - 08 - 0001 - G1297

Water Resources Research
Act of 1984

Project Starting Date : September 1, 1986
Project Termination date: August 31, 1988

Progress Report for the period
June 1, 1987, through August 31, 1987

by

Aris P. Georgakakos, Ph. D.
Professor of Hydrology and Water Resources
School of Civil Engineering
Georgia Institute of Technology
Atlanta, Georgia 30332
Tel.: (404) 894-2240 or -2201

September 14, 1987

The contents of this report were developed under a grant from the Department of the Interior, U. S. Geological Survey. However, those contents do not necessarily represent the policy of that agency, and you should not assume endorsement by the Federal Government.

The project period from June to August, 1987, was devoted to the development and testing of a computer code implementing the ELQG control method to the Savannah river system. The model was tested in several control and simulation experiments and demonstrated superior computational efficiency and reliability. The results of this analysis constituted the subject of a technical paper presented at the WATERPOWER '87 ASCE conference in Portland, Oregon (August 17-21). This paper is included in Appendix A and summarizes the work performed.

APPENDIX A

OPTIMAL OPERATION OF THE SAVANNAH RIVER SYSTEM

by

Aristidis P. Georgakakos

School of Civil Engineering, Georgia Institute of Technology, Atlanta

This paper presents an application of a stochastic control method to the real time operation of the Savannah river system which includes three reservoirs and is expected to meet energy generation, flood protection, and navigation requirements. The associated problem is formulated and the method is employed in a series of control and simulation experiments. The results indicate that the method is reliable, computationally efficient, and can effectively assist the decision making process.

INTRODUCTION

Reservoir operation has been an active research area for over 30 years (see, Rosenthal, 1980, Yeh, 1985, and Georgakakos and Marks, 1985, for survey papers). Reservoir systems are large scale projects with a variety of vital benefits (e.g., municipal, industrial, and agricultural water supply, energy generation, navigation, and recreation) as well as severe flood and drought risks. Although the need to combine mathematical models with the ever-expanding computer technology in the reservoir operation process has long been recognized by both researchers and practitioners (see Proceedings of National Workshop on Reservoir Operation Research, 1979), current practices are still primarily based on heuristic rules. The reasons are partially due to the problem's resilient difficulty and partially due to the existing communication

gap between researchers and reservoir system managers. Practical engineering experience is necessary in all cases but will suffice alone only in few relatively simple systems. In the majority of cases, the decision making process can greatly benefit from reservoir control research advances. In turn, this interaction can only stimulate more meaningful research.

This paper presents some computational experience with a recently developed reservoir control method. The emphasis is primarily on the practical interpretation of this method's capabilities rather than its theory. The case study utilizes data from the Savannah river system.

SYSTEM DESCRIPTION

The Savannah river system (Figure 1) originates in the North Carolina Blue Ridge mountains and flows in a south-easterly direction toward the Atlantic Ocean along the Georgia - South Carolina border. Since the Colonial times, the river has played an instrumental role in the development of the basin's economy, which is primarily agricultural in the north and industrial in the south.

The many economic and social benefits together with the severe flood risks have brought about several river control and utilization projects, the most notable of which are the Hartwell, R.B. Russell, and Clark Hill storage projects and an eleven-mile levee around the city of Augusta. Table 1 summarizes some relevant characteristics of the above-mentioned reservoirs whose optimal regulation is the scope of this study. This as well as all other hydrologic or operational data used here was compiled from the Savannah River Basin reservoir regulation manual (U.S. Army Corps of Engineers, 1974) or from personal communications with the engineers of the Savannah District.

Apart from power generation, these projects are expected to provide reliable flood protection and maintain a minimal downstream discharge (6000 cfs) for navigation purposes. Figure 2 displays the annual distribution of the mean net reservoir inflows, and Figure 3 shows a typical distribution of energy production targets. (The solid lines correspond to Hartwell, the dotted to Russell, and the dashed to Clark Hill.) The actual flows may deviate markedly from their respective means with this deviation often being several times the mean value. In other words, the probability distributions of inflows are distinctly skewed.

THE RESERVOIR CONTROL PROBLEM

The Savannah system is a cascade of three reservoirs whose dynamics can be modelled by the following water balance difference equations:

$$s_h(k+1) = s_h(k) - u_h(k) + w_h(k) \ , \qquad (1_a)$$

$$s_r(k+1) = s_r(k) - u_r(k) + u_h(k) + w_r(k) \ , \qquad (1_b)$$

$$s_c(k+1) = s_c(k) - u_c(k) + u_r(k) + w_c(k) \ , \qquad (1_c)$$

where

$s_j(k)$ is the water volume stored in reservoir j = h, r, or c at the beginning of time period k,

$u_j(k)$ is the volume released during period k,

$w_j(k)$ is the net reservoir inflow during period k, and

h, r, c are subscripts indicating quantities pertaining to Hartwell, Russell, or Clark Hill respectively.

Equations (1) describe a stochastic system. The randomness is a result of inflow uncertainty and practically implies that even if future releases are known, storage volumes cannot be precisely determined.

The restrictions of the physical system and the flood protection and navigation concerns impose upper and lower bounds on this system's storage and release variables:

$$s_j^{min}(k) \leq s_j(k) \leq s_j^{max}(k) \ , \qquad (2_a)$$

$$u_j^{min}(k) \leq u_j(k) \leq u_j^{max}(k) \ , \qquad (2_b)$$

$$j = h, r, c,$$

where $s_j^{max}(k)$ and $s_j^{min}(k)$ correspond to the capacity and dead storage values reported in Table 1, $u_j^{max}(k)$ is taken equal to 20000 cfs for all j, and $u_j^{min}(k)$ is taken equal to zero for $j = \{h,r\}$ and 6000 cfs for $j = c$. The value of 20000 cfs for the upper release bound was based on the results of flood-damage analyses conducted by the Corps of Engineers (1974) and represents the highest harmless release.

In view of the inflow uncertainty, the storage constraints must be more properly restated in the following probabilistic format:

$$\int_{-\infty}^{s_j^{min}(k)} f_j(x)\, dx \leq \beta_j^{min}(k) \qquad (2_c)$$

$$\int_{s_j^{max}(k)}^{+\infty} f_j(x)\, dx \leq \beta_j^{max}(k) \qquad (2_d)$$

where $f_j(x)$ denotes the probability density function of the storage variable $s_j(k)$; $\beta_j^{max}(k)$ and $\beta_j^{min}(k)$ are to be determined by the system managers according to their risk concept. These inequalities require that the probability of the storage variables exceeding their upper or lower bounds be less than or equal to some prespecified tolerance level.

Let $P_j(k)$ denote reservoir j's energy demand during period k and $g_j[s_j(k),u_j(k)]$ its energy production function. Then, the system's energy

generation objective is accomplished if $P_j(k) = g_j[\underline{s}_j(k), u_j(k)]$ for all j and k. Equivalently, the same goal is achieved if

$$J = E\{ \sum_k \sum_j (P_j(k) - g[\underline{s}_j(k), u_j(k)])^2 \} \qquad (3)$$

is minimized. In Performance Index (3), $E\{\cdot\}$ represents the expected value of the quantity inside the brackets, which is random as a result of the randomness of the storage variables; the first summation is over all periods of the control horizon while the second is over the three reservoirs. This quadratic penalty-type performance index is usually convenient because of its convex attributes. The power production functions g_j must be determined based on the power plant turbine characteristic curves; namely, the curves relating power production to turbine discharge and net hydraulic head, the latter being the difference between the forebay and tailwater elevations less the penstock hydraulic losses. In the case of the Hartwell and Russell projects, the net hydraulic head, and consequently the functions g_j, also depend upon the downstream reservoir's storage value. Thus, in their case, $\underline{s}_j$ is a vector of two storage variables. For Clark Hill, $\underline{s}_j$ includes only s_c. The power production functions were determined via nonlinear regression analyses and exhibit sufficient accuracy over all of the turbine operational range. The standard deviation of the fitted power values from the actual ones was within (0.3 - 0.5) MW for all projects.

The Savannah system control problem can now be mathematically stated as one which calls for finding the release sequences $\{u_h(k), u_r(k), u_c(k)\}$, $k = 0,1,2,\ldots$, which minimize Performance Index (3) subject to the system Equations (1) and Constraints (2).

In the above formulation, the flood and low flow concerns take precedence over energy generation. Namely, the identified optimal release policies will

attempt to satisfy the energy generation requirements as long as no constraints are active. However, during times of floods or droughts the releases will be determined to avoid exceeding the designated flood levels or to meet the required low flows.

Lastly, the time period k was intentionally left unspecified. In this study it will correspond to one week. However, the formulation presented in this section and the reservoir control method to be discussed next can be used with any time period of interest.

EXTENDED LINEAR QUADRATIC GAUSSIAN (ELQG) CONTROL

ELQG is a stochastic optimization method recently developed for the treatment of reservoir regulation problems (Georgakakos and Marks, 1985, $1987_{a,b}$). At each decision time ELQG is designed to perform the following operations:

1. Obtain probabilistic inflow forecasts over the specified control horizon. (Both statistical and physically-based inflow models may be used.)

2. Assume some initial nominal release sequence for each system reservoir and, based on the system equations, generate probabilistic forecasts of their storages.

3. Derive the first and second derivatives of the performance index J with respect to the release variables and construct the Newton optimization direction. If any release or storage constraints are violated, determine the Projected Newton direction or use a penalty function method respectively.

4. Perform the iteration using the Armijo stepsize selection rule and define new nominal release sequences.

5. If no further reduction of the performance index is possible and all release and storage trajectories are feasible, proceed to Step 6; otherwise return to Step 2 and repeat the previous process.

6. Apply the first period's optimal releases and repeat Steps 1 - 6 at the next decision time.

ELQG is designed to display reliability and computational efficiency. These properties are theoretically guaranteed as a result of the nature of the optimization directions and the stepsize selection rule employed; they have also been practically documented through extensive computational experience. For more details on the structure and the performance of the ELQG control algorithm, the reader is referred to the above-cited references.

Figures 4 and 5 present two typical ELQG control experiments with the Savannah system. Each figure has two sets of plots. The top plots display the identified optimal release rules; the bottom plots delineate the associated storage trajectories. Except for mean values, the storage plots also include the 97.5% and 2.5% probability limits. Release and storage boundaries are indicated by dashed lines. In both of these experiments, the initial storage values were 115, 44, and 110 billion cubic feet respectively for Lakes 1 (Hartwell), 2 (Russell), and 3 (Clark Hill), and the control horizon was equal to 10 weeks. Figure 4 shows the optimal sequences when no storage bounds are taken into account. These sequences basically satisfy the energy generation requirements shown in Figure 2. In fact, the generation from Clark Hill exceeds the required amount due to the more stringent navigation release. The storage trajectories indicate that if this release policy is adopted, there is high chance that at least Lakes 1 and 3 will exceed their capacity. Figure 5 shows what release schedules are necessary to avoid violation of the storage

constraints at the specified probabilistic level.

The above experiments are typical of the ELQG control of the Savannah reservoirs: In the absence of flood or drought conditions, the system is operated to meet the energy requirements; otherwise, the priority is shifted to the flood or drought objectives.

SIMULATION RESULTS

The simulation experiments presented here were run to quantify the average system performance under ELQG control. The basis of these experiments was 100 years of synthetically generated weekly flows assumed to follow lognormal probability distributions with historically estimated means and variances. The ELQG control algorithm was implemented with a six week control horizon and reliability parameters equal to 2.5% in the first experiment and 50% in the second. Figure 6 depicts the mean values and the (2.5%-97.5%) probability limits of the first experiment's storages, releases, and energy generation for Lake Hartwell; Figure 7 present the results of the second simulation experiment. The results for the other two lakes are similar and are not included. Some comments are now offered:

1. Under the stated hydrologic conditions and power commitments, the system reservoirs consistently undergo stressful periods where storages approach capacity values and higher flood risks. During these periods, the variability of releases and energy generation increases.

2. When the reservoirs are not stressed, they are basically operated to satisfy the energy requirements. The variability of these releases and energy generation is minimal.

3. Between the two experiments, the first results in lower storage levels

and fewer excessive releases. (An excessive release is a release above 20,000 cfs.) In fact, the release plots indicate that the occurrence of excessive releases is consistent with and can be controlled by ELQG's probability tolerance levels. When these levels are high, as in the second experiment, release constraint violations are more frequent. The first experiment allows constraint violation only 2.5% of the times.

4. Although the second experiment is characterized by higher storage levels, on the average its energy generation is comparable to that of the first. This result comes about because the second ELQG setup is "myopic" and reacts to the possibility of a storage bound violation only when there is high probability (50%) that such an event may happen. At that time, however, a good part of the emergency release cannot pass through the turbines and does not produce power. As a result, the gains from maintaining higher storages are lost. On the other hand, the first ELQG setup is more "cautious" and reacts to such circumstances in an anticipatory fashion; thus, it manages to pass most of the flood waters through the power turbines and makes up for the lesser hydraulic head.

5. The second experiment, with 50% tolerance levels, practically corresponds to deterministic (expected value) system operation. Thus, the previous two comments also reflect the benefits of stochastic versus deterministic optimization.

CONCLUSIONS

The ELQG stochastic control method was employed to study the real time operation of the Savannah reservoirs. The method was briefly outlined and its performance discussed in control and simulation experiments. ELQG is reliable

and computationally efficient and can handle release and probabilistic storage constraints and multiple objectives. In the Savannah study, ELQG was shown to effectively compromise between flood protection and energy generation.

Future work with the Savannah system will involve coupling of ELQG with physically-based inflow forecasting models for daily system regulation. With reliable foresight of future inflows, the method is expected to maximize the system's operational efficiency.

The results of the ELQG simulations can also assist in establishing operational policies. For example under the assumptions stated here, the Savannah system has the ability to reliably satisfy higher energy commitments. This will not only increase energy generation but will also enhance flood protection.

ACKNOWLEDGEMENTS

The author would like to thank the staff of the Savannah COE district office for providing the necessary case study data, and especially Engineers R. Parker and J. Hoke for their insightful discussions. This work was supported in part by U.S.G.S. through Grant 14-08-0001-G1297.

REFERENCES

Georgakakos, A.P., and Marks, D.H., "Real Time Control of Reservoir Systems," Technical Report No. 301, Ralph M. Parsons Laboratory for Hydrology and Water Resources, Dept. of Civil Engineering, Massachusetts Institute of Technology, Cambridge, Massachusetts, May 1985.

Georgakakos, A.P., and Marks, D.H., "A New Method for the Real Time Operation of Reservoir Systems," Water Resources Research, Vol. 23, No. 7, pg. 1376-1390, 1987.

Georgakakos, A.P., and Marks, D.H., "A New Method for the Control of the River Nile," International Journal of Water Resources Development, Vol. 3, No. 2, pg. 133-141, 1987.

Proceedings of the National Workshop on Reservoir Systems Operations, University of Colorado, Boulder Colorado, August 13-17, 1979.

Rosenthal, R., "The Status of Optimization Models for the Operation of Multireservoir Systems With Stochastic Inflows and Nonseparable Benefits," Technical Report No. 75, Tennessee Water Resources Research Center, Knoxville, 1980.

Yeh, W. W.-G., "Reservoir Management and Operation Models: A State-of-the-Art Review, Water Resources Research, Vol. 21, pg. 1797-1818, 1985.

Table 1: Some Data on the Savannah Reservoirs

	Hartwell	Russell	Clark Hill
Year Completed:	1962	1984	1953
Drainage Basin: (sq. mi.)	2088	802	3254
Dead Storage: (10^9 ft^3)	49.401	39.177	63.815
Storage Capacity: (10^9 ft^3)	123.830	50.798	126.324
Hydropower Capacity: (MW)	4x66+1x80=344	4x75=300	7x40=280

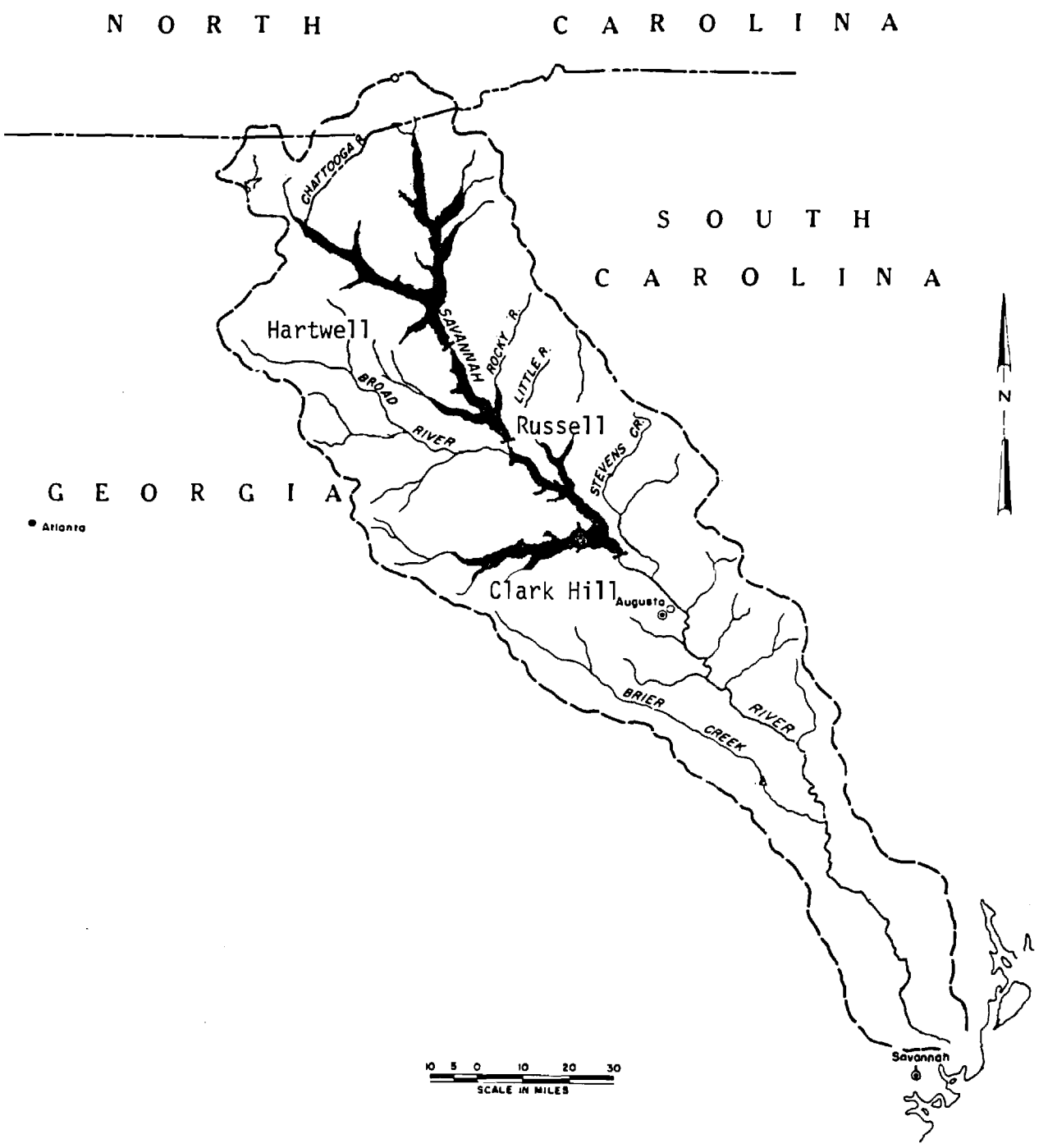

Figure 1: A Map of the Savannah River Basin

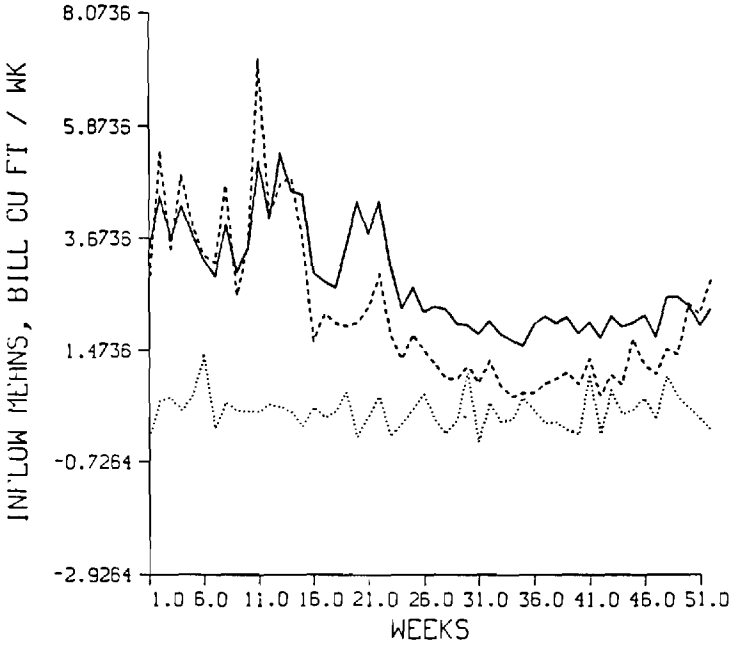

Figure 2: Mean Net Reservoir Inflow

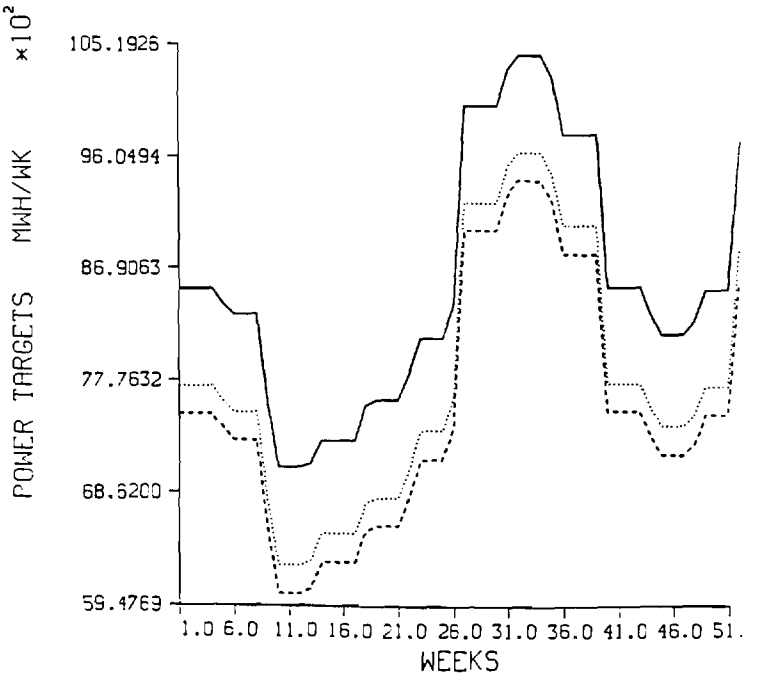

Figure 3: Typical Energy Targets

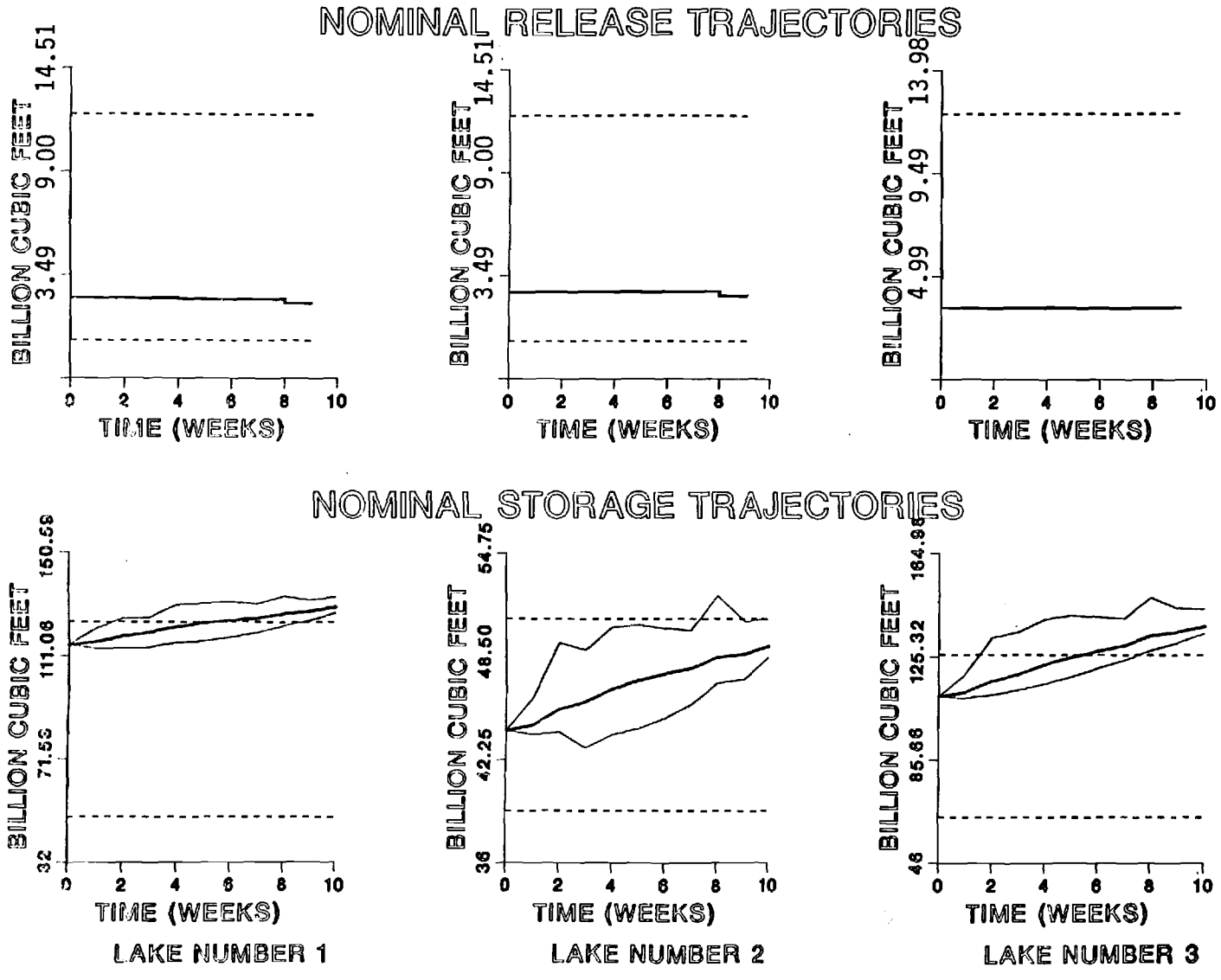

Figure 4: ELQG Control Without Storage Constraints

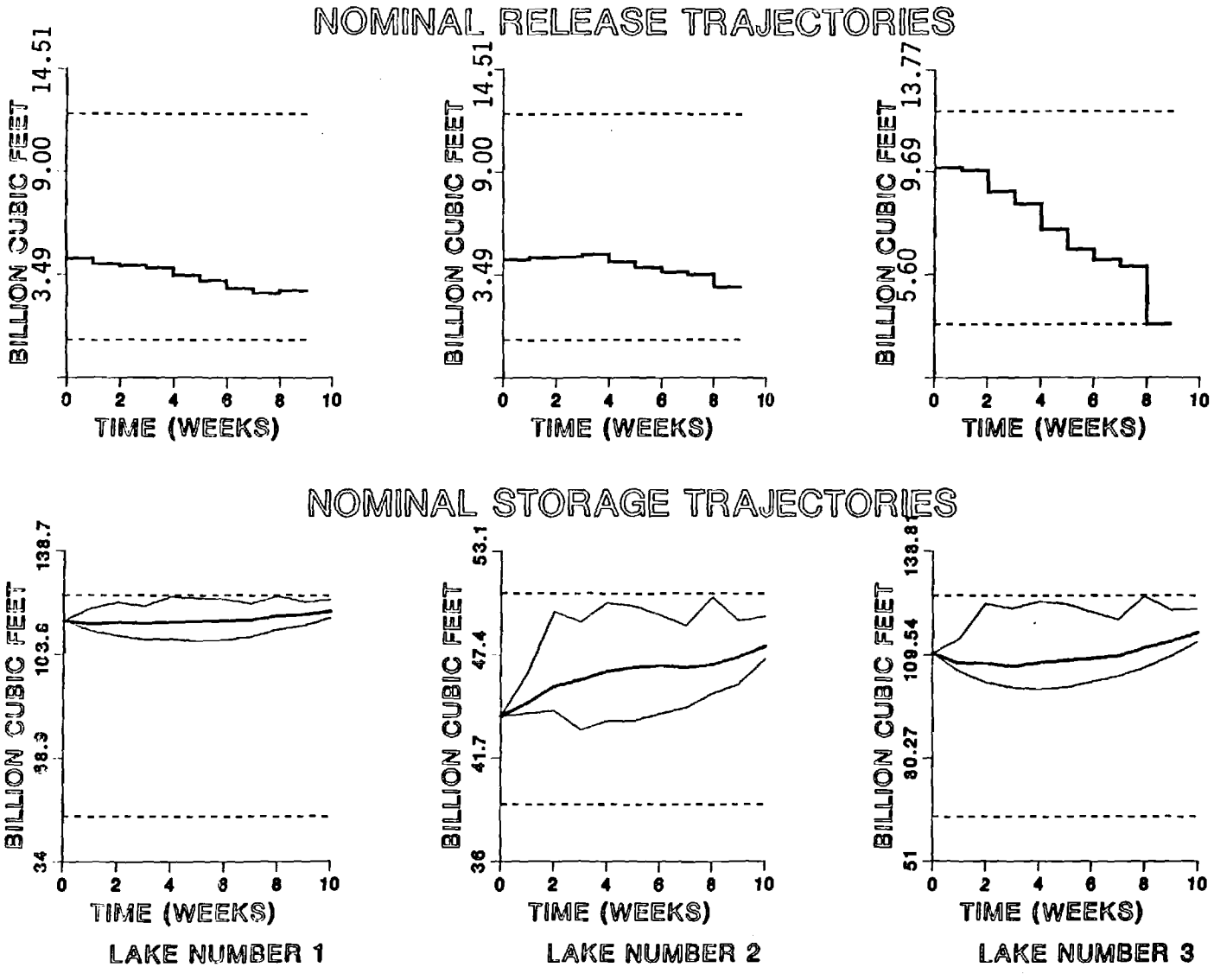

Figure 5: ELQG Control With Storage Constraints

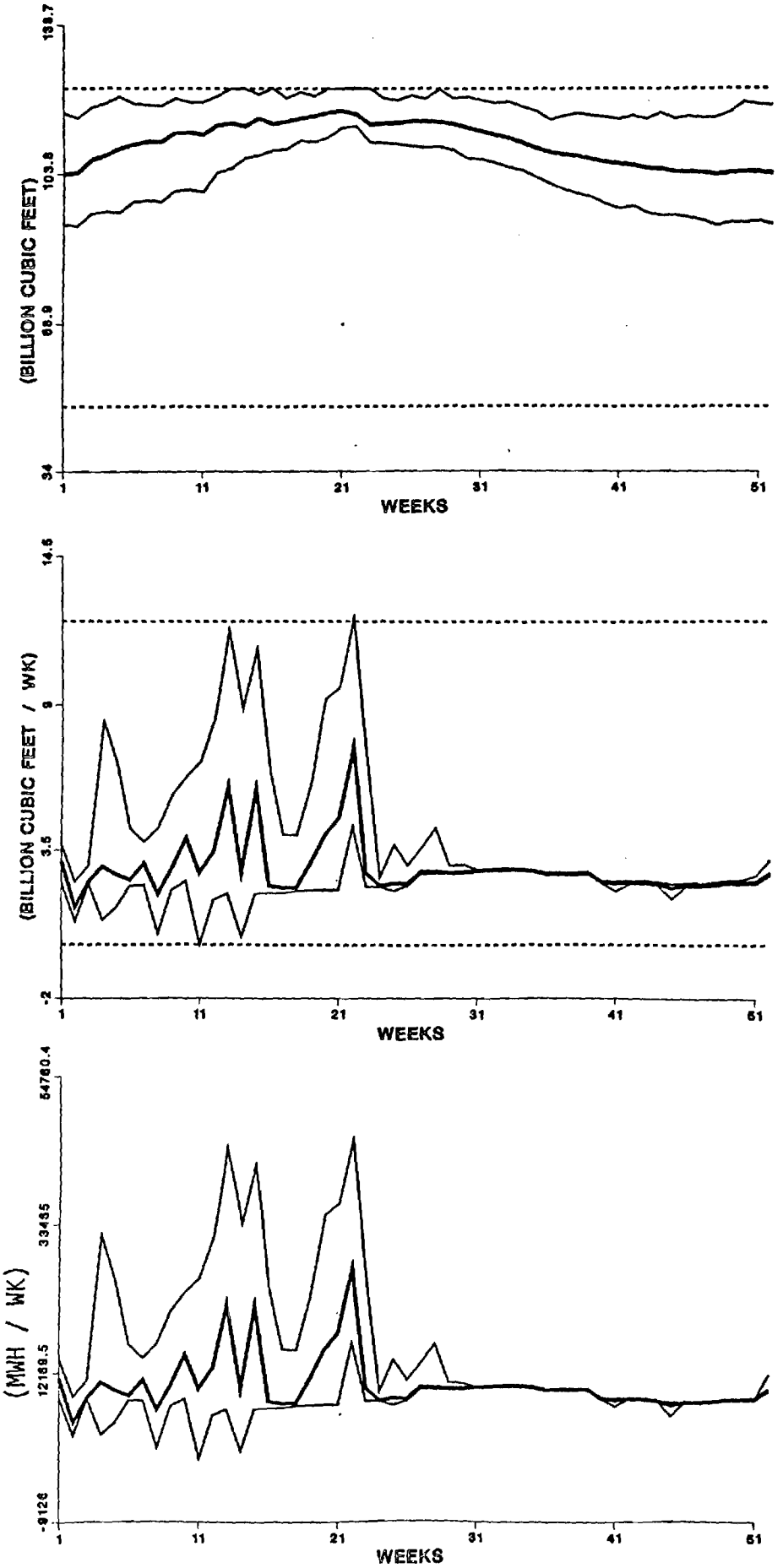

Figure 6: First Simulation Experiment: Hartwell Storage, Release, and Power

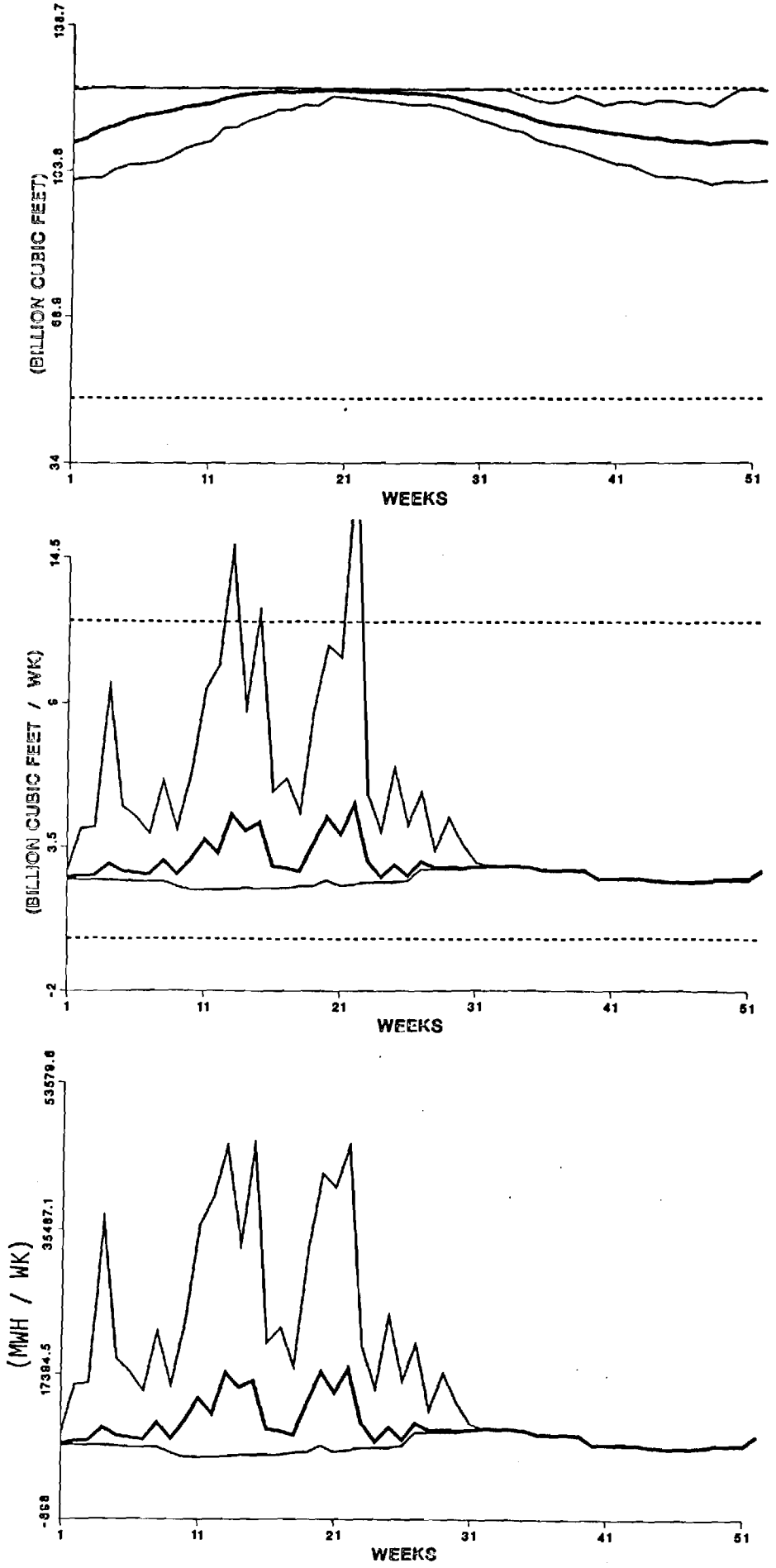

Figure 7: Second Simulation Experiment: Hartwell Storage, Release, and Power

"Optimal Real-Time Forecasting and Control of Reservoir Hydrosystems Using Remote and On-Site Sensors"

Supported by
the U.S. Geological Survey, Department of the Interior
under award number 14 - 08 - 0001 - G1297

Water Resources Research
Act of 1984

Project Starting Date : September 1, 1986
Project Termination date: August 31, 1988

Progress Report for the period
September 1 through November 30, 1987

by

Aris P. Georgakakos, Ph. D.
Professor of Hydrology and Water Resources
School of Civil Engineering
Georgia Institute of Technology
Atlanta, Georgia 30332
Tel.: (404) 894-2240 or -2201

December 4, 1987

The contents of this report were developed under a grant from the Department of the Interior, U. S. Geological Survey. However, those contents do not necessarily represent the policy of that agency, and you should not assume endorsement by the Federal Government.

Table of Contents

EXTENDED LINEAR QUADRATIC GAUSSIAN (ELQG) CONTROL: FURTHER EXTENSIONS

1. INTRODUCTION

The ELQG control method (Georgakakos and Marks, WRR, 1987) is a stochastic control algorithm for the optimal operation of multiobjective reservoirs. ELQG identifies release sequences which optimize the benefits from one system objective (typically hydropower) while satisfying the other objectives at prespecified reliability levels. Mathematically, this translates into optimizing a general functional of a stochastic system in state-space form with upper and lower release and probabilistic storage bounds. Extensive computational experience indicated that, although the method is reliable overall, it is more efficient in handling release rather than storage constraints. Furthermore, the treatment of probabilistic constraints is exact only for Gaussian disturbances.

In this work, ELQG is modified to more effectively handle nongaussian disturbances and storage constraints by taking into account higher order statistical moments and using a new barrier function method. The effectiveness of these extensions is evaluated through control and simulation experiments with the Savannah river system.

2. RESERVOIR CONTROL PROBLEM FORMULATION

A typical formulation of a multiobjective reservoir control problem (Georgakakos and Marks, 1987) is presented below and will serve as reference in the sections to follow:

Find the release sequences $\{u_j(k),\ j=1,\ldots,M,\ k=0,1,\ldots,N\}$ which minimize

$$J = E\ \{\ \sum_k\ \sum_j\ [P_j(k) - g_j(\underline{s}_j(k),u_j(k))]^{\alpha}\ \} \tag{1}$$

$j = 1,2,\ldots,M,$

$k = 0,1,2,\ldots,N-1,$

subject to

(a) the system equations,

$$\underline{s}(k+1) = \underline{\underline{A}}(k)\underline{s}(k) + \underline{\underline{B}}(k)\underline{u}(k) + \underline{\underline{\Gamma}}(k)\underline{w}(k), \tag{2}$$

$k = 0,1,2,\ldots,N-1,$

with $\underline{s}(0)$ known,

(b) the release constraints,

$$u_j^{min}(k) \le u_j(k) \le u_j^{max}(k), \tag{3}$$

$j = 1,2,\ldots,M,$

$k = 0,1,2,\ldots,N-1,$ and

(c) the storage reliability constraints,

$$Prob[s_j(k) \le s_j^{min}(k)] \le \gamma_j^{min}(k), \tag{4_a}$$

$$Prob[s_j(k) \le s_j^{max}(k)] \le \gamma_j^{max}(k), \tag{4_b}$$

$j = 1,2,\ldots,M,$

$k = 0,1,2,\ldots,N.$

In the above formulation,

M is the number of reservoirs,

N is the end of the control horizon,

$P_j(k)$ is the energy target for the j^{th} reservoir during period k,

$g_j(\underline{s}_j(k), u_j(k))$ is the energy generation of the j^{th} reservoir during period k,

$\underline{s}_j(k)$ is a vector including one or two storage variables: the storage of the j^{th} reservoir and that of the downstream one, the latter entering the energy function through the tailwater effect, if any,

$u_j(k)$ is the turbine release from reservoir j,

α is a real exponent (most often equal to 2) to induce convexity of the performance index,

$E\{\cdot\}$ denotes the expected value of the quantity in the brackets,

$\underline{s}(k)$ is the vector of all reservoir storages at the beginning of period k,

$\underline{u}(k)$ is the vector of all controllable reservoir releases during period k,

$\underline{w}(k)$ is the vector of all reservoir inflows during period k,

$\underline{\underline{A}}(k)$, $\underline{\underline{B}}(k)$, $\underline{\underline{\Gamma}}(k)$ are matrices with elements determined by the system's water budget relationships,

$u_j^{min}(k)$, $u_j^{max}(k)$ are lower and upper release bounds,

$s_j^{min}(k)$, $s_j^{max}(k)$ are lower and upper storage bounds,

$\gamma_j^{min}(k)$, $\gamma_j^{max}(k)$ are tolerance levels reflective of the reservoir managers' risk attitude.

3. NONGAUSSIAN STATISTICS

The need for nongaussian considerations arises mainly because, more often than not, streamflows exhibit such behavior. Moreover, in systems modelled by nonlinear dynamical relationships, even with gaussian inflows, the resulting storages deviate from normality. The greater this deviation, the less effectively the reliability constraints (4) are handled.

Discussing the full estimation of the joint probability density of the system's storages, Georgakakos and Marks, 1987, conclude that it is a rather involved task requiring excessive computational overhead even for small size systems. Alternatively, if a number of statistical moments could be computed, this function could be approximated with some other density function preserving these statistics. ELQG was initially designed to account for the storages' mean and covariance and employ a gaussian approximation of their probability density. This approach will now be extended to include higher order statistical moments.

The expected storage trajectory associated with a nominal control sequence $\{\bar{\underline{u}}(k),\ k=0,1,2,\ldots,N-1\}$, can be obtained from dynamical Equation (2):

$$\bar{\underline{s}}(k+1) = \underline{\underline{A}}(k)\bar{\underline{s}}(k) + \underline{\underline{B}}(k)\bar{\underline{u}}(k) + \underline{\underline{\Gamma}}(k)\bar{\underline{w}}(k), \qquad (5)$$

where $\bar{\underline{s}}(k)$ and $\bar{\underline{w}}(k)$ are the mean storage and inflow vectors and $\bar{\underline{s}}(0) = \underline{s}(0)$. Subtracting (5) from (2), one obtains the equation of the zero mean process:

$$\delta\underline{s}(k+1) = \underline{\underline{A}}(k)\delta\underline{s}(k) + \underline{\underline{B}}(k)\delta\underline{u}(k) + \underline{\underline{\Gamma}}(k)\delta\underline{w}(k), \qquad (6)$$

where $\delta\underline{x}(k) = \underline{x}(k) - \bar{\underline{x}}(k)$ for $x \in \{s,u,w\}$.
Equation (6) can be used to generate central statistical moments as soon as the nature of the release corrections $\delta\underline{u}(k)$ is defined. In the ELQG control algorithm, these corrections are obtained in feedback form:

$$\delta\underline{u}(k) = - \underline{\underline{D}}(k) \, [\underline{\underline{L}}(k)\delta\underline{s}(k) + \underline{\Lambda}(k)] \qquad (7)$$

$k = 0,1,2,\ldots,N-1,$

with the control gains $\underline{\underline{D}}(k)$, $\underline{\underline{L}}(k)$, and $\underline{\Lambda}(k)$ computed analytically. Substituting (7) in (6) and discarding $\Lambda(k)$, which becomes zero at the optimal $\bar{u}(k)$ sequence, results in

$$\delta\underline{s}(k+1) = [\underline{\underline{A}}(k) - \underline{\underline{B}}(k)\underline{\underline{D}}(k)\underline{\underline{L}}(k)]\delta\underline{s}(k) + \underline{\underline{\Gamma}}(k)\delta\underline{w}(k), \qquad (8)$$

$k = 0,1,2,\ldots,N-1.$

Equation (8) can now be used in the computation of central moments:

Postmultiplying with $[\delta\underline{s}(k+1)]^T$ and taking expectations leads to the covariance propagation equation:

$$\underline{\underline{P}}_s(k+1) = \underline{\underline{F}}(k)\underline{\underline{P}}_s(k)[\underline{\underline{F}}(k)]^T + \underline{\underline{\Gamma}}(k)\underline{\underline{Q}}(k)[\underline{\underline{\Gamma}}(k)]^T \qquad (9)$$

where $\underline{\underline{P}}_s(k) = E\{\delta\underline{s}(k)[\delta\underline{s}(k)]^T\}$, $\underline{\underline{Q}}(k) = E\{\delta\underline{w}(k)[\delta\underline{w}(k)]^T\}$, $\underline{\underline{F}}(k) = \underline{\underline{A}}(k) - \underline{\underline{B}}(k)\underline{\underline{D}}(k)\underline{\underline{L}}(k)$, and $\delta\underline{w}(k)$, $k=0,1,2,\ldots,N-1$, are assumed to be independent random vectors. This assumption is used for consistency with the ELQG derivation of the release corrections and associated control gains; nonetheless, the statistics of these random vectors are determined from forecasting models fully accounting for their dependencies (see, discussion in Georgakakos and Marks, 1987).

Although the results for the third central moment cannot be expressed in a matrix form similar to (9), the computations can proceed in much the same way: Consider for instance a three reservoir system whose Equation (8) is as follows:

$$x(k+1) = f_{11}(k)x(k) + f_{12}(k)y(k) + f_{13}(k)z(k) + \omega_1(k), \qquad (10_a)$$

$$y(k+1) = f_{21}(k)x(k) + f_{22}(k)y(k) + f_{23}(k)z(k) + \omega_2(k), \qquad (10_b)$$

$$z(k+1) = f_{31}(k)x(k) + f_{32}(k)y(k) + f_{33}(k)z(k) + \omega_3(k), \qquad (10_c)$$

where $x(k) = \delta s_1(k)$, $y(k) = \delta s_2(k)$, $z(k) = \delta s_3(k)$, and $\omega_j(k) = \delta w_j(k)$.

Raising each one of the above equations to the third power and taking expectations yields the following result:

$$E\{x^3(k+1)\} = f_{11}^3 E\{x^3\} + f_{12}^3 E\{y^3\} + f_{13}^3 E\{z^3\} + E\{\omega_1^3\}$$

$$+ 3f_{11}^2 f_{12} E\{x^2 y\} + 3f_{12}^2 f_{11} E\{y^2 x\} + 3f_{11}^2 f_{13} E\{x^2 z\} + 3f_{13}^2 f_{11} E\{z^2 x\}$$

$$+ 3f_{12}^2 f_{13} E\{y^2 z\} + 3f_{13}^2 f_{12} E\{z^2 y\} + 6f_{11} f_{12} f_{13} E\{xyz\}, \qquad (11)$$

(similar equations can be derived for $E\{y^3 k(+1)\}$ and $E\{z^3(k+1)\}$) where the time dependence of the terms in the right side of (11) has been dropped for notational convenience. As can be seen from (11), each storage's skewness at time $k+1$ depends not only on every storage and inflow skewness at the previous time k but also on all other third order central moments of the storage variables. Despite the assumed inflow independence, these moments do not vanish because of the interelationhips introduced through Equation (7). However, these third order moments may also be recursively propagated in the same fashion by means of Equations (10).

Although utilizing third moment information will suffice in most cases, fourth or higher order statistical moments may also be determined by similar considerations.

Having the mean, variance, and skewness of the storage variables at each time k, the storage distribution may be approximated by a suitable probability law. Then, probabilistic constraints (4) can be inverted into constraints on each expected storage:

$$\xi_j^{min}(k) \le \bar{s}_j(k) \le \xi_j^{max}(k), \qquad (12)$$

$$j = 1,2,\ldots,M,$$

where $\xi_j^{min}(k)$ and $\xi_j^{max}(k)$ are such that

$$Prob[s_j(k) \le \bar{s}_j(k) - \xi_j^{min}(k)] = \gamma_j^{min}(k) \quad \text{and} \qquad (13_a)$$

$$Prob[s_j(k) \ge \bar{s}_j(k) + \xi_j^{max}(k)] = \gamma_j^{max}(k). \qquad (13_b)$$

By also expressing the performance index in terms of the preserved statistical moments (as discussed in Georgakakos and Marks, 1987), control problem (1 - 4) can be reformulated into deterministic format and solved via the ELQG optimization algorithm. (The states of the reformulated problem are the statistical moments of the original storage variables.)

A last remark refers to the advantage in using the feedback Equation (7) to represent the release corrections. If these corrections were assumed deterministic, both the variance and skewness as well as all higher order moments would grow unbounded and would result in overly conservative operation. Instead, as will be seen in the case study section of this paper, usage of (7) makes (8) stable, resulting in bounded moments and augmenting the storages' feasible regions (12).

4. A BARRIER FUNCTION METHOD FOR RELIABILITY CONSTRAINTS

Extensive ELQG application experience has indicated that the method's computational requirements are largely expended for handling the reliability storage constraints. According to the penalty function method initially used, these constraints are examined at each iteration for possible violations. In the event of a constraint violation at time period k, a quadratic penalty term is added to the performance index:

$$C^i \left[s_j^{max}(k) - \delta\bar{s}_j(k) - s_j(k)\right]^2, \text{ (upper constraint violation)} \qquad (13)$$

with $s_j^{max}(k) - \delta\bar{s}_j(k)$ being the value of the mean storage where the constraint is just binding and C^i is a penalty coefficient. The problem (1-3) is then re-solved, the storage constraints re-examined, and the proper penalty terms added with a new coefficient $C^{i+1} > C^i$. The increment rate of this coefficient is a matter of experimentation and is crucial to this method's performance. A slow increment rate will result in slow convergence, while a very fast one will fail to identify which constraints are binding. Extensive control experiments with a single reservoir and relatively short control horizons (10 ~ 15 time periods) indicated that an increment formula

$$C^{i+1} = \beta\, C^i \qquad (14)$$

with $\beta \in [4,10]$ will generally perform well. In fact, these case studies illustrated that problem (1-3) does not have to be completely solved before each increment of the penalty coefficient; rather, the projected Newton and penalty function iterations can be performed simultaneously with substantial

computational savings. However, when the number of binding constraints is large (e.g., when longer control horizons or many reservoirs or both are considered), control and storage constraints cannot be reliably treated in this manner, and the computational requirements begin to grow. The main reason for this performance weakening is the nature of the penalty function method which prescribes penalty terms only when there are constraint violations. If in the next iteration all storage variables are forced inside the feasible region, penalty terms are not added, and the method tends to drive the storage trajectory back outside its bounds; this oscillation becomes more unstable as the penalty coefficient increases.

Alternatively, storage constraints can be treated via a barrier function method (Luenberger, 1973). The method researched in this study uses a function of the following form:

$$B[s_j(k)] = C \left[\frac{s_j^{max}(k) - s_j(k)}{s_j^{max}(k) - s_j^{min}(k)} \right]^{-\mu} \left[\frac{s_j(k) - s_j^{min}(k)}{s_j^{max}(k) - s_j^{min}(k)} \right]^{-\nu} \qquad (15)$$

where C, μ, and ν are real positive constants. Figure 1 shows plots of this function for $C = 1$, $s_j^{max}(k) = 123.8$, $s_j^{min}(k) = 49.4$, and different values of μ and ν.

The motivation for using this function is to prescribe increasingly higher costs as storage approaches either boundary while being virtually inconsequential within the feasible region. Thus, in contrast to the quadratic penalty (13), $B[s_j(k)]$ does not have to be added or removed depending on the constraint violation status, and the controller is always "aware" of its cost structure when searching for better release and storage sequences.

However, simply including this barrier function in the performance index will not be computationally efficient. The two main reasons are first that the

iterations may start from or initially generate infeasible trajectories and second that the barrier cost may drive a binding storage significantly afar from its boundary. To account for these effects, the following usage of this barrier function method is suggested:

At each ELQG iteration i, Performance Index (1) is expanded to include the following barrier function terms:

$$B^i[s_j(k)] = C \left[\frac{b_j^{max,i} + s_j^{max}(k) - \delta s_j^{-max}(k) - s_j(k)}{s_j^{max}(k) - s_j^{min}(k)} \right]^{-\mu} \cdot \left[\frac{- b_j^{min,i} + s_j^{min}(k) + \delta s_j^{-min}(k) - s_j(k)}{s_j^{max}(k) - s_j^{min}(k)} \right]^{-\nu} \quad (16)$$

where $\delta s_j^{-max}(k)$ and $\delta s_j^{-min}(k)$ are as in (13) and $b_j^{max,i}$ and $b_j^{min,i}$ are determined as follows:

$$b_j^{max,i} = \begin{cases} b_j \text{ , if there is no constraint violation,} \\ x^i + b_j \text{, if the constraint is violated by an amount } x^i \end{cases} \quad (17)$$

and similarly for $b_j^{min,i}$.

According to the above procedure, when there are constraint violations, the barrier function is broadened to include the storage trajectory, with the boundaries placed a distance b_j from it. Due to the associated high costs, the controller gradually brings the storage within the feasible region. Afterwards, the barrier function boundaries are placed a distance b_j from the upper and lower storage bounds and the procedure converges. Parameter b_j can be determined by preliminary experimentation or it can be adaptively adjusted

by inspecting the limiting trajectories and increasing or lowering its value so as to make the constraints barely binding. Toward this end, the following simple scheme was seen to work reliably: If the limiting storage is at a distance Δx_j from its bound (Δx_j is positive when storage does not violate the constraint and negative if it does), replace b_j with $b_j + \Delta x_j$ and continue the iterations until convergence; in a few such cycles the scheme will converge at the optimal sequences. In fact, the appropriate b_j value depends on the scaling coefficient C. This coefficient should be selected so that the flat segment of the barrier function is negligible with respect to the other terms in the performance index.

As it will be seen from the case study presented, this approach is reliable and efficient and facilitates simultaneous treatment of release and storage constraints, improving the overall ELQG efficiency.

5. CASE STUDY

The Savannah river system (Figure 2) originates in the North Carolina Blue Ridge mountains and flows in a south-easterly direction toward the Atlantic Ocean along the Georgia - South Carolina border. Since the Colonial times, the river has played an instrumental role in the development of the basin's economy, which is primarily agricultural in the north and industrial in the south. The many economic and social benefits together with the severe flood risks have brought about several river control and utilization projects, the most notable of which are the Hartwell, R.B. Russell, and Clark Hill storage projects and an eleven-mile levee around the city of Augusta. Table 1 summarizes some relevant characteristics of the above-mentioned reservoirs which are owned and operated by the U.S. Army Corps of Engineers. This as well as all other hydrologic or operational data used here was compiled from the Savannah River Basin reservoir regulation manual (U.S. Army Corps of Engineers, 1974) or from personal communications with the engineers of the Savannah District.

The primal objectives of the Savannah reservoirs are to generate energy, provide flood control, and facilitate navigation. The power production functions, included in Appendix A, were determined via nonlinear regression analysis on the power plant turbine characteristic curves; namely, the curves relating power production to turbine discharge and net hydraulic head, the latter being the difference between the forebay and tailwater elevations less various hydraulic losses. In the case of the Hartwell and Russell projects, the net hydraulic head, and consequently the power functions, also depend upon the downstream reservoir's storage value. The estimated functions exhibit sufficient accuracy over all of the turbine operational range. The standard

deviation of the fitted values from the actual ones is within (0.3 - 0.5) MW for all projects.

Flood-damage studies conducted by the Corps of Engineers have estimated the highest harmless release from Clark Hill to be about 20,000 cfs. In the interest of navigation, this release should not be less than 6,000 cfs. Figure 4 displays the weekly distribution of net reservoir inflows and typical energy production targets. The three lines on the inflow graphs delineate the mean and 97.5% confidence band levels. Clearly, the probability distributions of these inputs are skewed.

Figure 5 presents a typical ELQG control experiment with the Savannah system. This figure has two sets of plots. The top plots display the identified optimal release rules; the bottom plots delineate the associated storage trajectories. Except for mean values, the storage plots also include the 97.5% and 2.5% probability limits. Release and storage boundaries are indicated by dashed lines. In this experiment, the initial storage values were 111, 44, and 109 billion cubic feet respectively for Lakes 1 (Hartwell), 2 (Russell), and 3 (Clark Hill), and the control horizon was equal to 10 weeks. The figure shows the optimal sequences when no storage bounds are taken into account. These sequences basically satisfy the energy generation requirements shown on Figure 4. In fact, energy generation from Clark Hill exceeds the required amount due to the more stringent navigation release. In this experiment, the storage probability distributions were approximated by three parameter lognormal density functions preserving the three first statistical central moments as discussed in Section 3. ELQG converges to these trajectories in 4 to 5 iterations using approximately 5 seconds of CPU time on a Cyber 180/990 computer system. The storage trajectories indicate that if

this release policy is adopted, there is high chance that Lakes 1 and 3 will exceed their capacity.

The second control experiment is intended to evaluate the effectiveness of the proposed new barrier function method for reliability constraints. The procedure in Section 3 was implemented with $\mu = 1$, $\nu = 1$, and $C = 10^6$. ElQG iterations started from the sequences portayed on Figure 5 and converged to the ones shown on Figure 6. Convergence was completed in 8 iterations and required approximately 11.6 CPU seconds. Table 2 reports some iteration characteristics: W_i is a convergence index (see, Georgakakos and Marks, 1987, for a rigorous definition) reflecting the magnitude of the optimization direction. Small W_i values signify convergence. "Reliability Constraint Violations" is the cumulative violation amount for each reservoir. Lastly, "Energy Generation" reports the expected energy production associated with the nominal sequences of a certain iteration. As indicated by these results, ELQG demonstrates impressive efficiency and accounts for both release and storage constraints in very few iterations. By comparison, usage of the penalty function method would require at least 6 to 7 cycles of 4 to 5 iterations for convergence to the same solution. These computational savings are important, especially when one considers implementing the control scheme on microcomputers.

The above experiments are typical of the ELQG control of the Savannah reservoirs: In the absence of flood or drought conditions, the system is operated to meet the energy requirements; otherwise, the priority is shifted to the flood or drought objectives.

To quantify the average system performance under ELQG control, we run a simulation experiment. The basis of this experiment was 100 years of

synthetically generated weekly flows assumed to have lognormal probability distributions with historically estimated means and variances. The ELQG control algorithm was implemented with a ten-week control horizon and tolerance levels equal to 2.5% for all reliability constraints. Figure 7 depicts the mean values and the (2.5%-97.5%) probability bands of the simulated storages, releases, and energy generation for all three lakes. Some remarks are now noted:

1. Under the stated hydrologic conditions and power commitments, the system reservoirs consistently undergo stressful periods where storages approach capacity values and higher flood risks. During these periods, the variability of releases and energy generation increases.

2. When the reservoirs are not stressed, they are basically operated to satisfy the energy requirements. The variability of these releases and energy generation is minimal.

3. The release and storage plots indicate that the occurrence of constraint violations is consistent with and can be controlled by ELQG's probability tolerance levels. This result validates the developments in Section 3 whereby the approximation of the storage probability densities is based upon the first three statistical moments. If this approximation was based only on the mean and variance, given the distinctly skewed nature of the inputs, the upper constraint violations would exceed 2.5% while lower constraints would be reversely affected.

6. CONCLUSION

This work was concerned with two extensions of the ELQG reservoir control method: ELQG was enhanced to better handle nongaussian disturbances and storage constraints by considering higher order statistical moments and using a new barrier function method. These extensions were evaluated through control and simulation experiments with the Savannah river system. The results indicate that the extensions significantly improve the method's efficiency and facilitate its implementation on microcomputers.

REFERENCES

Georgakakos, A.P., and Marks, D.H., "A New Method for the Real Time Operation of Reservoir Systems," Water Resources Research, Vol. 23, No. 7, pg. 1376-1390, 1987.

Luenberger, D.G., "Introduction to Linear and Nonlinear Programming", Adison Wesley, 1973.

A P P E N D I X A

This appendix summarizes some information pertinent to the control of the reservoirs in the Savannah system.

1. **Hartwell**

Elevation vs Storage Relationship:

$h = e^{a_3} \; e^{a_1 s} \; s^{a_2}$

$a_3 = 0.55442029 \times 10^{+1}$

$a_1 = 0.19146204 \times 10^{-8}$

$a_2 = 0.63936589 \times 10^{-1}$

h: elevation (feet), s: storage (acre-ft).

Tailwater curve:

$t = e^{a_5} \; e^{a_1 u} \; u^{a_2} \; e^{a_3 h} \; h^{a_4}$

$a_5 = 0.53414559 \times 10^{+2}$

$a_1 = 0.10725323 \times 10^{-2}$

$a_2 = -0.24835179 \times 10^{-2}$

$a_3 = 0.37710725$

$a_4 = -0.17473616 \times 10^{+2}$

t: tailwater elevation (feet/10),

u: discharge (cfs/10000),

h: Russell elevation (feet/10).

Power: (5 turbines)

$P = e^{a_5} \; e^{a_1 u} \; u^{a_2} \; e^{a_3 h} \; h^{a_4}$

$a_5 = -0.61888698 \times 10^{+1}$

$a_1 = -0.11294264 \times 10^{-1}$

$a_2 = 0.16704826 \times 10^{+1}$

$a_3 = -0.58959841 \times 10^{-1}$

$a_4 = 0.19092384 \times 10^{+1}$

P: power (MW),

u: turbine discharge (cfs/100),

h: net head (feet/10).

2. **Russell**

Elevation vs Storage Relationship:

$h = e^{a_3} \; e^{a_1 s} \; s^{a_2}$

$a_3 = 0.51836143 \times 10^{+1}$

$a_1 = 0.10965342 \times 10^{-7}$

$a_2 = 0.69968157 \times 10^{-1}$

h: elevation (feet), s: storage (acre-ft).

Tailwater curve:

$t = e^{a_5} \; e^{a_1 u} \; u^{a_2} \; e^{a_3 h} \; h^{a_4}$

$a_5 = 0.12830082 \times 10^{+2}$

$a_1 = 0.11389940 \times 10^{-2}$

$a_2 = -0.30287137 \times 10^{-2}$

$a_3 = 0.14865647$

$a_4 = -0.40729693 \times 10^{+1}$

t: tailwater elevation (feet/10),

u: discharge (cfs/10000),

h: Clark Hill elevation (feet/10).

Power: (4 turbines)

$P = e^{a_7} \; e^{(a_1 u + a_2 u^3)} \; u^{a_3} \; u^{a_4 \, \ln u} \; u^{a_5 (\ln u)^2} \; h^{a_6}$

$a_7 = 0.44967871 \times 10^{+3}$

$a_1 = 0.38391504 \times 10^{+1}$

$a_2 = -0.16952332 \times 10^{-4}$

$a_3 = -0.46174283 \times 10^{+3}$

$a_4 = 0.15797048 \times 10^{+3}$

$a_5 = -0.20876873 \times 10^{+2}$

$a_6 = 0.11538901 \times 10^{+1}$

P: power (MW),

u: turbine discharge (cfs/100),

h: net head (feet/10).

3. **Clark Hill**

Elevation vs Storage Relationship:

$h = e^{a_5} \; e^{a_1 s} \; s^{a_2} \; s^{a_3 \, \ln s} \; s^{a_4 (\ln s)^2}$

$a_5 = 0.48770600 \times 10^{+2}$

$a_1 = 0.45747061 \times 10^{-3}$

$a_2 = -0.19238983 \times 10^{+2}$

$a_3 = 0.28889917 \times 10^{+1}$

$a_4 = -0.14707181$

h: elevation (feet), s: storage (acre-ft/1000).

Tailwater curve:

$t = e^{a_3} \; e^{a_1 u} \; u^{a_2}$

$a_3 = 0.29012214 \times 10^{+1}$

$a_1 = 0.12456147 \times 10^{-2}$

$a_2 = 0.46835476 \times 10^{-1}$

t: tailwater elevation (feet/10),

u: discharge (cfs/10000),

Power: (7 turbines)

$P = e^{a_5} \; e^{a_1 u} \; u^{a_2} \; e^{a_3 h} \; h^{a_4}$

$a_5 = -0.66354710 \times 10^{+1}$

$a_1 = -0.16620056 \times 10^{-1}$

$a_2 = 0.16010340 \times 10^{+1}$

$a_3 = -0.11566747$

$a_4 = 0.25655811 \times 10^{+1}$

P: power (MW),

u: turbine discharge (cfs/100),

h: net head (feet/10).

Table 1: Some Data on the Savannah Reservoirs

	Hartwell	Russell	Clark Hill
Year Completed:	1962	1984	1953
Drainage Basin: (sq. mi.)	2088	802	3254
Dead Storage: (10^9 ft^3)	49.401	39.177	63.815
Storage Capacity: (10^9 ft^3)	123.830	50.798	126.324
Hydropower Capacity: (MW)	4x66+1x80=344	4x75=300	7x40=280

Table 2: ELQG Control Experiment - Performance Evaluation

Iteration #	W_i 10^9 ft^3	Reliability Constraint Violations (10^9 ft^3) H	R	C	Energy Generation MWH
1	33.5	39.9	3.1	186.3	284,447.
2	62.5	19.1	3.5	48.6	365,979.
3	16.2	9.8	4.0	4.8	379,593.
4	9.9	0.2	0.6	0.4	392,435.
5	2.8	0.0	0.1	0.0	393,159.
6	0.5	0.0	0.0	0.0	393,189.
7	0.07	0.0	0.0	0.0	393,193.
8	0.0005	0.0	0.0	0.0	393,193.

CPU Time: 11.6 seconds - Cyber 180/990

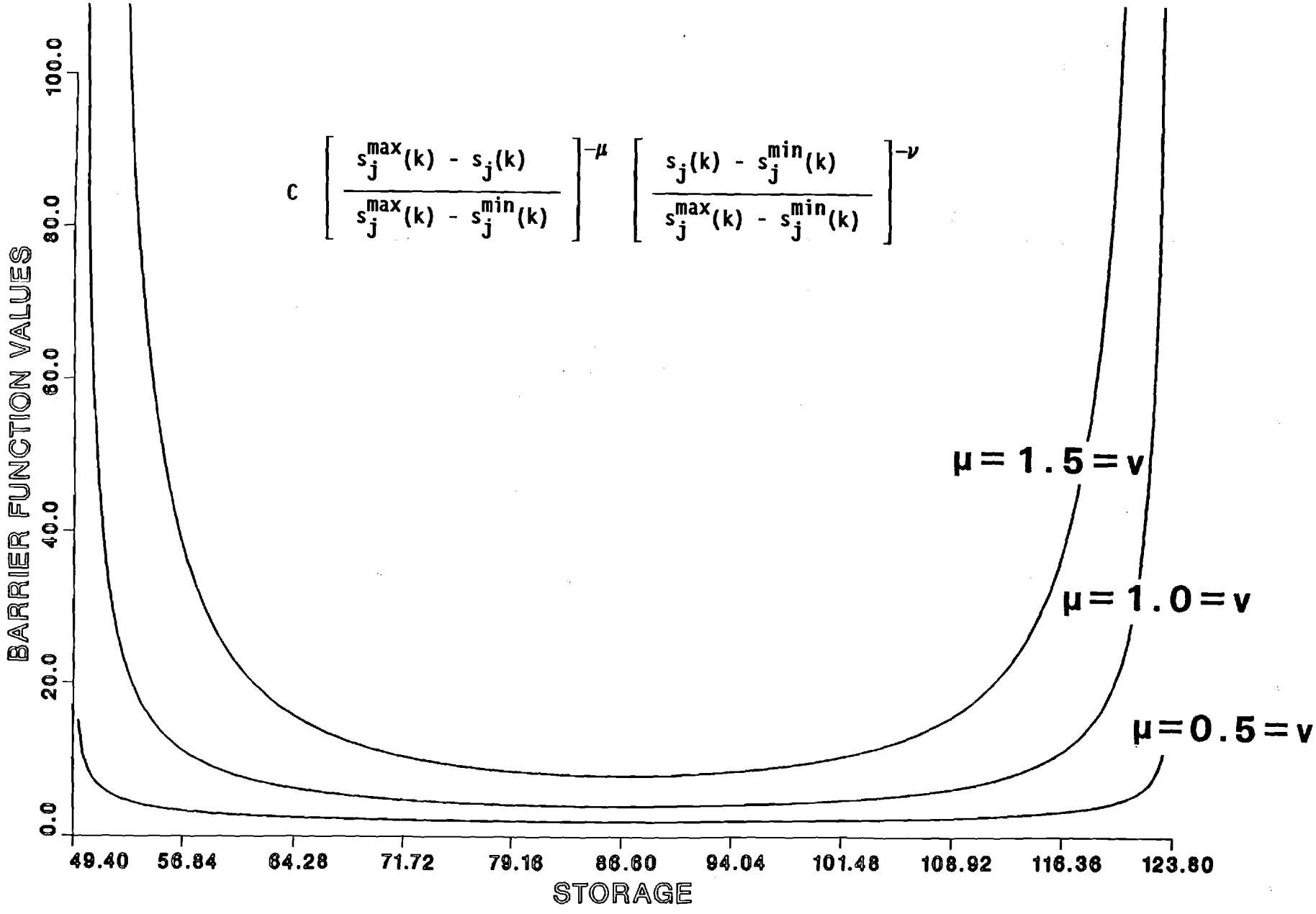

Figure 1: A Barrier Function Method For Storage Constraints

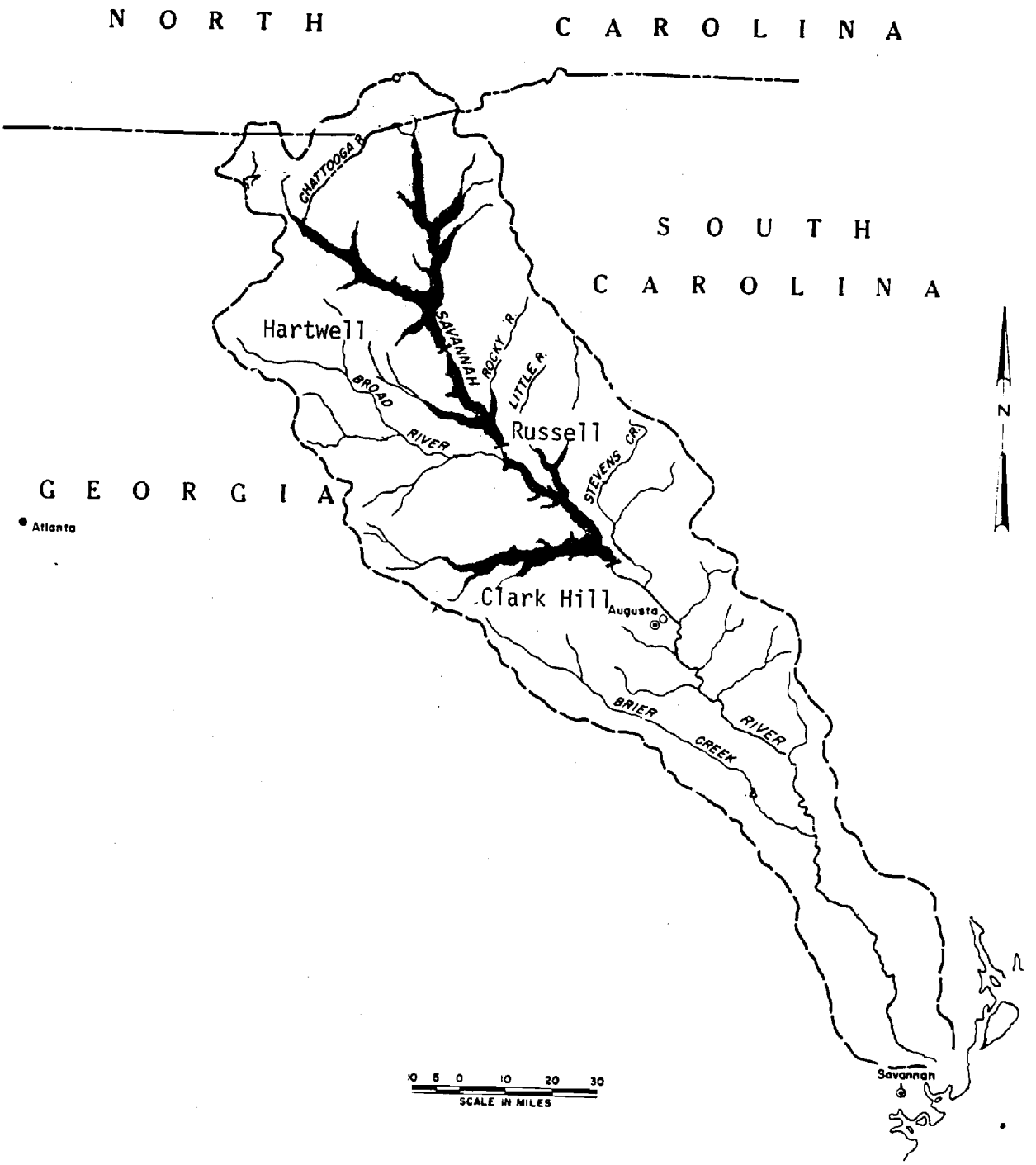

Figure 2: The Savannah River System

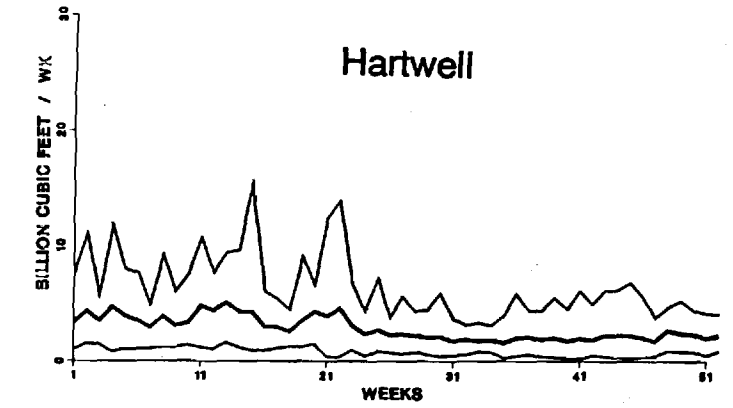

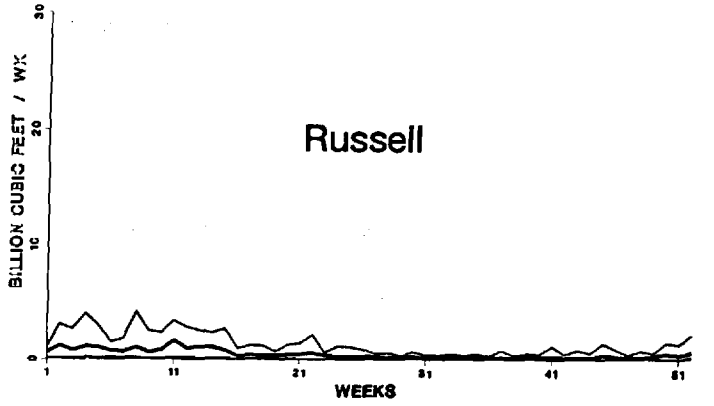

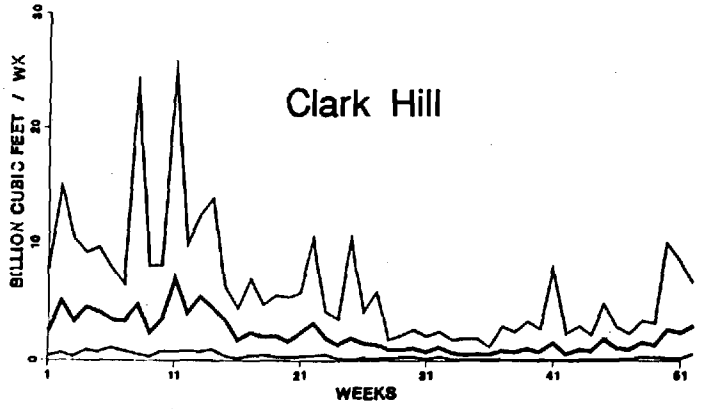

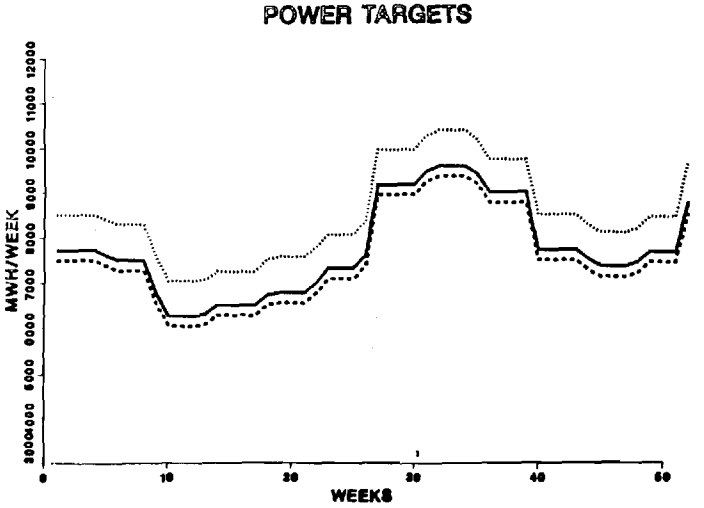

Figure 3: Inflow and Energy Target Distribution

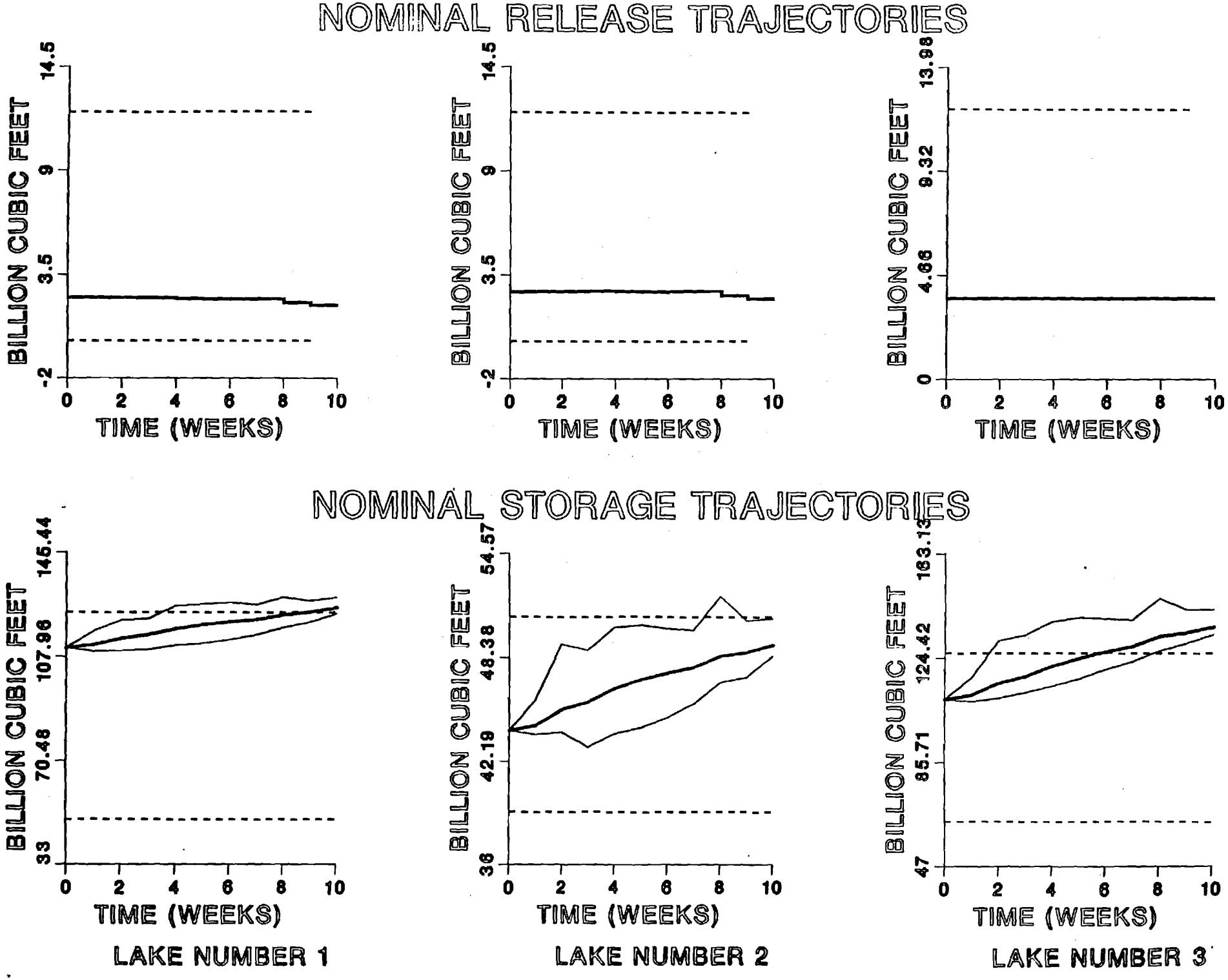

Figure 4: FLOC Control Without Storage C...

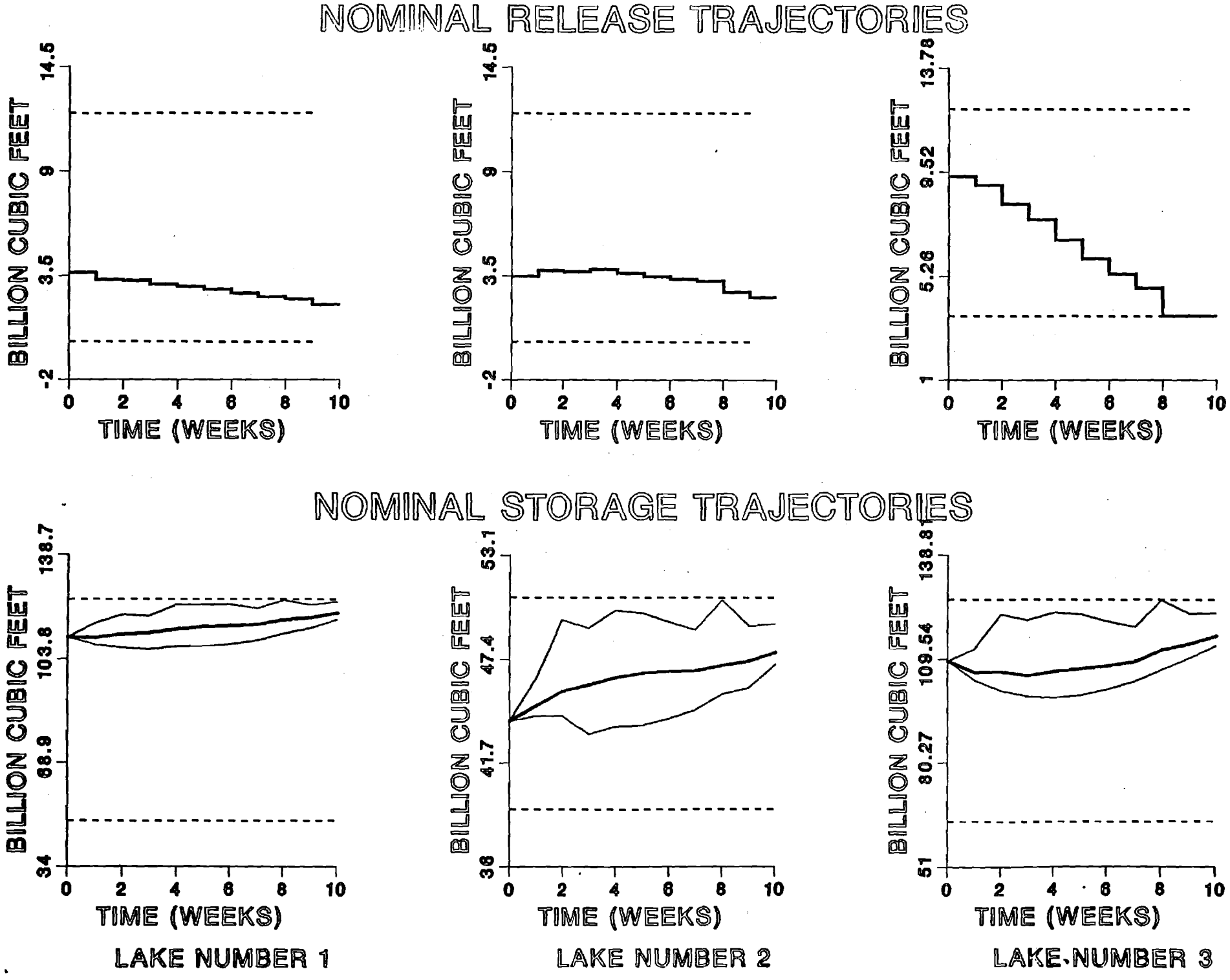

Figure 5: FLOC Control With Storage C

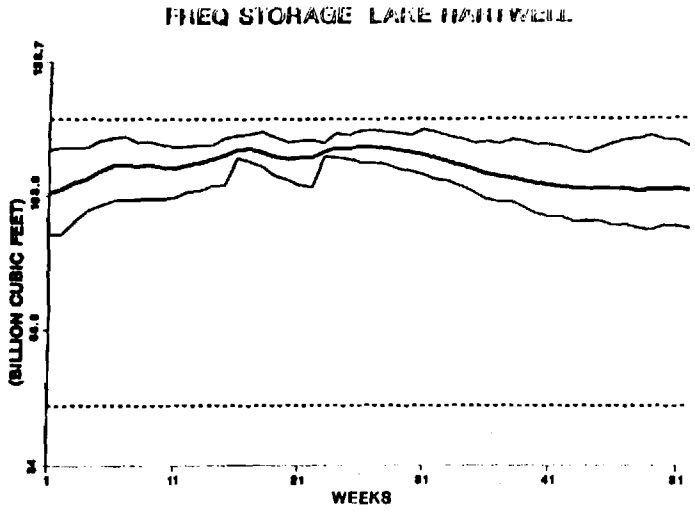

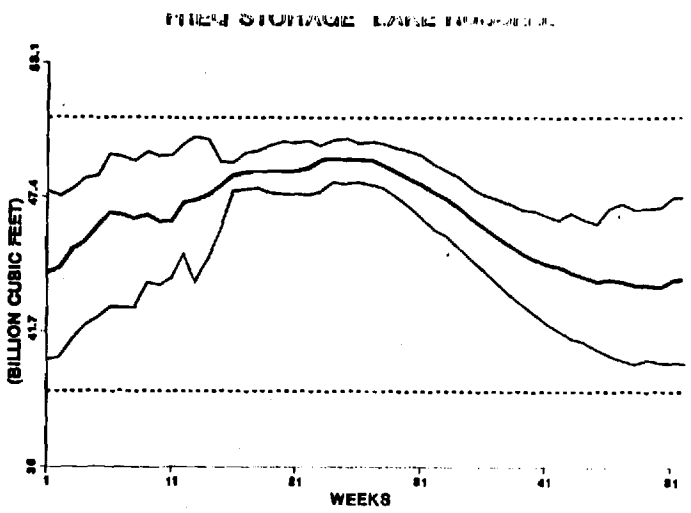

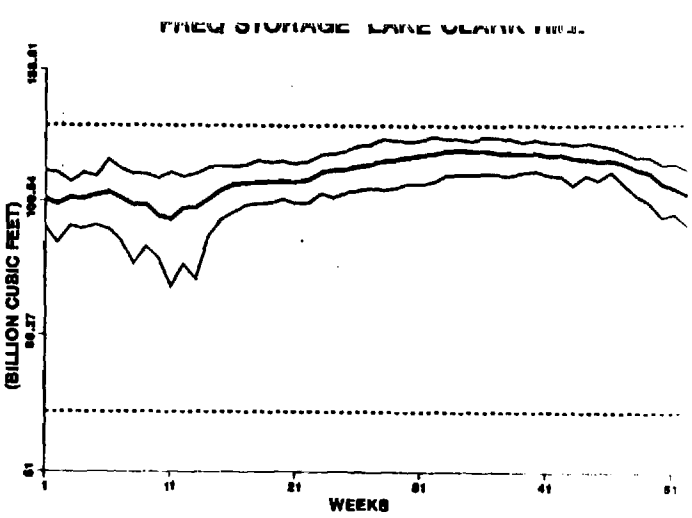

FREQ RELEASE LAKE HARTWELL

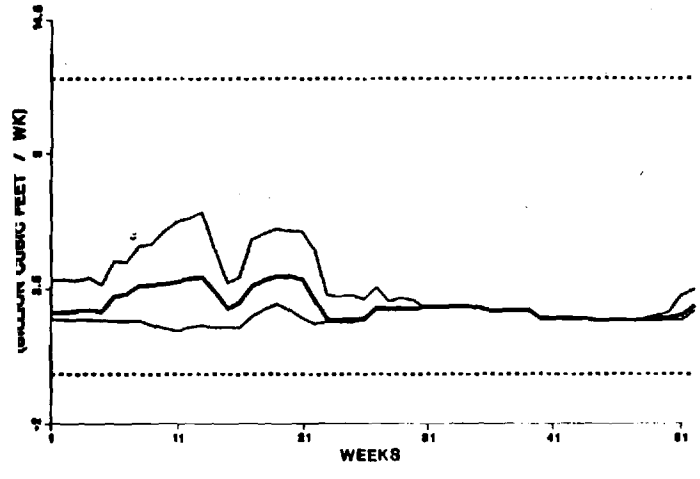

FREQ RELEASE LAKE RUSSELL

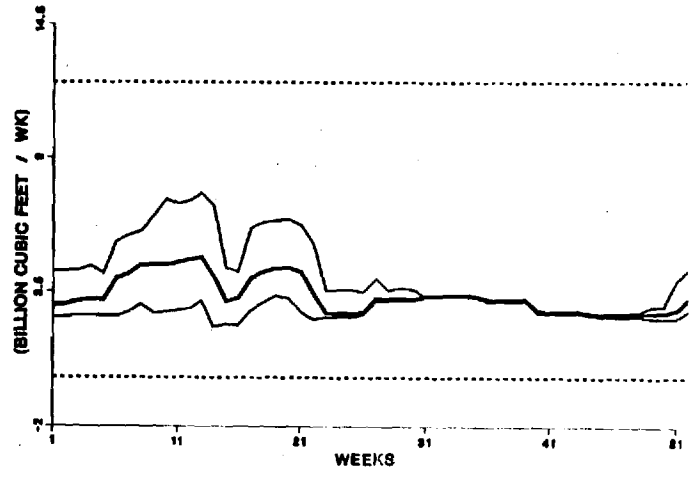

FREQ RELEASE LAKE CLARK HILL

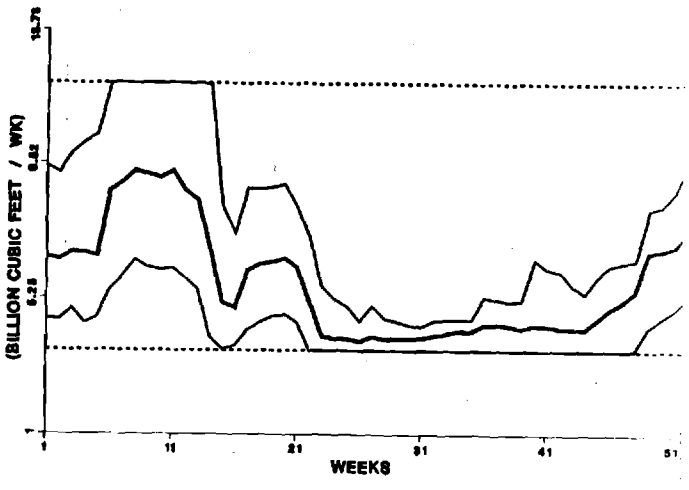

FREQ POWER LAKE HARTWELL

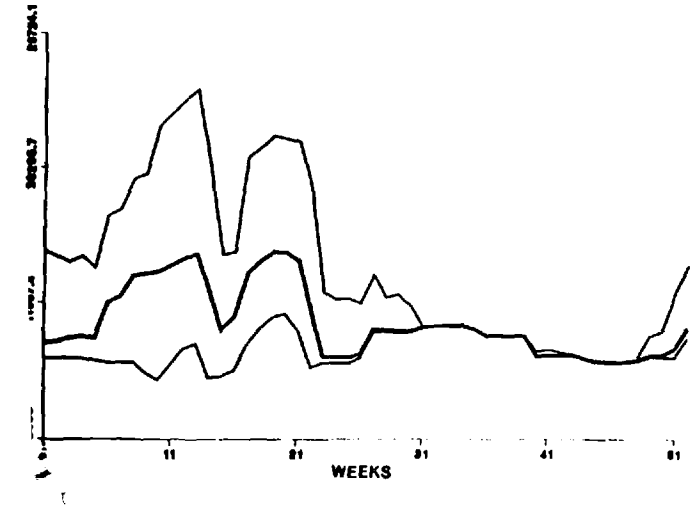

FREQ POWER LAKE RUSSELL

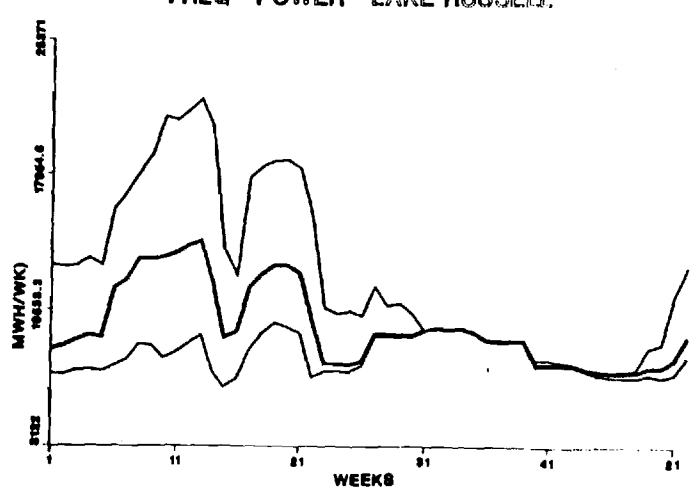

FREQ POWER LAKE CLARK HILL

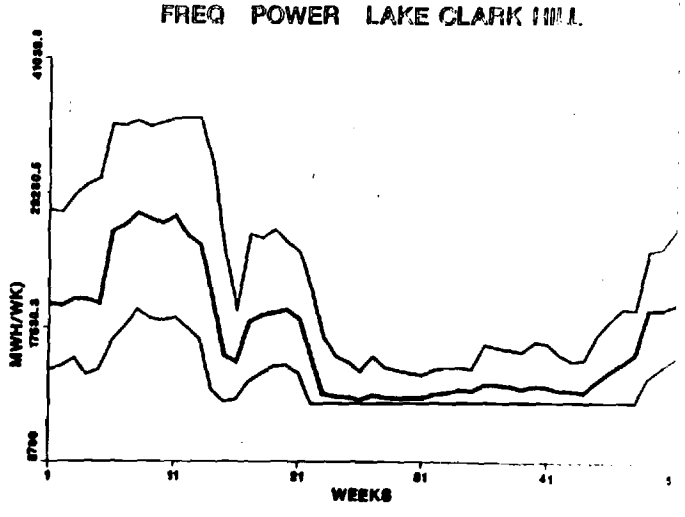

E-20-G 14

OPTIMAL REAL-TIME FORECASTING AND CONTROL OF RESERVOIR HYDROSYSTEMS USING REMOTE AND ON-SITE SENSORS

VOLUME II: RESERVOIR CONTROL

by

Aris P. Georgakakos

Assistant Professor

FINAL REPORT

United States Geological Survey
Grant No. 14-08-0001-G1297

August 1989

School of Civil Engineering
Georgia Institute of Technology
Atlanta, Georgia 30332

OPTIMAL REAL-TIME FORECASTING AND CONTROL OF RESERVOIR HYDROSYSTEMS USING REMOTE AND ON-SITE SENSORS
VOLUME II: RESERVOIR CONTROL

by

Aris P. Georgakakos
Assistant Professor

FINAL REPORT

United States Geological Survey
Grant No. 14-08-0001-G1297

School of Civil Engineering
Georgia Institute of Technology
Atlanta, Georgia 30332

August 1989

FOREWORD

This final report summarizes the second research phase performed with sponsorship of the United States Geological Survey, Water Resources research Act of 1984, under Grant No. 14-08-0001-G1297. The first phase was performed by the University of Iowa, Department of Civil and Environmental Engineering and Iowa Institute of Hydraulic Research, and it is summarized as a separate document (Georgakakos, K.P., T. H. Lee, and H. Shen, *Optimal Real-Time Forecasting and Control of Reservoir Hydrosystems Using Remote and On-Site Sensors, Volume I*, August 1989).

The author is grateful to Frank Coley and Robert Robinson of USGS, Reston, Virginia, for their administrative and technical advice throughout the two year project tenure. The author would also like to thank the staff of the Savannah district office of the U.S. Army Corps of Engineers and Mr. Marvin Meeks of Georgia Power for providing the data and insightful discussions for the Savannah River system and the LLoyd Shoals case studies.

The research work reported in Chapter 6 was also supported by Georgia Power Company, Research Project POE-06608.

DISCLAIMER

The contents of this report were developed under a grant from the Department of the Interior, U.S. Geological Survey. However, those contents do not necessarily represent the policy of that agency, and you should not assume endorsement by the Federal Government.

Table of Contents

Table of Contents Cont'd

Table of Contents Cont'd

List of Figures

List of Figures Cont'd — Page

List of Figures Cont'd — Page

List of Figures Cont'd Page

List of Tables Page

1. INTRODUCTION

Reservoir systems (Figure 1.1) are large scale projects with a variety of vital benefits (e.g., energy generation, municipal, industrial, and agricultural water supply, recreation, navigation, and fish conservation) as well as severe flood and drought risks. Fulfilling these objectives critically depends upon the successful management of the naturally uncertain river flows—a task which is quite complex. Although the need for combining mathematical models with the ever-growing computer technology in the reservoir operation process has long been recognized by both researchers and practitioners (see Proceedings of the National Workshop on Reservoir Systems Operations, Colorado, 1979), current practices are still primarily based on heuristic rules. The reasons are partially due to the problem's resilient difficulty and partially due to the existing communication gap between researchers and reservoir system managers. Practical engineering experience is necessary in all cases but will suffice alone only in few relatively simple systems. In the majority of cases, the decision making process can greatly benefit from hydrometeorological as well as operations research advances.

Hydrometeorological models are employed to forecast reservoir inflows based on real-time measurements of meteorological and hydrological variables (including temperature, pressure, mean areal precipitation, and streamflow discharge). Inflow forecasts are subsequently utilized by operations research (control) models to determine reservoir release sequences which optimize the tradeoff between the various system objectives. In general, the more accurate and extended the inflow forecasts, the better the control policies and the more effective the system utilization.

The goal of the project entitled *Optimal Real-Time Forecasting and Control of Reservoir Hydrosystems Using Remote and On-site Sensors* (U.S.G.S. Grant No. 14-08-0001-G1297) was to advance the state of the art in the aforementioned reservoir system management areas. Improvements in hydrometeorological forecasting models was the research subject of the University of Iowa project team and are discussed in Part I of the final report. Advances in optimal real-time control methods were researched by the Georgia Institute of Technology project team and are summarized in the present Part II volume.

This report includes eight chapters and four appendices. The research objectives are outlined in Chapter 2. Chapter 3 summarizes the research developments and the resulted products (publications and computer programs). Chapters 4, 5, 6, 7, and Appendix B describe the work performed by research objective. The report concludes with Chapter 8 which reviews the main research findings and provides recommendations for further study. Appendices A, C, and D include supplementary material pertaining to Chapter 4 and Appendix B.

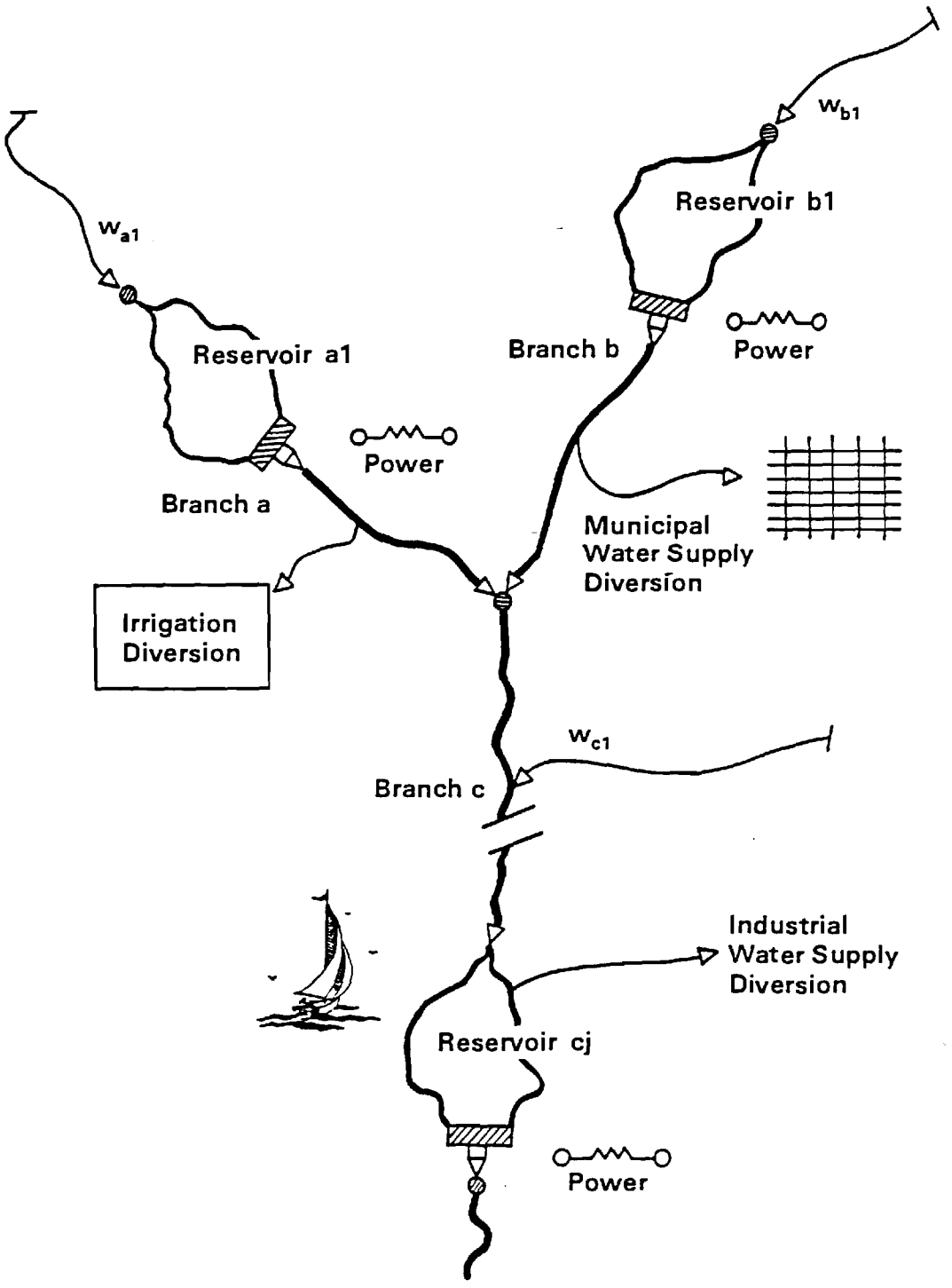

Figure 1.1: A Typical Reservoir System

2. BACKGROUND AND RESEARCH OBJECTIVES

2.1 Background

Over the years, reservoir system management has benefited from many Operations Research advances, and, conversely, reservoir management problems have motivated and continue to motivate advances in Operations Research. Yeh [1982, 1985] offers comprehensive surveys of reservoir control models. From a practical standpoint, the most relevant stochastic reservoir control models are based on Linear and Dynamic Programming.

Linear Programming (LP) models considering uncertainty are the Chance Constraint Programming [Revelle et al., 1969, Joeres et al., 1971, Eisel, 1972] and the Reliability Programming models (Colorni and Fronza, 1976, Simonovic and Marino, 1980, 1982, Marino and Mohamadi, 1983]. Mainly due to their simplified system representation, LP models are considered appropriate for design studies rather than for operation purposes [Loucks, 1970, Loucks and Dorfman, 1975].

Dynamic Programming models can further be distinguished as implicitly or explicitly stochastic models. Representative members of the first class are the models by Young, 1967, and Croley, 1974. Their approach consists of substituting the stochastic problem for a set of deterministic control problems corresponding to different synthetic inflow process realizations. The optimal releases resulting from the solution of these problems are regressed against selected system variables [Young, 1967] or fitted to probability density functions [Croley, 1974]. In the first case, the feedback laws are to be applied invariably at each decision time, while in the second, only the upcoming period's mean or mode is applied, and the procedure is sequentially repeated. Between the two, Croley's approach performs the best, yet its computational requirements make it operationally impractical.

The major explicitly stochastic DP model class employs Markov Chain inflow process description and uses Backward Stochastic DP for the solution of the resulting control problem (Schweig and Cole, 1968, Butcher, 1971, Su and Deininger, 1972, 1974, Arunkumar and Yeh, 1973, Alarcon and Marks, 1979, Buchanan and Bras, 1981]. Overall, this approach performs satisfactorily in small systems (e.g., one or two reservoirs); however, its application to multireservoir configurations is computationally prohibited due to "dimensionality" problems [Bellman and Dreyfus, 1962]. It is worth noting that the previous formulations have been extended to account for storage reliability constraints [Askew, 1974a,b, Sniedovich, 1979, 1980a,b] but only for a single reservoir with time-uncorrelated inflows.

Thus, DP models suffer primarily from dimensionality problems stemming from the need to implement the DP solution in discretized form. The

publications by Wasimi and Kitanidis [1983], Loaiciga and Marino [1985], and Georgakakos and Marks [1985 and 1987] introduced methods avoiding this numerical difficulty. Wasimi and Kitanidis [1983] and Loaiciga and Marino [1985] formulated unconstrained linear quadratic gaussian control problems and derived feedback solutions in analytical form. Neither model considers control or storage constraints since such restrictions would exclude analytical solutions. Georgakakos and Marks named their model Extended Linear Quadratic Gaussian (ELQG) control because it is applicable to linear quadratic gaussian (LQG) problems as well as problems with nonlinear dynamics, control and storage reliability constraints, and nonquadratic performance indices. ELQG is a trajectory iteration algorithm which iterates according to the Projected Newton and Penalty Function methods. Each iteration is based on analytically derived optimization directions. Extensive computational experience indicate that the method's computational efficiency is restricted by the handling of storage constraints (Penalty Function method). Furthermore, ELQG is exact only in systems with gaussian inputs.

2.2 Research Objectives

A major research objective was to improve ELQG effectiveness and applicability. Toward this goal, two areas were identified and pursued: (1) development of a methodology to account for nongaussian system inputs and (2) development of a more efficient algorithm for the treatment of storage constraints.

An important reservoir system objective is to optimize hydropower generation scheduling. Thus far, the methods developed have focussed on long term reservoir system management where energy generation can be approximately represented. Application of these techniques in short term hydropower generation scheduling is not straightforward due to several complicating idiosyncracies characterizing hydroelectric facilities. A third major research objective was to develop a control procedure that will handle these idiosyncracies and effectively assist the decision making process.

Usually, short term reservoir system models need to represent the dynamics of the river reaches connecting the system reservoirs. Extensive research experience already exists with the development and calibration of river routing models. However, such models are not directly compatible with the state-space form of the most efficient control methods. Thus, a fourth research objective was to develop a state-space river routing scheme which utilizes the existing research experience and can be combined with the new optimal control advances.

Streamflow forecasting models are generally expected to enhance reservoir operation by providing the foresight for better decision making. Operational streamflow models, however, require real time data

from expensive measurement devices (including rain and streamflow gages, radars, and satellites). Usage of such models is justified if forecast benefits outweigh the associated instrumentation costs. A fifth research objective was to quantify the benefits of forecasting in reservoir operation.

In an effort to close the communication gap between reservoir operation research and practice, a last project objective was to apply the previous developments to real-world systems and encourage their use by system managers and operators.

3. SUMMARY OF WORK

3.1 Project Team

The Georgia Institute of Technology project team consisted of the following individuals: Dr. Aris P. Georgakakos, Principal Investigator, Evangelos A. Baltas, Research Assistant, and Thomas W. Barr, Research Assistant. Mr. Baltas' participation was in the development of the state-space river routing model (Appendix B), while Mr. Barr's contribution was in the application of the new hydropower control method to the Southeastern U.S. reservoir system (Chapter 7).

3.2 Work Summary by Research Area

3.2.1 ELQG Extensions

The ELQG control method [Georgakakos and Marks, 1987] is a stochastic control algorithm for the optimal operation of multiobjective reservoirs. Mathematically, this method optimizes a general functional of a stochastic system in state-space form with upper and lower release constraints and probabilistic storage bounds. ELQG is a sequential algorithm which accounts for stochastic effects by preserving the first two statistical moments of the system inputs and storages. In this work, the method is first extended to handle nongaussian features which frequently characterize reservoir inputs. This extension is based on representing the storage probability densities by utilizing as many statistical moments as necessary. Secondly, ELQG's efficiency with respect to reliability storage constraints is evaluated, and a new barrier function method is researched. These modifications are tested in case studies with the Savannah system (three reservoirs) and are shown to improve ELQG efficiency and applicability. Detailed presentation of these developments is offered in Chapter 4.

3.2.2 A New Stochastic Control Method for Hydropower Scheduling

A stochastic control method for the real-time operation of hydropower systems is introduced, evaluated, and implemented. This method finds optimal hydropower schedules by invoking several control levels. The control levels distinguish between peak and off-peak generation periods and seek to maximize energy output during the former while meeting other operational objectives as constraints. Each control level is further decomposed into dynamic and static modules. The dynamic module accepts turbine discharge rates from the static module and utilizes probabilistic inflow forecasts with stochastic control techniques to determine optimal power generation schedules. The static module regulates each turbine to generate power at best efficiency or some specified output. The new method is applied to a real-world system and

is found to be reliable and computationally efficient. The simulation results indicate that the hydropower and economic gains from using such techniques in real-time reservoir management can be substantial. This method is discussed in Chapters 6 and 7.

3.2.3 A State Space Model for River Routing

In this part, a state-space formulation of the Muskingum-Cunge routing scheme is proposed. The state-space formulation utilizes real-time discharge measurements, accounts for modeling and observation errors, and allows real-time updating through a Kalman filter estimator. The new model is tested in two different geotechnical conditions to forecast six-hour discharge values in hypothetical channels. For realism, the geomorphologic characteristics of these case studies are determined based on the Regime theory. The model results are compared to those from DWOPER, a field-tested numerical dynamic routing model, and validate the usefulness of this approach. A comprehensive discussion of this model is provided in Appendix B.

3.2.4 The Value of Streamflow Forecasting in Reservoir Operation

The value of streamflow forecasts in reservoir operation depends on a number of factors and cannot be generally quantified. Assessment of forecast benefits is presented here for two specific systems. The first is the Savannah three-reservoir system, and the other consists of a single reservoir in the state of Georgia. Probabilistic streamflow models of increasing forecasting ability are coupled with the ELQG stochastic control method in extensive simulation experiments. The system performance is statistically evaluated with regard to energy generation and flood and drought prevention. This analysis indicates that forecast benefits are quite substantial yet system specific. Discussions of these results are included in Chapters 5 and 6.

3.2.5 Communication of Research Advances to Practicing Engineers

The aforementioned research advances are of interest to reservoir system managers and practicing engineers. In an effort to encourage their use in the decision making process, a number of agencies and electrical utilities were contacted and familiarized with the new developments. The U.S. Army Corps of Engineers and Georgia Power Company have already expressed explicit interest and support by sponsoring research projects for adapting these techniques to selected hydropower systems. Apart from seminar presentations to potentially interested agencies and companies, information dissemination has already begun and will continue through journal, conference, and technical report publications.

3.3 Products

3.3.1 Journal Publications

Georgakakos, A. P., "Extended Linear Quadratic Gaussian (ELQG) Control: Further Extensions", accepted for publication, *Water Resources Research*, Vol. 25, No. 2, pg. 191 - 201, 1989.

Georgakakos, A. P., "The Value of Forecasting in Reservoir Control", in press, *Water Resources Bulletin*, 1989.

Georgakakos, A.P., E. Baltas, and K.P. Georgakakos, "A New State-Space Model for River Routing, under review, *Water Resources Research*, 1989.

Georgakakos, A.P., "A Two-Level Control Method for Hydropower Scheduling," under review, *Water Resources Research*, 1989.

Georgakakos, A.P. and T. Barr, "Optimal Regulation of the Southeastern U.S. Reservoir System", under preparation, to be submitted to *Water Resources Research*, 1989.

3.3.2 Conference Presentations

Georgakakos, A.P., "Optimal Operation of the Savannah River System," *Waterpower '87 Conference of the American Society of Civil Engineers*, Oregon, Aug. 19-21, 1987.

Georgakakos, A.P., "The Value of Forecasting in Reservoir Control," *American Water Resources Association Conference*, Invited, Salt Lake City, Utah, Nov. 1-6, 1987.

Georgakakos, A. P., "Extended Linear Quadratic Gaussian (ELQG) Control: Further Extensions", *American Geophysical Union Meeting*, San Francisco, December 6-11, 1987.

Georgakakos, A. P., and M. Meeks, "Stochastic Control of Hydropower Systems", *ASCE Workshop on Computerized Decision Support Systems for Water Managers*, Fort Collins, Colorado, June 27-29, 1988.

Georgakakos, A. P., "Optimal Control of Water Resources Systems", *Invited Short Course*, University of Lisbon, Portugal, July 25-29, 1988.

Georgakakos, A. P., "Optimal Operation of the Southeastern U.S. Reservoir System," *24th National Conference of the American Water Resources Association*, Invited, Milwaukee, Wisconsin, Nov. 6-11, 1988.

Georgakakos, A. P., "Advances in Integrated Forecasting and Control of Reservoir Systems in Real-Time," *Special Workshop on Real Time Hydrometeorology*, University of Iowa, Iowa City, November 15-16, 1988.

Georgakakos, A. P., and M. Meeks, "Real Time Control of Hydropower Systems", *1989 Georgia Water Resources Conference*, Invited, University of Georgia, Athens, Georgia, May 16-17, 1989.

3.3.3 **Seminar Presentations to Electrical Utilities and Agencies**

Georgakakos, A.P., "Optimal Operation Schemes for Hydropower Systems," Georgia Power Co., December 1, 1986.

Georgakakos A.P., "Optimal Operation of the Savannah River System," Savannah District Office of the U.S. Army Corps of Engineers, September 10, 1987.

Georgakakos A.P., "A Multilevel Control Method for the Savannah River System," Savannah District Office of the U. S. Army Corps of Engineers, November 22, 1988.

Georgakakos, A.P., "Optimal Control of Hydropower Systems," Pacific Gas and Electric Co., San Francisco, December 14, 1988.

3.3.4 **Master Theses**

Baltas, E. A., "A State Space Model for River Routing," School of Civil Engineering, Georgia Institute of Technology, June 1988.

Barr, T. W., "Optimal Regulation of the Southeastern U.S. Reservoir System, School of Civil Engineering, Georgia Institute of Technology, 1989.

3.3.5 **Software**

1. Program for the Real-Time Control of the Lloyd Shoals Hydroelectric Project.
2. Program for the Simulation of the Lloyd Shoals Hydroelectric Project.
3. Program for the Real-Time Control of the Savannah River System.
4. Program for the Simulation of the Savannah River System Operations.
5. Program for the Control of the U.S. Reservoir System.
6. State-Space Model for River Routing.

The first two programs have been developed in a user-friendly form for use by the Georgia Power Company. Programs 3, 4, 5, and 6 are in research form.

4. EXTENDED LINEAR QUADRATIC GAUSSIAN (ELQG) CONTROL: FURTHER EXTENSIONS

4.1 Introduction and Overview

Reservoir management has been the theme of numerous Operations Research applications. The associated problem may be treated by ordinary nonlinear programming methods, but the solution process can greatly benefit by exploiting the system's dynamical nature and employing optimal control techniques. Depending on the modeling assumptions, optimal control problems may be deterministic or stochastic. Deterministic problems are conceptually easier to solve. Stochastic formulations can be more subtle and, in many cases, computationally intractable. Both types can be treated via the main optimal control solution methodologies; namely, the Minimum Principle of Pontryagin [Pontryagin et al., 1962, Kushner and Sshweppe, 1964, Athans and Falb, 1966] and Bellman's Dynamic Programming [Bellman, 1961, Bellman and Dreyfus, 1962, Larson and Casti, 1978, Maybeck, 1982, Ch. 13]. Being an open-loop methodology, the Minimum Principle is more efficient in deterministic cases where open-loop and feedback solutions coincide. Dynamic Programming (D.P.) is conceptually better-suited to stochastic problems where feedback policy solutions are ideally sought. Had it not been for the well-known D.P.'s numerical predicament, this distinction between open-loop and feedback control techniques would have settled the issue of what to use and where. However, feedback solutions are, in most cases, chimerical, and this has spawned a plethora of second generation D.P. adaptations [Larson 1968, Jacobson and Mayne, 1970, Bertsekas, 1976, Ch. 5].

Among others, some open-loop procedures applied to reservoir management can be found in Papageorgiou [1985], Turgeon [1981], Murray and Yakowitz [1979], Jamshidi and Heidari [1977], Larson and Keckler [1969]. Similarly, feedback approaches have been presented in Kitanidis and Foufoula-Georgiou [1987], Loaiciga and Marino [1985], Stedinger et al. [1984], Bras et al. [1983], Alarcon and Marks [1979], Su and Deininger [1972,1974]. Many more reservoir management techniques can be found in a comprehensive review by Yeh [1985].

Extended Linear Quadratic Gaussian (ELQG) control [Georgakakos and Marks, 1987] is a stochastic control method with both open-loop and feedback features. The feedback element results from ELQG's sequential character, suggesting controls which depend on the current system conditions. However, at each decision time these controls are obtained from an open-loop solution process. This process also generates linear approximations of the feedback control laws and uses them to locally simulate the true feedback operation. Thus, ELQG's computational efficiency is comparable to that of the open-loop procedures, while its performance exhibits the feedback nature of the optimal controller, the difference being that only the active neighborhoods of the feedback laws

are generated at each decision time and not the entire functionals. Furthermore, the solution process involves no discretizations.

Extensive computational experience indicated that, although the ELQG method is reliable overall, it is more efficient in handling release rather than storage constraints. Furthermore, the treatment of probabilistic constraints is exact only for Gaussian disturbances. In this paper, ELQG is modified to more effectively handle nongaussian disturbances and storage constraints by taking into account higher order statistical moments and using a new barrier function method. The effectiveness of these extensions is evaluated through control and simulation experiments with the Savannah river system.

4.2 Problem Statement

A typical formulation of a reservoir control problem can be stated as follows:

Find the release sequences $\{u_j(k),\ j=1,\ldots,M,\ k=0,1,\ldots,N\}$ which minimize

$$J = E\left\{ \sum_k \sum_j [P_j(k) - g_j(s_j(k),u_j(k))]^{\alpha} \right\}, \tag{4.1}$$

$j = 1,2,\ldots,M,$
$k = 0,1,2,\ldots,N-1,$

subject to

(a) the system equations,

$$s(k+1) = A(k)s(k) + B(k)u(k) + \Gamma(k)w(k), \tag{4.2}$$

$k = 0,1,2,\ldots,N-1,$
with $s(0)$ known;

(b) the release constraints,

$$u_j^{min}(k) \le u_j(k) \le u_j^{max}(k), \tag{4.3}$$

$j = 1,2,\ldots,M,$
$k = 0,1,2,\ldots,N-1;$ and

(c) the storage reliability constraints,

$$Prob[s_j(k) \le s_j^{min}(k)] \le \gamma_j^{min}(k), \tag{4.4a}$$

$$Prob[s_j(k) \ge s_j^{max}(k)] \le \gamma_j^{max}(k), \tag{4.4b}$$

$j = 1,2,\ldots,M,$
$k = 0,1,2,\ldots,N.$

In the above formulation, M is the number of reservoirs; N is the end of the control horizon; $P_j(k)$ is the energy target of the j^{th} reservoir during period k; $g_j(s_j(k),u_j(k))$ is the energy generation of

the j^{th} reservoir during period k; $\mathbf{s}_j(k)$ is a vector including the storage of the j^{th} reservoir and that of the downstream one if the latter affects the energy function through the tailwater effect; $u_j(k)$ is the turbine release from reservoir j; α is an even integer (most often equal to 2) to induce convexity of the performance index; $E\{\cdot\}$ denotes the expected value of the quantity in the brackets; $\mathbf{s}(k)$ is the vector of all reservoir storages at the beginning of period k; $\mathbf{u}(k)$ is the vector of all controllable reservoir releases during period k; $\mathbf{w}(k)$ is the vector of all reservoir inflows during period k; $\mathbf{A}(k)$, $\mathbf{B}(k)$, $\mathbf{\Gamma}(k)$ are matrices with elements determined by the system's water budget relationships; $u_j^{min}(k)$, $u_j^{max}(k)$ are lower and upper release bounds; $s_j^{min}(k)$, $s_j^{max}(k)$ are lower and upper storage bounds; and $\gamma_j^{min}(k)$, $\gamma_j^{max}(k)$ are tolerance levels reflective of the reservoir manager's risk attitude.

4.3 Extended Linear Quadratic Gaussian (ELQG) Control

ELQG [Georgakakos and Marks, 1987] is a control method which solves the previous problem in the following manner: First, it invokes a streamflow forecasting model—which may be physically based or statistical—to produce probabilistic forecasts of the upcoming reservoir inputs. These forecasts together with a nominal release sequence are then converted into probabilistic forecasts of the system storages through Equations (4.2). Nominal release and probabilistic storage sequences become input to the controller which checks whether they violate any release or storage bounds and whether the performance index has any improvement margin. If any improvement is possible, the controller analytically generates constrained gradient vectors and hessian matrices and suggests new nominal release sequences according to the projected Newton and penalty function methods and the Armijo stepsize selection rule. The iterations continue until no further improvement of the performance index is possible, generally implying the identification of a locally optimal sequence; however, under convexity conditions, which can usually be induced in the formulation of the control problem, this sequence also constitutes a globally optimal solution. At that point, the first period's optimal releases are implemented, and this process is repeated at the next decision time. ELQG is computationally an open-loop control method, because it sequentially solves the open-loop control problem formulated above; yet, due to its sequential nature, the method suggests releases which are functions of all current system conditions as in the feedback approaches.

Another comment concerns the specification of probabilistic versus deterministic release constraints. Problem (4.1–4.4), which is solved at each decision time, includes the latter constraint type; however, due

to the physical storage limitations, these constraints are essentially probabilistic. This results because in the actual operation the undesirable situation where a reservoir storage is about to exceed its capacity is averted by increasing the release to whichever rate is necessary. Thus, the likelihood of a release constraint violation is governed by the probabilistic tolerance level established for the associated storage constraints.

Originally, in the forecasting of future inflows and storages, ELQG utilized information on the first two statistical moments—mean vectors and covariance matrices—and employed a Gaussian representation of the associated probability densities. However, for a number of reasons, these distributions may be asymmetric and usage of only the first two statistical moments may not suffice.

4.4 Nongaussian Statistics

The need for nongaussian considerations arises mainly because, more often than not, streamflows exhibit such behavior. Moreover, in systems modelled by nonlinear dynamical relationships, even with gaussian inflows, the resulting storages deviate from normality. The greater this deviation, the less effective is the handling of reliability constraints (4.4).

Discussing the full estimation of the joint probability density of the system's storages, Georgakakos and Marks [1987] conclude that it is a rather involved task requiring excessive computational overhead even for small size systems. Alternatively, if a number of statistical moments could be computed, this function could be approximated with some other density function preserving these statistics. ELQG was initially designed to account for the storages' mean and covariance and employ a gaussian approximation of their probability density. This approach will now be extended to include higher order statistical moments.

The expected storage trajectory associated with a nominal control sequence

$\{\bar{u}(k),\ k = 0,1,2,\ldots,N-1\}$, can be obtained from dynamical equation (4.2):

$$\bar{s}(k+1) = A(k)\bar{s}(k) + B(k)\bar{u}(k) + \Gamma(k)\bar{w}(k), \qquad (4.5)$$

where $\bar{s}(k)$ and $\bar{w}(k)$ are the mean storage and inflow vectors and $\bar{s}(0) = s(0)$. Subtracting (4.5) from (4.2), one obtains the equation of the zero mean process:

$$\delta s(k+1) = A(k)\delta s(k) + B(k)\delta u(k) + \Gamma(k)\delta w(k), \qquad (4.6)$$

where $\delta x(k) = x(k) - \bar{x}(k)$ for $x \in \{s,u,w\}$.

Equation (4.6) can be used to generate central statistical moments as

soon as the nature of the release corrections $\delta u(k)$ is defined. These corrections can be storage independent, as in the open-loop optimization procedures, or can be functionally related to the system's storages through feedback laws. Although more complex, the second possibility is also more desirable, because it reduces the spread of the forecasted probability distributions. In the ELQG iterative solution process, the control corrections are related to the system's states through a linear approximation of the true feedback control laws in the neighborhood of the nominal state sequences:

$$\delta u(k) = - D(k) [L(k)\delta s(k) + \Lambda(k)], \quad k = 0,1,2,\ldots,N-1, \tag{4.7}$$

where the control gains $D(k)$, $L(k)$, and $\Lambda(k)$ are obtained analytically [Georgakakos and Marks, 1987]. Matrix $D(k)L(k)$ is the linear mapping of the states on the controls; $\Lambda(k)$ is essential in the iteration process but does not describe the feedback character of $\delta u(k)$. Actually, $\Lambda(k)$ becomes zero at the unconstrained optimal points, while when the controls are binding, they are not related to the states in a feedback manner [Georgakakos and Marks, 1987]. Substituting (4.7) in (4.6) and discarding $\Lambda(k)$, results in

$$\delta s(k+1) = [A(k) - B(k)D(k)L(k)]\delta s(k) + \Gamma(k)\delta w(k), \quad k = 0,1,2,\ldots,N-1. \tag{4.8}$$

Equation (4.8) can now be used in the computation of central moments: Postmultiplying with $[\delta s(k+1)]^T$ and taking expectations leads to the covariance propagation equation:

$$P_S(k+1) = F(k)P_S(k)[F(k)]^T + \Gamma(k)Q(k)[\Gamma(k)]^T \tag{4.9}$$

where $P_S(k) = E\{\delta s(k)[\delta s(k)]^T\}$, $Q(k) = E\{\delta w(k)[\delta w(k)]^T\}$, $F(k) = A(k) - B(k)D(k)L(k)$, and $\delta w(k)$, $k = 0,1,2,\ldots,N-1$, are assumed to be independent random vectors. This assumption is used for consistency with the ELQG derivation of the release corrections and associated control gains; nonetheless, the statistics of these random vectors are determined from forecasting models fully accounting for their dependencies [see, discussion in Georgakakos and Marks, 1987].

Although the results for the third central moment cannot be expressed in a matrix form similar to (4.9), the computations can proceed in much the same way. Consider for instance a three reservoir system whose Equation (4.8) is as follows:

$$x(k+1) = f_{11}(k)x(k) + f_{12}(k)y(k) + f_{13}(k)z(k) + \omega_1(k), \tag{4.10a}$$

$$y(k+1) = f_{21}(k)x(k) + f_{22}(k)y(k) + f_{23}(k)z(k) + \omega_2(k), \tag{4.10b}$$

$$z(k+1) = f_{31}(k)x(k) + f_{32}(k)y(k) + f_{33}(k)z(k) + \omega_3(k), \tag{4.10c}$$

where $x(k) = \delta s_1(k)$, $y(k) = \delta s_2(k)$, $z(k) = \delta s_3(k)$, and $\omega_j(k) = \delta w_j(k)$. Raising each one of the above equations to the third power and taking

expectations yields the following result:

$$E\{x^3(k+1)\} = f_{11}^3 E\{x^3\} + f_{12}^3 E\{y^3\} + f_{13}^3 E\{z^3\} + E\{\omega_1^3\}$$
$$+ 3f_{11}^2 f_{12} E\{x^2y\} + 3f_{12}^2 f_{11} E\{y^2x\} + 3f_{11}^2 f_{13} E\{x^2z\} + 3f_{13}^2 f_{11} E\{z^2x\}$$
$$+ 3f_{12}^2 f_{13} E\{y^2z\} + 3f_{13}^2 f_{12} E\{z^2y\} + 6f_{11} f_{12} f_{13} E\{xyz\}, \qquad (4.11)$$

where the time dependence of the terms in the right side of (4.11) has been dropped for notational convenience. (Similar equations can also be derived for $E\{y^3(k+1)\}$ and $E\{z^3(k+1)\}$.) As can be seen from (4.11), each storage's skewness at time $k+1$ depends not only on every storage and inflow skewness at the previous time k but also on all other third order central moments of the storage variables. Despite the assumed inflow independence, these moments do not vanish because of the interelationhips introduced through equation (4.7). However, these third order moments may also be recursively propagated in the same fashion by means of Equations (4.10).

Although utilizing third moment information will suffice in most cases, fourth or higher order statistical moments may also be determined by similar considerations.

Having the mean, variance, and skewness of the storage variables at each time k, the storage distribution may be approximated by a suitable probability law. Then, probabilistic constraints (4.4) can be inverted into constraints on each expected storage:

$$\xi_j^{min}(k) \le \bar{s}_j(k) \le \xi_j^{max}(k), \qquad (4.12)$$
$$j = 1,2,\ldots,M,$$

where $\xi_j^{min}(k)$ and $\xi_j^{max}(k)$ are the mean storage levels such that

$$Prob[s_j(k) \le s_j^{min}(k)] = \gamma_j^{min}(k), \qquad (4.13a)$$

$$Prob[s_j(k) \ge s_j^{max}(k)] = \gamma_j^{max}(k). \qquad (4.13b)$$

By also expressing the performance index in terms of the preserved statistical moments [as discussed in Georgakakos and Marks, 1987], the ELQG control procedure converts problem (4.1 – 4.4) into a deterministic format with a new set of states: the statistical moments of the original storage variables. Subsequently, this problem is solved in an iterative fashion as discussed in the previous section.

Although this extension for nongaussian statistics was discussed in the context of a discrete time problem formulation, it can also be employed when the system is modelled in continuous time. In that case, the propagation of the storage statistical moments can be accomplished

either by the procedure presented here in connection with a discretization scheme [e.g., see Georgakakos and Marks, 1987] or, more directly, by the procedure discussed in Jazwinski [1970, pg. 136–139].

A last remark refers to the advantage in using feedback Equation (4.7) to represent the release corrections. If these corrections were assumed storage independent, both the variance and skewness as well as all higher order moments would grow unbounded and would result in overly conservative operation. Instead, as will be seen in the case study section of this paper, usage of (4.7) makes (4.8) stable, resulting in bounded moments and augmenting the storages' feasible regions (4.12).

4.5 A Barrier Function Method for Reliability Constraints

Extensive ELQG application experience has indicated that the method's computational requirements are largely expended by handling the reliability storage constraints. According to the penalty function method initially used, these constraints are examined at each iteration for possible violations. In the event of a constraint violation at time period k, a quadratic penalty term is added to the performance index:

$$C^i \, [\xi_j^{max}(k) - s_j(k)]^2, \text{ (upper constraint violation)} \qquad (4.14)$$

with $\xi_j^{max}(k)$ being the value of the mean storage where the constraint is just binding (as in Equation (4.12)) and C^i is a penalty coefficient. The problem (4.1-4.3) is then resolved, the storage constraints reexamined, and the proper penalty terms added with a new coefficient $C^{i+1} > C^i$. The increment rate of this coefficient is a matter of experimentation and is crucial to this method's performance. A slow increment rate will result in slow convergence, while a very fast one will fail to identify which constraints are binding. Extensive control experiments with a single reservoir and relatively short control horizons (10 – 15 time periods) indicated that an increment formula

$$C^{i+1} = \beta \, C^i \qquad (4.15)$$

with $\beta \in [4,10]$ will generally perform well. In fact, these case studies illustrated that problem (4.1–4.3) does not have to be completely solved before each increment of the penalty coefficient; rather, the projected Newton and penalty function iterations can be performed simultaneously with substantial computational savings. However, when the number of binding constraints is large (e.g., when longer control horizons or many reservoirs or both are considered), control and storage constraints cannot be reliably treated in this manner, and the computational requirements begin to grow. The main reason for this performance weakening is the nature of the penalty function method which prescribes penalty terms only when there are constraint violations. If in the next iteration all storage variables are forced inside the feasible region, then penalty terms are not added, and the method tends to drive the storage trajectory back outside its

bounds; this oscillation becomes more unstable as the penalty coefficient increases.

Alternatively, storage constraints can be treated via a barrier function method [Luenberger, 1973]. The method researched in this study uses a function of the following form:

$$B[s_j(k)] = C \left[\frac{s_j^{max}(k) - s_j(k)}{s_j^{max}(k) - s_j^{min}(k)} \right]^{-\mu} \left[\frac{s_j(k) - s_j^{min}(k)}{s_j^{max}(k) - s_j^{min}(k)} \right]^{-\nu} \quad (4.16)$$

where C, μ, and ν are real positive constants. Figure 4.1 shows plots of this function for $C = 1$, $s_j^{max}(k) = 123.8$, $s_j^{min}(k) = 49.4$, and different values of μ and ν.

The motivation for using this function is to prescribe increasingly higher costs as storage approaches either boundary while being virtually inconsequential within the feasible region. Thus, in contrast to the quadratic penalty (4.14), $B[s_j(k)]$ does not have to be added or removed depending on the constraint violation status, and the controller is always "aware" of its cost structure when searching for better release and storage sequences.

However, simply including this barrier function in the performance index will not be computationally efficient. The two main reasons are first that the iterations may start from or initially generate infeasible trajectories and second that the barrier cost may drive a binding storage significantly afar from its boundary. To account for these effects, the following usage of this barrier function method is suggested:

At each ELQG iteration i, the reformulated performance index is expanded to include the following barrier function terms:

$$B^i[s_j(k)] = C \left[\frac{b_j^{max,i} + \xi_j^{max}(k) - \bar{s}_j(k)}{\xi_j^{max}(k) - \xi_j^{min}(k)} \right]^{-\mu} \cdot \left[\frac{- b_j^{min,i} + \xi_j^{min}(k) - \bar{s}_j(k)}{\xi_j^{max}(k) - \xi_j^{min}(k)} \right]^{-\nu} \quad (4.17)$$

where $\xi_j^{max}(k)$ and $\xi_j^{min}(k)$ are as in (13) and $b_j^{max,i}$ and $b_j^{min,i}$ are determined as follows:

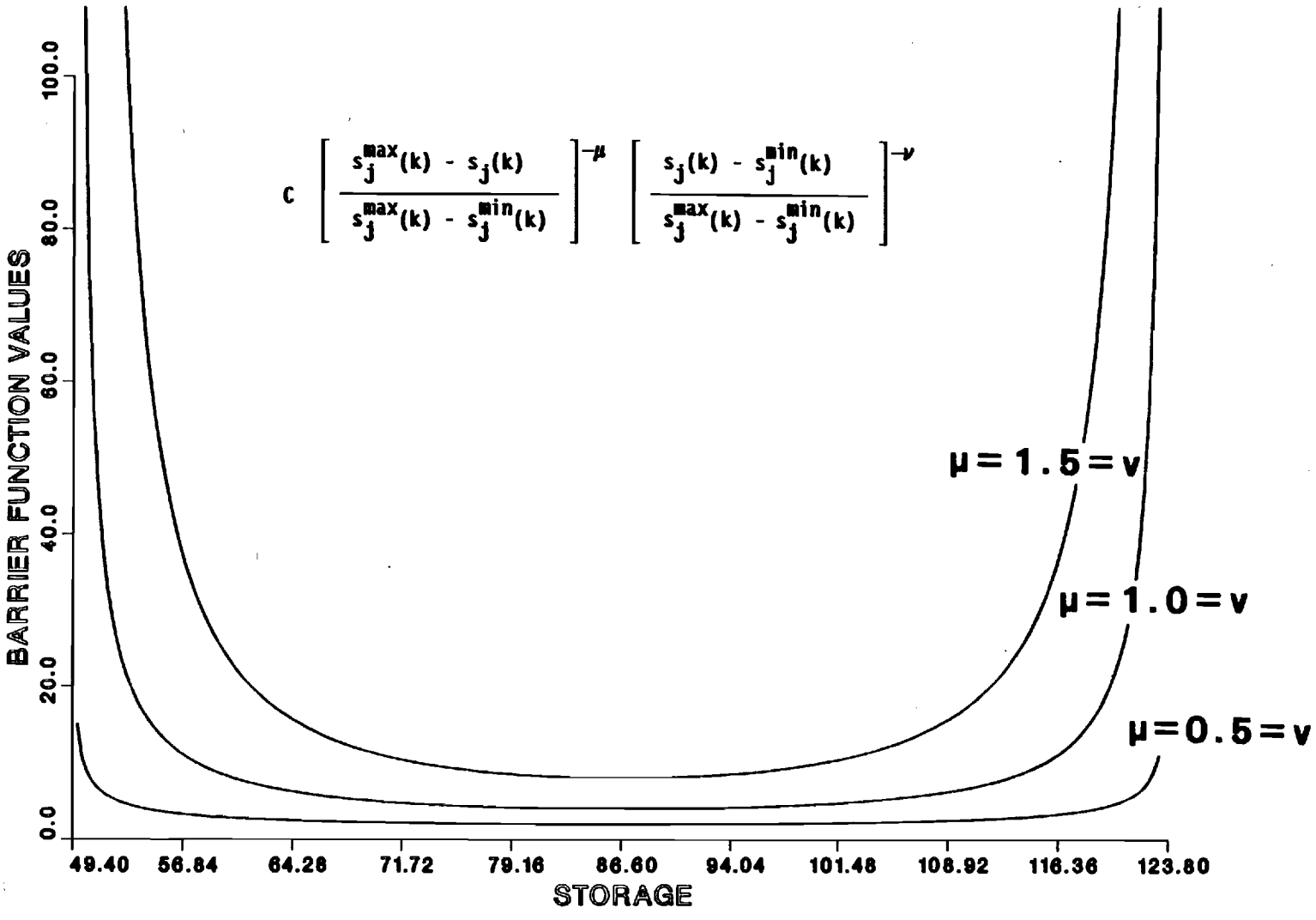

Figure 4.1: A Barrier Function for Storage Constraints

$$b_j^{max,i} = \begin{cases} b_j \text{ , if there is no constraint violation,} \\ x^i + b_j \text{, if the constraint violation is } x^i \end{cases} \quad (4.18)$$

and similarly for $b_j^{min,i}$.

According to the above procedure, when there are constraint violations, the barrier function is broadened to include the storage trajectory, with the boundaries placed a distance b_j from it. Due to the associated high costs, the controller gradually brings the storage within the feasible region. Afterwards, the barrier function boundaries are placed a distance b_j from the upper and lower storage bounds and the procedure converges. Parameter b_j can be determined by preliminary experimentation or it can be adaptively adjusted by inspecting the limiting trajectories and increasing or lowering its value so as to make the constraints barely binding. Toward this end, the following simple scheme was seen to work reliably: If the limiting storage is at a distance Δx_j from its bound (Δx_j is positive when storage does not violate the constraint and negative if it does), replace b_j with $b_j + \Delta x_j$ and continue the iterations until convergence; in a few such cycles the scheme will converge at the optimal sequences. In fact, the appropriate b_j value depends on parameters μ and ν and scaling coefficient C. This coefficient should be selected so that the flat segment of the barrier function is negligible with respect to the other terms in the performance index.

As it will be seen from the case study presented, this approach is reliable and facilitates simultaneous treatment of release and storage constraints, improving the overall ELQG efficiency.

4.6 Case Study

4.6.1 The Savannah River System

The Savannah river system (Figure 4.2) originates in the North Carolina Blue Ridge mountains and flows in a south-easterly direction toward the Atlantic Ocean along the Georgia – South Carolina border. Since the Colonial times, the river has played an instrumental role in the development of the basin's economy, which is primarily agricultural in the north and industrial in the south. The many economic and social benefits together with the severe flood risks have brought about several river control and utilization projects, the most notable of which are the Hartwell, R. B. Russell, and Clark Hill storage projects and an eleven-mile levee around the city of Augusta. Table 4.1 summarizes some relevant characteristics of the above-mentioned reservoirs which are owned and operated by the U.S. Army Corps of Engineers. This as well as

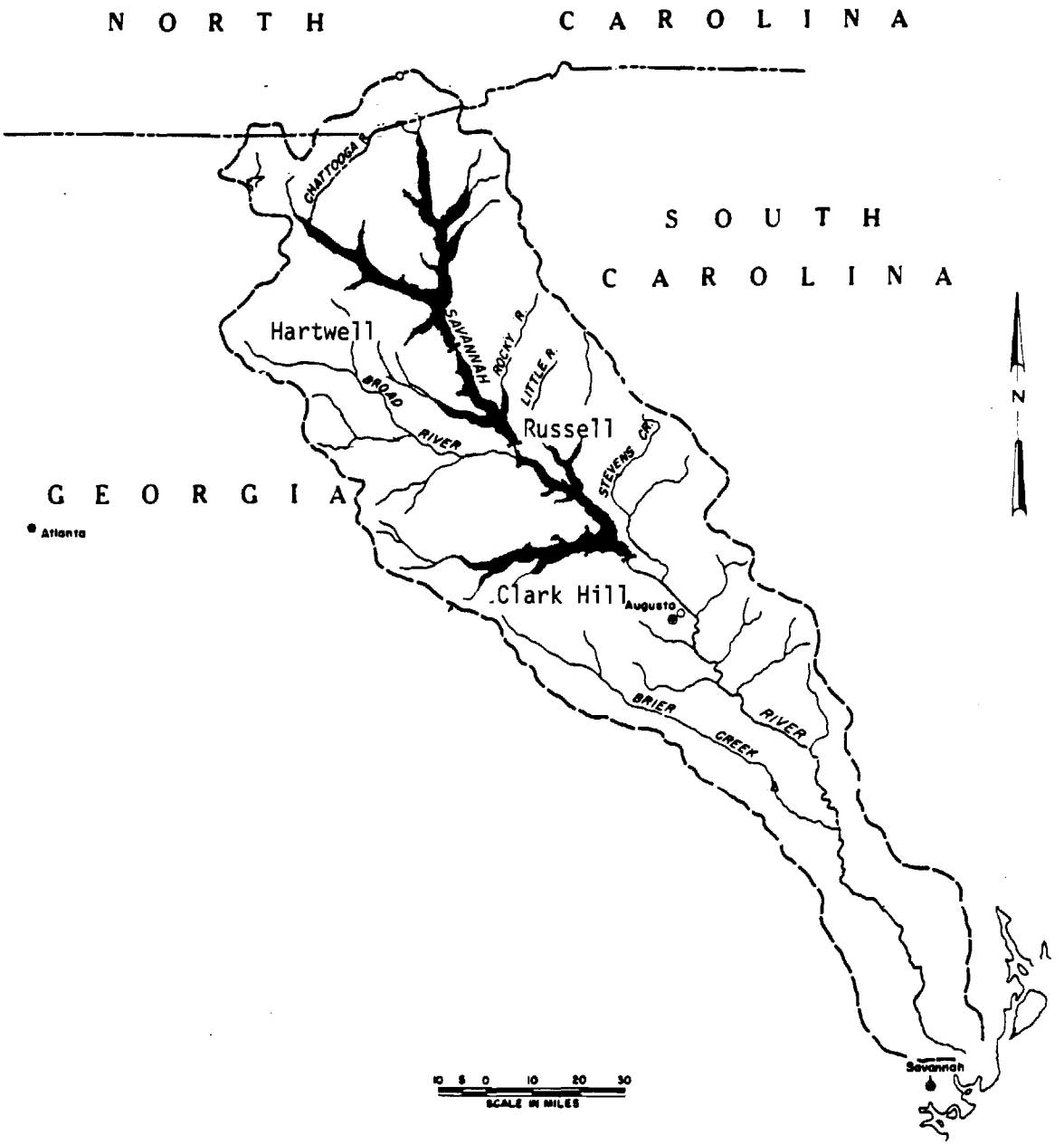

Figure 4.2: The Savannah River Basin

all other hydrologic or operational data used here were compiled from the Savannah River Basin reservoir regulation manual (U.S. Army Corps of Engineers, 1974) or from personal communications with the engineers of the Savannah District.

Table 4.1: Some Data on the Savannah Reservoirs

	Hartwell	Russell	Clark Hill
Year Completed:	1962	1984	1953
Drainage Basin: (sq. mi.)	2088	802	3254
Dead Storage: (10^9 ft^3)	49.401	39.177	63.815
Storage Capacity: (10^9 ft^3)	123.830	50.798	126.324
Hydropower Capacity: (MW)	4x66+1x80=344	4x75=300	7x40=280

The primary objectives of the Savannah reservoirs are to generate energy, provide flood control, and facilitate navigation. For purposes of this study, the power production functions were determined via regression analysis on the power plant turbine characteristic curves; namely, the curves relating power production to turbine discharge and net hydraulic head, the latter being the difference between the forebay and tailwater elevations less various hydraulic losses. In the case of the Hartwell and Russell projects, the net hydraulic head, and consequently the power functions, also depend upon the downstream reservoir's storage value. For example, Russell's power function has the following form:

$$g_r(s_r,s_c,u) = \exp\{a_0 + a_1 u + a_2 u^3 + a_3 \ell n(u) + a_4[\ell n(u)]^2 + a_5[\ell n(u)]^3 + a_6 \ell n(H)\} \quad (4.19a)$$

$$H = h_r - t_r \quad (4.19b)$$

$$h_r = \exp\{b_0 + b_1 s_r + b_2 \ell n(s_r)\} \quad (4.19c)$$

$$t_r = \exp\{c_0 + c_1 u_r + c_2 \ell n(u_r) + c_3 h_c + c_4 \ell n(h_c)\} \quad (4.19d)$$

$$h_c = \exp\{d_0 + d_1 s_c + d_2 \ell n(s_c) + d_3[\ell n(s_c)]^2 + d_4[\ell n(s_c)]^3\} \quad (4.19e)$$

where $g_r(s_r,s_c,u)$ denotes turbine power production; u, turbine discharge; H, net hydraulic head; h_r, Russell pool level; t_r, Russell tailwater elevation; s_r, Russell storage; u_r, total Russell release; h_c, Clark Hill pool level; s_c, Clark Hill storage; and a_i, b_j, c_k, d_ℓ, $i\epsilon[0,1,2,3,4,5,6]$, $j\epsilon[0,1,2]$, $k\epsilon[0,1,2,3,4]$, $\ell\epsilon[0,1,2,3,4]$ are regression coefficients. The total power production is the sum of four (4.19a) terms corresponding to the four turbines presently installed at the Russell power plant facilities. Following the operational practices at the Savannah system, reservoir release is apportioned fairly evenly

among the plant turbines so that $u = u_r/4$. Similar expressions were derived for the other two projects and are reported in Appendix A. The estimated functions exhibit sufficient accuracy over all of the turbine operational range. The standard deviation of the fitted values from the actual ones is within (0.3 – 0.5) MW for all projects.

Flood-damage studies conducted by the Corps of Engineers have estimated the highest harmless release from Clark Hill to be about 20,000 cfs. In the interest of navigation, this release should not be less than 6,000 cfs. Figure 4.3 displays the weekly distribution of net reservoir inflows and typical energy production targets. The three lines on the inflow graphs delineate the mean and 97.5% confidence band levels. Clearly, the probability distributions of these inputs are skewed.

4.6.2 Control Experiments

Figure 4.4 presents a typical ELQG control experiment with the Savannah system. This figure has two sets of plots. The top plots display the identified optimal release rules; the bottom plots delineate the associated storage trajectories. Except for mean values, the storage plots also include the 97.5% and 2.5% probability limits. Release and storage boundaries are indicated by dashed lines. In this experiment, the initial storage values were 111, 44, and 109 billion cubic feet respectively for Lakes 1 (Hartwell), 2 (Russell), and 3 (Clark Hill), and the control horizon was equal to 10 weeks. The figure shows the optimal sequences when no storage bounds are taken into account. These sequences basically satisfy the energy generation requirements shown on Figure 4.4. In fact, energy generation from Clark Hill exceeds the required amount due to the more stringent navigation release. In this experiment, the storage probability distributions were approximated by three parameter lognormal density functions preserving the three first statistical central moments as discussed earlier. ELQG converges to these trajectories in 4 to 5 iterations using approximately 5 seconds of CPU time on a Cyber 180/990 computer system. The storage trajectories indicate that if this release policy is adopted, there is high chance that Lakes 1 and 3 will exceed their capacity. For comparison, Figure 4.5 includes the same sequences with open-loop propagation of statistics. Clearly, this approach drastically narrows the feasible storage regions and leads to overly conservative operation.

The second control experiment is intended to evaluate the effectiveness of the proposed new barrier function method for reliability constraints. The procedure in the previous section was implemented with $\mu = 1$, $\nu = 1$, and $C = 10^6$. ELQG started from the sequences portrayed on Figure 4.4 and converged to the ones shown on Figure 4.6. Convergence was completed in 8 iterations and required

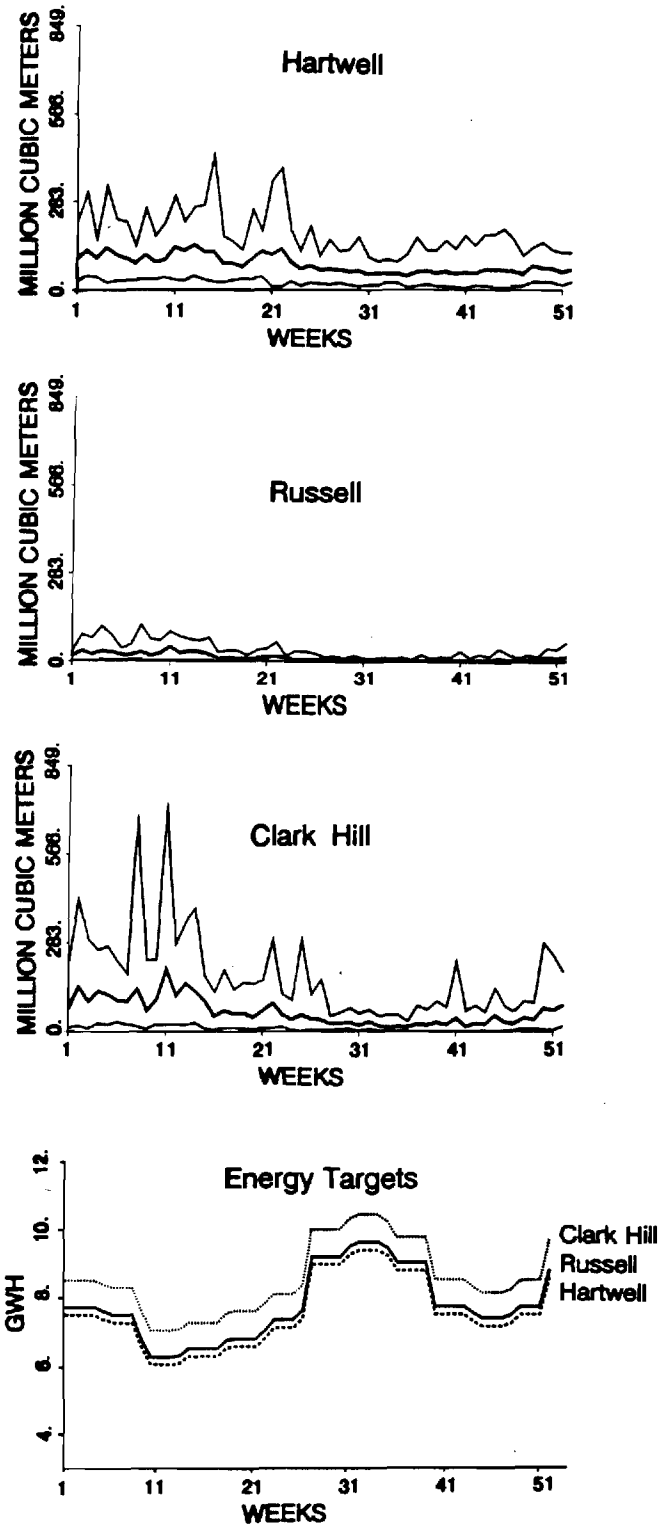

Figure 4.3: Net Reservoir Inflow and Energy Target Distributions

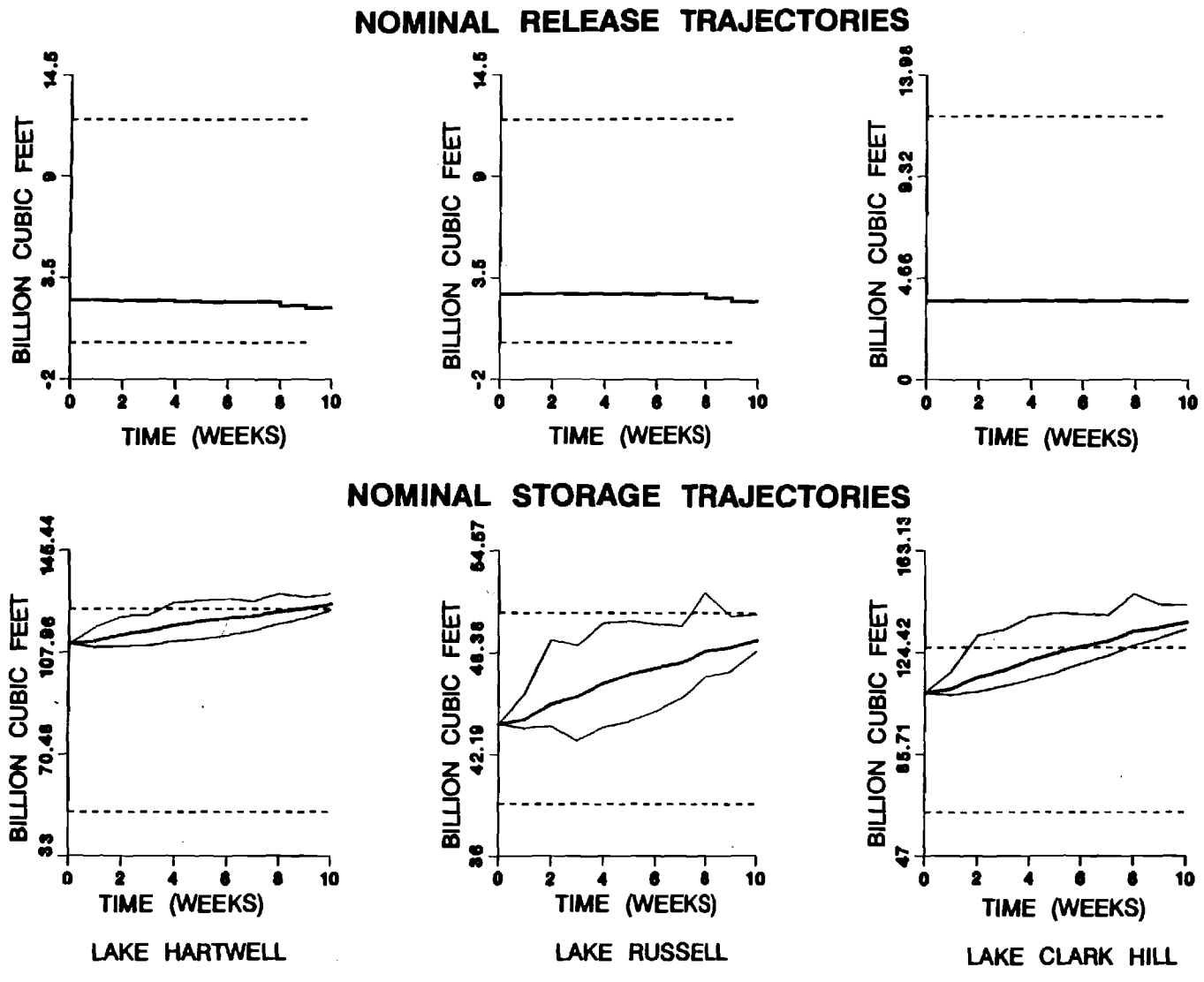

Figure 4.4: ELQG Control Without Storage Constraints

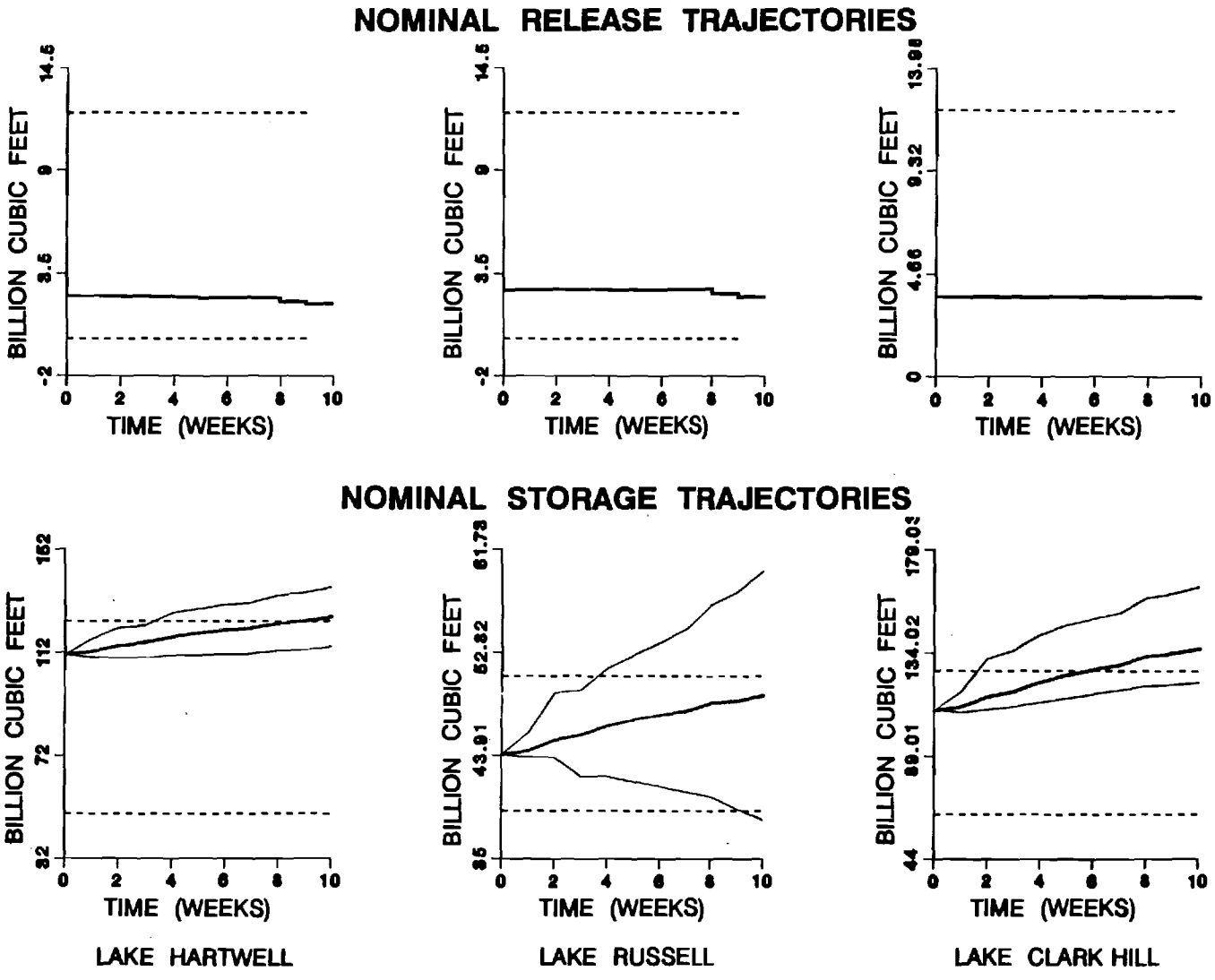

Figure 4.5: Open-Loop ELQG Control

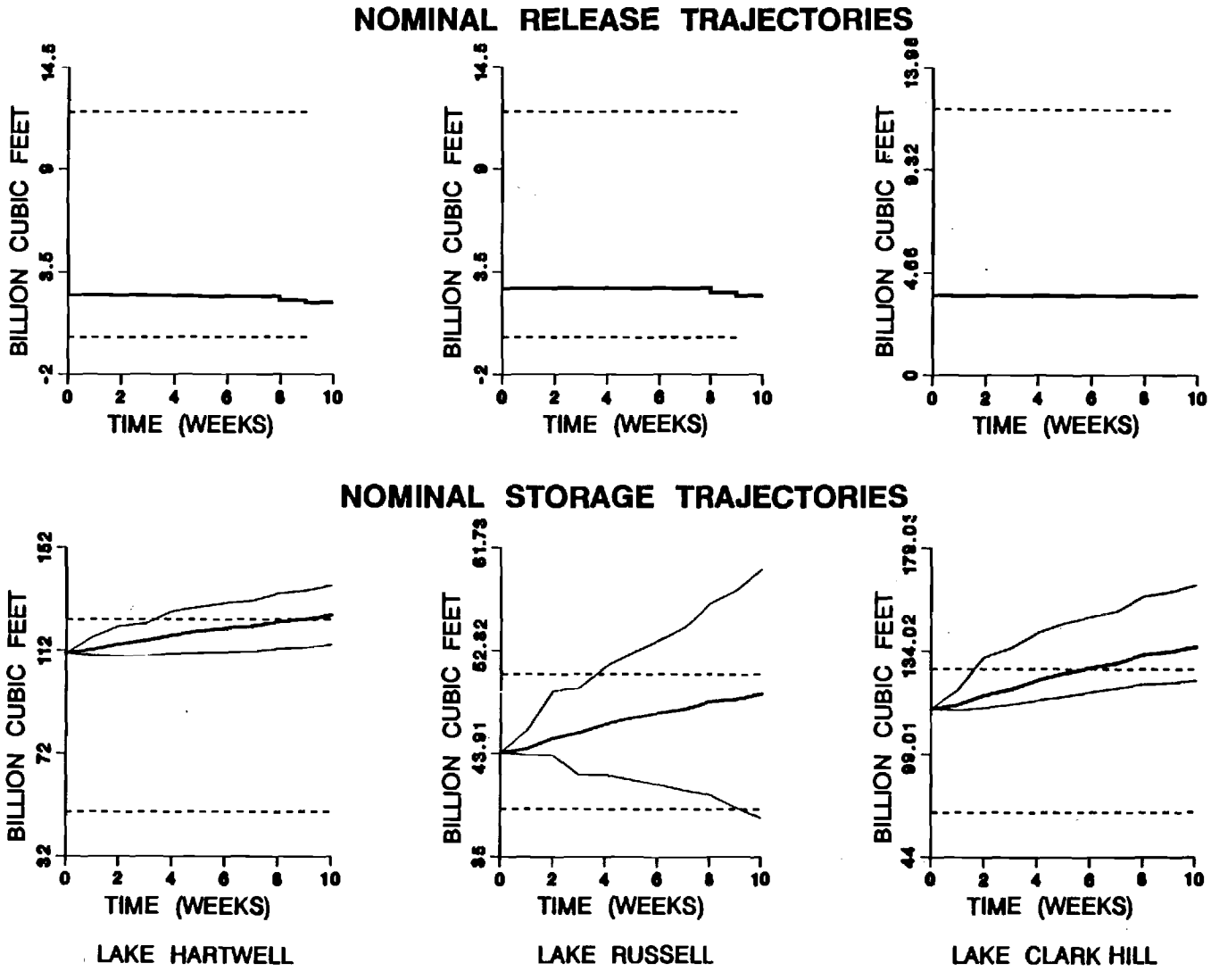

Figure 4.5: Open-Loop ELQG Control

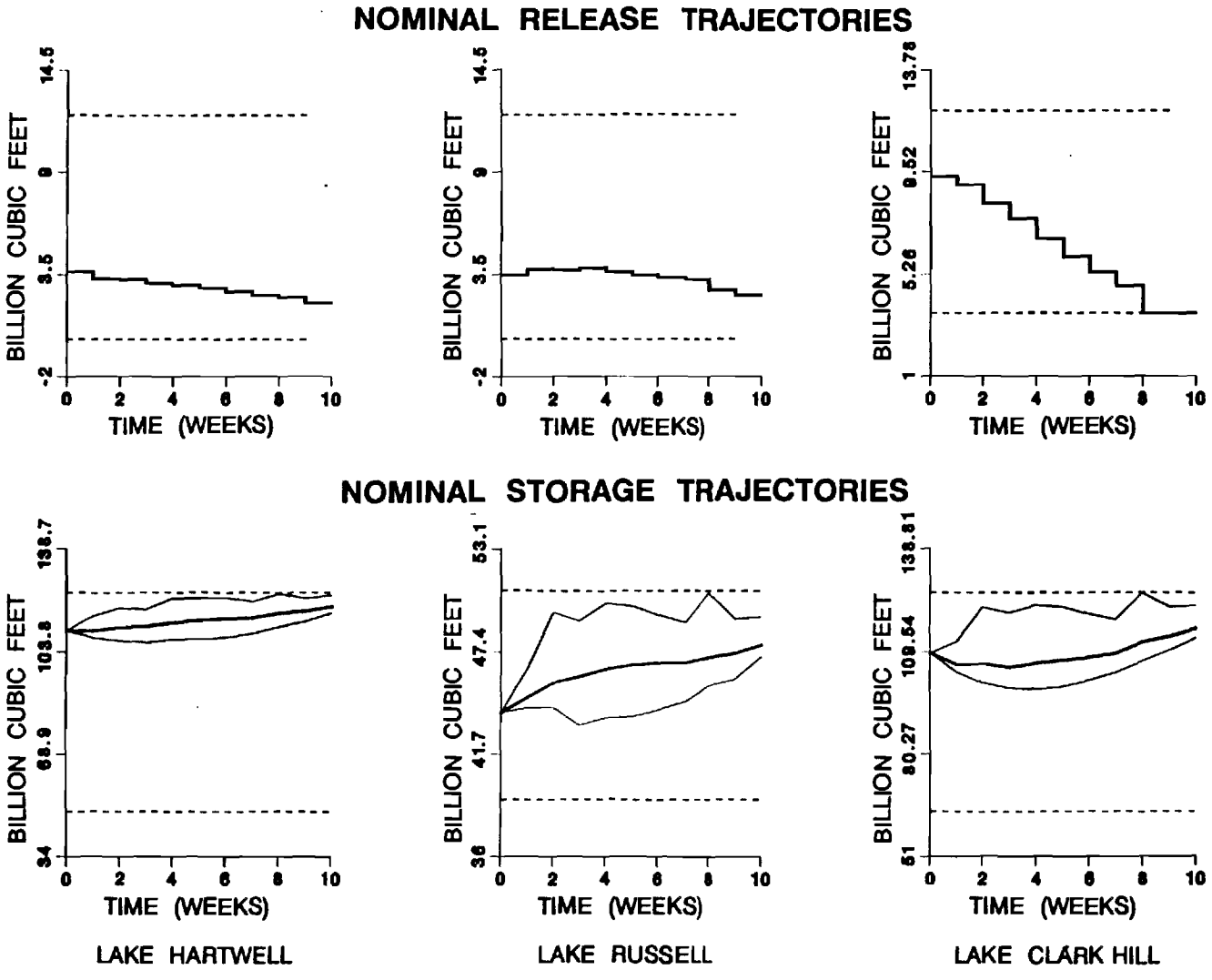

Figure 4.6: ELQG Control With Storage Contraints

approximately 11.6 CPU seconds. Table 4.2 reports some iteration characteristics. W_i is a convergence index [see, Georgakakos and Marks, 1987, for a rigorous definition] reflecting the magnitude of the optimization direction. Small W_i values signify convergence. "Reliability Constraint Violations" is the cumulative violation amount for each reservoir. Lastly, "Energy Generation" reports the expected energy production associated with the nominal sequences of a certain iteration. As indicated by these results, ELQG demonstrates notable efficiency and accounts for both release and storage constraints in very few iterations. By comparison, the penalty function method would require at least 6 to 7 cycles of 4 to 5 iterations for convergence to the same solution. These computational savings are important, especially when the control scheme is to be implemented on microcomputers.

Table 4.2: ELQG Control Experiment - Performance Evaluation

		Reliability Constraint Violations (10^9 ft^3)			Energy
	W_i				Generation
Iteration #	(10^9 ft^3)	H	R	C	(MWH)
1	33.5	39.9	3.1	186.3	284,447.
2	62.5	19.1	3.5	48.6	365,979.
3	16.2	9.8	4.0	4.8	379,593.
4	9.9	0.2	0.6	0.4	392,435.
5	2.8	0.0	0.1	0.0	393,159.
6	0.5	0.0	0.0	0.0	393,189.
7	0.07	0.0	0.0	0.0	393,193.
8	0.0005	0.0	0.0	0.0	393,193.

CPU Time: 11.6 seconds - Cyber 180/990

The above experiments are typical of the ELQG control of the Savannah reservoirs. In the absence of flood or drought conditions, the system is operated to meet the energy requirements; otherwise, the priority is shifted to the flood or drought objectives.

A last comment refers to the specification of the upper release bounds: If turbine release at full gate exceeds flood control or other channel flow constraints, the upper bounds $u^{max}(k)$ are initially set equal to the most binding flow rates. The model is then run, and the identified release and storage sequences are examined. If the storage sequences are feasible (releases are always feasible), the control process terminates, and the optimal release rates are implemented. In

the event that the storage sequences exceed their upper bounds while releases attain their maximum rates, the conclusion is that, under the forecasted hydrologic scenario, the downstream flow constraints cannot be met at the specified reliability levels. In this case, the operators have two options: (1) Reduce the specified reliability or (2) increase the upper release bounds. If they choose the first, they can eventually find the highest reliability level that these constraints can be met. The second option allows for higher release rates depending on the operators' judgement. Eventually, the upper bounds can be placed at the highest turbine release with the intention to maximize energy generation. If this does not suffice and the storage levels still exceed the associated bounds, the optimal decision is to run the turbines at full gate knowing that the chances of spillage are increased. Similar options and operations take place when full gate turbine release is lower than the downstream flow rate constraints. The upper release bound should now initially correspond to the highest turbine release. If this does not result in feasible solutions, the chances of spillage and flow rate constraint violation are increased above those specified by the parameters γ.

4.6.3 A Simulation Experiment

The average system performance under ELQG control was evaluated through a simulation experiment. The basis of this experiment was 100 years of synthetically generated weekly flows assumed to have lognormal probability distributions with historically estimated means and variances. The ELQG control algorithm was implemented with a ten-week control horizon and tolerance levels equal to 2.5% for all reliability constraints. Figure 4.7 depicts the mean values and the (2.5% – 97.5%) probability bands of the simulated storages, releases, and energy generation for all three lakes.

The most notable observation is that the release and storage plots indicate that the occurrence of constraint violations is consistent with and can be controlled by ELQG's probability tolerance levels; namely, constraint violations do no occur more frequently than 2.5 times every one hundred experiments for each week of the year. This result verifies ELQG's ability to effectively handle reliability constraints and justifies the consideration of skewness in addition to the mean and covariance. Other observations specific to the Savannah system are noted below:

Under the stated hydrologic conditions and power commitments, the system reservoirs consistently undergo stressful periods where storages approach capacity values and higher flood risks. During these periods, the variability of releases and energy generation increases. When the reservoirs are not stressed, they are basically operated to satisfy the energy requirements. The variability of these releases and energy

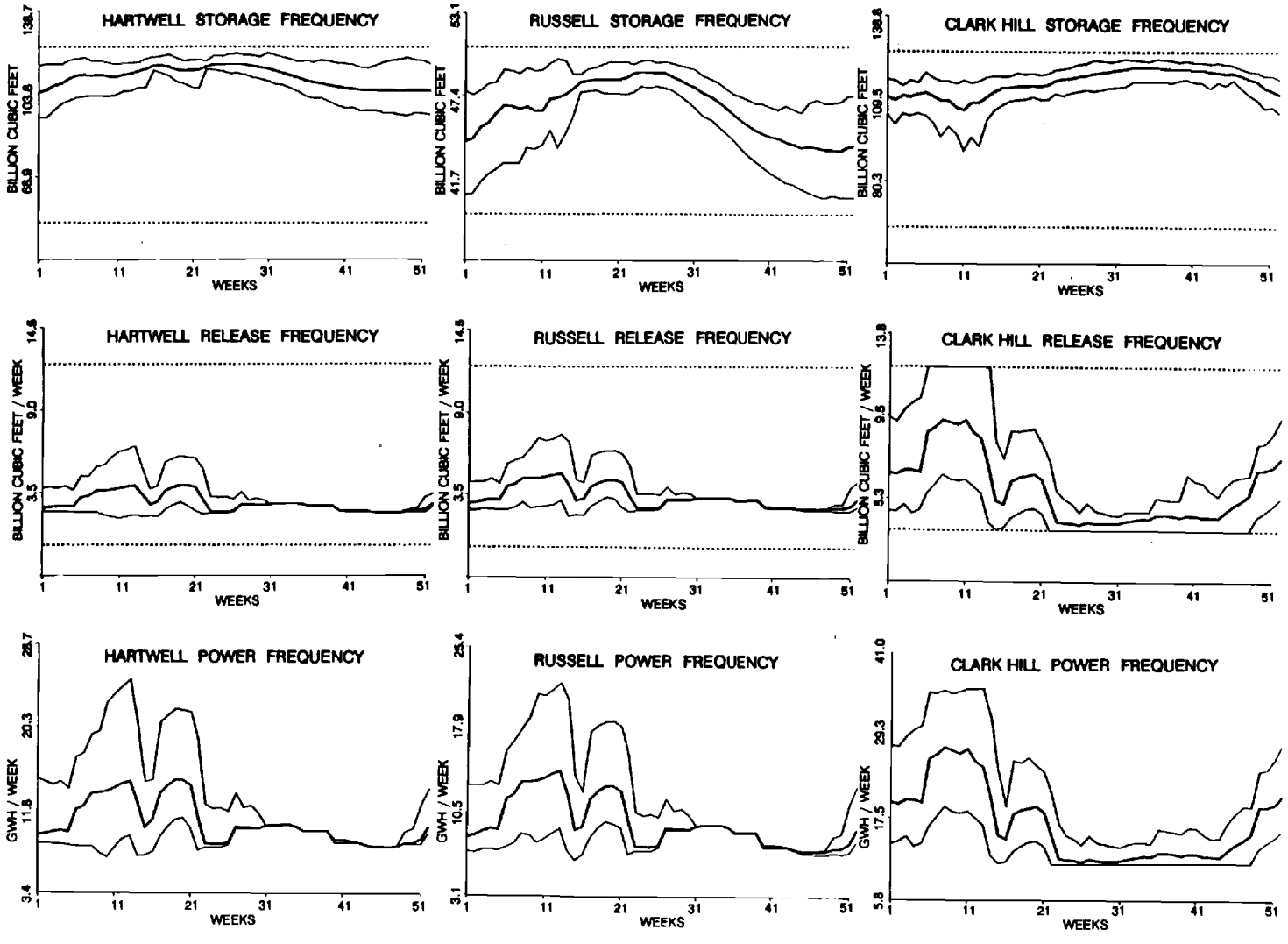

Figure 4.7: Simulation Experiment

generation is minimal.

4.7 Closing Remarks

This chapter presented and evaluated two extensions of the ELQG reservoir control method: (1) ELQG was modified to more accurately represent the system uncertainties by not only considering their mean vector and covariance matrix, but also their skewness and possibly other significant higher order moments. (2) ELQG's efficiency with respect to probabilistic constraints was also enhanced as a result of a new barrier function method. This barrier function method allows simultaneous control and storage constraint iterations and thereby improves ELQG's overall efficiency. The merit of these changes was evaluated and verified in control and simulation experiments with a three-reservoir system. An important conclusion of the case study is that ELQG's nominal reliability is in agreement with the reliability realized during actual operation.

Overall, the method is well-suited for the real time control of reservoir systems with multiple objectives. ELQG is presently under implementation for the Savannah River reservoirs on a microcomputer system.

5. THE VALUE OF FORECASTING IN RESERVOIR OPERATION

5.1 Introduction

Better streamflow foresight is expected to improve reservoir operation because it allows more time for better decision making. However, forecasting systems can be costly, and the question that frequently arises is whether their benefits outweigh their costs. Unfortunately, the process of reservoir control is complex, and the value of forecasting cannot be generally quantified. Among many other factors, forecast benefits are influenced by reservoir size and spatial distribution, the nature and timing of system objectives, the relation of the objectives to the region's hydrology, and the control approach adopted.

Forecasting models have been classified in a number of ways [Rodriguez-Iturbe, et al., 1978, Kitanidis and Bras, 1978] and have been utilized with a variety of control schemes [Yeh, et al., 1976, 1979, Bras, et al., 1983, Wasimi and Kitanidis, 1983, Stedinger, et al., 1984, Loaiciga and Marino, 1985, Georgakakos and Marks, 1987]. However, assessments of forecast benefits have not as yet been the subject of published investigations.

The goal of this section is to evaluate the benefit of forecasting in the Savannah River System in the state of Georgia.

5.2 Control Experiments

A description of the Savannah River System has already been presented in the previous section. The ELQG control method will be employed here in simulation experiments under different hydrologic and operational scenarios to evaluate the potential benefits of better streamflow forecasts.

Two control experiments will first be presented to highlight the effect of streamflow forecasting on the optimal release policies. Figure 5.1 exhibits the results of an ELQG control experiment with the Savannah River System. The control problem is identical to that of Section 4 and is solved with a ten-week control horizon and reliability parameters γ equal to 0.025. The inflow statistics—mean, variance, and skewness—were those of the historical sequences, and reservoir storages were initially set equal to 111, 44, and 109 billion cubic feet for Hartwell, Russell, and Clark Hill respectively. The figure shows this problem's optimal release and storage trajectories. Except for mean values, the storage plots also include the 97.5% probability limits. In this experiment, the expected energy generation is roughly 400,000 MWH while the corresponding energy target is about 275,000 MWH. Namely, ELQG is more concerned with the binding storage constraints than the

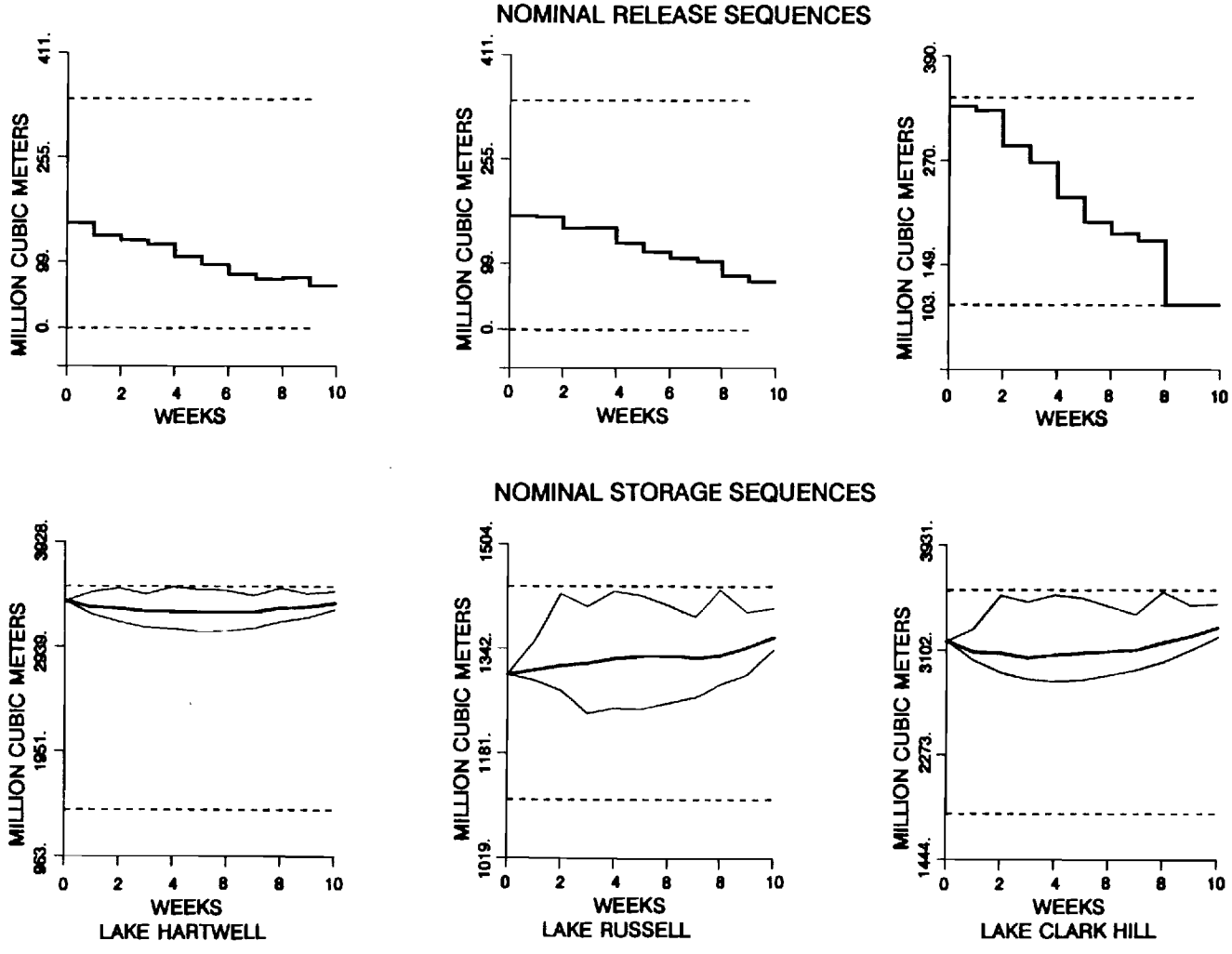

Figure 5.1: An ELQG Control Experiment

energy generation requirements.

Figure 5.2 includes the results of a second ELQG experiment. The problem is the same as before, but the controller is now assumed to have better foresight of the upcoming inflows. Better foresight was here simulated by reducing the forecasted inflow variance and, consequently, narrowing the associated inflow probability band. As a result, the storage probability bands are also reduced, and the controller allows for higher storage levels, at the same risk of constraint violation. The energy generation expected to result from the new optimal release and storage sequences is about 325,000 MWH. Eventually, however, higher hydraulic head should increase energy generation. The question is *how much* increase can one expect.

5.3 Simulation Experiments

The benefits of forecasting were here assesed by simulating the Savannah system response under ELQG control with four streamflow models of varying forecasting power.

The first model was simply a predictor of the historical weekly inflow statistics, models 2 and 3 were lag-one seasonal autoregressive models, and the fourth model had perfect foresight of the upcoming inflows. Models 2 and 3 predicted the conditional inflow mean and associated error variance according to the following equations:

$$\hat{w}_i(\ell) = \bar{w}(i+\ell) + \rho_{i+\ell,i+\ell-1} \cdots \rho_{i+1,i} \frac{\sigma_{i+\ell}}{\sigma_i} [w(i) - \bar{w}(i)], \qquad (5.1)$$

$$\hat{P}_{w,i}(\ell) = [1 - \rho^2_{i+\ell,i+\ell-1} \cdots \rho^2_{i+1,i}] \sigma^2_{i+\ell}. \qquad (5.2)$$

In the above equations, $\hat{w}_i(\ell)$ is the forecast issued from time period i for the inflow at time $i+\ell$, with ℓ being the lead time of the forecast; $w(i+\ell)$ is the historical inflow mean at time $i+\ell$; $\rho_{i+\ell,i+\ell-1}$ is the historical correlation coefficient between periods $i+\ell$ and $i+\ell-1$; $\sigma_{i+\ell}$ is the historical standard deviation for period $i+\ell$; $w(i)$ is the observed inflow at time period i; and $\hat{P}_{w,i}(\ell)$ is the ℓ–lead forecast error variance.

As these equations indicate, the forecasting ability of this model improves as the correlation coefficients approach one. For forecasting model 2, these coefficients were set equal to their historically estimated values; the correlation coefficients of model 3 were arbitrarily set at the middle point between their true value and one. These models assumed that the three reservoir inputs were independent and followed three-parameter lognormal distributions. Model 4 was included to provide an upper performance bound. It should be noted that

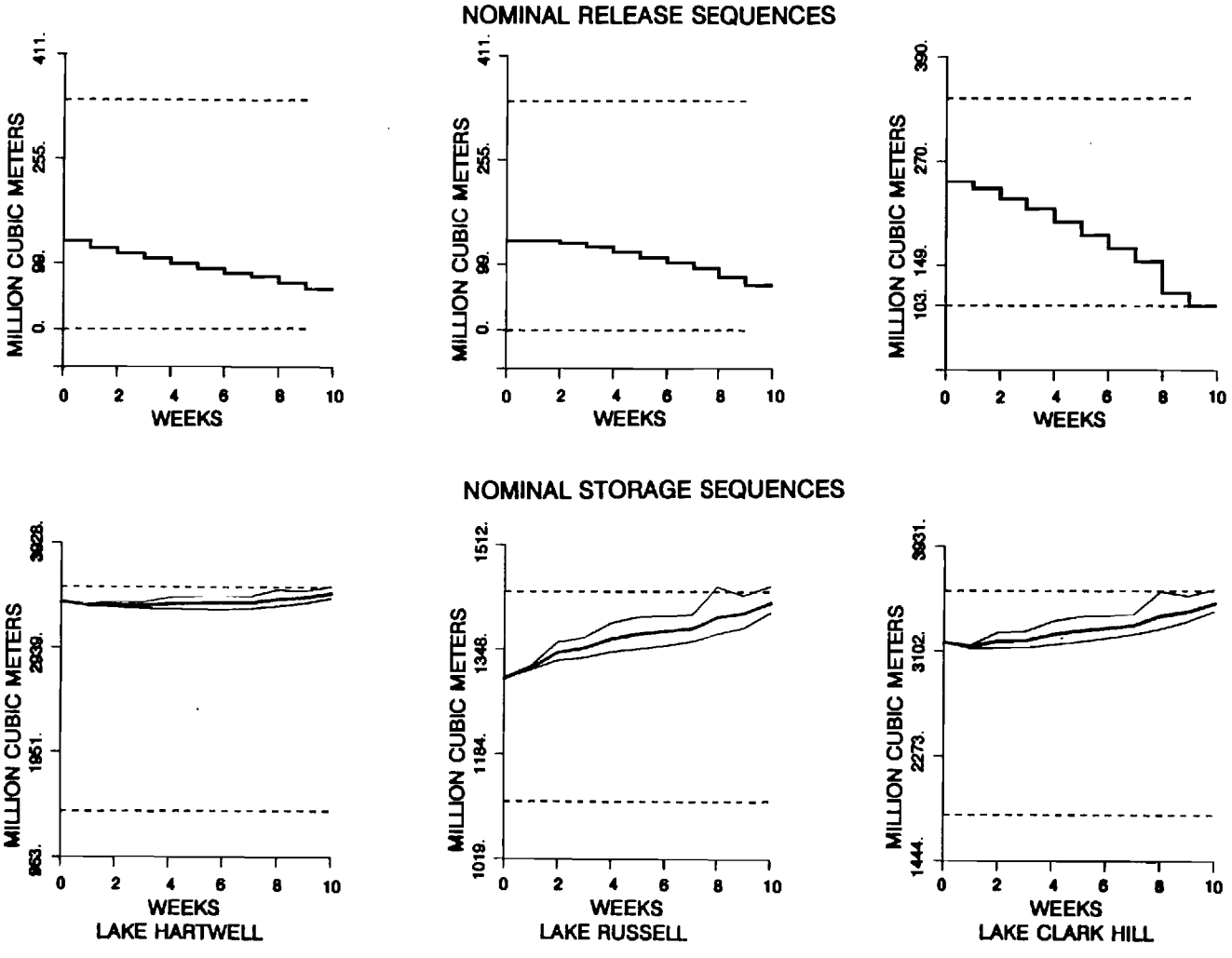

Figure 5.2: ELQG Control with Forecasting

all models share the same historical (apriori) variances σ^2. However, the forecasted error variances are largest in model 1 (equal to σ^2) and gradually decline to zero in the other models.

The simulation process was based on 100 years of synthetic weekly inflows generated from model 3. At the beginning of every week, each forecasting model was first invoked to predict the upcoming inflows over the control horizon [0,N-1]. The control routine was subsequently called upon to determine the optimal release sequences $\{u_j^*(k), j=h,r,c, k=0,1,...N-1\}$. The first period's optimal releases $\{u_j^*(0), j=h,r,c\}$ and generated inflows $\{w_j(0), j=h,r,c\}$ were then implemented and stored along with the resulting storages and energy generation. At the end of the simulation horizon, 100 values of the above quantities had been recorded for each week of the year, each reservoir, and ELQG-forecast model combination. These data-sets were then analyzed and their mean and 97.5% probability bands were calculated. The results appear on Figures 5.3 through 5.6, and some remarks are noted below.

In all cases, release and storage trajectories do not exceed their respective bounds (dashed lines) for more than 2.5% of the time. This is the level set for the reliability parameters γ in the ELQG routine and verifies the ability of the controller to handle probabilistic constraints as claimed. As streamflow forecasts improve, ELQG allows higher average reservoir storages. However, because the available storage capacity decreases, the control horizons required to maintain the same risk levels for constraint violation become longer. Thus, the results on Figures 5.3 through 5.6 were respectively obtained with control horizons 8, 10, 14, and 16 weeks.

During the first half of the year where inflow rates are high, the system's operation is mainly concerned with flood prevention. During this period, reservoir releases are highly variable and energy generation is well above the required targets. The second half is strictly dedicated to satisfying energy demands. The previous simulation experiments can also provide an estimate of the system's energy generation potential. Two relevant quantities are the mean annual energy production and the mean energy output which is available at 97.5% of the time. Figure 5.7 includes plots of these quantities and summarizes the worth of forecasting for the Savannah River System. The percentages indicate that better forecasting models can increase the mean energy production by about 1% and the 97.5%-available energy output by 2.5 to 3%. In absolute terms, these percentages represent 15 and 50 GWH gains respectively, primarily incurred over the first half of the year.

Another beneficial effect of forecasting may be a reduction in the highest necessary release during flood periods. Namely, more accurate

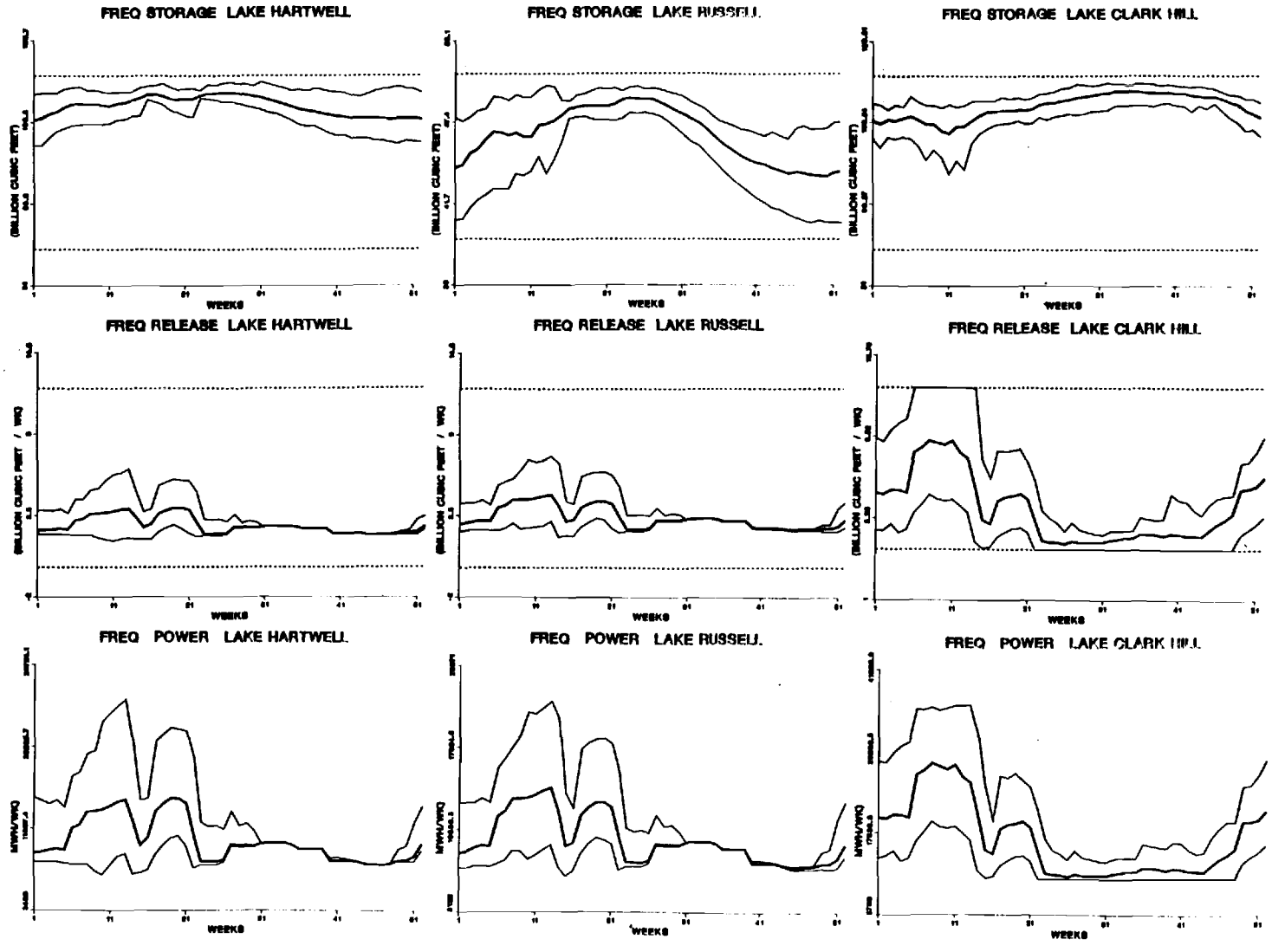

Figure 5.3: Simulation Experiments: Forecasting Model #1

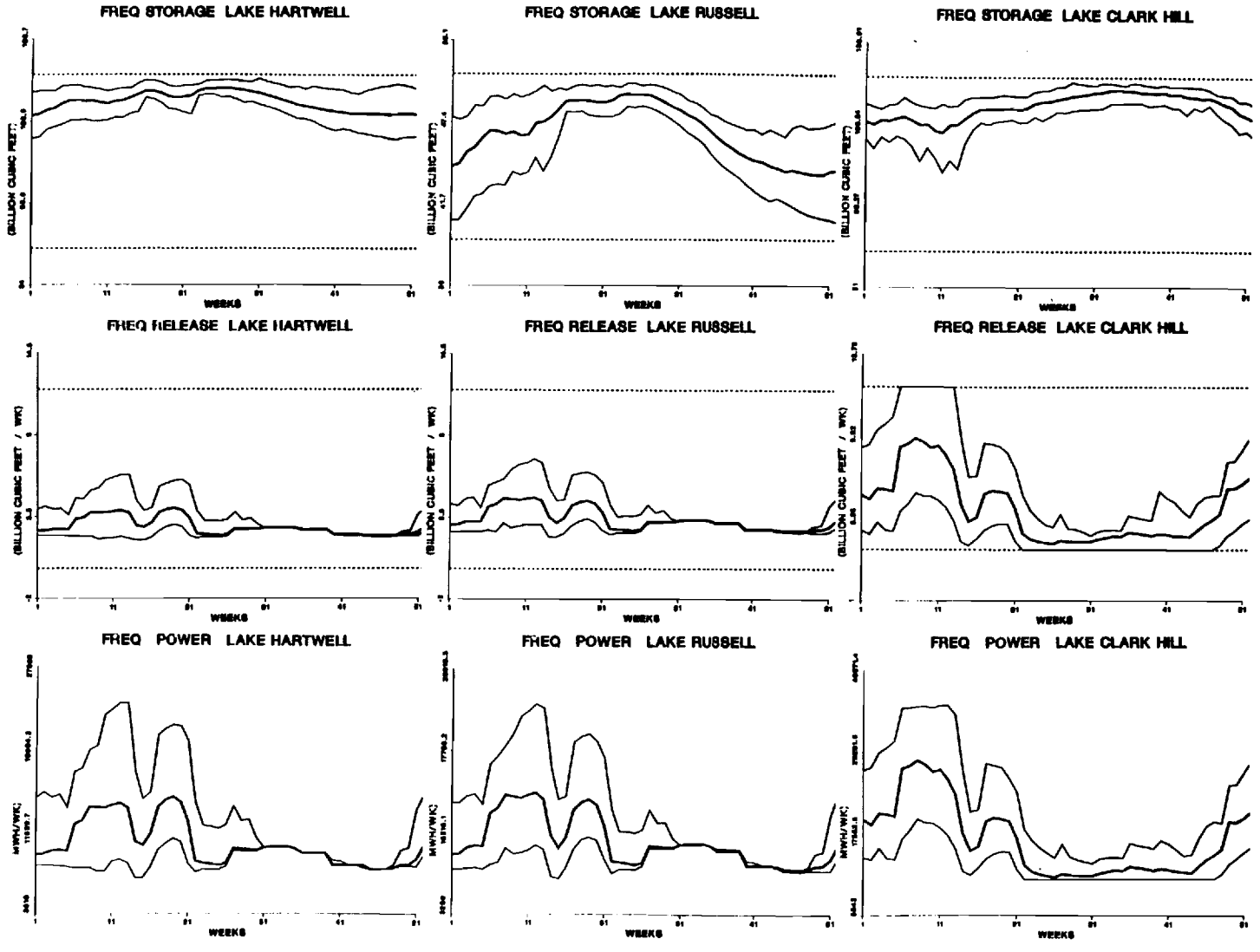

Figure 5.4: Simulation Experiments: Forecasting Model #2

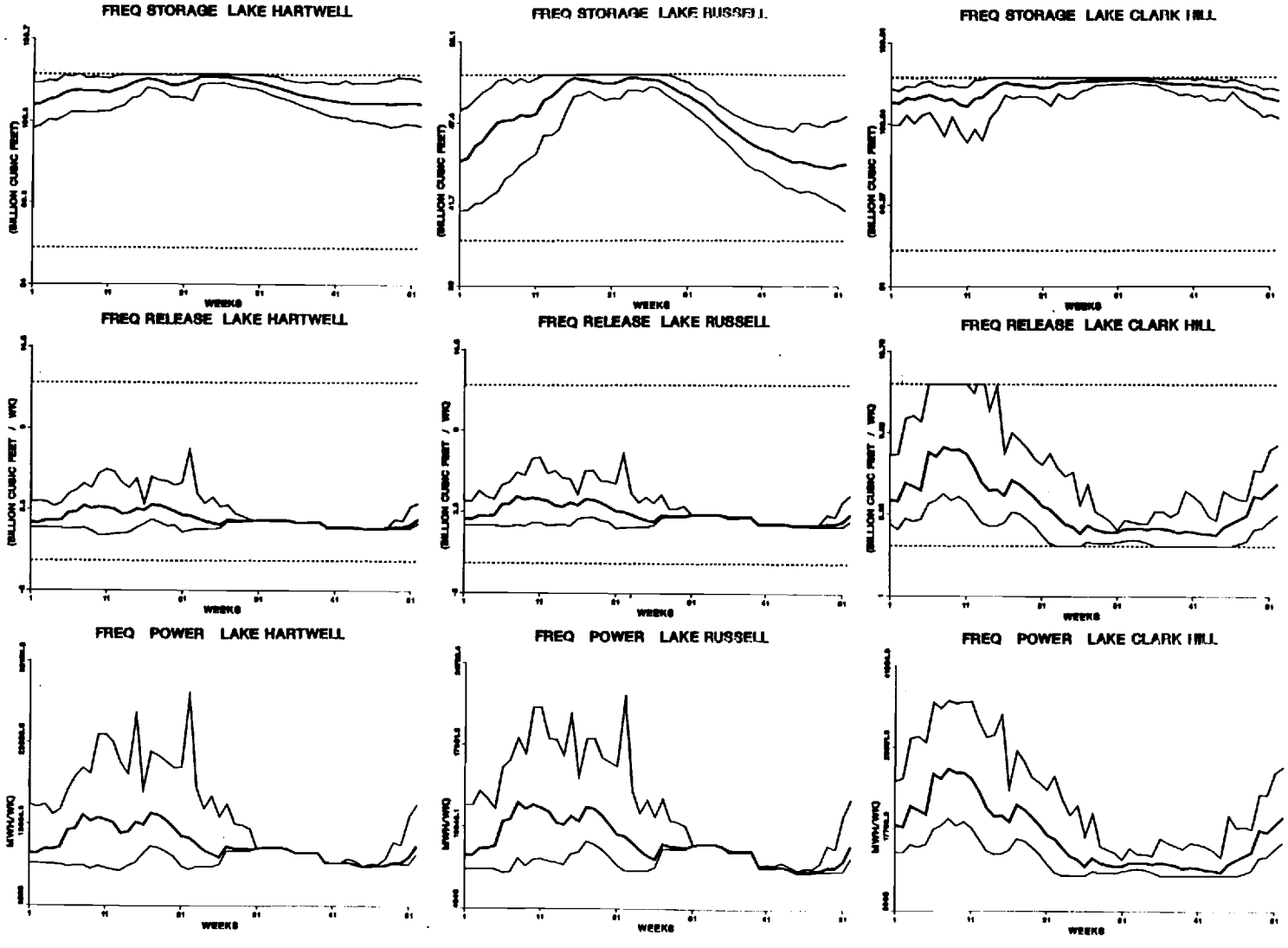

Figure 5.5: Simulation Experiments: Forecasting Model #3

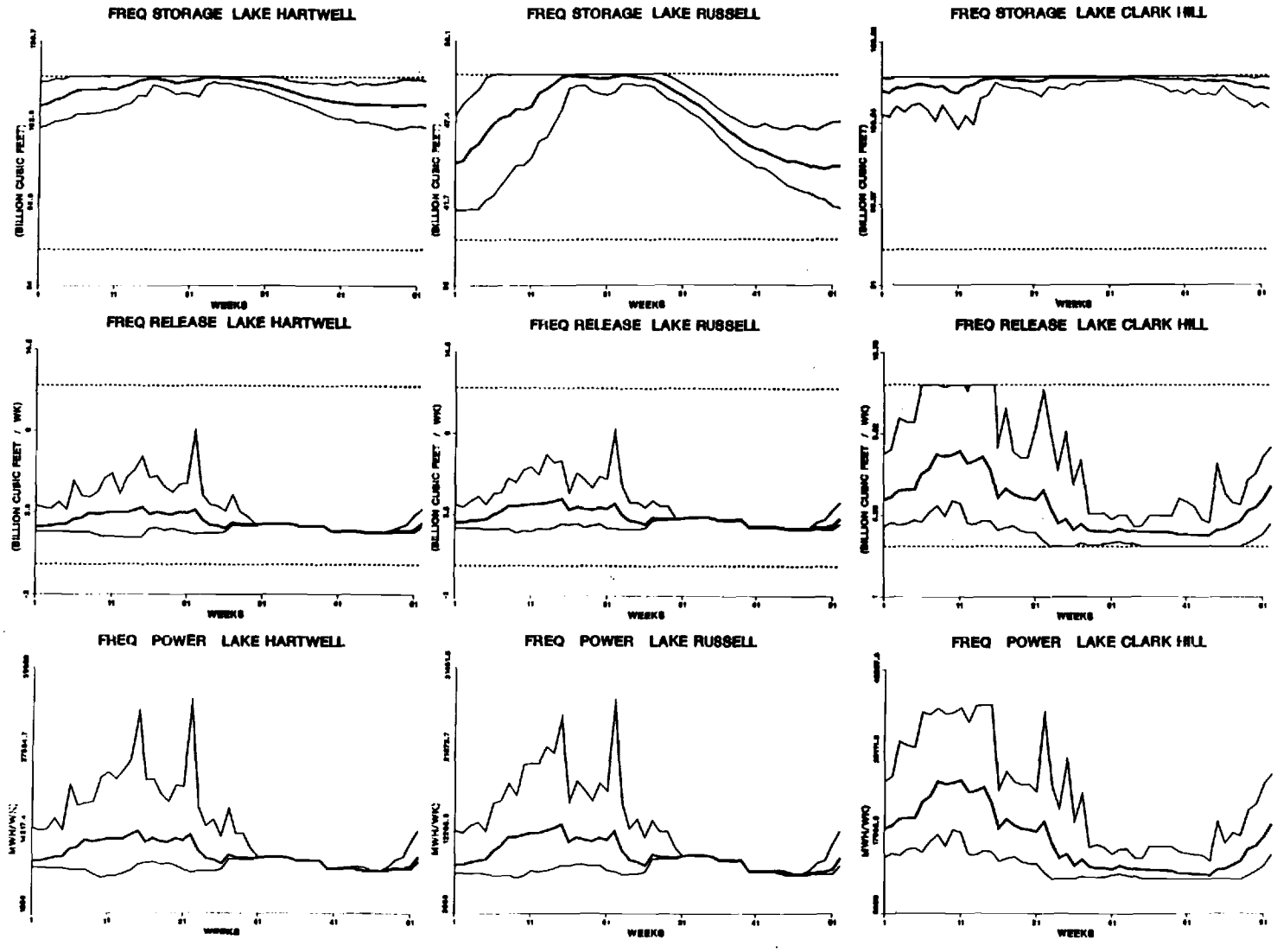

Figure 5.6: Simulation Experiments: Forecasting Model #4

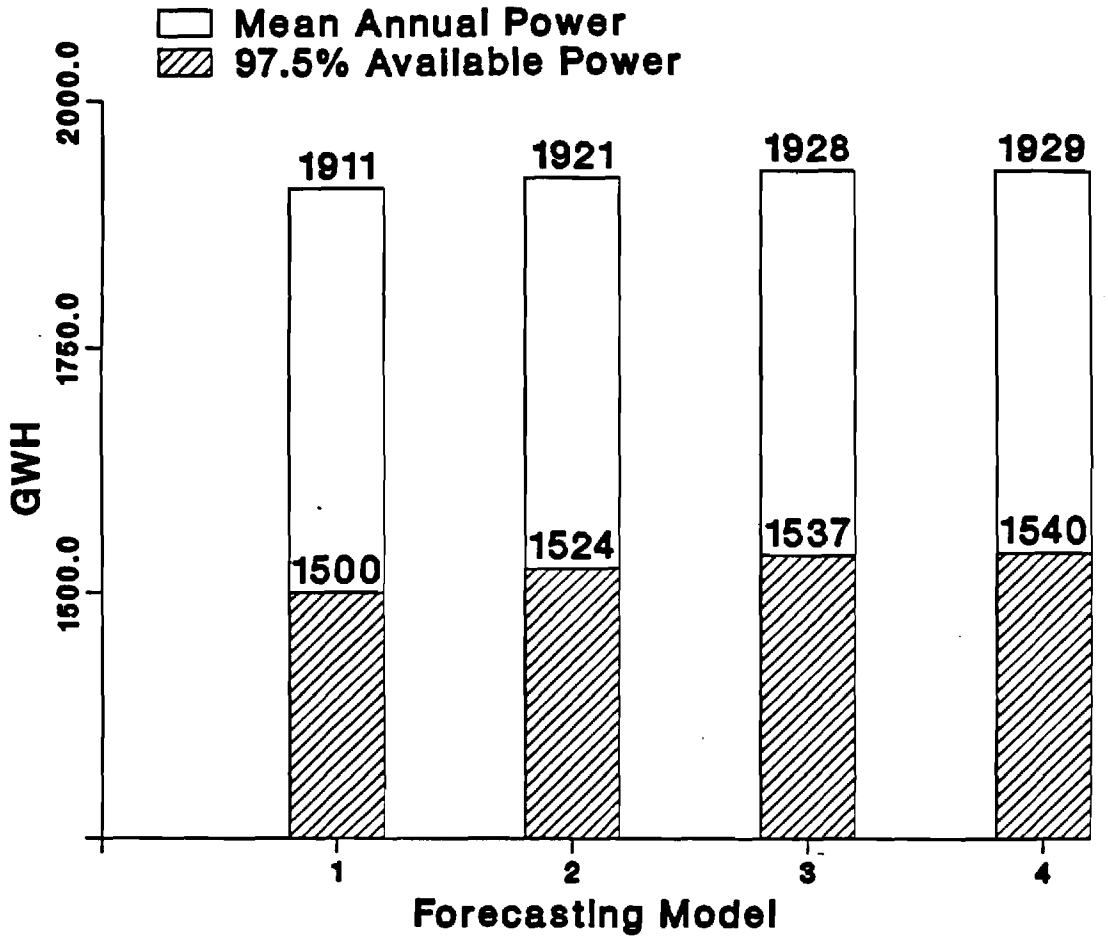

Figure 5.7: The Value of Streamflow Forecasting

and farsighted models are expected to better manage flood volumes and prevent excessive releases. In the above experiments, however, this effect could not be demonstrated. In all cases, the highest release did not exceed the upper bound.

A last comment refers to the role of the reliability parameters γ. For the same forecast-control model combination, their levels also affect thedistribution of the simulated storages. Larger γ values would not only result in higher mean reservoir storages but also in more frequent constraint violations. This, in turn, would result in more water bypassing the turbines and less energy output. In fact, there is an optimal level γ where the spilled water and the average hydraulic head combine for optimal power production. Above this level, power output is limited by spillage; below it, power output declines due to the reduced hydraulic head.

5.4 Closing Remarks

In summary, probabilistic streamflow forecasting can considerably improve reservoir operation, but the benefits are system specific. Some general observations are that forecasting increases energy output and reliability by raising the turbine hydraulic head and minimizing spillage; it mitigates drought repercussions by enhancing dependable water supply; and it reduces flood damages by avoiding excessive releases. These improvements may be rather attractive, particularly in reservoirs frequently operated under flood or drought conditions.

6. A STOCHASTIC CONTROL METHOD FOR HYDROPOWER SCHEDULING

6.1 Introduction and Overview

Optimal scheduling of hydropower operations is a process involving a plethora of complicating factors. At any given day, reservoir operators must skillfully balance upcoming inflow forecasts against available storage, turbine power, and discharge capacities to maximize energy generation. Hydropower is most valuable during the day's "peak" generation period, and, therefore, hydro-plants must generate as much energy as possible during the peak hours. Hydropower turbines should optimally operate at best efficiency, where a given release volume generates the most energy. However, at times of high flows, it pays to abandon best efficiency operation and "run" at full gate. During off-peak hours, energy is normally produced at a required minimum except when peak generation cannot maintain desirable reservoir levels. During such occasions, off-peak generation should be invoked as much as necessary. At times of extremely high flows, emergency flood gates may have to be considered, while during extreme droughts, power generation may have to cease.

Recent optimal control developments have successfully demonstrated the merit of using such techniques in long term reservoir management (Wasimi and Kitanidis [1983], Marino and Loaiciga [1985], Kitanidis and Foufoula-Georgiou [1987], Georgakakos and Marks [1987], Foufoula-Georgiou and Kitanidis [1988], and Georgakakos [1989a,b]. However, as the operation focuses on day-to-day management, system modeling requirements grow (see also Trezos and Yeh [1987]), and direct application of the existing control models becomes inadequate.

This chapter introduces a new control structure which is more attuned to the idiosyncracies of short-term hydropower scheduling. The essence of this approach is to organize the solution of the associated control problem in several levels. Each level formulates and seeks to solve a control problem whose solution is more desirable than those of higher level problems. Thus, if successful, the process terminates, and the optimal generation schedules are implemented. In the opposite event, the solution process resumes at the immediately higher control level. The control level problems differ by the turbine operational modes, generation time constraints, system priorities, and operational controls. This problem breakdown facilitates the formulation of subproblems amenable to optimal control methods. Further decoupling in dynamic and static modules enhances controller flexibility and overall computational efficiency.

This chapter includes five additional sections. Section 6.2 provides a general description of the case study system—the Lloyd Shoals hydroelectric facility and dam. Section 6.3 compiles all data and relationships necessary for the development of the mathematical system

model. Section 6.4 outlines the control model structure and provides the mathematical details of the algorithms used. Section 6.5 includes two parts. The first presents some computational experience with the new control model, and the second elaborates on the results from five simulation experiments. Section 6.6 summarizes the primary findings of this research and provides the basis for potential system improvements.

6.2 System Description

The subject of this study is the Lloyd Shoals Hydroelectric Project, which is owned and operated by the Georgia Power Company. As shown in Figure 6.1, the project is located on the Ocmulgee River approximately 45 miles southeast of Atlanta, Georgia. Also indicated in the figure are the operational hydrologic stations. None of the four major streams supplying Lake Jackson are gauged near their confluence with the lake.

Originally built and owned by the Central Georgia Power Company, Lloyd Shoals began producing electricity in 1911 with four 2400-kilowatt units. A fifth 2400-kilowatt unit was completed in 1916, and a sixth 2400-kilowatt unit was added a year later, bringing the plant's output to 14,400 kilowatts. Today, as a result of improvements made over the years, the Lloyd Shoals plant can generate 20,000 kilowatts.

From east to west the dam consists of an earth embankment section with a concrete core wall about 530 feet long, a concrete gravity structure including a 728.5-foot long overflow spillway, an intake section (198 feet), and a non-overflow section (143 feet). The crests of the earth embankment and the non-overflow sections are at elevations 542 and 540 respectively, and the top of the spillway flashboards are at elevation 530. The maximum dam height is about 100 feet.

The overflow spillway section consists of a 180-foot section on the east end and a 128.5-foot section on the west end with a crest elevation of 528. These two sections are equipped with two-foot high flashboards which trip slightly above elevation 530. The 420-foot middle section has a crest elevation of 525 feet and is equipped with five-foot high flashboards that also trip slightly above elevation 530. Included in the western section is a 20-foot wide by 6.2-foot high gate with a sill at elevation 518. This gate is provided for reservoir regulation and trash release as well as supplemental spillway discharge.

The reservoir formed by the dam, Jackson Lake, has a surface area of 4750 acres at the normal pool elevation of 530 feet. The drainage area is approximately 1400 square miles.

The Georgia Power Company hydroelectric plants operate for the primary purpose of power generation. In general, flood control, water supply, or navigation are not operational objectives. The total hydroelectric

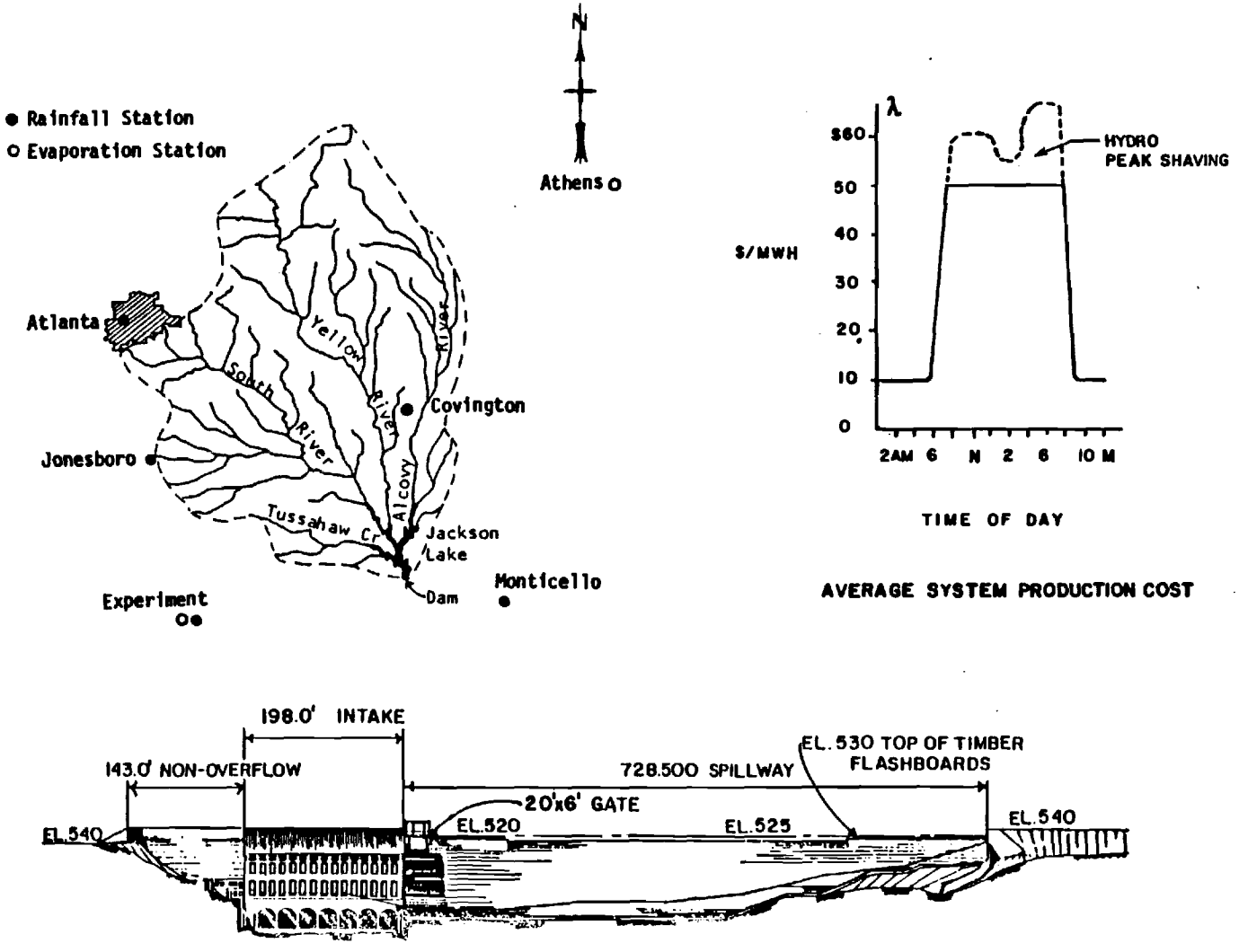

Figure 6.1: The Lloyd Shoals Hydroelectric Project

capacity of the Georgia Power Company system is approximately 5.5 percent of the total system generating capacity. From an energy standpoint, the hydroelectric plants supply roughly 3 percent of Georgia's energy needs.

The daily demand on the system typically varies from a low during late night/early morning hours to a peak during the normal business hours. The annual maximum load generally occurs during the summer between 4 and 6 p.m. due to air conditioning needs. The peak generation period lasts approximately fourteen hours each week day. As the load increases from the late night/early morning minimum to the peak period, variable production costs also increase due to the use of fossil-fueled plants. The average system production cost at any time is termed the system lambda. Figure 6.1 additionally includes an example of a lambda curve. The values shown are for illustration only. Since the variable cost of hydroelectric plant is essentially zero, they are operated when they are most effective—on the peak of the lambda curve. Consequently, Georgia Power Company's hydroelectric plants are "peaking" plants.

From the previous discussion, it is obvious that the operating objective at the Lloyd Shoals Project is to maximize the energy generated during the fourteen hour peak period Monday through Friday of each week. This requires maximizing the hydraulic head while avoiding overtopping/tripping the flashboards at elevation 530. Additional reservoir level constraints are that the level should not be lower than elevation 522 from September 1 to June 1 and elevation 528 the remainder of the year. The elevation 528 constraint occurs because Lake Jackson is used as a water source in extreme droughts to supply Georgia Power Company thermal plants located downstream. During off-peak periods a minimum generation level is desired. Normally this is 2000 kilowatts per hour; however, during dry periods, the plant's generation may be reduced to 500 kilowatts per hour or even down to zero to minimize the drawdown in the lake level. Finally, a minimum instantaneous downstream flow of 100 cfs must be maintained. This last requirement is usually satisfied by turbine wicked-gate leakage.

6.3 System Model

Scheduling reservoir operation requires models of the following key system elements: dynamics, operational constraints, and objectives.

System dynamics describe the system response to various inputs and outputs and on a day-to-day basis can be modelled by:

$$s(k+1) = s(k) - u(k) - g(k) - \ell(k) - f(k) + w(k), \qquad (6.1)$$
$$k = 0,1,\ldots,N,$$

where s(k) represents reservoir storage at the beginning of time period k; u(k) represents turbine release during the scheduled generation hours; g(k) is the release from the turbine assigned to meet the minimum

generation requirement of 2000 KW per day; $\ell(k)$ is turbine leakage; f(k) is flood gate or spillway outflow; w(k) is net reservoir inflow; k is the time discretization interval (corresponding here to one day); and N is the length of the control horizon.

The turbine release volume u(k) can be expressed as

$$u(k) = \left[\sum_{i=1}^{6} u_i(k) \right] t(k), \tag{6.2}$$

where $u_i(k)$ represents the discharge of the i^{th} turbine and t(k) is the scheduled power generation time during period k. These discharges depend upon the reservoir level and may correspond to best turbine efficiency, maximum power output, or some other operational mode.

The minimum generation release g(k) is given by

$$g(k) = [24 - t(k)] \, u_j^{min}(k), \tag{6.3}$$

where $u_j^{min}(k)$ is the discharge required to generate 2000 KW from the turbine designated for this purpose.

Turbine leakage is related to storage through

$$\ell_i(k) = \ell_i^{ref} \sqrt{(h[s(k)] - h_0) / h^{ref}}, \tag{6.4a}$$

$$\ell(k) = \sum_{i=1}^{6} \ell_i(k), \tag{6.4b}$$

where h_0 corresponds to the elevation of the turbine centerline; ℓ_i^{ref} are the leakage rates at some reference head h^{ref}, and h[s(k)] is the reservoir's elevation–storage relationship (Georgia Power, 1988). The values of these parameters are reported in Table 6.1:
The elevation–storage relationship (Figure 6.2) was determined via regression analysis on actual elevation–storage data:

$$\begin{aligned} h[s(k)] = {} & 443.81903 + 0.32732543\, s(k) - 0.79649653 \times 10^{-3} \, [s(k)]^2 \\ & + 21.076469 \, \ell n[s(k)] - 1.7542414 \, (\ell n[s(k)])^2 \\ & + 10.757541/s(k), \end{aligned} \tag{6.5}$$

where h is obtained in feet when s(k) is expressed in 1000 acre–feet. Some regression statistics are reported in Table 6.2.

Table 6.1: Parameters of the Leakage Functions

h_0 = 446 feet	h^{ref} = 81.24 feet
Turbine	ℓ_i^{ref} [cfs]
1	37.2
2	76.9
3	27.5
4	37.9
5	39.6
6	45.9
Total	265.0

Table 6.2: Statistics of the Elevation Storage Regression Equation

% of Variation Explained by Regression	99.9925
St. Deviation of Residuals [ft]	0.2183
Max. Pos. Deviation of Residuals [ft] (Predicted - Actual)	0.5893
Max. Neg. Deviation of Residuals [ft] (Predicted - Actual)	-0.3207

Flood gate outflow is also related to storage in a nonlinear fashion and is modelled as orifice or weir flow depending on whether or not the gate opening is submerged. The associated equations are as follows:

(i) If 518 feet $\leq h[s(k)] \leq$ 524.4 feet (orifice),

$$f(k) = \alpha_0 \, [L - \alpha_1 \, (h(s(k) - h_0)] \, [h[s(k)] - h_0]^{1.5} \, , \qquad (6.6a)$$

where α_0=3.1, L=20 feet, α_1=0.2, h_0=518 feet, h in feet, and f(k) in cfs.

(ii) If $h[s(k)] \geq$ 524.4 feet (weir),

$$f(k) = L \, d \, \beta_0 \, [\, 2 \, g \, (h[s(k)] - h_1)]^{0.5} \, , \qquad (6.6b)$$

where d=6 feet, g=32.17 feet/sec^2, h_1=521 feet, h in feet, f(k) in cfs, and β_0 is a coefficient which depends on the water depth as follows (Brater and King, 1967):

Table 6.3: Weir Flow Coefficients

H = h(s(k)) - 521 [feet]	β_0
3.4	0.530
3.9	0.535
5.7	0.569
7.6	0.584
9.4	0.595
≥ 12.0	0.600

Operational and physical constraints limit the variation of storage, release, and generation time to their feasible ranges:

$$s^{min}(k) \le s(k) \le s^{max}(k), \tag{6.7a}$$

$$u_i^{min}(k) \le u_i(k) \le u_i^{max}(k), \quad i=1,2,\ldots,6, \tag{6.7b}$$

$$t^{min}(k) \le t(k) \le t^{max}(k), \tag{6.7c}$$

$$k = 0,1,\ldots,N,$$

where s^{min} and s^{max} correspond to the minimum and maximum allowable storages; u_i^{min} and u_i^{max} are the discharges corresponding to the minimum and maximum turbine power output; and t^{min} and t^{max} determine the hours of energy generation within a day. Based on the discussion in the previous section, s^{min} can be taken equal to 3218 x10^6 ft^3 (522 feet) from September 1st through June 1st and 4247 x10^6 ft^3 (528 feet) for the remainder of the year, and s^{max} is equal to 4660 x10^6 ft^3. The minimum power output for all turbines is equal to 500 KW, while the maximum power output equals 3200 KW for turbines 1 to 4, and 3400 KW for turbines 5 and 6. t^{min} is equal to zero, and t^{max} can be 14 or 24 hours on a week day depending on the operational mode (14 corresponds to the duration of the peak period), and 0 or 24 hours on Saturdays and Sundays.

Due to inflow uncertainty, constraints (6.7a) should be restated in a probabilistic format:

$$Prob[s(k) \le s^{min}(k)] \le \gamma^{min}(k), \quad k=1,\ldots,N-1, \tag{6.8a}$$

$$Prob[s(k) \ge s^{max}(k)] \le \gamma^{max}(k), \quad k=1,\ldots,N-1, \tag{6.8b}$$

where γ^{min} and γ^{max} are the probabilistic tolerance levels.

The purpose of the Lloyd Shoals project is to maximize energy output. The power generation functions for each turbine were developed via regression analysis on simultaneous head, flow, and power measurements

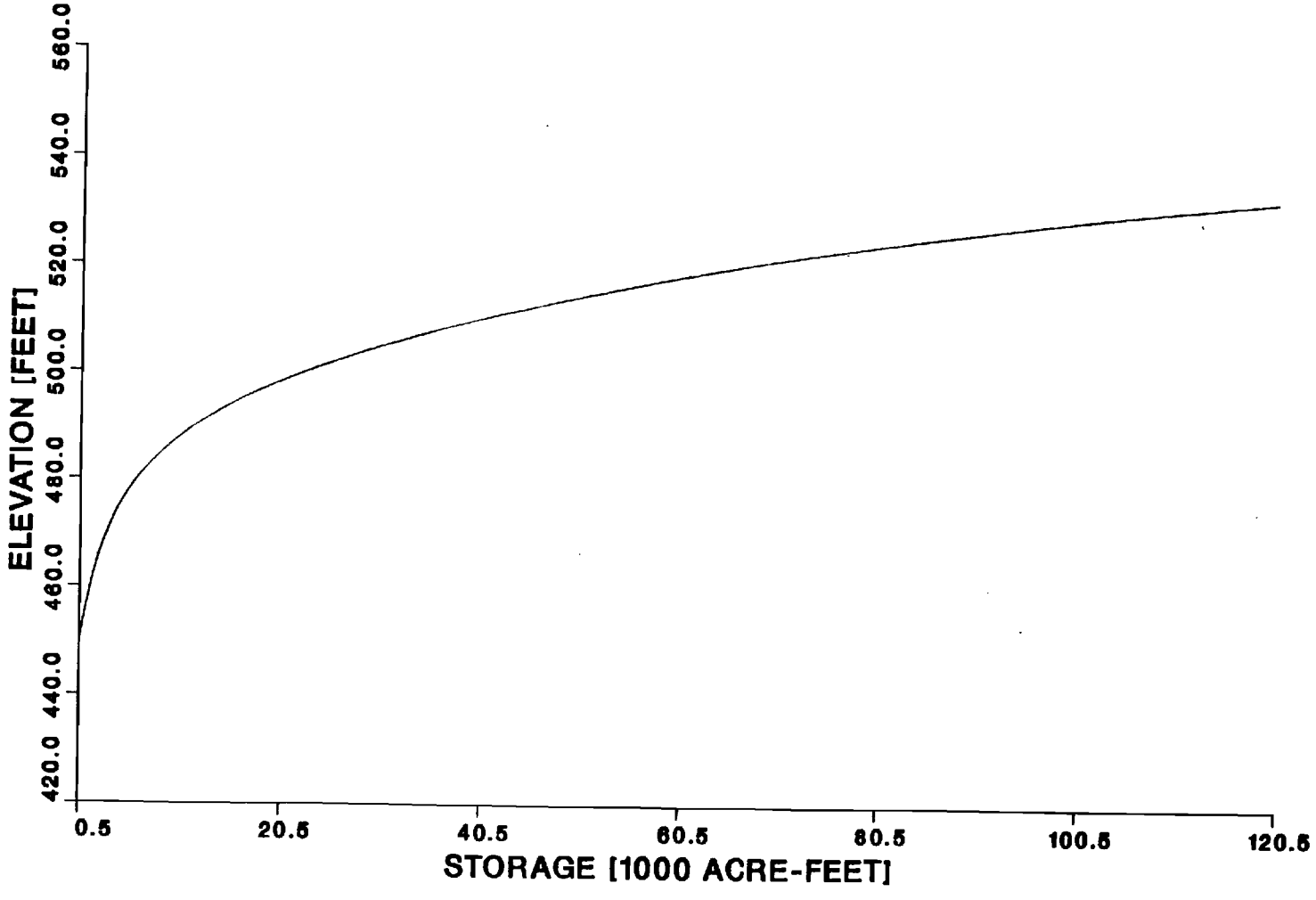

Figure 6.2: Elevation Versus Storage Relationship

and have the following form (Georgia Power, 1988):

$$p_i[h_i^n, u_i] = a_{i,1} + a_{i,2}\, h_i^n + [b_{i,1} + b_{i,2}\, h_i^n]\, u_i + [c_{i,1} + c_{i,2}\, h_i^n]\, u_i^2, \qquad (6.9)$$

$$i = 1,2,\ldots,6,$$

where $p_i[\ ]$ is the power output (KW), h_i^n is the net hydraulic head (feet), u_i is the turbine discharge (cfs) and a,b, and c are regression coefficients. The values of these coefficients are reported below:

Table 6.4: Coefficients of the Turbine Power Functions

$a_{1,1} = -1144.1307$	$a_{1,2} = 5.153575$
$b_{1,1} = 5.314086$	$b_{1,2} = 0.0283214167$
$c_{1,1} = -0.004464149$	$c_{1,2} = 0.0000172344$
$a_{2,1} = -1694.5590$	$a_{2,2} = 5.0963333$
$b_{2,1} = 5.511485$	$b_{2,2} = 0.03296675$
$c_{2,1} = -0.00428132$	$c_{2,2} = 0.000015404833$
$a_{3,1} = -1539.152$	$a_{3,2} = 5.0631667$
$b_{3,1} = 5.619713$	$b_{3,2} = 0.03401$
$c_{3,1} = -0.004682089$	$c_{3,2} = 0.00001684275$
$a_{4,1} = -1757.187$	$a_{4,2} = 5.096$
$b_{4,1} = 5.568577$	$b_{4,2} = 0.033434$
$c_{4,1} = -0.004446496$	$c_{4,2} = 0.000016007917$
$a_{5,1} = -2219.861$	$a_{5,2} = 5.70675$
$b_{5,1} = 6.171604$	$b_{5,2} = 0.036911167$
$c_{5,1} = -0.004794143$	$c_{5,2} = 0.000017251417$
$a_{6,1} = -1425.7394$	$a_{6,2} = 4.7300083$
$b_{6,1} = 5.099076$	$b_{6,2} = 0.03046375$
$c_{6,1} = -0.003934244$	$c_{6,2} = 0.0000141565$

Figure 6.3 displays the power function of the first turbine.

The net hydraulic head is determined based on the reservoir forebay elevation, the tailwater elevation, and the frictional energy losses. For a total outflow Q, the tailwater elevation can be computed from (Figure 6.4)

$$Q \le 3300 \text{ cfs} : t_w(Q) = 423.43666 + 2.8724141\, Q - 1.7019926\, Q^2 + 0.69391531\, Q^3 - 0.09701342\, Q^4, \qquad (6.10a)$$

$$Q \ge 3300 \text{ cfs} : t_w(Q) = \exp\{\, 6.0498451 + 0.75771347 \times 10^{-2}\, [\ell n(Q)] + 0.64189658 \times 10^{-3}\, [\ell n(Q)]^2 - 0.98717478 \times 10^{-3}\, [\ell n(Q)]^3 + 0.28708173 \times 10^{-3}\, [\ell n(Q)]^4\, \}, \qquad (6.10b)$$

where t_w in obtained in feet when Q is expressed in 1000 cfs. Some statistics of the above regression equations are included in the Table 6.5:

The frictional energy losses can be estimated from

$$f_r(u_i) = 1.5\ [u_i/580]^2, \qquad (6.11)$$

where f_r is obtained in feet when u_i is expressed in cfs (Figure 6.5, Georgia Power, 1988).

Table 6.5: Statistics of the Tailwater Regression Equations

	$Q \leq 3300$ cfs	$Q \geq 3300$ cfs
% of Variation Explained by Regression	99.9603	99.9976
St. Deviation of Residuals [ft]	0.0246	0.0234
Max. Pos. Deviation of Residuals [ft] (Predicted - Actual)	0.0352	0.0352
Max. Neg. Deviation of Residuals [ft] (Predicted - Actual)	-0.0360	-0.0340

Lastly, the net hydraulic head is obtained as follows:

$$h_i^n = h[s(k)] - t_w(Q) - f_r(u_i). \qquad (6.12)$$

It is noted that although the previous system model was motivated by the Lloyd Shoals hydroelectric project, it includes all elements characterizing any reservoir system expected to provide hydroelectric services. Furthermore, the control method presented in the next section is also generally applicable.

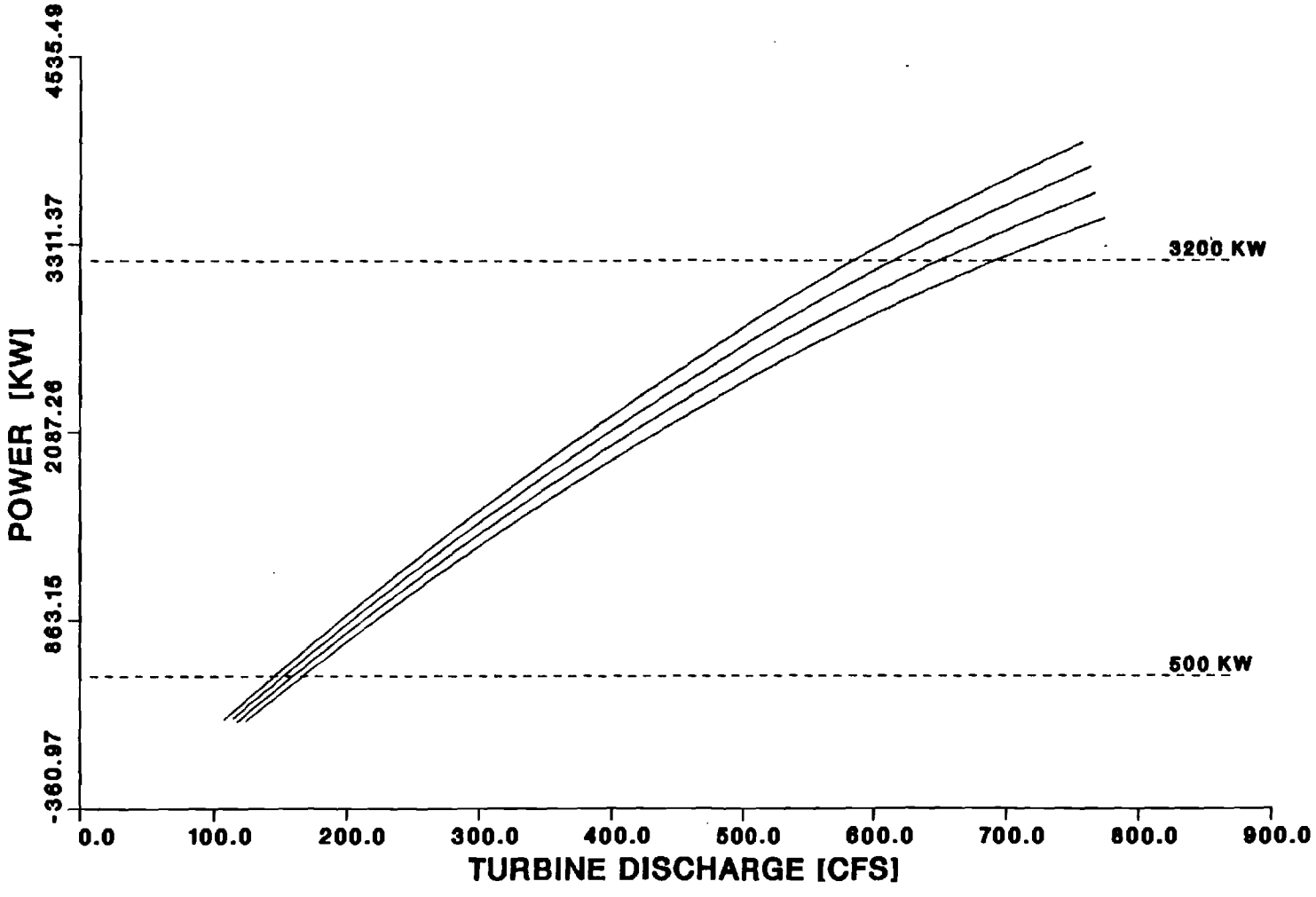

Figure 6.3: The Power Function of the First Turbine

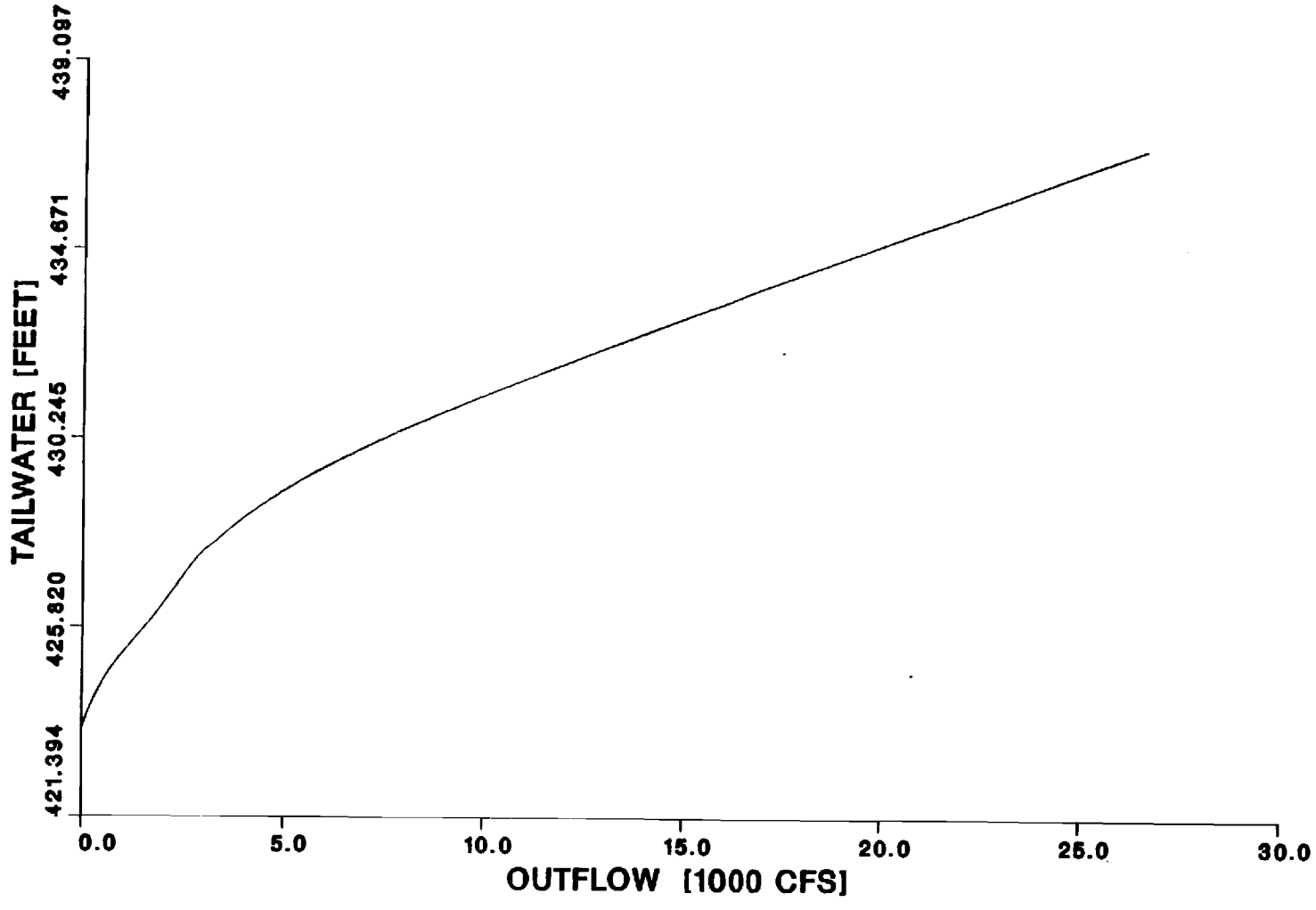

Figure 6.4: Tailwater Curve

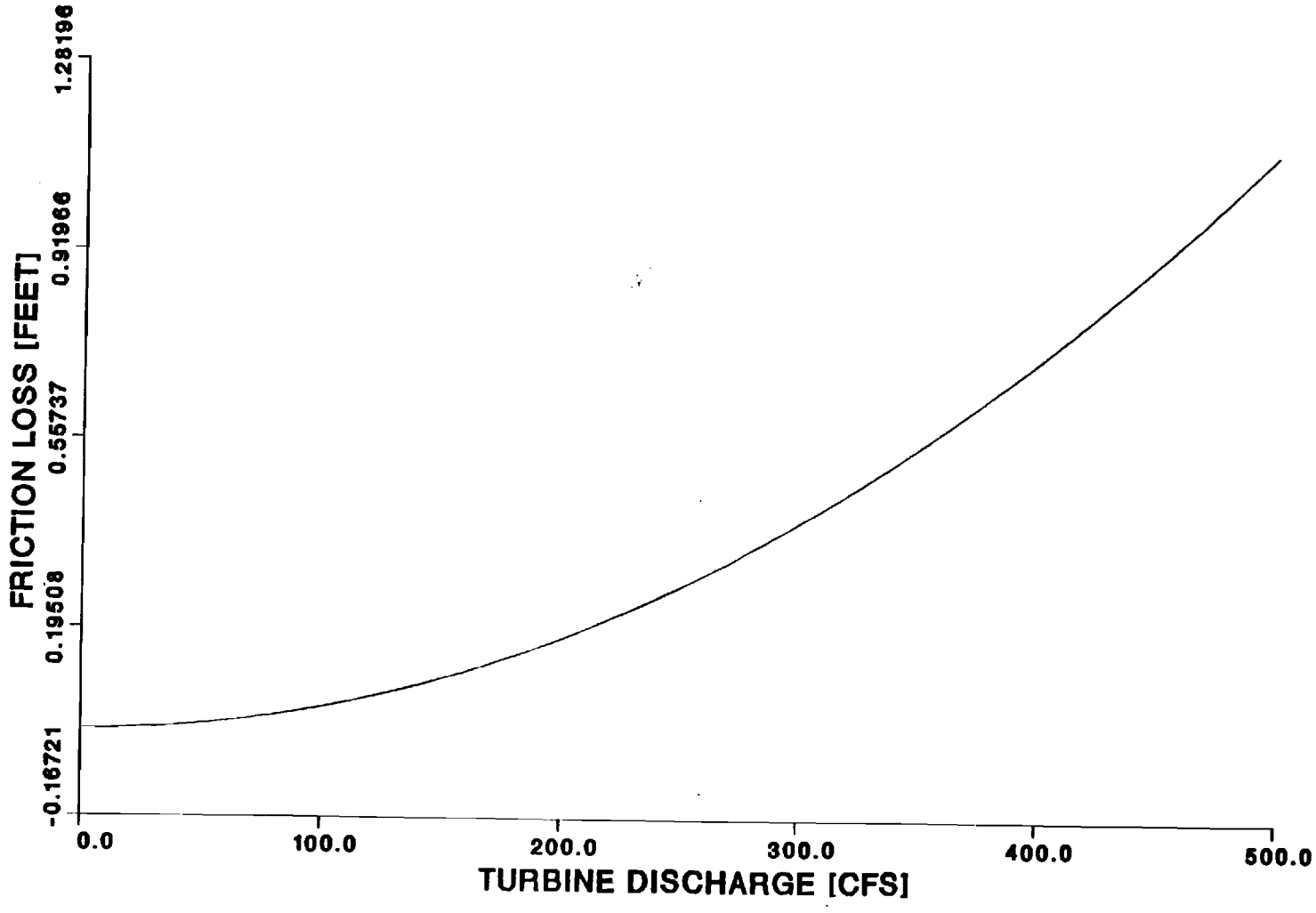

Figure 6.5: Hydraulic Frictional Losses

6.4 Control Model

6.4.1 Overview

The control model is a stochastic dynamic optimization scheme which determines optimal daily release and power generation schedules. This model is based on the Extended Linear Quadratic Gaussian (ELQG) reservoir control method (Georgakakos and Marks, 1987, Georgakakos, 1989a,b), but it also includes certain new enhancements which make it more suitable for hydropower systems.

The control model (Figure 6.6) includes five operational levels which are activated in the following sequential manner: The goal of the first level is to determine the optimal generation time schedule and associated discharges which maximize turbine efficiency during the peak generation periods. If a feasible solution is found here, the process terminates. The optimal power generation schedules for the next day are implemented, and the decision process is repeated at the beginning of the next day. If, on the other hand, some of the upper storage bounds are violated, indicating high inflows, the controller activates its second level.

The second level abandons best efficiency operation and attempts to find a solution with the turbines running fully open; that is, at maximum power. Generation times are again constrained within the peak period. If this level fails to bring the reservoir storage within its bounds, the controller invokes its third level.

The third level relaxes the peak period restriction and additionally allows for off-peak generation at maximum power. If a feasible solution cannot be found still, the controller activates its fourth level.

The fourth level operates the hydroelectric plant at maximum power for 24 hours a day and additionally invokes the flood gate. The flood gate is the last operational control and, if it is unable to control the water levels from rising past the flash boards, the prescribed action is to run all available turbines and flood gate wide open.

If while in the first control level, the storage sequence violates its lower bounds (low flows), the controller actuates its fifth level. This level decreases the minimum generation requirement until the storage sequence becomes feasible. If this is not viable, the controller prescribes complete shut-down of the hydroelectric facility.

Each of the previous five levels, solves the real-time scheduling problem by utilizing a new, two-module, stochastic control procedure. A more detailed discussion of the functions of each control level and module follows next.

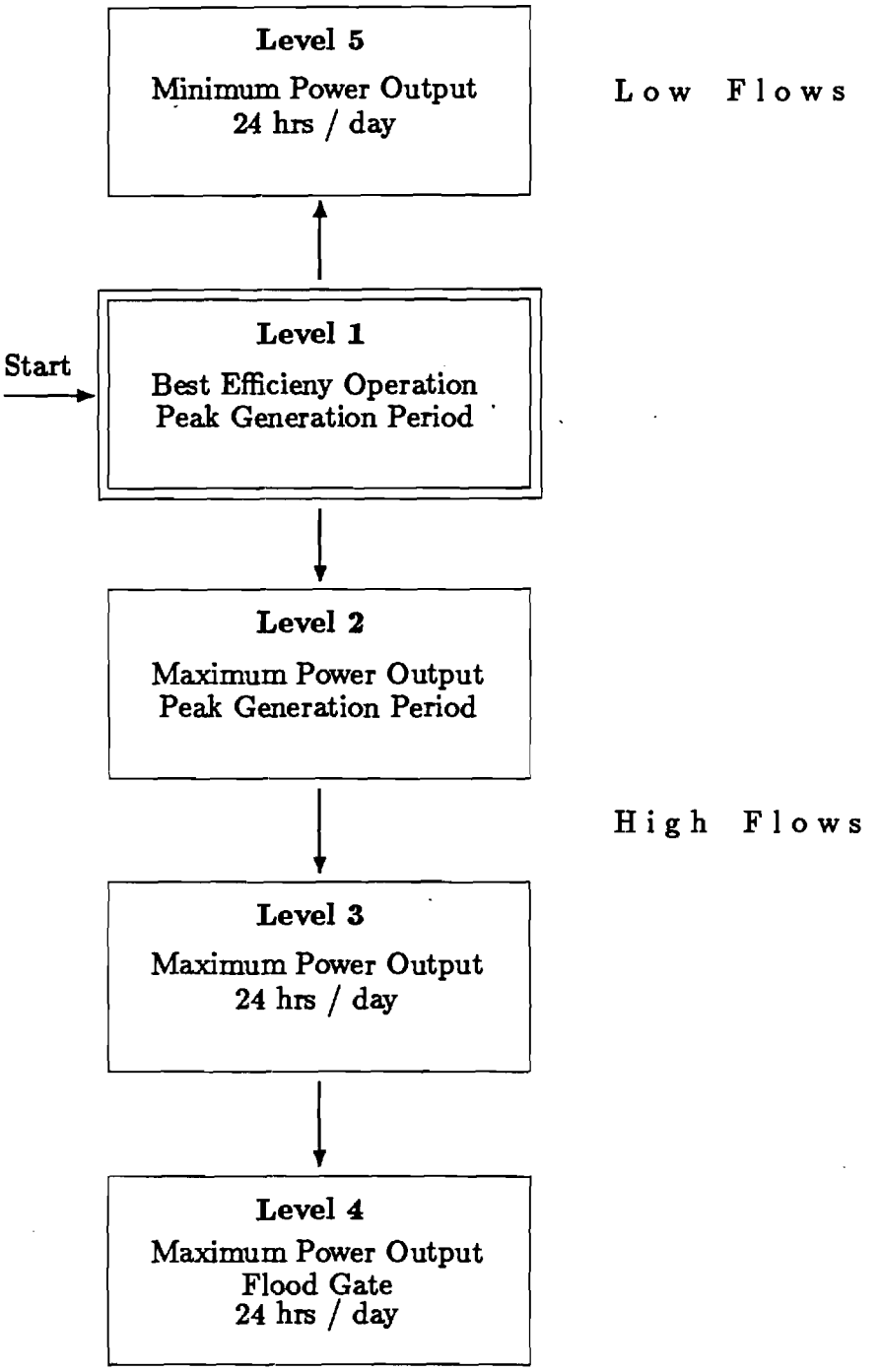

Figure 6.6: Control Model Structure

6.4.2 The First Control Level

The first control level is activated first and attempts to find optimal power generation and discharge schedules which maximize the efficiency of the turbines during the peak generation periods. In general, a streamflow forecasting model can be invoked at this stage to predict reservoir inflows over the control horizon. (Due to luck of adequate hydrologic data records, inflow forecasting can only be simulated here.) Subsequently, the control algorithm is called upon to solve the scheduling problem by iteratively activating two optimization modules (Figure 6.7).

The first optimization module (I) accepts the inflow forecasts from the forecasting model and estimates of the turbine discharges and leakage rates from the second module (II) and finds optimal power generation schedules (hours of generation within the peak generation period of each day.

The problem solved in this module is to find the optimal $\{t(k), k=0,\ldots,N-1\}$ sequence which minimizes

$$J = E\left\{ \sum_{k=0}^{N-1} \sum_{i=1}^{6} \xi_i(k) \left[P_i^{max} t_p - t(k)\, p_i[h_i^n, u_i] \right]^2 + L[s(N),N] \right\} \quad (6.13)$$

subject to

(α) the storage dynamics:

$$s(k+1) = A(k)\, s(k) + B(k)\, t(k) + \omega(k) \quad (6.14)$$

where $A(k) = 1$,

$$B(k) = -\sum_{i=1}^{6} [\xi_i(k)\, u_i(k) + \psi_i(k)\, u_i^{min}(k) + (\xi_i(k) - \psi_i(k))\, \ell_i(k)],$$

$$\omega(k) = w(k) - 24 \sum_{i=1}^{6} [\psi_i(k)\, u_i^{min}(k) + (1 - \xi_i(k))\, \ell_i(k) + (\xi_i(k) - \psi_i(k))\, \ell_i(k)],$$

$$\xi_i(k) = \begin{cases} 1, & \text{if turbine i is operational during period k,} \\ 0, & \text{if turbine i is unavailable during period k,} \end{cases}$$

$$\psi_i(k) = \begin{cases} 1, & \text{if turbine i is designated to cover the minimum generation requirements during period k,} \\ 0, & \text{if turbine i will not cover the minimum generation requirements during period k;} \end{cases}$$

(β) the storage and generation time constraints:

$$Prob[s(k) \le s^{min}(k)] \le \gamma^{min}(k), \quad k=1,2,\ldots,N, \quad (6.15a)$$

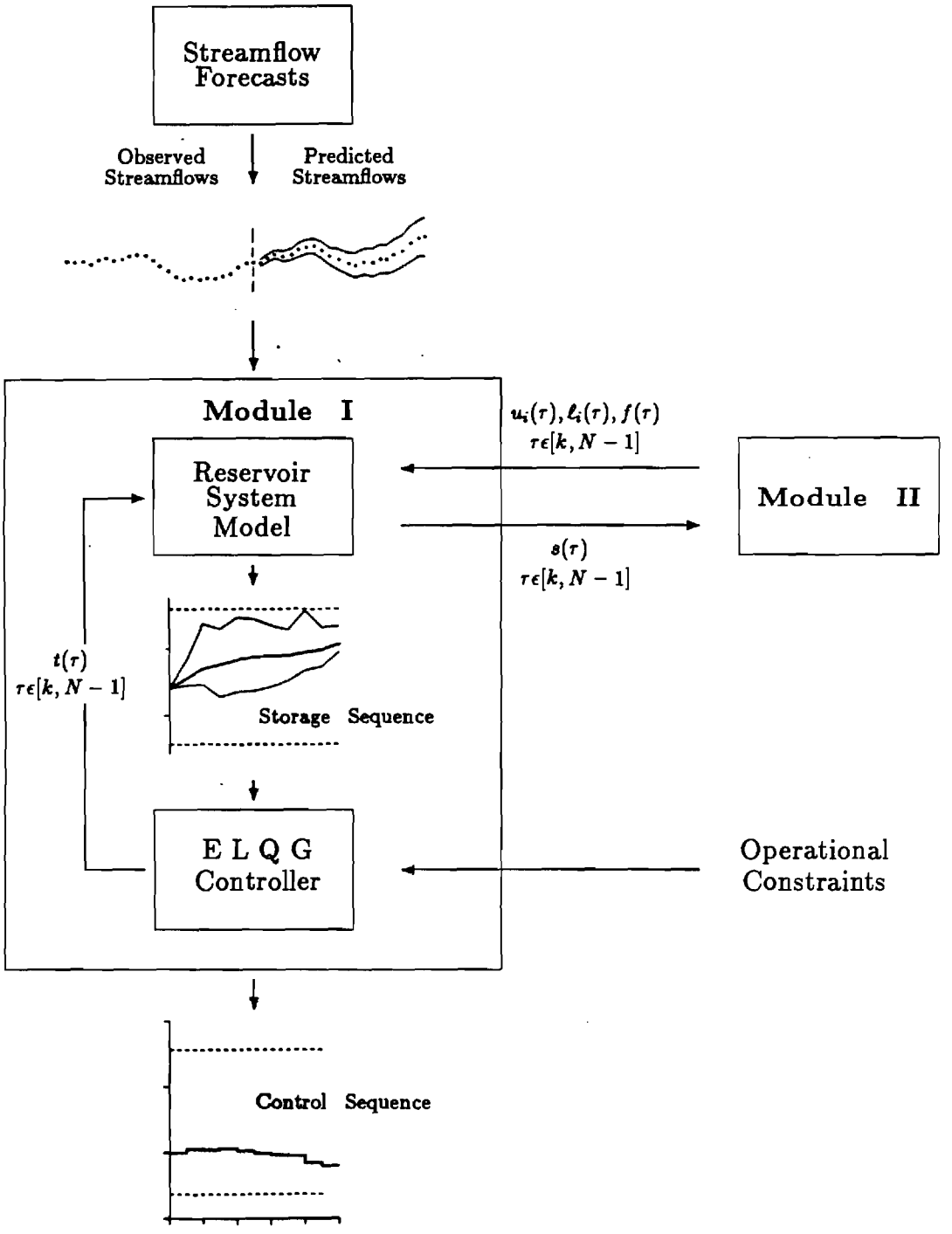

Figure 6.7: A Two-Module Control Method

$$\text{Prob}[s(k) \geq s^{max}(k)] \leq \gamma^{max}(k), \quad k=1,2,\ldots,N, \tag{6.15b}$$

$$t^{min}(k) \leq t(k) \leq t^{max}(k), \quad k=0,1,\ldots,N-1. \tag{6.15c}$$

In the above index, t_p represents the target generation period (hours), and P_i^{max} is the maximum power output of turbine i. Equation (6.14) follows directly from the definitions given in the previous section. The values of ξ, ψ, s^{min}, s^{max}, γ^{min}, γ^{max}, t^{min}, and t^{max} are specified by the user. In this level, $[t^{min},t^{max}]$ represents the peak generation period of each day (8:00 am to 10:00 pm for Monday through Friday), and s^{min} and s^{max} are the minimum and maximum storages as discussed in the previous section. The terminal cost term L[s(N),N] is a quadratic function with origin at the upper storage bound to reflect the long-term operation policy of maintaining high reservoir levels.

This is a stochastic control problem which can be solved via the ELQG control method (Georgakakos and Marks, 1987, Georgakakos, 1989a,b). For a detailed discussion of this method, the reader is referred to the previous citations. Herein the emphasis will be on the new method enhancements. The main difference between this and the more traditional reservoir control problem formulations (see, for instance, Georgakakos, 1989a) is that the optimization variables do not represent release volumes but rather power generation hours. As will be seen, this novelty leads to a more accurate description of the system's hydroelectric function.

In this level, the second control module (II) is commissioned to determine the discharge rates which maximize turbine efficiency over the interval [0,t(k)] and satisfy the minimum generation requirements for the remainder of the day [t(k),24]. The efficiency e_i of the ith turbine is defined by

$$e_i = p_i / [\eta\, u_i\, h_i^n], \tag{6.16}$$

where p_i is the power generation function given by Equation (6.9), u_i is turbine discharge, h_i^n is the net hydraulic head, and η is a constant equal to 0.08465 when u_i is in cfs, h_i^n in feet, and p_i in KW. Figure 6.7 displays the power and efficiency curves of the first turbine for a net head of 100 feet.

Efficiency maximization is subject to power generation constraints,

$$P_i^{min} \leq p_i \leq P_i^{max}, \quad i=1,2,\ldots,6, \tag{6.17}$$

and involves all turbines due to the coupling introduced by the net hydraulic head. Thus, the problem to be solved in this module is to find the discharges, $\{u_i, i=1,\ldots,6\}$, which maximize the efficiency

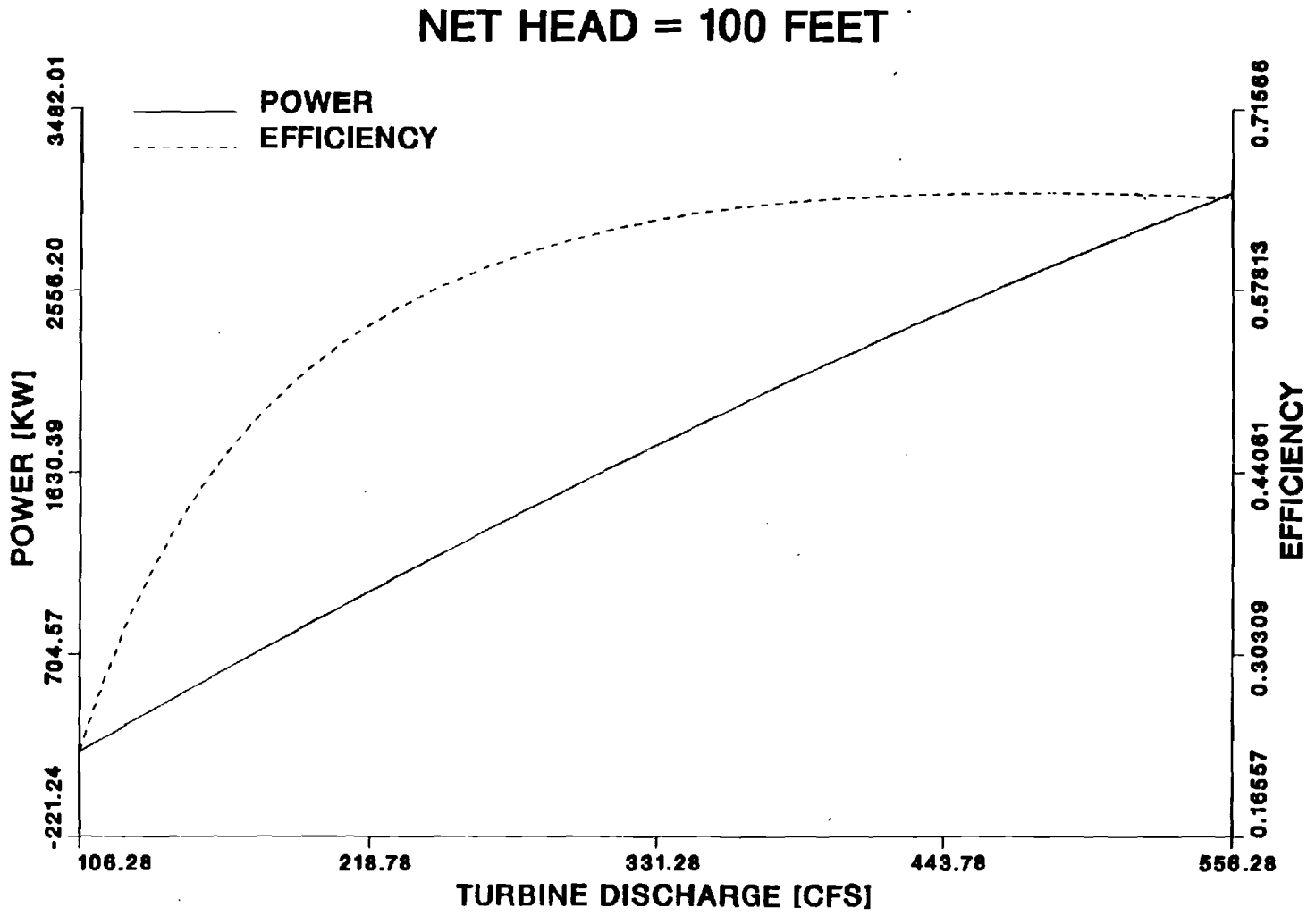

Figure 8: Efficiency–Power Curves for the First Turbine

of the available turbines, $\{e_i,\ i=1,\ldots,6\}$, subject to the power constraints (6.17). For this problem, reservoir storage is specified by the first control module. If the first module problem is stochastic, reservoir storage can be set equal to its expected value.

Substituting the power expression (6.9) in Equation (6.16), yields

$$e_i = \frac{1}{\eta\, u_i}\left[a_{i,1} + \frac{a_{i,2}}{h_i^n}\right] + \frac{1}{\eta}\left[b_{i,1} + \frac{b_{i,2}}{h_i^n}\right] + \frac{u_i}{\eta}\left[c_{i,1} + \frac{c_{i,2}}{h_i^n}\right], \quad (6.18)$$

where h_i^n depends on the discharge u_i through Equation (6.12).

Taking the first and second derivatives of the above expression with respect to u_i is a tedious task, but it establishes that $\partial^2 e_i/\partial u_i^2$ is negative and therefore demonstrates that e_i is a concave function of u_i. Thus, the optimal u_i's are those which set the first derivative of (6.18) equal to zero or, if this happens outside the feasible ranges defined by (6.16), those which correspond to the exceeded power bound. These optimal values are obtained here by the following algorithm:

Algorithm IIα: Specification of Turbine Discharge Rates for $[0,t(k)]$

1. Set $\{u_i(k),\ i=1,..,6\}$ equal to some initial values.

2. Determine the forebay elevation $H = h[\bar{s}(k)]$, where $\bar{s}(k)$ is the mean storage value specified by the first control module.

3. Determine the total reservoir outflow rate:

$$Q = \sum_{i=1}^{6} [\xi i(k)\ u_i(k) + (1 - \xi_i(k))\ \ell_i(k)], \quad (6.19)$$

where $\ell_i(k)$ is the leakage rate given by Equation (6.4a).

4. Compute the net hydraulic head for each turbine:

$$h_i^n = H - t_w(Q) - f_r[u_i(k)],\ i=1,\ldots,6, \quad (6.20)$$

where $f_r[\ ]$ is the frictional loss function (Eq. (6.11)).

5. Determine the discharge rates $\bar{u}_i(k)$ which maximize turbine efficiency (Eq. (6.18)). Assuming that h^n are constant, these discharges can be analytically computed by taking the derivative of Equation (6.18) and setting it equal to zero. The result is the following:

$$\bar{u}_i(k) = \sqrt{\frac{a_{i,1} + \dfrac{a_{i,2}}{h_i^n}}{c_{i,1} + \dfrac{c_{i,2}}{h_i^n}}},\ i=1,\ldots,6, \quad (6.21)$$

6. Compute the power, $p_i[h^n,\bar{u}_i]$, i=1,...,6, associated with the previous net heads and discharge rates from Equation (6.9).

$$\text{If} \quad p_i^{min} > p_i[h^n,\bar{u}_i] \quad \text{or} \quad p_i[h^n,\bar{u}_i] > p_i^{max},$$

compute the discharge rates that correspond to the exceeded power bound. These discharge rates can be computed by setting the left-hand side of Equation (6.9) equal to the exceeded power bound and solving the resulting quadratic equation with respect to u_i. The solution is obtained from

$$\bar{u}_i(k) = \frac{-B_i + \sqrt{B_i^2 - 4 A_i C_i}}{2 A_i}, \tag{6.22}$$

where $A_i = c_{i,1} + c_{i,2} h_i^n$,

$B_i = b_{i,1} + b_{i,2} h_i^n$,

$Ci = a_{i,1} + a_{i,2} h_i^n - p^{bound}$,

and the values of $a_{i,1}$, $a_{i,2}$, $b_{i,1}$, $b_{i,2}$, $c_{i,1}$, and $c_{i,2}$ are given in Table 6.4.

7. Update the total reservoir outflow rate,

$$\bar{Q} = \sum_1^6 [\xi_i(k)\ \bar{u}_i(k) + (1 - \xi_i(k))\ \ell_i(k)], \tag{6.23}$$

and compute the difference $D = [\bar{Q} - Q]$. If $|D| \leq \epsilon$, terminate; otherwise repeat Steps 4 through 7. The value of ϵ controls the accuracy of the solution and can be set, for instance, equal to 1 cfs.

The rational behind this algorithm is that turbine efficiency and power output are primarily controlled by turbine discharge while net head adjustments from iteration to iteration are relatively small. As a result, this optimization scheme is characterized by fast convergence rate requiring about 2 to 3 iterations to convergence.

The second task of the second module is to determine the discharge $u_i^{min}(k)$ of the ith turbine which is designated to cover the minimum generation requirement of 2,000 KW over the remainder of the day [t(k),24]. These computations can also be organized in a similar algorithmic manner.

Algorithm IIβ: Specification of Turbine Discharge Rates for [t(k),24]

1. Set $u_i^{min}(k)$ equal to some initial value.

2. Determine the forebay elevation $H = h[\bar{s}(k)]$, where $\bar{s}(k)$ is the mean storage value specified by the first control module.

3. Determine the total reservoir outflow rate:

$$Q = u_i^{min}(k) + \sum_{j=1}^{6} [(1 - \psi_j(k))\ \ell_j(k)], \tag{6.28}$$

where $\ell_j(k)$ is the leakage rate given by Equation (6.4a).

4. Compute the net hydraulic head for the ith turbine:

$$h_i^n = H - t_w(Q) - f_r[u_i^{min}(k)], \tag{6.29}$$

where $f_r[\ ]$ is the frictional loss function (Eq. (6.11)).

5. Compute the discharge rates that correspond to the minimum generation requirement P^{mg} :

$$\bar{u}_i^{min}(k) = \frac{-B_i + \sqrt{B_i^2 - 4\ A_i\ C_i}}{2\ A_i}, \tag{6.30}$$

where $A_i = c_{i,1} + c_{i,2}\ h_i^n$,

$B_i = b_{i,1} + b_{i,2}\ h_i^n$,

$Ci = a_{i,1} + a_{i,2}\ h_i^n - P^{mg}$,

and the values of $a_{i,1}$, $a_{i,2}$, $b_{i,1}$, $b_{i,2}$, $c_{i,1}$, and $c_{i,2}$ are given in Table 6.4.

6. Update the total reservoir outflow rate,

$$\bar{Q} = \bar{u}_i^{min}(k) + \sum_{j=1}^{6} [(1 - \psi_j(k))\ \ell_j(k)], \tag{6.31}$$

and compute the difference $D = [\bar{Q} - Q]$. If $|D| \leq \epsilon$, terminate; otherwise repeat Steps 4 through 6. Again, the value of ϵ controls the accuracy of the solution and can be set equal to 1 cfs.

The previous tasks of the second control module are to be performed for all time periods k of the control horizon [0,N-1]. Thus, the second control module accepts values of the mean storage trajectory from the solution of the first module problem, and it generates best efficiency and minimum generation discharge rates. These discharges are fed back and help update the first module solution, with this exchange continuing until convergence. At the completion of this process, the storage trajectory is examined for possible constraint violations. If storage constraints (6.8) are not violated, the model terminates and the first day's optimal generation schedule is implemented. If upper storage constraints are violated (probability of exceedance is higher than the specified tolerance γ^{max}, indicating flood condition), the controller activates its second level. If, on the other hand, lower constraints cannot be satisfied (drought condition), the controller activates its fifth level.

6.4.3 The Second Control Level

The second level is activated when best efficiency discharges and the peak generation time of 14 hours daily excluding weekends cannot lower reservoir storage within its feasible range. The purpose here is to investigate whether maximizing power output within the peak period will prevent storage constraint violations. The solution is again obtained using the two-module control scheme described in the previous section with the following specifications:

Module I: As in the first level.

Module II: Step 5 of Algorithm IIα for the computation of the best efficiency discharge rates is replaced by Step 6 which is now performed for all available turbines.

If this level's solution is feasible, the model terminates. Otherwise, it invokes the third level.

6.4.4 The Third Control Level

The third level lifts the peak generation period restriction and allows for up to 24-hour daily generation time for both week-days and weekends. The solution is obtained as in the previous levels with the following specifications:

Module I: The values of the parameters t_p and $\{t^{max}(k),\ k=0,\ldots,N-1\}$ in Index (6.13) and Constraints (6.15c) are set equal to 24 hours.

Module II: As in the second control level.

As before, if the solution is feasible, the model terminates; otherwise, it activates the fourth level.

6.4.5 The Fourth Control Level

The fourth level is activated when turbine discharge rates at maximum power output are inadequate to prevent reservoir levels from exceeding the flash board tripping threshold of 530 feet. The last operational control is to force reservoir storage within the permissible bounds by utilizing the flood gate. Generation times are now fixed to 24 hours, and turbine discharges correspond to the highest allowable power output. The problem here is to find the necessary flood gate operation schedules which produce feasible reservoir storages. The solution can again be found by using the two-module control scheme introduced earlier in the following manner:

Module I: The problem solved in this Module can be stated as follows: Determine the optimal flood gate operation schedule $\{t_f(k),\ k=0,1,\ldots,N-1\}$ which minimizes

$$J = E\left\{ \sum_{k=0}^{N-1} [s(k) - s^*(k)]^2 + [s(N) - s^*(N)]^2 \right\} \tag{6.32}$$

subject to

(α) the storage dynamics:

$$s(k+1) = A(k)\ s(k) + B(k)\ t_f(k) + \omega(k) \tag{6.33}$$

where $A(k) = 1$,

$B(k) = f(k)$ (flood gate outflow rate as computed by Eq. (6.6))

$$\omega(k) = w(k) - 24 \sum_{i=1}^{6} [\xi_i(k)\ u_i(k) + (1 - \xi_i(k)\ \ell_i(k)]$$

$$\xi_i(k) = \begin{cases} 1\ , & \text{if turbine i is operational during period k,} \\ 0\ , & \text{if turbine i is unavailable during period k,} \end{cases}$$

(β) the storage and generation time constraints:

$$\text{Prob}[s(k) \le s^{\min}(k)] \le \gamma^{\min}(k), \quad k=1,2,\ldots,N, \tag{6.34a}$$

$$\text{Prob}[s(k) \ge s^{\max}(k)] \le \gamma^{\max}(k), \quad k=1,2,\ldots,N, \tag{6.34b}$$

$$0 \le t_f(k) \le 24, \quad k=0,1,\ldots,N-1. \tag{6.34c}$$

In the above formulation, $s^*(k)$, $k=1,..,N$, can be set equal to the upper storage bounds, the purpose being to determine the necessary flood gate releases which will satisfy the violated storage constraints. As before, the solution of this stochastic control problem may be obtained by the ELQG control method.

Module II: The purpose of this Module is simply to determine the discharge rates which maximize power output. The procedure is similar to the one presented in the third level with the exception of Steps 3 and 7, in Algorithm IIα, where the total reservoir outflows should be computed by

$$Q = \sum_{i=1}^{6} [\xi i(k)\ u_i(k) + (1 - \xi_i(k))\ \ell_i(k)] + f(k), \tag{6.35}$$

$$\tilde{Q} = \sum_{i=1}^{6} [\xi i(k)\ \tilde{u}_i(k) + (1 - \xi_i(k))\ \ell_i(k)] + f(k). \tag{6.36}$$

Flood gate release is the last control that can be exercised by the operator and even if reservoir storage cannot be sufficiently lowered, the model terminates suggesting that all turbines and the flood gate be

operated fully open 24 hours a day. The reason for letting water through the flood gate is to keep reservoir storage from exceeding the level of 530 feet. As discussed in Section 2, when water level rises above this threshold, the flash boards trip and cannot be repositioned until water level falls below 528 feet, causing a substantial loss of hydraulic head and water volume.

6.4.6 The Fifth Control Level

Levels 2, 3, and 4 are sequentially invoked depending on the severity of the upcoming flood. The fifth level is invoked during droughts when the optimal generation times are zero, and certain lower storage constraints are still violated. This level simply reduces the initially specified 2000 KW minimum generation requirements by 500 KW at a time, and it terminates when storage becomes feasible. The solution is obtained by following the procedures outlined in the first level; the only difference is that Algorithm IIβ is implemented with reduced values of the minimum generation P^{mg}. These reductions amount to 500 KW each time. If P^{mg} is reduced to 500 KW without attaining storage feasibility, the controller prescribes that the power plant be completely shut down.

6.5 Case Studies

6.5.1 Control Experiments

This section presents some computational experience with the control scheme presented earlier. The purpose here is (1) to provide engineering insight to this method's performance in real time decision operations and (2) to familiarize the user with the program's result presentation format.

For all three control experiments to be presented, the reservoir is initially assumed to have a storage of 4,000 million cubic feet and the control horizon is taken equal to 14 days. The lower and upper storage bounds are equal to 3,118 and 4,660 million cubic feet respectively (corresponding to 522 and 530 feet reservoir elevations). The starting date is Friday, January 1st, 1988. Apart from maximizing peak energy output, the controller also attempts to maintain end-of-horizon storage as high as possible. The tolerance levels γ are set equal to 2.5%. The objective of the control experiments is to maximize peak power generation under three different hypothetical inflow forecast scenarios. The inflow forecast statistics are shown on Figure 6.9. The forecast probability distributions are assumed to be lognormal with mean and standard deviation as indicated. Table 6.6 presents the optimal schedules for the first experiment. (Results are included for the first ten days of the control horizon.) For each period (day) the following quantities are reported: turbine discharge and power output during the daily generation time; turbine leakage for the non-generation period; power generation time; mean end-of-day storage and reservoir level; minimum generation output, designated turbine, and discharge; and flood gate discharge and operation time. Figure 6.10 portrays the optimal generation time and storage sequences. The dashed lines delineate the associated bounds; the three lines in the storage graph represent the mean and the 95% probability band about the mean. As can be seen from these results, the controller finds the optimal solution while in the first operational level. Namely, turbines "run" at best efficiency for a portion of the 14-hour peak generation period. The second, third, ninth, and tenth days, corresponding to Saturdays and Sundays, have no peak generation periods. For Turbines 2, 4, and 5 best efficiency generation implies maximum power output.

Table 6.7 and Figure 6.11 summarize the results of the second computational experiment with intermediate flow statistics. The optimal sequences are now found with the system in the third level of operation where all six turbines "run" at full gate for up to 24 hours a day including weekends.

Lastly, Table 6.8 and Figure 6.12 report the results of the third computational experiment. Anticipating high flows, the controller resorts to the fourth level where the flood gate may be opened to

prevent overtopping of the flash boards. Although overtopping may happen 14 days into the future, the controller indicates that the flood gate must be operated from the first day (3.48 hours) if the associated risk is to be kept lower than or equal to 2.5%.

The previous experiments were performed on a CYBER 180/990 digital computer. Each experiment required approximately 2 CPU seconds. High computational efficiency is a distinctive characteristic of this approach and is due to the excellent convergence properties of the control algorithms developed. As a result, microcomputer implementations are also feasible.

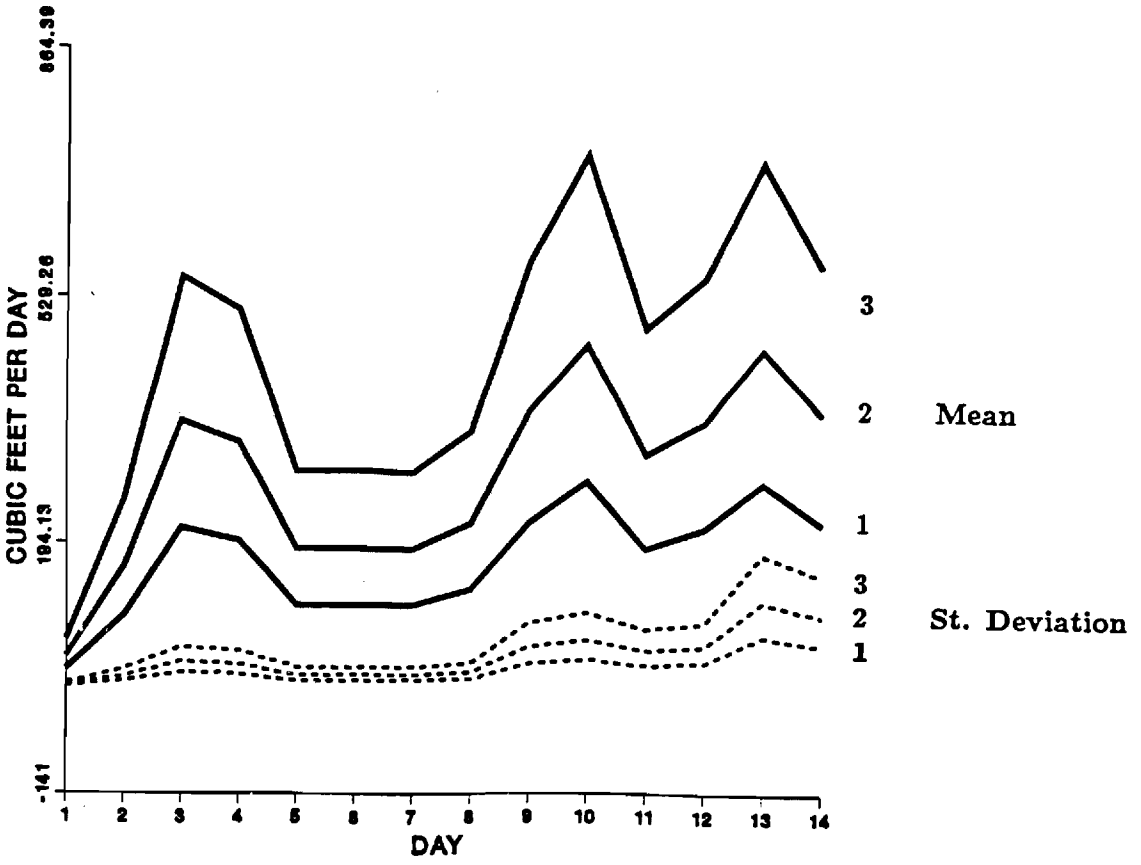

Figure 6.9: Inflow Forecast Statistics

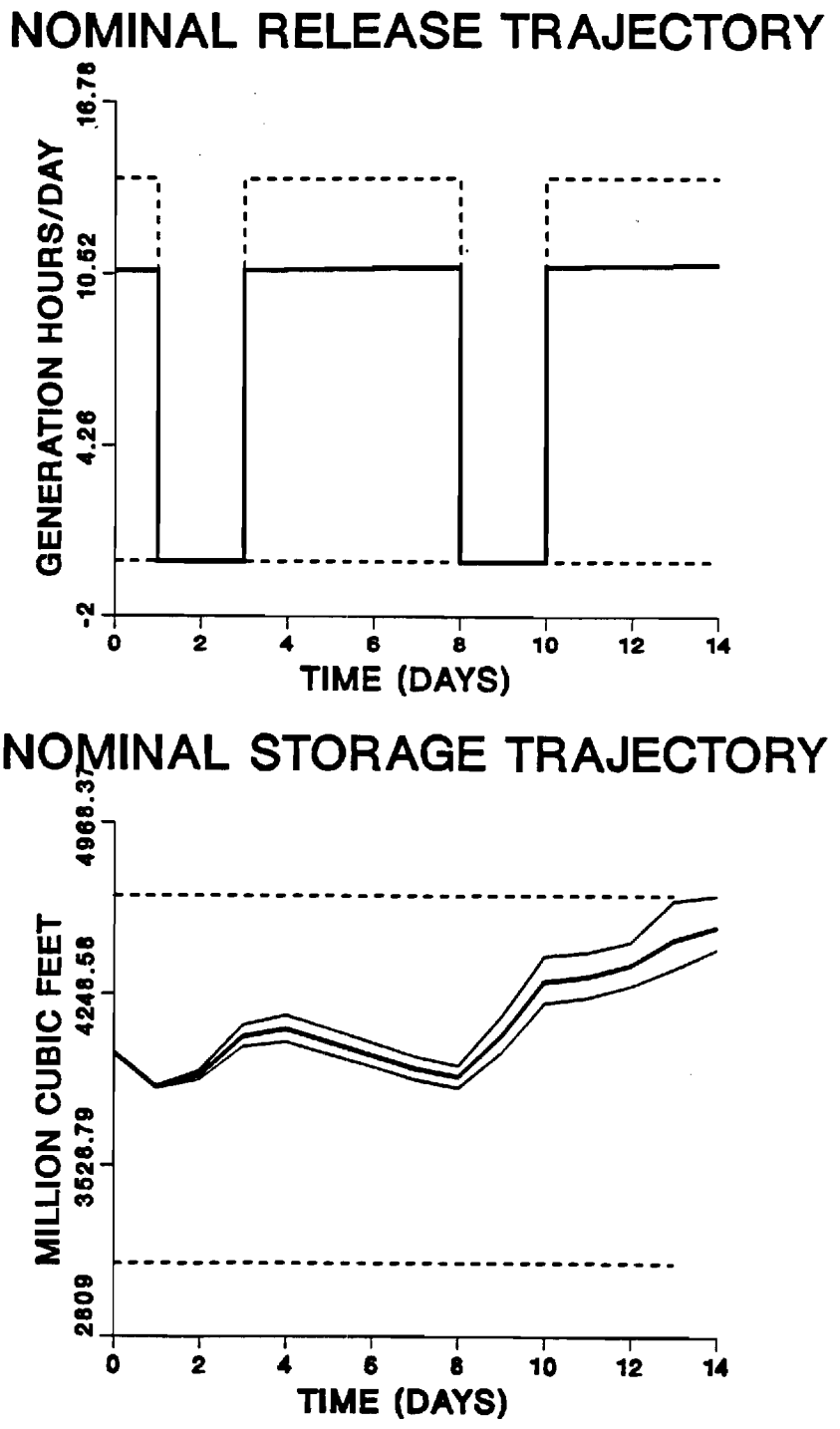

Figure 6.10: Optimal Sequences for Experiment #1

Table 6.6: Optimal Schedules for Experiment #1

OPTIMAL RELEASE AND POWER GENERATION SCHEDULES
STARTING DATE: 1/1/1988

PERIOD 1

TURBINE #	1	2	3	4	5	6
DISCHARGE (CFS):	480.06	634.94	586.36	643.23	660.35	614.44
POWER (KW):	2595.39	3200.00	3135.85	3200.00	3400.00	3012.80
LEAKAGE (CFS)	37.08	76.65	27.41	37.77	39.47	45.75

GENERATION TIME: 10.65 HRS
FORECASTED END-OF-PERIOD STORAGE: 3857.75 MILLION CUBIC FEET
FORECASTED END-OF-PERIOD RESERVOIR LEVEL: 525.92 FT
MINIMUM GENERATION: 2000.00 KW FROM TURBINE #1 AT 364.18 CFS DISCHARGE
FLOOD GATE RELEASE: 0.00 CFS
FULL GATE OPERATION: 0.00 HRS

PERIOD 2

TURBINE #	1	2	3	4	5	6
DISCHARGE (CFS):	0.00	0.00	0.00	0.00	0.00	0.00
POWER (KW):	0.00	0.00	0.00	0.00	0.00	0.00
LEAKAGE (CFS)	36.90	76.27	27.27	37.59	39.28	45.52

GENERATION TIME: 0.00 HRS
FORECASTED END-OF-PERIOD STORAGE: 3904.02 MILLION CUBIC FEET
FORECASTED END-OF-PERIOD RESERVOIR LEVEL: 526.17 FT
MINIMUM GENERATION: 2000.00 KW FROM TURBINE #1 AT 366.47 CFS DISCHARGE
FLOOD GATE RELEASE: 0.00 CFS
FULL GATE OPERATION: 0.00 HRS

PERIOD 3

TURBINE #	1	2	3	4	5	6
DISCHARGE (CFS):	0.00	0.00	0.00	0.00	0.00	0.00
POWER (KW):	0.00	0.00	0.00	0.00	0.00	0.00
LEAKAGE (CFS)	36.96	76.39	27.32	37.65	39.34	45.60

GENERATION TIME: 0.00 HRS
FORECASTED END-OF-PERIOD STORAGE: 4068.52 MILLION CUBIC FEET
FORECASTED END-OF-PERIOD RESERVOIR LEVEL: 527.07 FT
MINIMUM GENERATION: 2000.00 KW FROM TURBINE #1 AT 365.71 CFS DISCHARGE
FLOOD GATE RELEASE: 0.00 CFS
FULL GATE OPERATION: 0.00 HRS

PERIOD 4

TURBINE #	1	2	3	4	5	6
DISCHARGE (CFS):	479.90	632.52	586.44	640.69	657.74	614.51
POWER (KW):	2603.03	3200.00	3147.80	3200.00	3400.00	3023.94
LEAKAGE (CFS)	37.16	76.82	27.47	37.86	39.56	45.85

GENERATION TIME: 10.68 HRS
FORECASTED END-OF-PERIOD STORAGE: 4099.93 MILLION CUBIC FEET
FORECASTED END-OF-PERIOD RESERVOIR LEVEL: 527.24 FT
MINIMUM GENERATION: 2000.00 KW FROM TURBINE #1 AT 363.12 CFS DISCHARGE
FLOOD GATE RELEASE: 0.00 CFS
FULL GATE OPERATION: 0.00 HRS

PERIOD 5

TURBINE #	1	2	3	4	5	6
DISCHARGE (CFS):	479.82	631.44	586.47	639.56	656.58	614.54
POWER (KW):	2606.48	3200.00	3153.21	3200.00	3400.00	3028.99
LEAKAGE (CFS)	37.20	76.90	27.50	37.90	39.60	45.90

GENERATION TIME: 10.70 HRS
FORECASTED END-OF-PERIOD STORAGE: 4045.68 MILLION CUBIC FEET
FORECASTED END-OF-PERIOD RESERVOIR LEVEL: 526.95 FT
MINIMUM GENERATION: 2000.00 KW FROM TURBINE #1 AT 362.64 CFS DISCHARGE
FLOOD GATE RELEASE: 0.00 CFS
FULL GATE OPERATION: 0.00 HRS

PERIOD 6

TURBINE #	1	2	3	4	5	6
DISCHARGE (CFS):	479.95	633.32	586.41	641.53	658.60	614.49
POWER (KW):	2600.50	3200.00	3143.84	3200.00	3400.00	3020.25
LEAKAGE (CFS)	37.13	76.76	27.45	37.83	39.53	45.82

GENERATION TIME: 10.72 HRS
FORECASTED END-OF-PERIOD STORAGE: 3990.40 MILLION CUBIC FEET
FORECASTED END-OF-PERIOD RESERVOIR LEVEL: 526.65 FT
MINIMUM GENERATION: 2000.00 KW FROM TURBINE #1 AT 363.47 CFS DISCHARGE
FLOOD GATE RELEASE: 0.00 CFS
FULL GATE OPERATION: 0.00 HRS

PERIOD 7

TURBINE #	1	2	3	4	5	6
DISCHARGE (CFS):	480.09	635.28	586.35	643.59	660.72	614.43
POWER (KW):	2594.31	3200.00	3134.16	3200.00	3400.00	3011.22
LEAKAGE (CFS)	37.06	76.62	27.40	37.76	39.46	45.73

GENERATION TIME: 10.75 HRS
FORECASTED END-OF-PERIOD STORAGE: 3933.54 MILLION CUBIC FEET
FORECASTED END-OF-PERIOD RESERVOIR LEVEL: 526.34 FT
MINIMUM GENERATION: 2000.00 KW FROM TURBINE #1 AT 364.33 CFS DISCHARGE
FLOOD GATE RELEASE: 0.00 CFS
FULL GATE OPERATION: 0.00 HRS

PERIOD 8

TURBINE #	1	2	3	4	5	6
DISCHARGE (CFS):	480.23	637.35	586.29	645.76	662.94	614.36
POWER (KW):	2587.85	3200.00	3124.07	3200.00	3400.00	3001.80
LEAKAGE (CFS)	36.99	76.47	27.35	37.69	39.38	45.64

GENERATION TIME: 10.78 HRS
FORECASTED END-OF-PERIOD STORAGE: 3897.91 MILLION CUBIC FEET
FORECASTED END-OF-PERIOD RESERVOIR LEVEL: 526.14 FT
MINIMUM GENERATION: 2000.00 KW FROM TURBINE #1 AT 365.24 CFS DISCHARGE
FLOOD GATE RELEASE: 0.00 CFS
FULL GATE OPERATION: 0.00 HRS

PERIOD 9

TURBINE #	1	2	3	4	5	6
DISCHARGE (CFS):	0.00	0.00	0.00	0.00	0.00	0.00
POWER (KW):	0.00	0.00	0.00	0.00	0.00	0.00
LEAKAGE (CFS)	36.95	76.38	27.31	37.64	39.33	45.59

GENERATION TIME: 0.00 HRS
FORECASTED END-OF-PERIOD STORAGE: 4069.93 MILLION CUBIC FEET
FORECASTED END-OF-PERIOD RESERVOIR LEVEL: 527.08 FT
MINIMUM GENERATION: 2000.00 KW FROM TURBINE #1 AT 365.81 CFS DISCHARGE
FLOOD GATE RELEASE: 0.00 CFS
FULL GATE OPERATION: 0.00 HRS

PERIOD 10

TURBINE #	1	2	3	4	5	6
DISCHARGE (CFS):	0.00	0.00	0.00	0.00	0.00	0.00
POWER (KW):	0.00	0.00	0.00	0.00	0.00	0.00
LEAKAGE (CFS)	37.16	76.82	27.47	37.86	39.56	45.85

GENERATION TIME: 0.00 HRS
FORECASTED END-OF-PERIOD STORAGE: 4298.07 MILLION CUBIC FEET
FORECASTED END-OF-PERIOD RESERVOIR LEVEL: 528.26 FT
MINIMUM GENERATION: 2000.00 KW FROM TURBINE #1 AT 363.10 CFS DISCHARGE
FLOOD GATE RELEASE: 0.00 CFS
FULL GATE OPERATION: 0.00 HRS

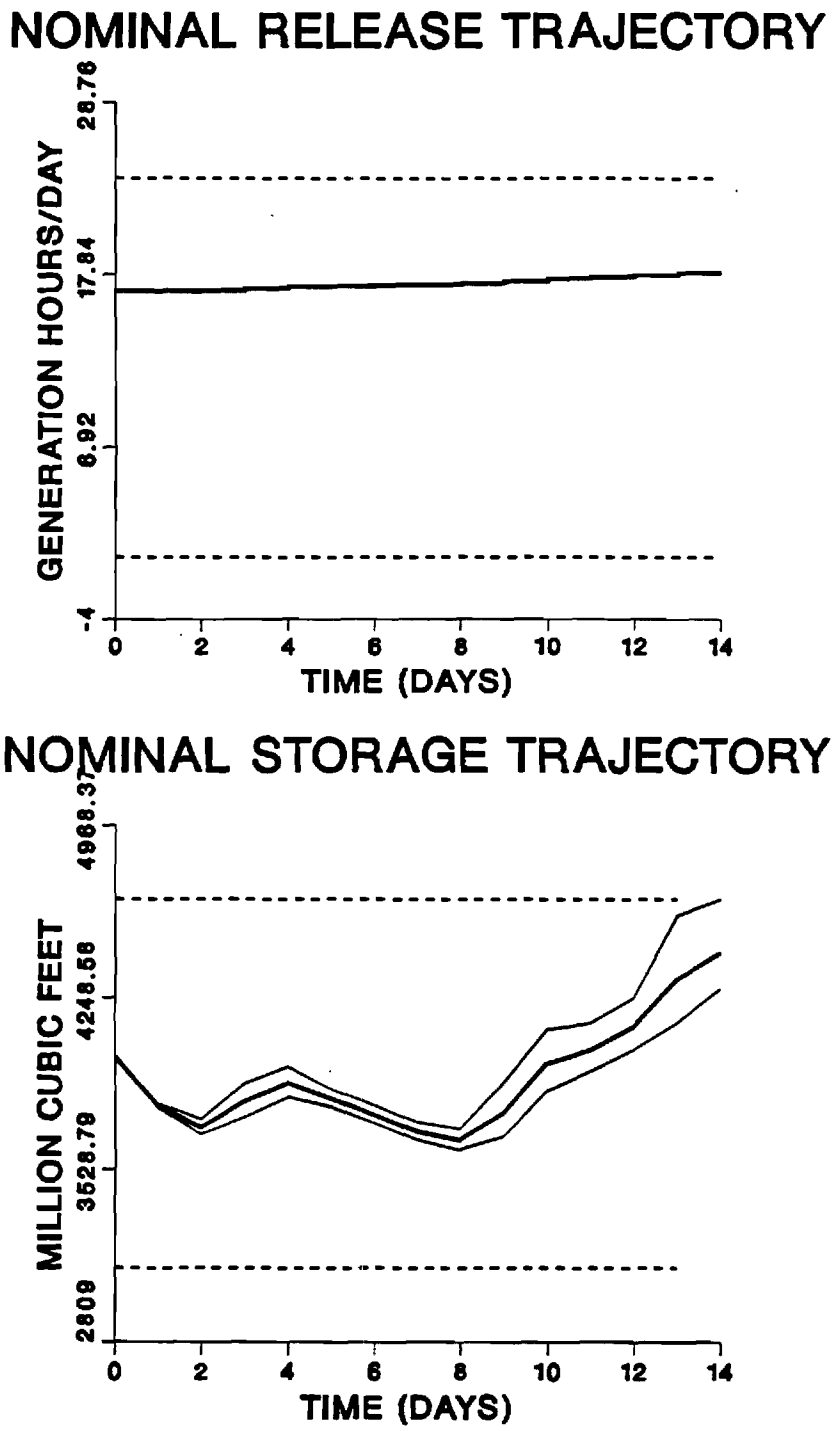

Figure 6.11: Optimal Sequences for Experiment #2

Table 6.7: Optimal Schedules for Experiment #2

OPTIMAL RELEASE AND POWER GENERATION SCHEDULES
STARTING DATE: 1/1/1988

PERIOD 1

TURBINE #	1	2	3	4	5	6
DISCHARGE (CFS):	603.88	636.09	599.93	644.44	661.59	702.09
POWER (KW):	3200.00	3200.00	3200.00	3200.00	3400.00	3400.00
LEAKAGE (CFS)	37.08	76.65	27.41	37.77	39.47	45.75

GENERATION TIME: 16.81 HRS
FORECASTED END-OF-PERIOD STORAGE: 3793.43 MILLION CUBIC FEET
FORECASTED END-OF-PERIOD RESERVOIR LEVEL: 525.55 FT
MINIMUM GENERATION: 2000.00 KW FROM TURBINE #1 AT 364.18 CFS DISCHARGE
FLOOD GATE RELEASE: 0.00 CFS
FULL GATE OPERATION: 0.00 HRS

PERIOD 2

TURBINE #	1	2	3	4	5	6
DISCHARGE (CFS):	611.52	643.97	607.43	652.72	670.09	711.63
POWER (KW):	3200.00	3200.00	3200.00	3200.00	3400.00	3400.00
LEAKAGE (CFS)	36.81	76.10	27.21	37.50	39.19	45.42

GENERATION TIME: 16.78 HRS
FORECASTED END-OF-PERIOD STORAGE: 3704.96 MILLION CUBIC FEET
FORECASTED END-OF-PERIOD RESERVOIR LEVEL: 525.04 FT
MINIMUM GENERATION: 2000.00 KW FROM TURBINE #1 AT 367.54 CFS DISCHARGE
FLOOD GATE RELEASE: 0.00 CFS
FULL GATE OPERATION: 0.00 HRS

PERIOD 3

TURBINE #	1	2	3	4	5	6
DISCHARGE (CFS):	615.01	647.56	610.86	656.51	673.98	716.00
POWER (KW):	3200.00	3200.00	3200.00	3200.00	3400.00	3400.00
LEAKAGE (CFS)	36.69	75.85	27.12	37.38	39.06	45.27

GENERATION TIME: 16.82 HRS
FORECASTED END-OF-PERIOD STORAGE: 3811.63 MILLION CUBIC FEET
FORECASTED END-OF-PERIOD RESERVOIR LEVEL: 525.65 FT
MINIMUM GENERATION: 2000.00 KW FROM TURBINE #1 AT 369.06 CFS DISCHARGE
FLOOD GATE RELEASE: 0.00 CFS
FULL GATE OPERATION: 0.00 HRS

PERIOD 4

TURBINE #	1	2	3	4	5	6
DISCHARGE (CFS):	610.82	643.24	606.75	651.96	669.31	710.75
POWER (KW):	3200.00	3200.00	3200.00	3200.00	3400.00	3400.00
LEAKAGE (CFS)	36.84	76.15	27.23	37.53	39.21	45.45

GENERATION TIME: 16.96 HRS
FORECASTED END-OF-PERIOD STORAGE: 3889.82 MILLION CUBIC FEET
FORECASTED END-OF-PERIOD RESERVOIR LEVEL: 526.10 FT
MINIMUM GENERATION: 2000.00 KW FROM TURBINE #1 AT 367.24 CFS DISCHARGE
FLOOD GATE RELEASE: 0.00 CFS
FULL GATE OPERATION: 0.00 HRS

PERIOD 5

TURBINE #	1	2	3	4	5	6
DISCHARGE (CFS):	607.87	640.20	603.85	648.76	666.02	707.06
POWER (KW):	3200.00	3200.00	3200.00	3200.00	3400.00	3400.00
LEAKAGE (CFS)	36.94	76.36	27.31	37.63	39.32	45.58

GENERATION TIME: 17.08 HRS
FORECASTED END-OF-PERIOD STORAGE: 3825.22 MILLION CUBIC FEET
FORECASTED END-OF-PERIOD RESERVOIR LEVEL: 525.73 FT
MINIMUM GENERATION: 2000.00 KW FROM TURBINE #1 AT 365.95 CFS DISCHARGE
FLOOD GATE RELEASE: 0.00 CFS
FULL GATE OPERATION: 0.00 HRS

PERIOD 6

TURBINE #	1	2	3	4	5	6
DISCHARGE (CFS):	610.30	642.71	606.24	651.40	668.73	710.10
POWER (KW):	3200.00	3200.00	3200.00	3200.00	3400.00	3400.00
LEAKAGE (CFS)	36.85	76.18	27.24	37.55	39.23	45.47

GENERATION TIME: 17.13 HRS
FORECASTED END-OF-PERIOD STORAGE: 3758.21 MILLION CUBIC FEET
FORECASTED END-OF-PERIOD RESERVOIR LEVEL: 525.35 FT
MINIMUM GENERATION: 2000.00 KW FROM TURBINE #1 AT 367.01 CFS DISCHARGE
FLOOD GATE RELEASE: 0.00 CFS
FULL GATE OPERATION: 0.00 HRS

PERIOD 7

TURBINE #	1	2	3	4	5	6
DISCHARGE (CFS):	612.89	645.38	608.78	654.21	671.62	713.35
POWER (KW):	3200.00	3200.00	3200.00	3200.00	3400.00	3400.00
LEAKAGE (CFS)	36.76	76.00	27.18	37.46	39.14	45.36

GENERATION TIME: 17.18 HRS
FORECASTED END-OF-PERIOD STORAGE: 3687.85 MILLION CUBIC FEET
FORECASTED END-OF-PERIOD RESERVOIR LEVEL: 524.94 FT
MINIMUM GENERATION: 2000.00 KW FROM TURBINE #1 AT 368.14 CFS DISCHARGE
FLOOD GATE RELEASE: 0.00 CFS
FULL GATE OPERATION: 0.00 HRS

PERIOD 8

TURBINE #	1	2	3	4	5	6
DISCHARGE (CFS):	615.70	648.27	611.54	657.26	674.75	716.87
POWER (KW):	3200.00	3200.00	3200.00	3200.00	3400.00	3400.00
LEAKAGE (CFS)	36.67	75.80	27.11	37.36	39.04	45.25

GENERATION TIME: 17.23 HRS
FORECASTED END-OF-PERIOD STORAGE: 3652.06 MILLION CUBIC FEET
FORECASTED END-OF-PERIOD RESERVOIR LEVEL: 524.73 FT
MINIMUM GENERATION: 2000.00 KW FROM TURBINE #1 AT 369.36 CFS DISCHARGE
FLOOD GATE RELEASE: 0.00 CFS
FULL GATE OPERATION: 0.00 HRS

PERIOD 9

TURBINE #	1	2	3	4	5	6
DISCHARGE (CFS):	617.16	649.78	612.98	658.85	676.38	718.71
POWER (KW):	3200.00	3200.00	3200.00	3200.00	3400.00	3400.00
LEAKAGE (CFS)	36.62	75.70	27.07	37.31	38.98	45.18

GENERATION TIME: 17.29 HRS
FORECASTED END-OF-PERIOD STORAGE: 3764.79 MILLION CUBIC FEET
FORECASTED END-OF-PERIOD RESERVOIR LEVEL: 525.39 FT
MINIMUM GENERATION: 2000.00 KW FROM TURBINE #1 AT 369.99 CFS DISCHARGE
FLOOD GATE RELEASE: 0.00 CFS
FULL GATE OPERATION: 0.00 HRS

PERIOD 10

TURBINE #	1	2	3	4	5	6
DISCHARGE (CFS):	612.63	645.11	608.53	653.93	671.33	713.02
POWER (KW):	3200.00	3200.00	3200.00	3200.00	3400.00	3400.00
LEAKAGE (CFS)	36.77	76.02	27.18	37.47	39.15	45.37

GENERATION TIME: 17.43 HRS
FORECASTED END-OF-PERIOD STORAGE: 3971.05 MILLION CUBIC FEET
FORECASTED END-OF-PERIOD RESERVOIR LEVEL: 526.54 FT
MINIMUM GENERATION: 2000.00 KW FROM TURBINE #1 AT 368.03 CFS DISCHARGE
FLOOD GATE RELEASE: 0.00 CFS
FULL GATE OPERATION: 0.00 HRS

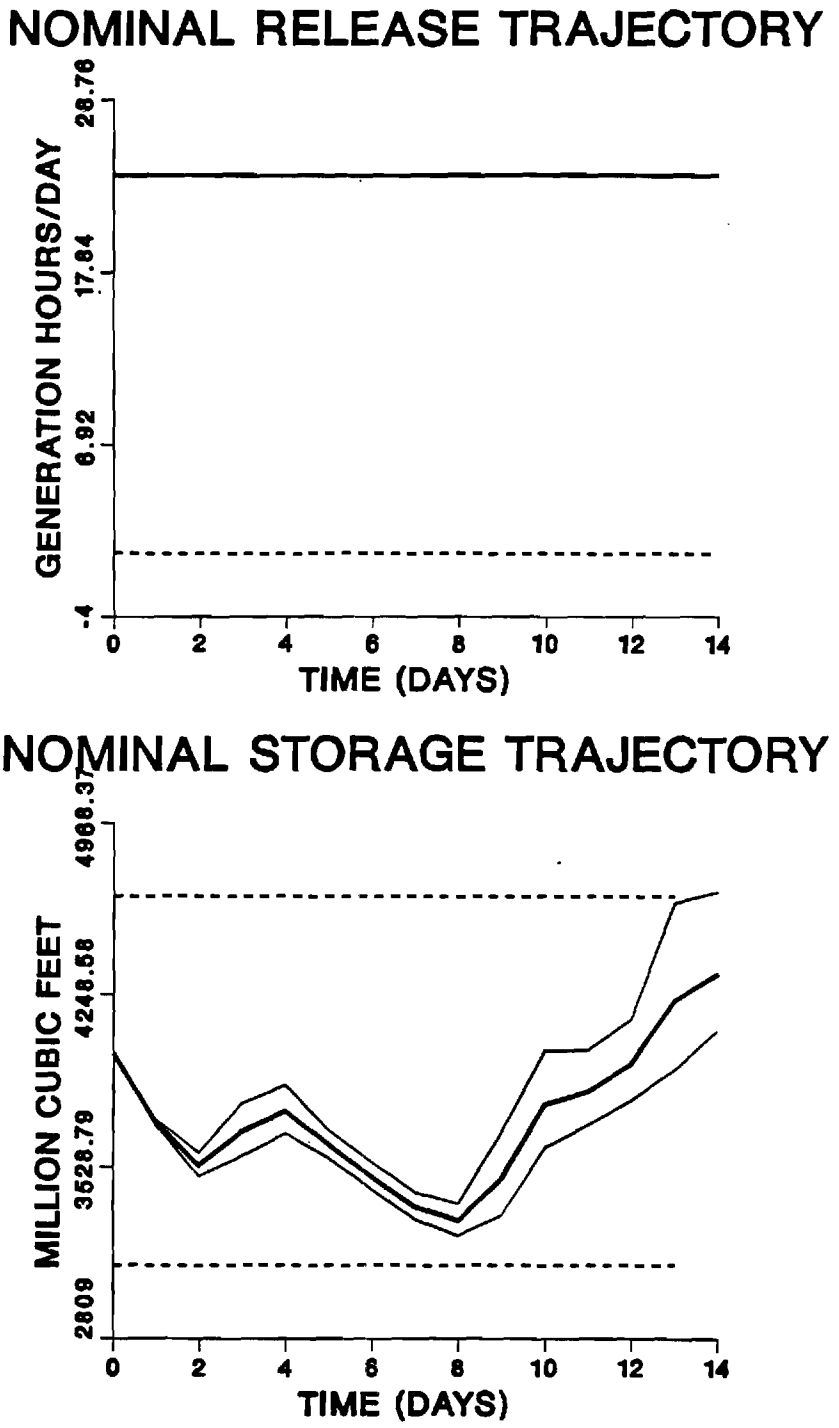

Figure 6.12: Optimal Sequences for Experiment #3

Table 6.8: Optimal Schedules for Experiment #3

OPTIMAL RELEASE AND POWER GENERATION SCHEDULES
STARTING DATE: 1/1/1988

PERIOD 1

TURBINE #	1	2	3	4	5	6
DISCHARGE (CFS):	609.41	641.79	605.36	650.43	667.74	708.99
POWER (KW):	3200.00	3200.00	3200.00	3200.00	3400.00	3400.00
LEAKAGE (CFS)	0.00	0.00	0.00	0.00	0.00	0.00

GENERATION TIME: 24.00 HRS
FORECASTED END-OF-PERIOD STORAGE: 3712.45 MILLION CUBIC FEET
FORECASTED END-OF-PERIOD RESERVOIR LEVEL: 525.08 FT
MINIMUM GENERATION: COVERED BY ABOVE SCHEDULE
FLOOD GATE RELEASE: 1308.55 CFS
FULL GATE OPERATION: 3.48 HRS

PERIOD 2

TURBINE #	1	2	3	4	5	6
DISCHARGE (CFS):	621.05	653.78	616.79	663.08	680.72	723.61
POWER (KW):	3200.00	3200.00	3200.00	3200.00	3400.00	3400.00
LEAKAGE (CFS)	0.00	0.00	0.00	0.00	0.00	0.00

GENERATION TIME: 24.00 HRS
FORECASTED END-OF-PERIOD STORAGE: 3535.20 MILLION CUBIC FEET
FORECASTED END-OF-PERIOD RESERVOIR LEVEL: 524.02 FT
MINIMUM GENERATION: COVERED BY ABOVE SCHEDULE
FLOOD GATE RELEASE: 1006.43 CFS
FULL GATE OPERATION: 24.00 HRS

PERIOD 3

TURBINE #	1	2	3	4	5	6
DISCHARGE (CFS):	627.77	660.70	623.38	670.39	688.22	732.12
POWER (KW):	3200.00	3200.00	3200.00	3200.00	3400.00	3400.00
LEAKAGE (CFS)	0.00	0.00	0.00	0.00	0.00	0.00

GENERATION TIME: 24.00 HRS
FORECASTED END-OF-PERIOD STORAGE: 3676.49 MILLION CUBIC FEET
FORECASTED END-OF-PERIOD RESERVOIR LEVEL: 524.87 FT
MINIMUM GENERATION: COVERED BY ABOVE SCHEDULE
FLOOD GATE RELEASE: 810.18 CFS
FULL GATE OPERATION: 24.00 HRS

PERIOD 4

TURBINE #	1	2	3	4	5	6
DISCHARGE (CFS):	622.17	654.94	617.89	664.30	681.97	725.03
POWER (KW):	3200.00	3200.00	3200.00	3200.00	3400.00	3400.00
LEAKAGE (CFS)	0.00	0.00	0.00	0.00	0.00	0.00

GENERATION TIME: 24.00 HRS
FORECASTED END-OF-PERIOD STORAGE: 3762.04 MILLION CUBIC FEET
FORECASTED END-OF-PERIOD RESERVOIR LEVEL: 525.37 FT
MINIMUM GENERATION: COVERED BY ABOVE SCHEDULE
FLOOD GATE RELEASE: 980.00 CFS
FULL GATE OPERATION: 24.00 HRS

PERIOD 5

TURBINE #	1	2	3	4	5	6
DISCHARGE (CFS):	618.85	651.53	614.64	660.69	678.27	720.85
POWER (KW):	3200.00	3200.00	3200.00	3200.00	3400.00	3400.00
LEAKAGE (CFS)	0.00	0.00	0.00	0.00	0.00	0.00

GENERATION TIME: 24.00 HRS
FORECASTED END-OF-PERIOD STORAGE: 3621.36 MILLION CUBIC FEET
FORECASTED END-OF-PERIOD RESERVOIR LEVEL: 524.54 FT
MINIMUM GENERATION: COVERED BY ABOVE SCHEDULE
FLOOD GATE RELEASE: 1062.48 CFS
FULL GATE OPERATION: 24.00 HRS

PERIOD 6

TURBINE #	1	2	3	4	5	6
DISCHARGE (CFS):	624.07	656.89	619.76	666.36	684.09	727.43
POWER (KW):	3200.00	3200.00	3200.00	3200.00	3400.00	3400.00
LEAKAGE (CFS)	0.00	0.00	0.00	0.00	0.00	0.00

GENERATION TIME: 24.00 HRS
FORECASTED END-OF-PERIOD STORAGE: 3487.83 MILLION CUBIC FEET
FORECASTED END-OF-PERIOD RESERVOIR LEVEL: 523.73 FT
MINIMUM GENERATION: COVERED BY ABOVE SCHEDULE
FLOOD GATE RELEASE: 930.37 CFS
FULL GATE OPERATION: 24.00 HRS

PERIOD 7

TURBINE #	1	2	3	4	5	6
DISCHARGE (CFS):	629.12	662.09	624.71	671.86	689.74	733.84
POWER (KW):	3200.00	3200.00	3200.00	3200.00	3400.00	3400.00
LEAKAGE (CFS)	0.00	0.00	0.00	0.00	0.00	0.00

GENERATION TIME: 24.00 HRS
FORECASTED END-OF-PERIOD STORAGE: 3362.82 MILLION CUBIC FEET
FORECASTED END-OF-PERIOD RESERVOIR LEVEL: 522.95 FT
MINIMUM GENERATION: COVERED BY ABOVE SCHEDULE
FLOOD GATE RELEASE: 767.97 CFS
FULL GATE OPERATION: 24.00 HRS

PERIOD 8

TURBINE #	1	2	3	4	5	6
DISCHARGE (CFS):	634.16	667.27	629.65	677.36	695.38	740.27
POWER (KW):	3200.00	3200.00	3200.00	3200.00	3400.00	3400.00
LEAKAGE (CFS)	0.00	0.00	0.00	0.00	0.00	0.00

GENERATION TIME: 24.00 HRS
FORECASTED END-OF-PERIOD STORAGE: 3304.07 MILLION CUBIC FEET
FORECASTED END-OF-PERIOD RESERVOIR LEVEL: 522.57 FT
MINIMUM GENERATION: COVERED BY ABOVE SCHEDULE
FLOOD GATE RELEASE: 619.40 CFS
FULL GATE OPERATION: 24.00 HRS

PERIOD 9

TURBINE #	1	2	3	4	5	6
DISCHARGE (CFS):	636.58	669.76	632.02	680.00	698.09	743.37
POWER (KW):	3200.00	3200.00	3200.00	3200.00	3400.00	3400.00
LEAKAGE (CFS)	0.00	0.00	0.00	0.00	0.00	0.00

GENERATION TIME: 24.00 HRS
FORECASTED END-OF-PERIOD STORAGE: 3482.08 MILLION CUBIC FEET
FORECASTED END-OF-PERIOD RESERVOIR LEVEL: 523.70 FT
MINIMUM GENERATION: COVERED BY ABOVE SCHEDULE
FLOOD GATE RELEASE: 552.95 CFS
FULL GATE OPERATION: 24.00 HRS

PERIOD 10

TURBINE #	1	2	3	4	5	6
DISCHARGE (CFS):	628.98	661.95	624.57	671.71	689.58	733.67
POWER (KW):	3200.00	3200.00	3200.00	3200.00	3400.00	3400.00
LEAKAGE (CFS)	0.00	0.00	0.00	0.00	0.00	0.00

GENERATION TIME: 24.00 HRS
FORECASTED END-OF-PERIOD STORAGE: 3790.04 MILLION CUBIC FEET
FORECASTED END-OF-PERIOD RESERVOIR LEVEL: 525.53 FT
MINIMUM GENERATION: COVERED BY ABOVE SCHEDULE
FLOOD GATE RELEASE: 772.23 CFS
FULL GATE OPERATION: 24.00 HRS

6.5.2 Simulation Experiments

Simulation experiments are intended to evaluate the system performance using the new control method. Among the issues to be investigated are the hydroelectric potential of Lloyd Shoals, the value of better inflow forecasts, the value of an additional (7th) turbine, and the hydroelectric losses due to turbine leakage.

6.5.2.1 Data Base

Simulation experiments may be conducted using historically observed or synthetically generated inflow sequences. In the case of the Lloyd Shoals Project, reservoir inflows can only be estimated through lake level and outflow discharge measurements. However, such records are not yet computerized and, therefore, prohibit the estimation of long historical inflow sequences. Thus, synthetic simulation experiments are only viable here. A brief description of the available data base follows.

(a) The rainfall data record includes daily values for the period from October 1980 through September 1981 from the five most relevant National Weather Service (NWS) stations located in Georgia. These stations are in Atlanta (WSO), Covington, Experiment, Jonesboro, and Monticello and are representative of the rainfall activity over the southern part of the Lloyd Shoals watershed. Unfortunately, the NWS station network does not adequately cover the upper basin. Mean areal precipitation estimates were obtained using the Thiessen estimation procedure (Figure 6.13).

(b) Evaporation data were compiled for October 1980 through September 1981 from two NWS stations located at Experiment and Athens. This study, however, primarily utilizes the Athens data (Figure 6.13) because the Experiment record is incomplete.

(c) The streamflow record includes daily values for the 1980-1981 water year from USGS station 02210500 on the Ocmulgee river near the City of Jackson. This station is approximately one mile downstream from Lloyd Shoals Dam, and its readings are considered representative of the total reservoir outflow.

(d) Daily reservoir elevations for the 1980-1981 water year were compiled from Georgia Power records. These values were used with the streamflow record to generate the sequence of net reservoir inflows to the Lloyd Shoals project. This analysis was performed using water balance considerations and the reservoir elevation versus storage relationship, derived from regression analysis of surveying data. A plot of the estimated net reservoir inflow values appears on Figure 6.13.

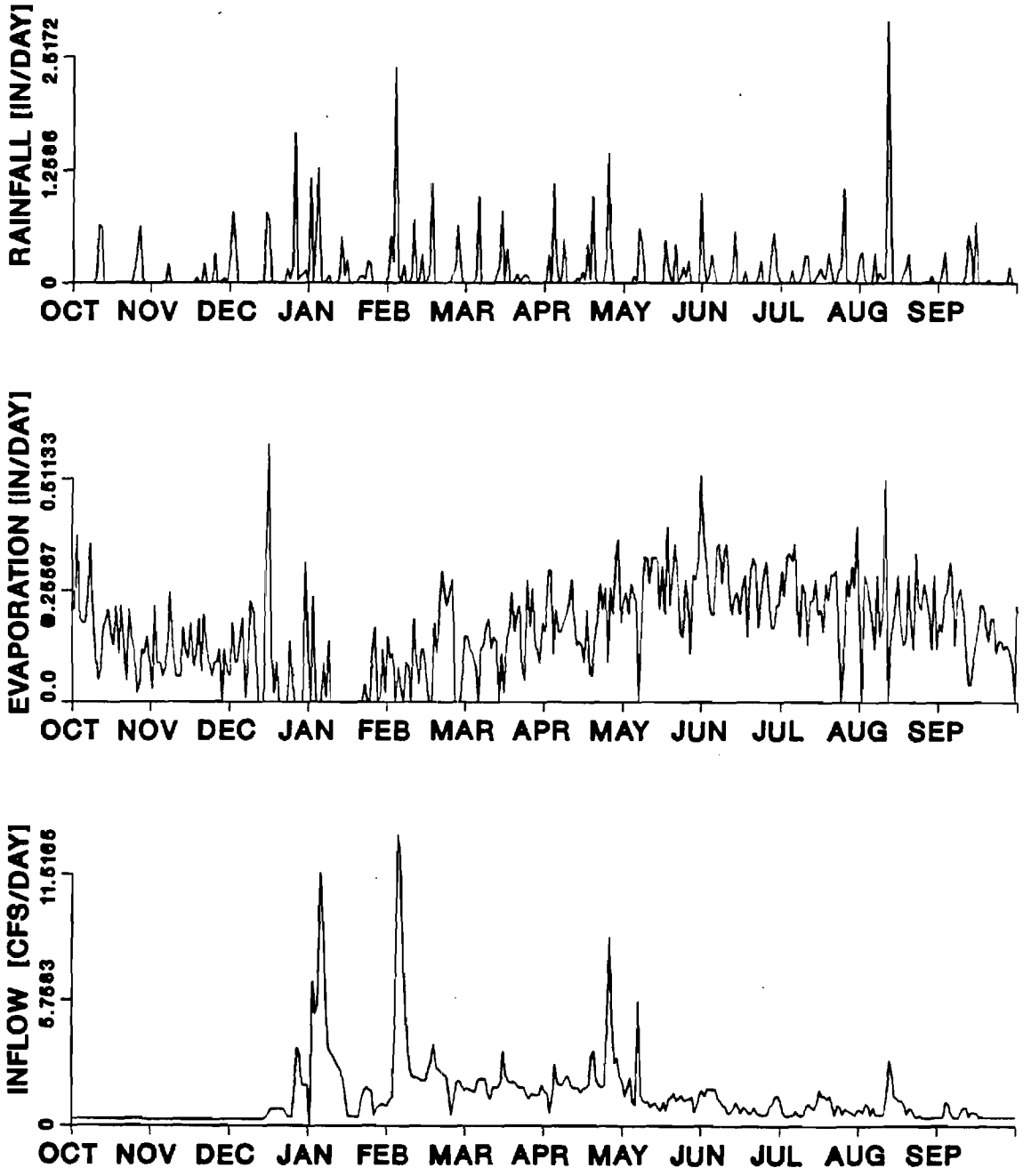

Figure 6.13: Rainfall, Evaporation, and Net Reservoir Inflows for Lloyd Shoals (1980 – 1981 Water Year)

(e) The geomorphologic characteristics of the Lloyd Shoals watershed were compiled from USGS 1:100,000 scale maps. The watershed was divided into five subbasins drained by the Alcovy River, Yellow, South River, Walnut Creek, and Tussahaw Creek. In each subbasin, each stream was delineated and ranked according to the Strahler ranking system. Then the following characteristics were measured and computerized: stream order, order of receptor stream, length, and slope. This information was processed for a total of 664 streams.

Based on the above geomorphoclimatic data, a physically-based rainfall-runoff model was calibrated and subsequently used to generate thirty years of daily net reservoir inflows. This model (Georgakakos and Kabouris, 1989) utilizes the concept of geomorphologic instantaneous unit hydrographs and requires a series of rainfall inputs. These inputs were generated using a statistical rainfall model, which was developed as follows:

The daily rainfall data in (a) were grouped into the following two sets depending on season: one included the rainfall events over the rainy season (December through June) and the other included the events over the dry season (July through November). The assumption was made that the events in each group follow a Poisson process (Benjamin and Cornell, 1970, Eagleson, 1978) with exponentially-distributed storm durations and interstorm periods and gamma-distributed storm depths. More specifically, it was assumed that t_s (storm duration), t_i (interstorm period), and d (rainfall depth) have the following probability distributions:

$$f_{T_s}(t_s) = \lambda_s \, e^{-\lambda_s t_s}, \tag{6.37}$$

$$f_{T_i}(t_i) = \lambda_i \, e^{-\lambda_i t_i}, \text{ and} \tag{6.38}$$

$$f_D(d) = \frac{\lambda_d \, (\lambda_d \, d)^{\kappa_d - 1} \, e^{-\lambda_d d}}{\Gamma(\kappa_d)}, \tag{6.39}$$

where $f_X(x)$ represents the probability density of the random variable X evaluated at x; λ_s, λ_i, λ_d, κ_d are calibration parameters; and $\Gamma(\kappa_d)$ is the incomplete gamma function:

$$\Gamma(\kappa_d) = \int_0^\infty e^{-x} \, x^{\kappa_d - 1} \, dx \, . \tag{6.40}$$

The previous parameters were calibrated for each period and were set equal to the following estimated values:

Table 6.9: Parameters of the Rainfall Model

Parameter	Rainy Season (December – June)	Dry Season (July – November)
λ_s [days^{-1}]	0.2605	0.3200
λ_i [days^{-1}]	0.3263	0.3243
λ_d [intches^{-1}]	1.4045	0.7324
κ_d	1.4841	0.4480

The rational behind this simple rainfall generation model is to preserve the statistical nature of the basic storm characteristics (duration, interstorm period, and storm depth) for both the rainy and the dry seasons. A synthetic storm sequence can be developed by generating independent random values for the triplet $[t_i, d, t_r]$ that defines each storm event. In this study, the generated synthetic storm sequence was thirty years long. This sequence constituted the rainfall input for the previously mentioned rainfall–runoff model which was then used to generate a 30–year long sequence of net reservoir inflows. These inflows are the basis of the simulation process presented in the next section.

6.5.2.2 The Simulation Process

The simulation process (Figure 6.14) seeks to imitate the operation of the Lloyd Shoals reservoir under the guidance of the control model previously discussed. At the beginning of each day, an inflow forecasting model is first invoked to provide inflow forecasts over the control horizon. These forecasts become available to the control model which finds optimal power generation and discharge schedules according to the methodology presented in Section 4. The schedules for the first day are implemented, the actual inflow values are generated, and the system outputs (end–of–day reservoir storage, actual turbine release, leakage rates, flood gate and flash board releases, peak and off-peak power generation) are computed and recorded. This process is repeated at the beginning of each day for the duration of the simulation horizon (30 years).

The lack of sufficient hydrologic data prohibits the valid calibration of an inflow forecasting model. Instead, this model operation is herein simulated as follows: Let the daily, apriori, inflow means and variances be denoted as $\mu(k)$ and $\sigma^2(k)$ respectively. These statistics were obtained from the generated net reservoir inflow series. Then, at the beginning of each day, the forecasts (mean, m(k), and forecast error

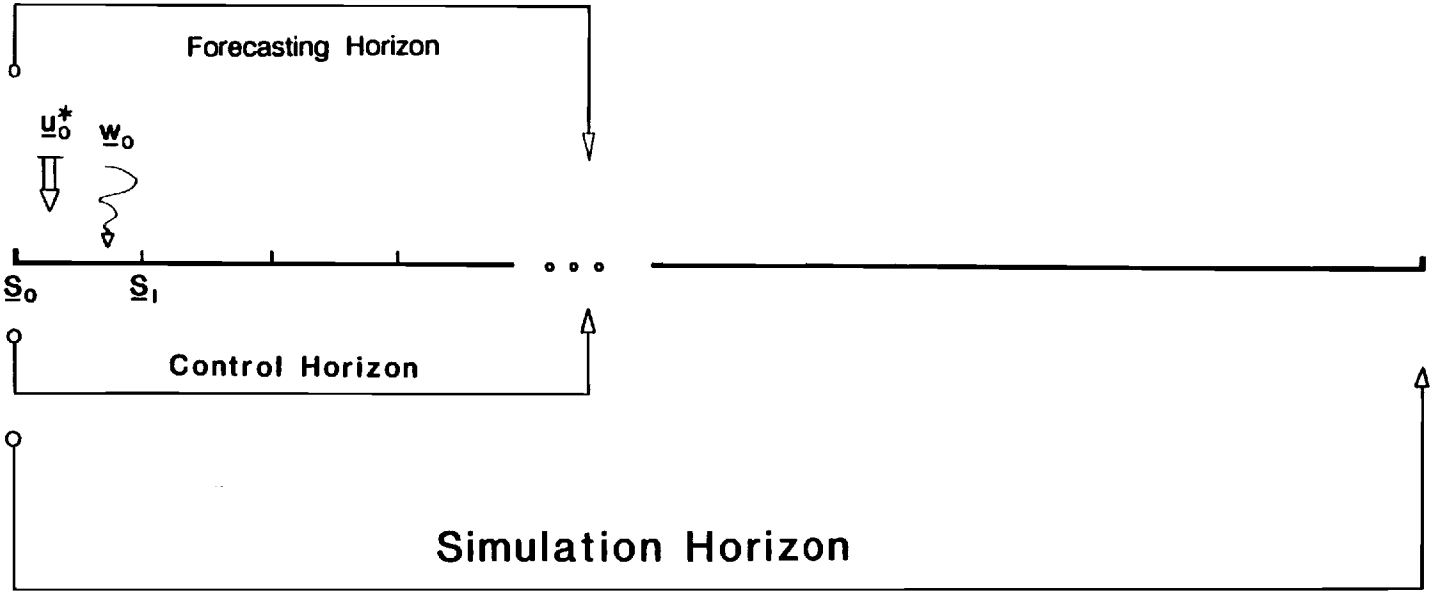

Figure 6.14: The Simulation Process

variance, $s^2(k)$) are computed by the following process:

1. Generate N independent standard normal variables $\omega(k)$, k=1,...,N.

2. Transform the previous variables into normal variables with mean q(k) and variance $[0.05\ q(k)\ (1-\rho)]^2$, where q(k) is the net reservoir inflow for day k and ρ is a forecast parameter in the range [0,1].

$$w(k) = \omega(k)\ 0.05\ q(k)\ [1 - \rho] + q(k),\ k=1,\ldots,N. \tag{6.41}$$

3. Forecast the upcoming inflows from

$$m(k) = \mu(k) + [w(k) - \mu(k)]\ \rho^k,\ k=1,\ldots,N. \tag{6.42}$$

4. Compute the associated forecast error variance from

$$s^2(k) = \sigma^2(k)\ [1 - (\rho^2)^k],\ k=1,\ldots,N. \tag{6.43}$$

This procedure has the following characteristics:

(i) For a given ρ, the forecast statistics tend to the apriori means $\mu(k)$ and the associated variances $\sigma^2(k)$ with time. This becomes evident from Equations (6.42) and (6.43) as ρ^k tends to 0 and $[1 - (\rho^2)^k]$ tends to 1.

(ii) As ρ tends to 1, the forecasting accuracy improves, since w(k) tends to q(k), m(k) tends to w(k), and $s^2(k)$ tends to zero. For ρ=1, this model generates perfect forecasts.

(iii) As ρ tends to 0, the forecasting accuracy deteriorates, since m(k) tends to $\mu(k)$ and $s^2(k)$ tends to $\sigma^2(k)$. For ρ=0, the previous scheme simply generates the apriori statistics.

(iv) For realism, the forecasts are assumed to follow lognormal probability distributions.

Thus, at the beginning of each day and depending on the value of ρ, the previous model generates inflow forecasts for the upcoming days of the control horizon. Then, the control model determines the optimal power generation and release schedules, and the system response is simulated. For accuracy, this simulation is performed on hourly intervals and is based on the following assumptions:

(a) If the optimal generation time schedule, $t^*(k)$, is less than or equal to 16 hours, power generation is assumed to begin at 8:00 am; otherwise, power generation begins at $[24 - t^*(k)]$ am and ends at 12:00 midnight.

(b) If the optimal decision calls for flood gate releases, flood gate operation begins at 12:00 midnight.

(c) If at any time within the day, the reservoir level exceeds the threshold of 530 feet, the flash boards trip and cannot be reset until the water level has receded below elevation 528 feet. To maximize energy generation during this time, the flood gate is completely shut, and all turbines operate at maximum power. The spillway outflow is determined from

$$Q_S = 0.2547755 \times 10^7 - 0.14145744 \times 10^5\ H + 0.2615793 \times 10^2\ H^2 - 0.16108972 \times 10^{-1}\ H^3, \tag{6.44}$$

where H is the reservoir elevation in feet and Q_S is the spillway

outflow in thousands of cfs.

(d) The hourly net reservoir inflow is equal to q(k)/24, where q(k) is the daily synthetic inflow value generated as explained in Section 5.2.1.

(e) For each hourly interval, the simulation routine computes the following quantities: end-of-the-hour reservoir storage, turbine release and leakage, spillway and flood gate outflows, and peak and off-peak power generation. At the end of each day, the corresponding daily values are determined by summation.

6.5.2.3 Five Simulation Experiments

The simulation experiments differ in the values of the forecast parameter ρ, the tolerance levels γ, the number of the operational turbines, and the turbine leakage rate. Some common features are that the initial storage is set equal to 4,247 million cubic feet and that the control horizon is 14 days. More specifically, the characteristics of each experiment are summarized below:

Table 6.10: Characteristics of the Simulation Experiments

	Simulation Experiment				
	I	II	III	IV	V
ρ	0.01	0.01	0.01	0.90	0.90
γ	50%	2.5%	2.5%	2.5%	2.5%
Turbines	6	6	7	6	6
Leakage	ℓ^{ref}	ℓ^{ref}	ℓ^{ref}	ℓ^{ref}	0.01 ℓ^{ref}

In the previous table, the 50% value for γ indicates that the corresponding control model is only concerned with maintaining the mean storage sequence within the storage bounds (deterministic optimization). When γ=2.5%, the storage constraints are satisfied 2.5% of the time (stochastic optimization). The turbines of Model V are assumed to have parameters ℓ^{ref} which are ten times lower than the values reported in Table 6.1.

Statistical analysis was employed to evaluate the performance of each control model over the 30-year simulation period. Table 6.11 reports the results of this analysis on a yearly basis; the monthly statistics are presented in Tables 6.12 through 6.16. Each table includes the mean and 5% and 95% percentiles of the reservoir storage, flood gate and flash board releases, turbine release and leakage, inflow, peak and off-peak energy generation. Several comments are now in order.

Table 6.11: Annual Statistics for the Simulation Experiments

Expmnt.	Storage 10^6 cf	Flood Gate Release 10^6 cf	Flash Board Release 10^6 cf	Turbine Release 10^6 cf	Leakage 10^6 cf	Inflow 10^6 cf	Peak Power MWH	Off-Pk. Power MWH
I								
5%	2,779	0	188	12,641	5,136	19,619	13,138	4,163
Mean	3,635	0	5,150	26,751	5,737	37,446	28,998	9,320
95%	3,906	0	11,969	37,367	6,411	51,921	40,587	13,643
II								
5%	2,515	0	0	12,947	4,857	19,619	13,724	4,231
Mean	3,504	260	2,631	29,162	5,528	37,446	29,791	12,091
95%	3,876	1,026	6,099	41,394	6,213	51,921	41,508	19,479
III								
5%	2,537	0	0	13,145	5,243	19,619	13,997	4,095
Mean	3,461	76	2,492	29,209	5,799	37,446	30,621	11,333
95%	3,841	348	5,772	41,187	6,365	51,921	43,009	18,258
IV								
5%	2,947	0	0	13,382	4,705	19,619	12,651	5,415
Mean	3,810	455	262	31,208	5,556	37,446	30,277	14,926
95%	4,063	1,918	1,891	45,331	6,551	51,921	43,061	24,592
V								
5%	3,575	0	0	19,251	448	19,619	18,612	8,058
Mean	3,896	470	261	36,216	533	37,446	35,515	16,888
95%	4,108	2,044	1,891	49,483	634	51,921	46,824	26,240

Table 6.12: Monthly Simulation Statistics for Experiment I

Month		Storage 10^6 cf	Fl. Gt. Release 10^6 cf	Fl. Bd. Release 10^6 cf	Turbine Release 10^6 cf	Leakage 10^6 cf	Inflow 10^6 cf	Peak Power MWH	Off-Pk. Power MWH
	5 %	3059.7	0.0	0.0	188.3	271.2	753.9	167.2	87.3
J	Mean	3581.7	0.0	488.2	2589.2	470.5	3465.0	2792.0	905.8
	95 %	4360.7	0.0	3635.3	5979.5	584.2	9897.0	5703.4	2899.5
	5 %	3152.6	0.0	0.0	433.9	290.4	845.6	334.3	221.0
F	Mean	3625.7	0.0	392.2	2524.9	419.6	3406.7	2824.0	781.9
	95 %	4396.6	0.0	2136.6	4785.2	541.5	7186.6	5270.4	1782.5
	5 %	2976.5	0.0	0.0	9.9	333.3	259.0	7.7	2.8
M	Mean	3539.0	0.0	275.9	2617.2	469.0	3212.1	2921.7	806.6
	95 %	4195.6	0.0	1943.3	4956.9	585.2	7791.3	5494.0	1985.7
	5 %	2708.8	0.0	0.0	0.0	264.6	107.0	0.0	0.0
A	Mean	3531.7	0.0	518.7	2551.2	445.8	3537.2	2810.5	828.2
	95 %	4387.7	0.0	3226.1	5731.0	567.2	9493.6	5795.9	2465.1
	5 %	2644.9	0.0	0.0	0.0	265.9	134.8	0.0	0.0
M	Mean	3565.1	0.0	700.9	2413.3	473.7	3880.5	2581.2	858.5
	95 %	4406.5	0.0	5323.4	6127.6	585.3	11675.7	5449.3	3332.6
	5 %	2185.3	0.0	0.0	0.0	353.5	51.1	0.0	0.0
J	Mean	3872.6	0.0	684.3	1458.8	515.7	2689.5	1353.7	764.9
	95 %	4422.2	0.0	4517.4	4529.2	588.6	9270.2	3618.1	2938.2
	5 %	2048.2	0.0	0.0	0.0	405.8	161.9	0.0	0.0
J	Mean	3989.0	0.0	499.3	1603.2	531.7	2784.5	1555.9	779.9
	95 %	4392.7	0.0	3519.4	3982.9	609.2	7815.3	3546.8	2373.7
	5 %	1664.4	0.0	0.0	0.0	359.5	83.8	0.0	0.0
A	Mean	4068.8	0.0	572.8	1995.9	510.4	2979.5	2073.7	835.0
	95 %	4417.3	0.0	2968.9	4676.8	607.2	7878.2	4499.9	2450.7
	5 %	1269.5	0.0	0.0	0.0	305.9	213.3	0.0	0.0
S	Mean	3495.6	0.0	273.5	2691.5	438.2	2705.2	3123.9	724.0
	95 %	4332.5	0.0	2058.9	5094.9	542.4	6895.1	5575.1	1784.0
	5 %	1612.0	0.0	0.0	0.0	301.9	284.2	0.0	0.0
O	Mean	3319.4	0.0	277.8	1936.5	496.7	2720.9	2093.2	664.1
	95 %	4249.9	0.0	2133.5	5471.1	581.9	7984.7	5533.8	2311.6
	5 %	2965.3	0.0	0.0	109.3	341.4	321.7	75.1	39.6
N	Mean	3443.3	0.0	123.9	2022.3	482.7	2890.7	2269.8	605.7
	95 %	4291.9	0.0	1142.2	4550.0	565.1	6456.3	5439.9	1143.1
	5 %	2961.9	0.0	0.0	0.0	315.2	562.9	0.0	0.0
D	Mean	3586.5	0.0	342.8	2346.8	483.2	3174.0	2598.0	765.0
	95 %	4352.8	0.0	2385.7	5262.1	585.6	7417.7	5739.7	2047.0

Table 6.13: Monthly Simulation Statistics for Experiment II

Month		Storage 10^6 cf	Fl. Gt. Release 10^6 cf	Fl. Bd. Release 10^6 cf	Turbine Release 10^6 cf	Leakage 10^6 cf	Inflow 10^6 cf	Peak Power MWH	Off-Pk. Power MWH
	5 %	3153.2	0.0	0.0	295.9	206.4	753.9	201.9	218.7
J	Mean	3740.5	29.8	284.9	2707.7	469.5	3465.0	2614.8	1305.9
	95 %	4470.3	222.6	2371.7	6973.2	588.4	9897.0	5474.5	4608.0
	5 %	3244.3	0.0	0.0	433.0	216.8	845.6	287.5	282.4
F	Mean	3812.2	12.1	215.1	2670.8	415.9	3406.7	2691.4	1175.4
	95 %	4458.2	95.7	1142.5	5977.8	546.1	7186.6	5145.3	3556.0
	5 %	3072.1	0.0	0.0	0.0	282.0	259.0	0.0	0.0
M	Mean	3720.4	11.3	203.5	2702.2	470.7	3212.1	2807.9	1094.4
	95 %	4331.7	127.0	1286.0	5747.8	588.2	7791.3	5345.3	2999.3
	5 %	2803.4	0.0	0.0	0.0	126.7	107.0	0.0	0.0
A	Mean	3658.6	70.2	171.3	2873.2	430.0	3537.2	2741.4	1401.0
	95 %	4451.5	599.0	1058.5	7831.5	570.0	9493.6	5833.6	5562.6
	5 %	2750.7	0.0	0.0	0.0	131.4	134.8	0.0	0.0
M	Mean	3629.9	72.2	262.0	2994.8	440.8	3880.5	2970.0	1330.5
	95 %	4436.3	475.3	3110.9	8140.6	588.3	11675.7	6085.5	5618.1
	5 %	1731.5	0.0	0.0	750.8	256.1	51.1	813.3	119.0
J	Mean	3433.5	10.1	311.6	2365.4	443.9	2689.5	2476.5	877.5
	95 %	4453.7	102.4	3121.3	5853.5	509.5	9270.2	5010.2	3560.4
	5 %	1185.4	0.0	0.0	0.0	327.6	161.9	0.0	0.0
J	Mean	3060.0	4.0	166.4	2277.0	460.0	2784.5	2452.0	733.4
	95 %	4315.9	56.9	1554.6	5004.1	531.2	7815.3	4643.6	2941.8
	5 %	810.5	0.0	0.0	0.0	312.7	83.8	0.0	0.0
A	Mean	3162.2	11.8	281.4	2260.6	461.1	2979.5	2420.9	759.8
	95 %	4431.4	159.7	2201.7	5284.6	528.9	7878.2	4842.4	2805.0
	5 %	484.8	0.0	0.0	0.0	265.8	213.3	0.0	0.0
S	Mean	3279.2	9.9	96.3	2081.2	464.4	2705.2	2174.3	837.7
	95 %	4372.2	145.8	1001.2	5712.6	560.4	6895.1	5362.6	2926.6
	5 %	917.9	0.0	0.0	0.0	252.9	284.2	0.0	0.0
O	Mean	3280.1	16.5	173.4	1984.8	489.9	2720.9	1971.3	894.4
	95 %	4393.8	169.8	1516.0	6225.7	586.2	7984.7	5633.1	3378.7
	5 %	2100.0	0.0	0.0	0.0	321.0	321.7	0.0	0.0
N	Mean	3521.9	7.9	108.7	1899.8	491.2	2890.7	2009.6	738.2
	95 %	4338.9	89.3	992.2	4877.5	568.3	6456.3	5181.7	2199.8
	5 %	2864.1	0.0	0.0	0.0	340.7	562.9	0.0	0.0
D	Mean	3749.4	4.1	356.4	2344.9	490.6	3174.0	2460.9	942.7
	95 %	4375.1	49.3	2544.0	4934.6	589.2	7417.7	5202.7	2172.1

Table 6.14: Monthly Simulation Statistics for Experiment III

Month		Storage 10^6 cf	Fl. Gt. Release 10^6 cf	Fl. Bd. Release 10^6 cf	Turbine Release 10^6 cf	Leakage 10^6 cf	Inflow 10^6 cf	Peak Power MWH	Off-Pk. Power MWH
	5 %	3116.5	0.0	0.0	286.2	271.9	753.9	189.6	183.5
J	Mean	3726.6	7.5	289.9	2692.2	496.1	3465.0	2645.1	1258.3
	95 %	4417.2	84.9	2373.0	6948.6	598.4	9897.0	5810.4	4452.8
	5 %	3244.9	0.0	0.0	424.0	269.9	845.6	281.1	282.4
F	Mean	3802.3	1.5	229.9	2655.1	442.2	3406.7	2766.3	1084.4
	95 %	4452.0	20.6	1304.6	6007.0	556.7	7186.6	5581.1	3169.8
	5 %	3064.8	0.0	0.0	0.0	329.7	259.0	0.0	0.0
M	Mean	3709.8	2.2	189.7	2688.0	497.2	3212.1	2849.4	1040.7
	95 %	4319.3	32.2	1192.4	5858.2	597.9	7791.3	5793.4	2732.7
	5 %	2795.5	0.0	0.0	0.0	187.7	107.0	0.0	0.0
A	Mean	3643.7	17.4	173.0	2919.2	455.2	3537.2	2927.2	1288.8
	95 %	4424.5	154.3	1153.7	8070.4	579.1	9493.6	6494.5	5184.7
	5 %	2736.8	0.0	0.0	0.0	180.3	134.8	0.0	0.0
M	Mean	3604.7	27.1	236.3	3025.1	467.8	3880.5	3090.6	1260.0
	95 %	4418.9	241.8	2800.2	8609.0	597.6	11675.7	6949.5	5471.4
	5 %	1719.1	0.0	0.0	697.0	310.0	51.1	782.5	86.4
J	Mean	3359.8	.6	325.1	2439.3	461.7	2689.5	2637.5	814.8
	95 %	4431.5	8.8	3323.0	5862.4	516.9	9270.2	5329.9	3124.7
	5 %	1264.7	0.0	0.0	0.0	375.2	161.9	0.0	0.0
J	Mean	2913.1	0.0	144.6	2300.2	476.5	2784.5	2545.5	643.1
	95 %	4298.0	0.0	1435.3	4953.5	538.8	7815.3	4717.7	2719.7
	5 %	880.9	0.0	0.0	0.0	343.4	83.8	0.0	0.0
A	Mean	3026.6	2.9	232.6	2314.4	477.0	2979.5	2529.1	714.5
	95 %	4402.3	39.9	1774.0	5554.8	534.6	7878.2	5293.5	2746.8
	5 %	541.6	0.0	0.0	0.0	309.8	213.3	0.0	0.0
S	Mean	3227.2	1.8	92.4	1943.6	490.5	2705.2	2089.6	730.4
	95 %	4364.8	24.5	949.6	5870.2	576.1	6895.1	5782.9	2738.7
	5 %	960.7	0.0	0.0	0.0	293.3	284.2	0.0	0.0
O	Mean	3266.2	9.3	148.2	1992.1	510.3	2720.9	2003.5	879.7
	95 %	4384.6	117.1	1226.4	6496.8	594.9	7984.7	6023.1	3469.1
	5 %	2047.1	0.0	0.0	0.0	370.8	321.7	0.0	0.0
N	Mean	3510.3	4.9	105.2	1879.0	511.6	2890.7	2023.9	699.6
	95 %	4294.1	72.8	1061.7	4772.1	577.5	6456.3	5311.4	1844.6
	5 %	2798.7	0.0	0.0	0.0	369.0	562.9	0.0	0.0
D	Mean	3738.3	.6	324.5	2360.4	512.7	3174.0	2513.3	919.0
	95 %	4370.5	9.1	2172.4	5218.2	599.1	7417.7	5430.4	2230.3

Table 6.15: Monthly Simulation Statistics for Experiment IV

Month		Storage 10^6 cf	Fl. Gt. Release 10^6 cf	Fl. Bd. Release 10^6 cf	Turbine Release 10^6 cf	Leakage 10^6 cf	Inflow 10^6 cf	Peak Power MWH	Off-Pk. Power MWH
	5 %	3252.8	0.0	0.0	340.9	132.9	753.9	219.5	245.4
J	Mean	3784.7	64.2	53.9	2905.3	460.9	3465.0	2753.2	1444.4
	95 %	4460.2	770.9	765.7	8082.1	590.0	9897.0	5875.7	5844.0
	5 %	3301.8	0.0	0.0	454.1	162.3	845.6	273.4	310.1
F	Mean	3842.4	16.0	0.0	2903.6	405.9	3406.7	2818.9	1374.7
	95 %	4529.3	180.5	0.0	6792.7	546.5	7186.6	5362.8	4607.2
	5 %	3151.5	0.0	0.0	8.0	226.4	259.0	5.2	2.8
M	Mean	3772.6	20.0	0.0	2885.3	463.6	3212.1	2937.8	1221.5
	95 %	4295.7	274.3	0.0	6670.6	589.2	7791.3	5711.5	3983.4
	5 %	2884.4	0.0	0.0	0.0	66.6	107.0	0.0	0.0
A	Mean	3711.0	45.6	0.0	3060.7	424.6	3537.2	2841.2	1578.5
	95 %	4440.2	597.7	0.0	8738.7	571.1	9493.6	5983.5	6684.6
	5 %	2798.7	0.0	0.0	0.0	64.1	134.8	0.0	0.0
M	Mean	3712.1	91.5	89.7	3100.8	438.5	3880.5	2985.7	1484.6
	95 %	4470.6	1195.5	1211.3	9133.7	589.5	11675.7	6231.4	6955.6
	5 %	2335.9	0.0	0.0	0.0	133.9	51.1	0.0	0.0
J	Mean	3969.0	66.9	31.8	1956.4	484.8	2689.5	1738.8	1131.4
	95 %	4525.4	829.6	429.1	7729.1	592.3	9270.2	5634.7	5572.8
	5 %	2189.5	0.0	0.0	0.0	221.6	161.9	0.0	0.0
J	Mean	4087.2	44.2	23.4	2084.5	502.9	2784.5	1913.6	1148.5
	95 %	4478.4	455.8	315.7	6698.4	612.5	7815.3	4875.8	4996.9
	5 %	1791.1	0.0	0.0	0.0	181.8	83.8	0.0	0.0
A	Mean	4164.3	37.2	0.0	2520.6	479.1	2979.5	2372.7	1328.4
	95 %	4509.4	462.3	0.0	7301.1	609.4	7878.2	5636.3	4979.3
	5 %	1389.7	0.0	0.0	0.0	200.4	213.3	0.0	0.0
S	Mean	3747.2	19.0	0.0	2800.9	443.7	2705.2	2893.7	1170.4
	95 %	4440.6	278.4	0.0	6710.3	563.7	6895.1	5731.8	4237.4
	5 %	1725.7	0.0	0.0	0.0	192.2	284.2	0.0	0.0
O	Mean	3525.1	17.5	12.7	2183.9	493.8	2720.9	2048.4	1098.5
	95 %	4408.3	185.7	171.6	7212.2	590.3	7984.7	5773.3	4663.5
	5 %	3120.1	0.0	0.0	118.9	279.9	321.7	74.7	64.4
N	Mean	3638.6	2.8	0.0	2177.9	482.9	2890.7	2274.4	854.4
	95 %	4448.7	37.4	0.0	5512.5	570.9	6456.3	5359.6	2720.9
	5 %	3140.1	0.0	0.0	10.2	238.8	562.9	8.2	2.8
D	Mean	3763.5	30.1	50.3	2627.7	475.1	3174.0	2698.2	1090.6
	95 %	4417.0	383.9	547.0	6499.7	590.4	7417.7	5969.5	3696.1

Table 6.16: Monthly Simulation Statistics for Experiment V

Month		Storage 10^6 cf	Fl. Gt. Release 10^6 cf	Fl. Bd. Release 10^6 cf	Turbine Release 10^6 cf	Leakage 10^6 cf	Inflow 10^6 cf	Peak Power MWH	Off-Pk. Power MWH
	5 %	3309.2	0.0	0.0	825.4	12.5	753.9	676.3	483.4
J	Mean	3807.4	63.6	53.9	3342.9	43.8	3465.0	3217.8	1608.9
	95 %	4481.8	771.4	765.7	8208.9	58.3	9897.0	5935.5	5971.5
	5 %	3294.2	0.0	0.0	961.5	15.7	845.6	724.4	565.6
F	Mean	3851.6	15.4	0.0	3276.2	38.6	3406.7	3224.6	1511.2
	95 %	4535.1	180.8	0.0	6912.3	53.4	7186.6	5426.8	4767.8
	5 %	3244.3	0.0	0.0	288.3	21.4	259.0	164.7	168.2
M	Mean	3792.5	20.7	0.0	3277.3	44.2	3212.1	3364.6	1351.7
	95 %	4320.3	254.4	0.0	6874.2	58.9	7791.3	5731.2	4217.2
	5 %	3227.5	0.0	0.0	98.0	6.1	107.0	42.1	75.4
A	Mean	3761.0	48.1	0.0	3409.7	40.7	3537.2	3202.0	1708.0
	95 %	4452.6	614.3	0.0	8816.5	57.0	9493.6	5996.8	6790.3
	5 %	3221.3	0.0	0.0	96.9	5.9	134.8	43.4	57.3
M	Mean	3792.8	92.1	89.7	3442.0	42.2	3880.5	3309.3	1640.2
	95 %	4474.9	1201.4	1211.3	9211.2	59.0	11675.7	6257.3	7043.6
	5 %	3215.0	0.0	0.0	0.0	12.6	51.1	0.0	0.0
J	Mean	4143.1	66.9	31.8	2309.6	47.3	2689.5	2094.6	1300.7
	95 %	4526.5	830.8	429.0	7849.3	59.0	9270.2	5717.9	5695.2
	5 %	3297.9	0.0	0.0	0.0	21.4	161.9	0.0	0.0
J	Mean	4273.7	53.5	23.4	2586.6	48.5	2784.5	2389.7	1408.6
	95 %	4484.5	491.1	315.6	6858.1	61.1	7815.3	5090.4	5140.2
	5 %	3365.3	0.0	0.0	41.5	17.1	83.8	41.7	17.8
A	Mean	4313.2	37.7	0.0	2944.3	46.3	2979.5	2794.6	1526.4
	95 %	4512.6	466.8	0.0	7468.2	60.7	7878.2	5771.8	5080.7
	5 %	3244.5	0.0	0.0	257.5	19.4	213.3	146.4	163.2
S	Mean	3894.6	19.0	0.0	3205.2	42.6	2705.2	3343.8	1299.4
	95 %	4451.1	279.6	0.0	6819.7	57.0	6895.1	5731.7	4326.5
	5 %	3256.6	0.0	0.0	358.6	17.6	284.2	243.3	203.4
O	Mean	3659.7	19.7	12.8	2679.1	47.6	2720.9	2565.0	1286.7
	95 %	4422.7	208.7	173.0	7447.6	58.8	7984.7	5830.9	4944.4
	5 %	3267.9	0.0	0.0	559.1	26.4	321.7	339.5	337.6
N	Mean	3681.7	2.8	0.0	2697.0	45.7	2890.7	2872.1	991.5
	95 %	4461.4	37.7	0.0	5788.2	56.9	6456.3	5532.7	2939.9
	5 %	3267.8	0.0	0.0	433.7	22.1	562.9	260.8	301.4
D	Mean	3785.0	30.8	49.3	3046.0	45.5	3174.0	3137.2	1254.1
	95 %	4435.5	395.4	531.8	6774.4	58.8	7417.7	6016.2	3941.2

1. Models I and II differ only in the value of the tolerance level γ (50% and 2.5% respectively). Smaller values of γ maintain lower reservoir storages, lessen the flash board mandatory releases, and, consequently, generate more peak and off-peak energy. Thus on the average, Model II generates approximately 1,000 MWH more peak and 2,500 MWH more off-peak energy per year and experiences almost half the spillway losses of Model I.

2. Models II and III have the same forecasting and tolerance levels but differ in the number of turbines. Model III is assumed to have an additional (7th) turbine which is identical to Turbine #1 but leaks at a rate ten times lower. As expected, the addition of the 7th turbine causes an average increase in peak energy generation by about 830 MWH per year and a corresponding decrease in off-peak energy generation. This improvement is more substantial in "wet" seasons where peak annual generation may improve by 1,500 MWH (95% percentile).

3. Models II and IV differ by the accuracy of the forecasting scheme. More accurate streamflow forecasting allows the reservoir to maintain higher storage levels without compromising constraint reliability. As a result, flash board outflow was drastically reduced from 2,631 $x10^6$ ft^3 to 261 $x10^6$ ft^3, while average annual peak and off-peak energy generation rose by 1,300 and 2,800 MWH respectively. Based on average system production costs shown in Figure 1, these improvements represent an approximate average gain of $100,000 per year. The actual gains during "wet" years are considerably higher, while the value of forecasting declines during "dry" years.

4. A comparison of the results for Models I and IV reveals the value of stochastic control methods with accurate streamflow forecasting. The improvements amount to a yearly average of 1,300 MWH peak and 5,600 MWH off-peak energy production and an economic gain of approximately $135,000. These results demonstrate that fully stochastic optimal control methods in connection with streamflow forecasting can substantially improve hydropower revenues.

5. Models IV and V differ by the turbine leakage rates. The turbines of Model V leak at a rate ten times lower than Model IV. The results indicate that the average peak and off-peak energy generation of Model V improved by 5,250 and 2,000 MWH respectively over those of Model IV. Based on Figure 1, these improvements amount to about $300,000 to $350,000 per year. Similar improvements are also realized in the 95% reliable energy output. In this regard, peak energy improved by 6,000 MWH, and off-peak energy by 2,600 MWH.

Figures 6.15 through 6.44 include plots of the simulation data and their daily and monthly frequencies. For clarity, the simulation data are plotted for the first 5,000 days. In the frequency plots, the thicker lines delineate the mean trajectories, while the thinner ones,

the 95% probability limits. The frequency plots and tables can be used to determine the 95% reliable peak and off-peak energy outputs.

The following section summarizes the results of this work and offers further recommendations.

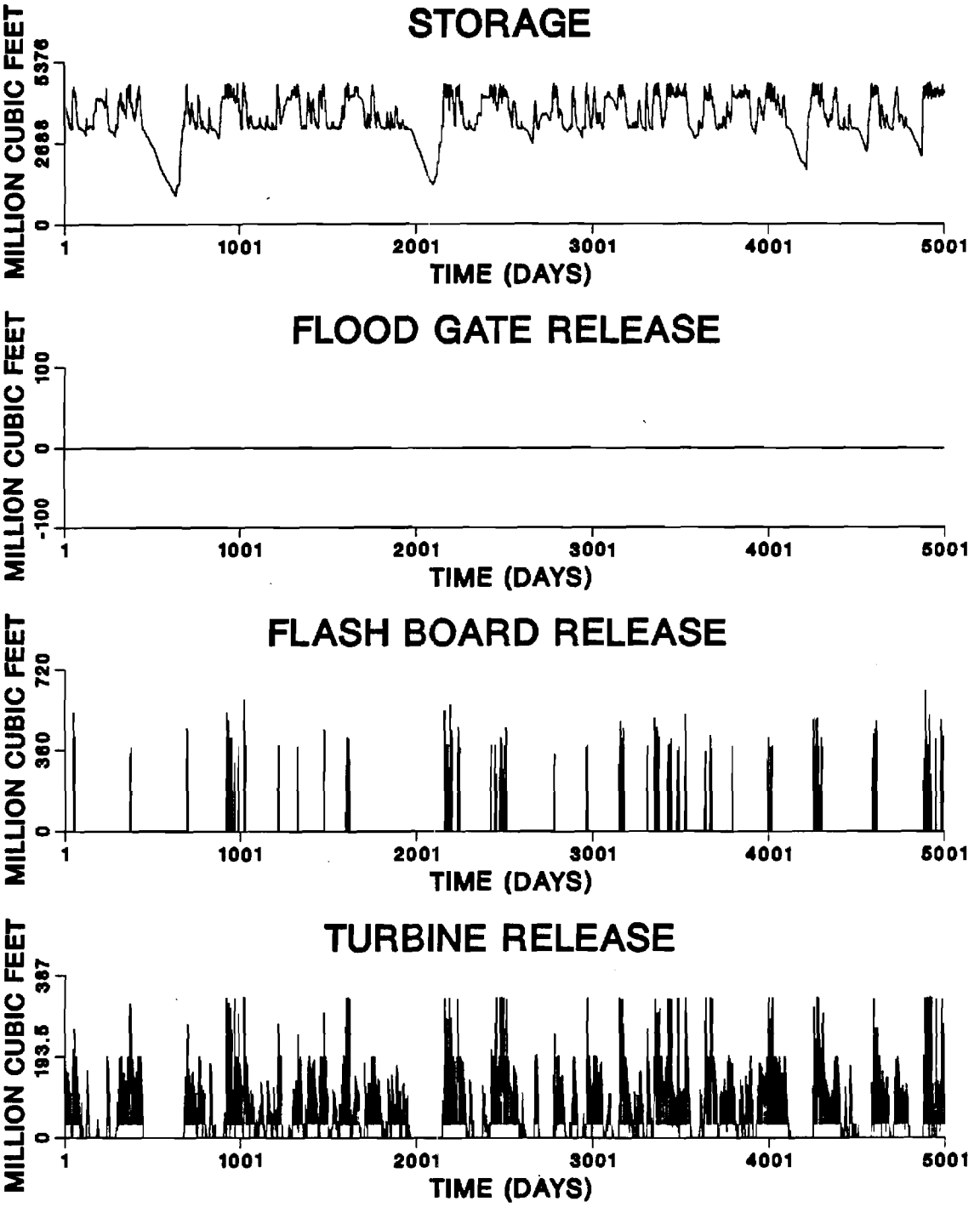

Figure 6.15: Simulation Results — Experiment I

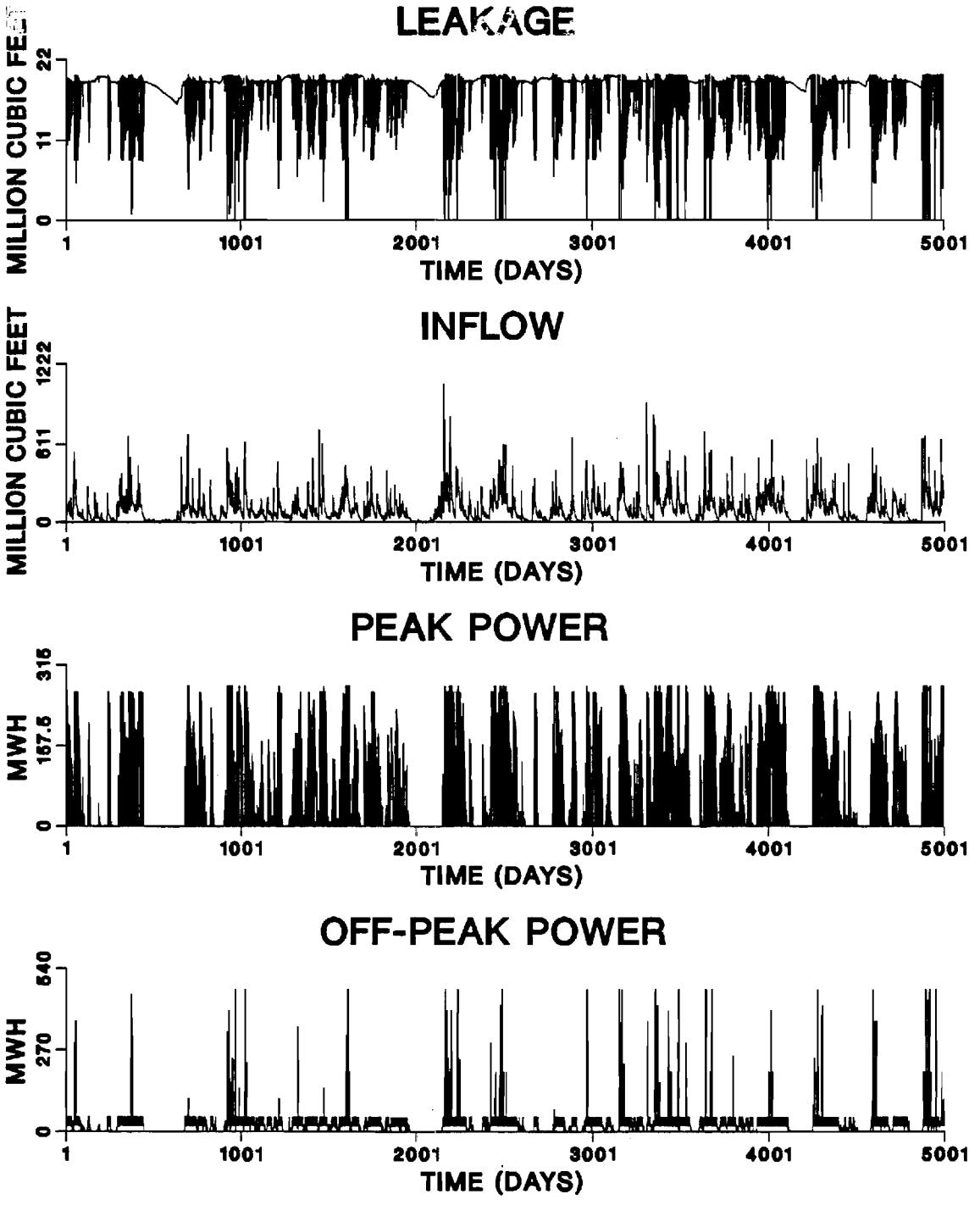

Figure 6.16: Simulation Results — Experiment I

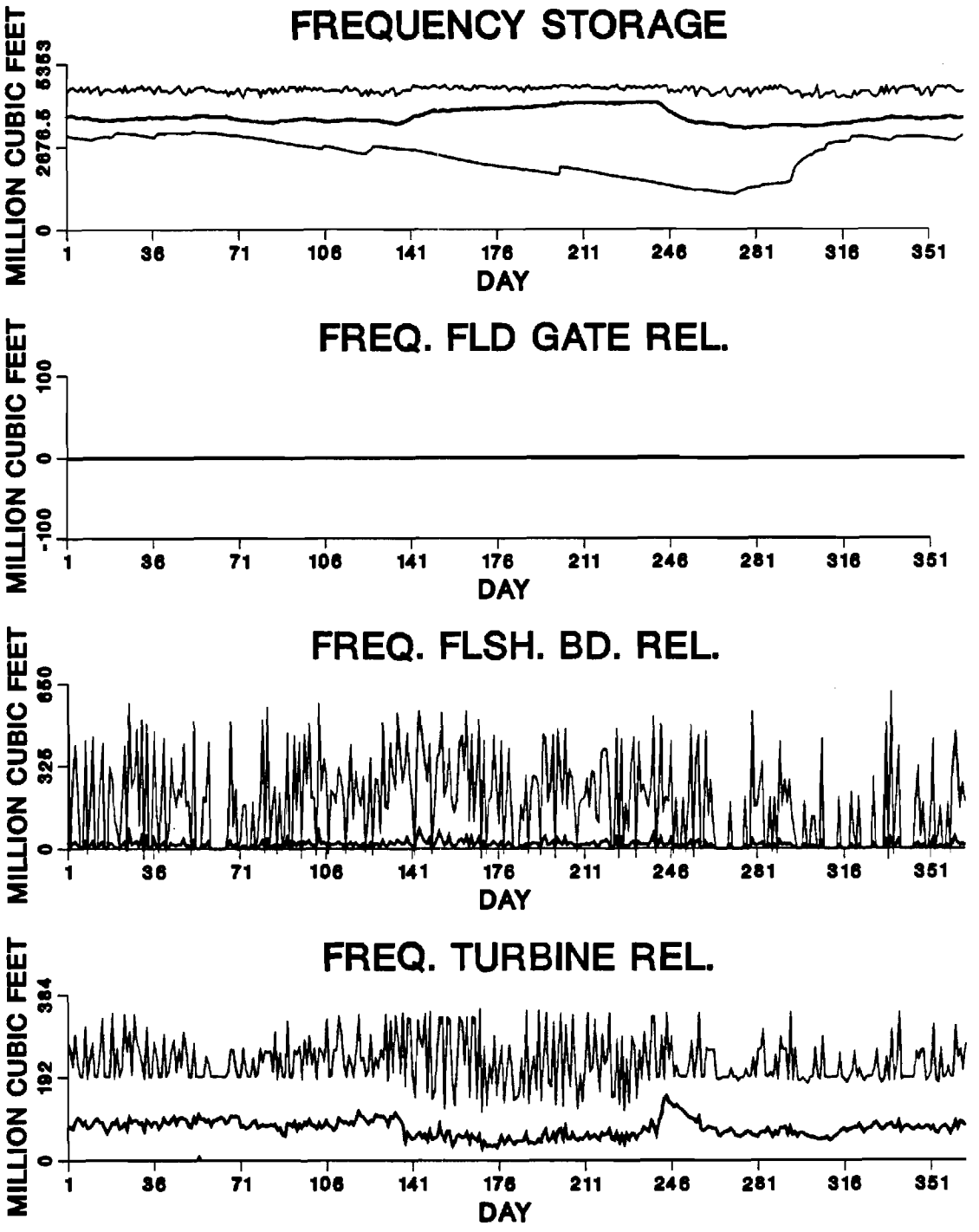

Figure 6.17: Daily Frequencies — Experiment I

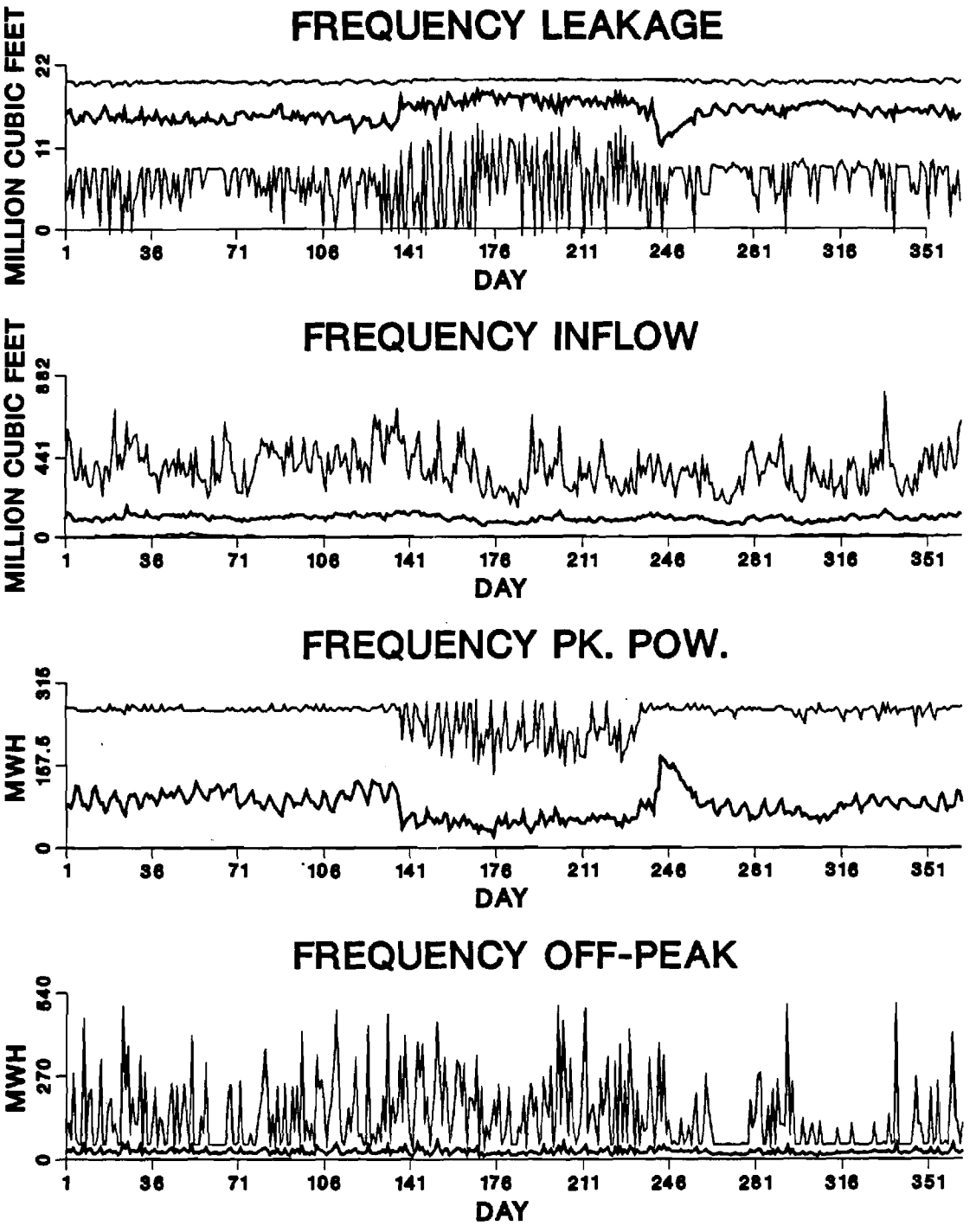

Figure 6.18: Daily Frequencies — Experiment I

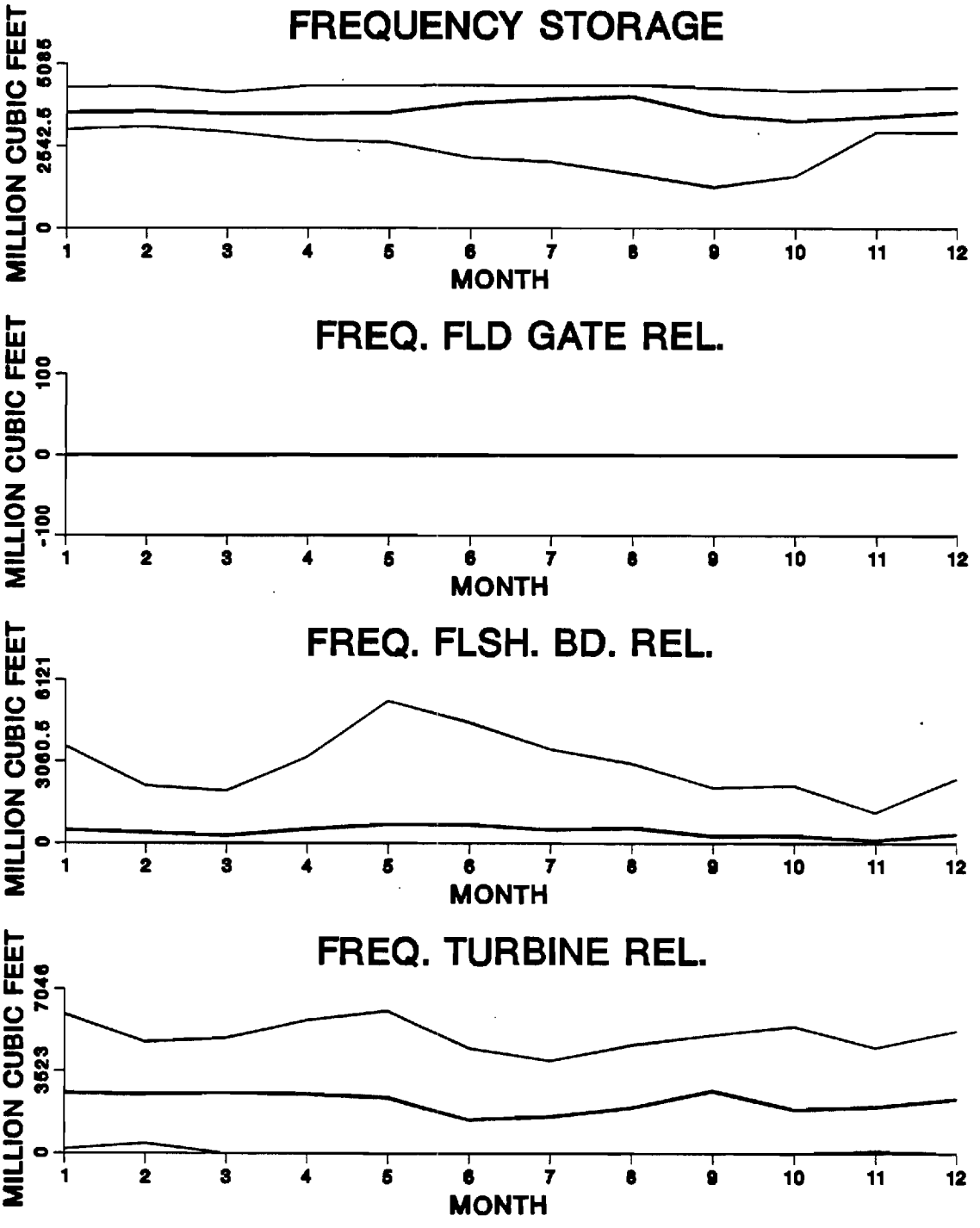

Figure 6.19: Monthly Frequencies — Experiment I

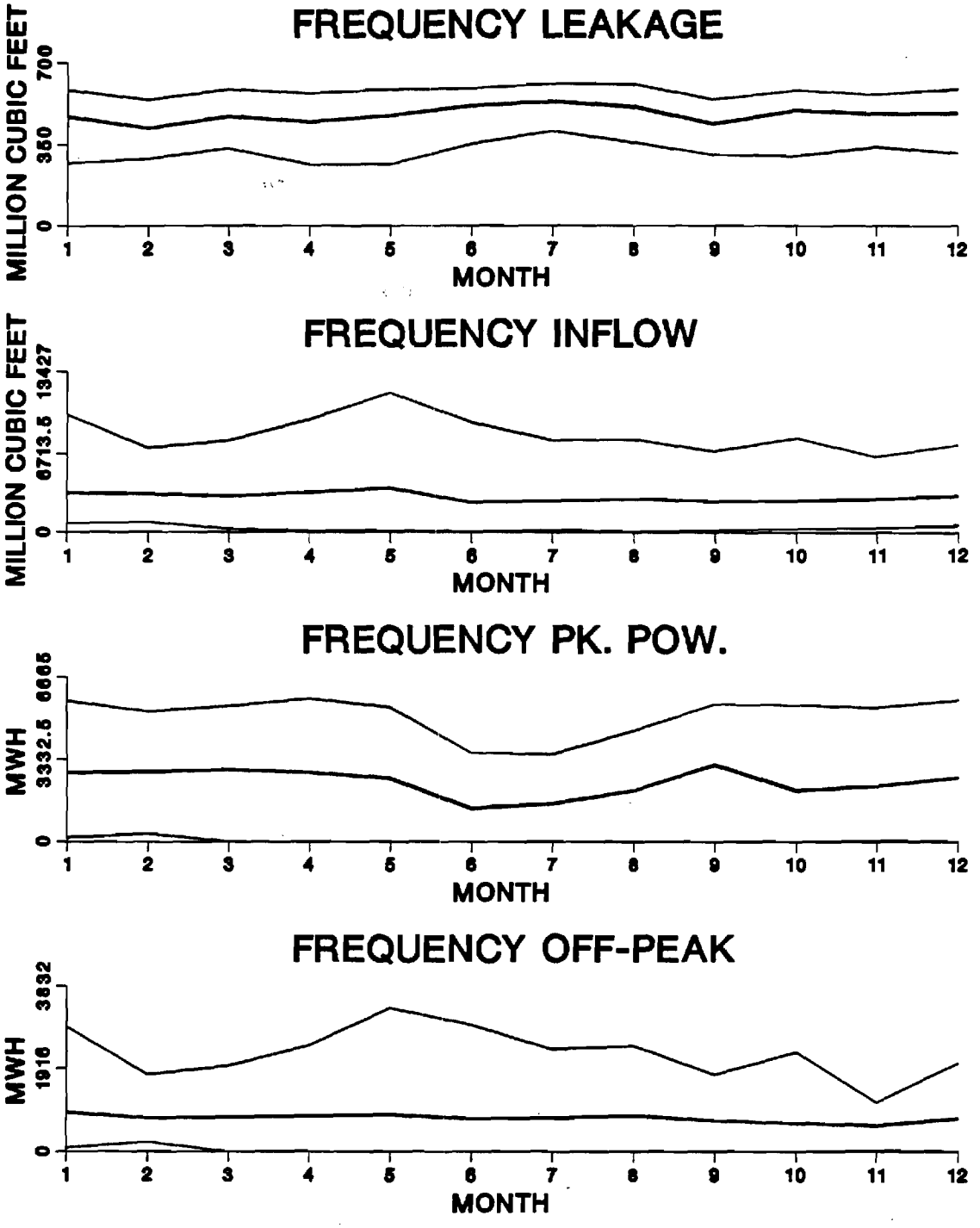

Figure 6.20: Monthly Frequencies — Experiment I

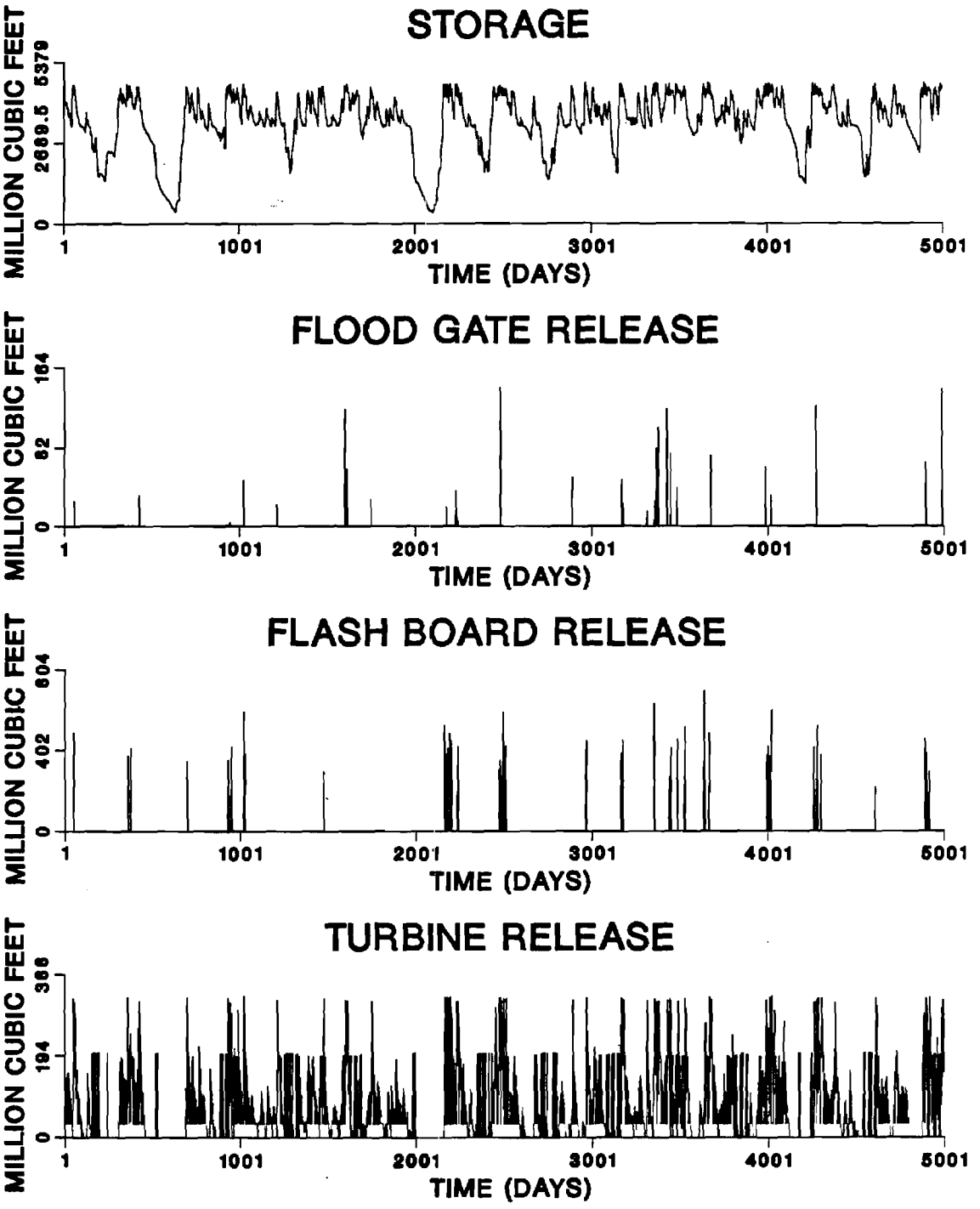

Figure 6.21: Simulation Results — Experiment II

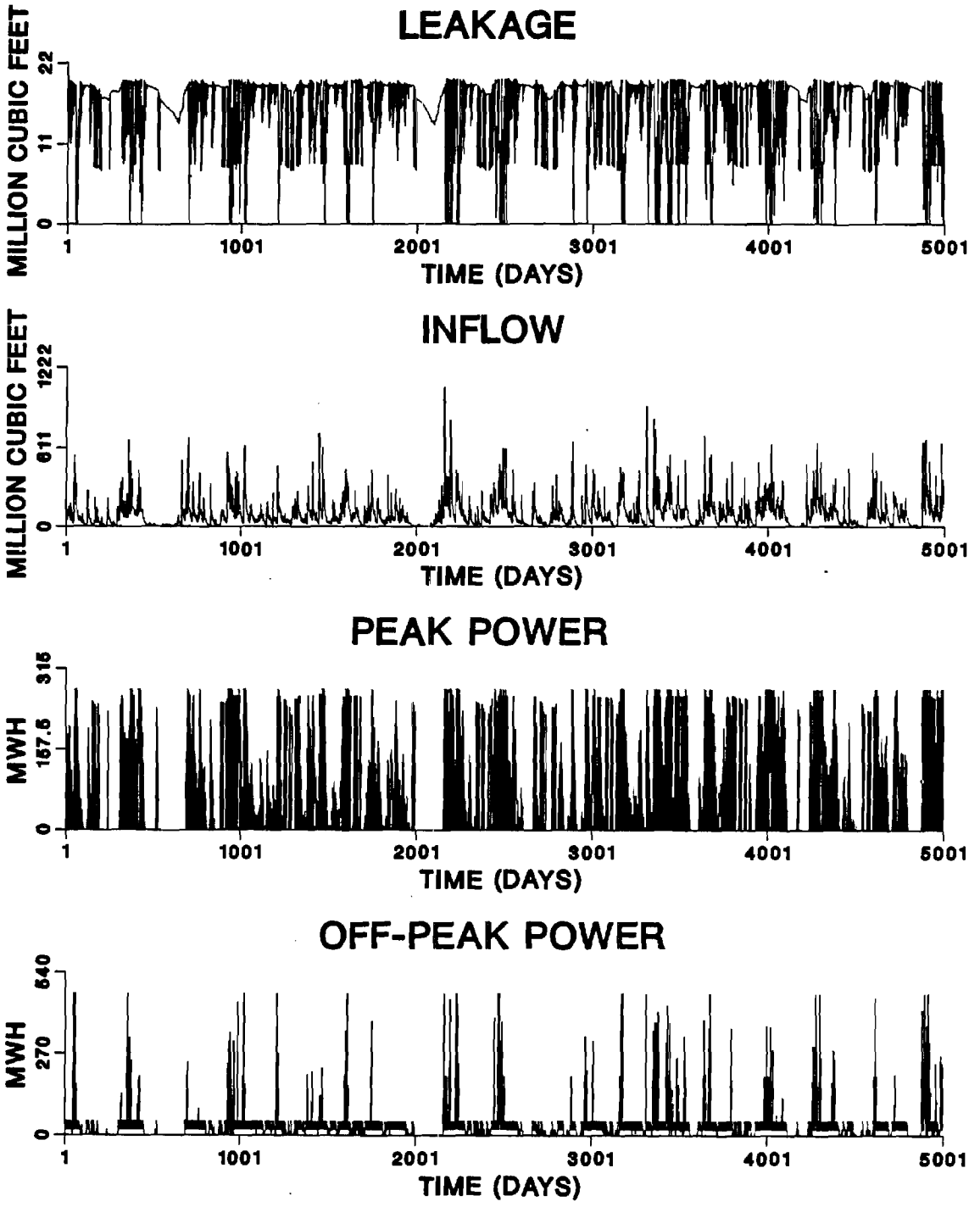

Figure 6.22: Simulation Results — Experiment II

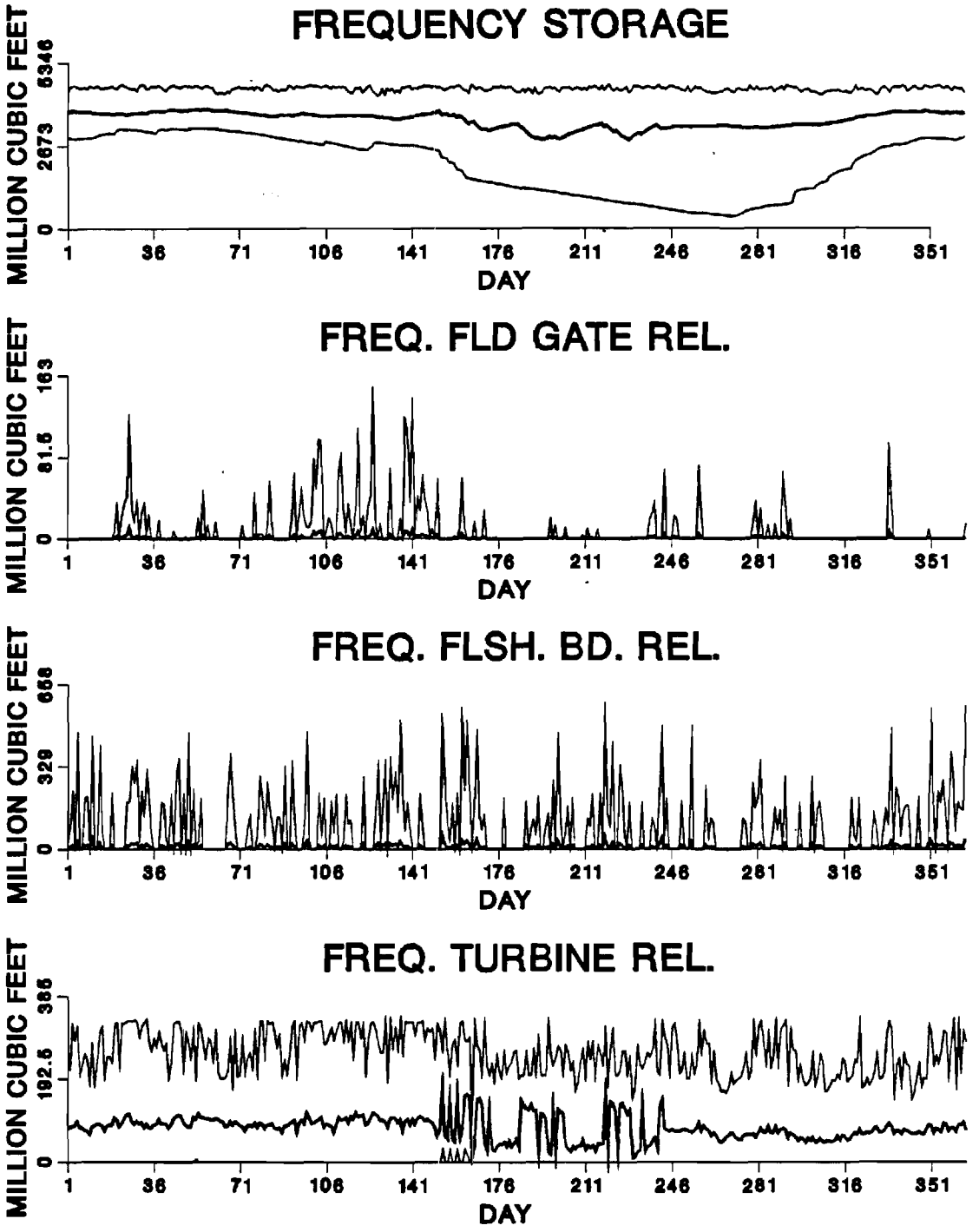

Figure 6.23: Daily Frequencies — Experiment II

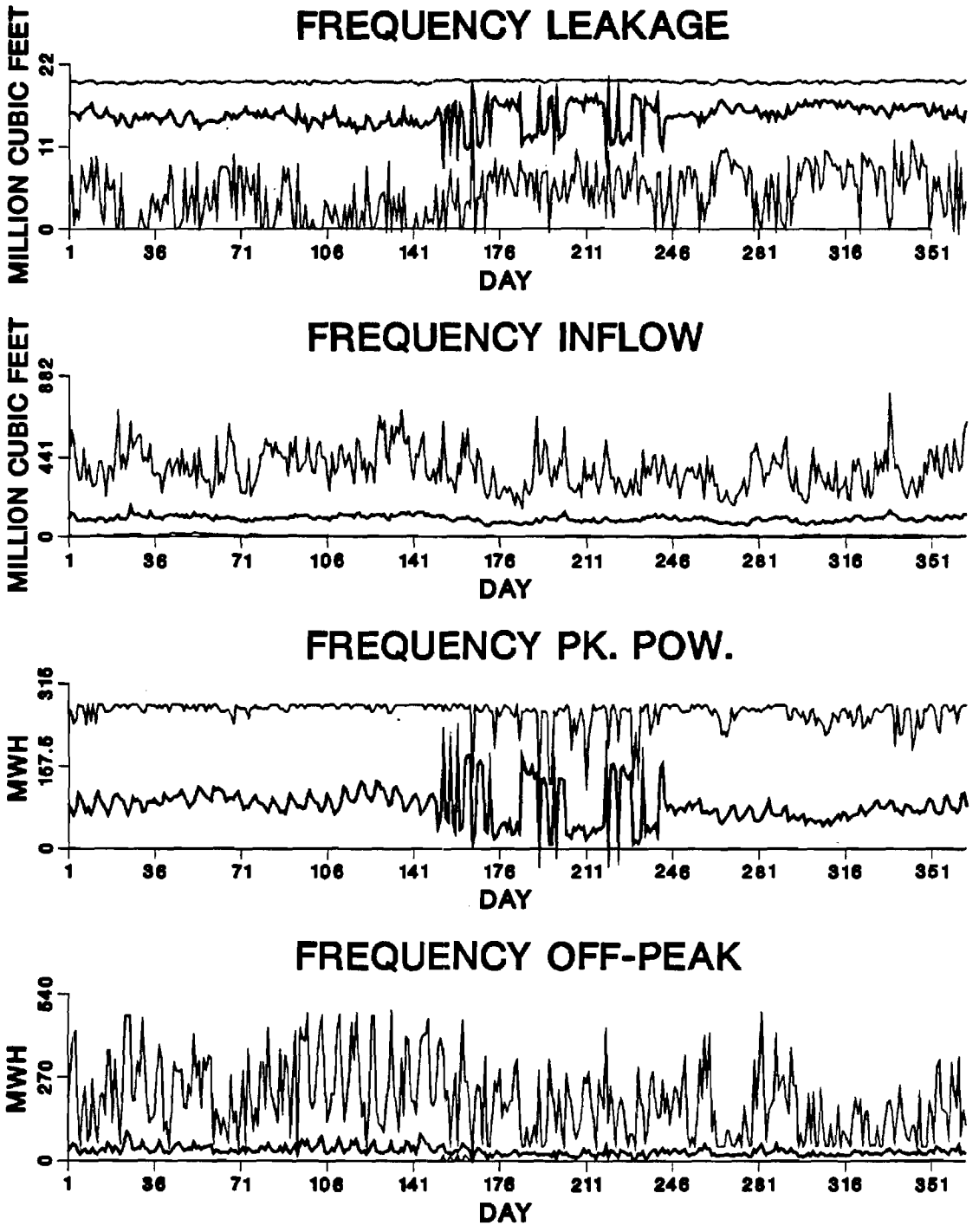

Figure 6.24: Daily Frequencies — Experiment II

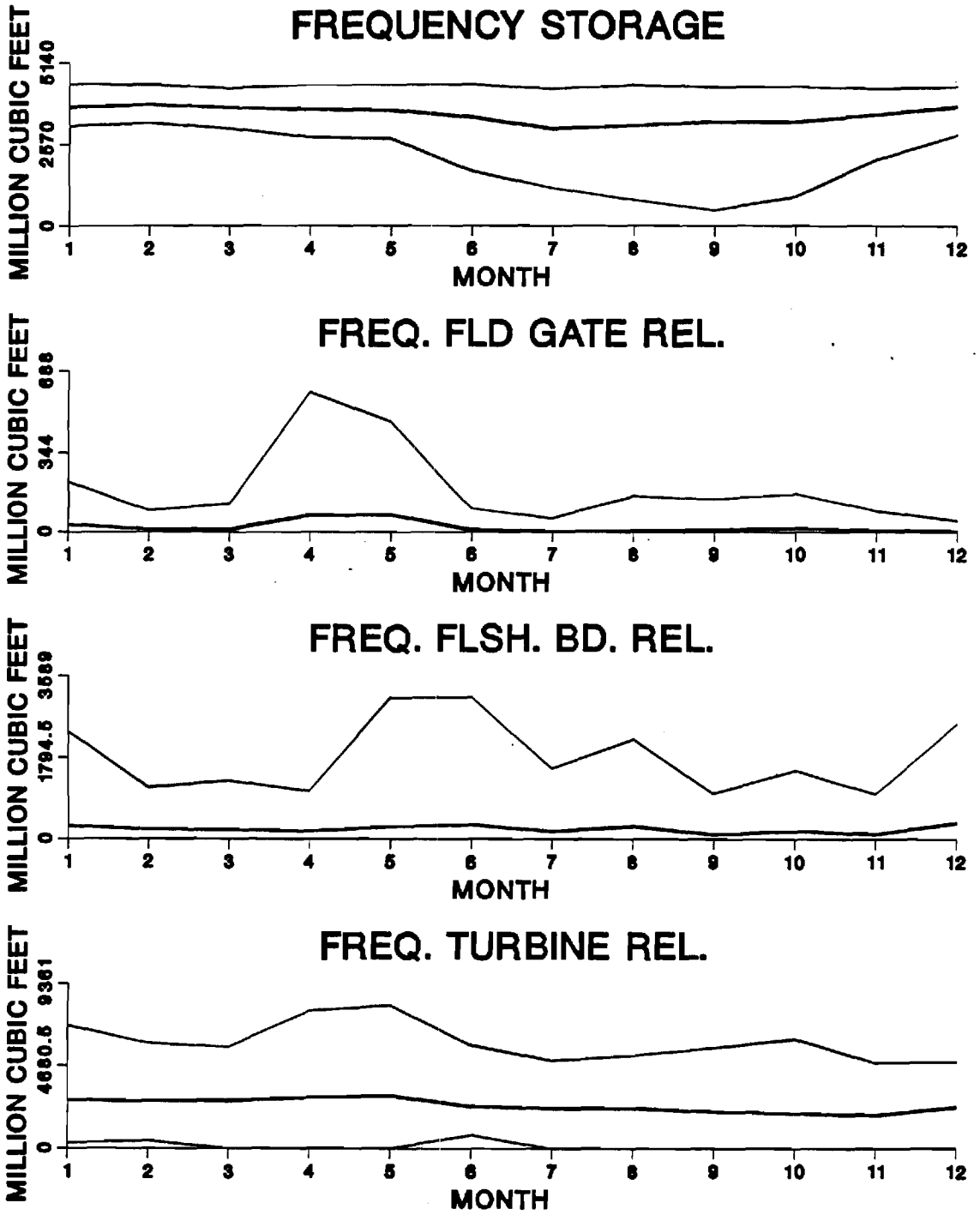

Figure 6.25: Monthly Frequencies — Experiment II

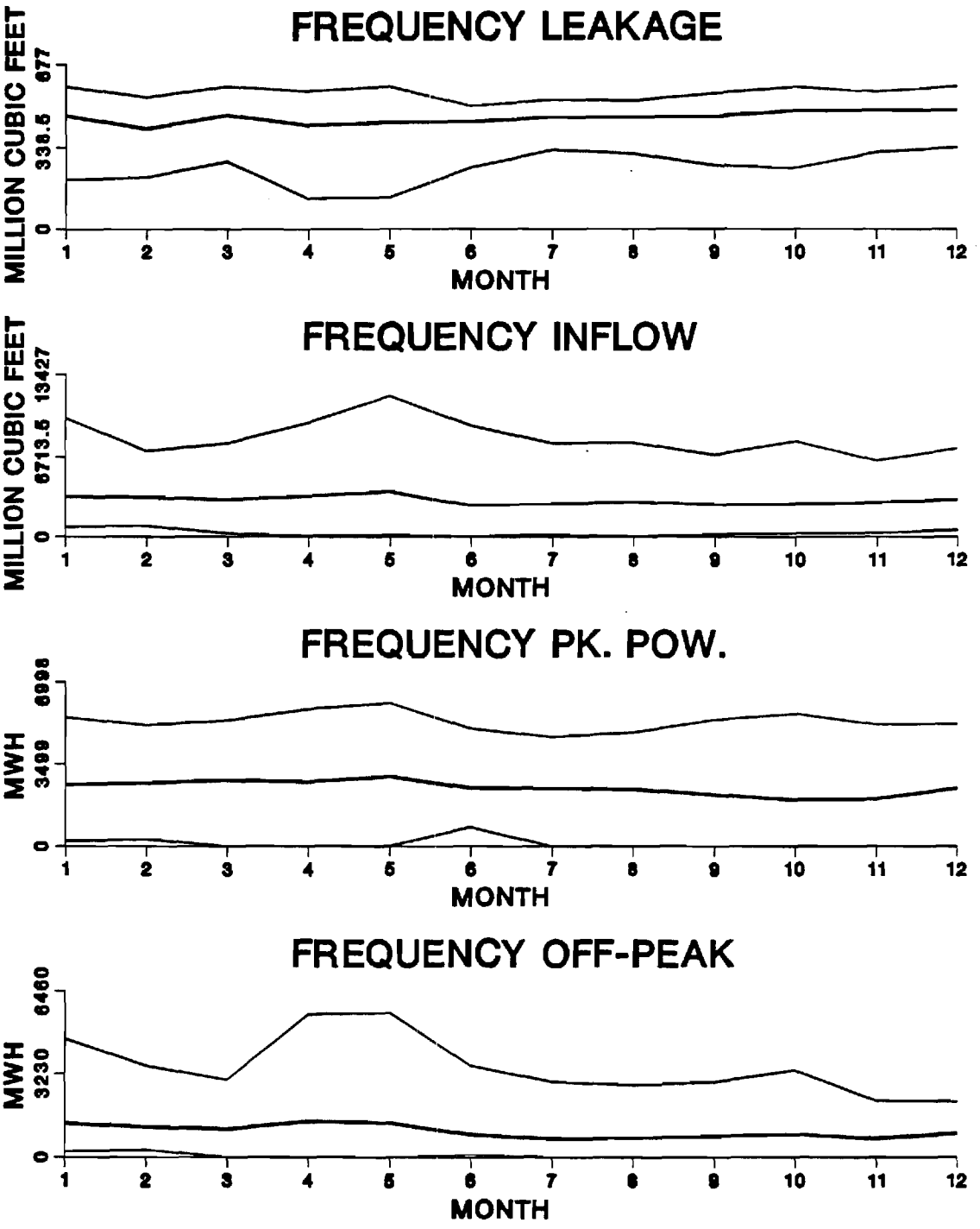

Figure 6.26: Monthly Frequencies — Experiment II

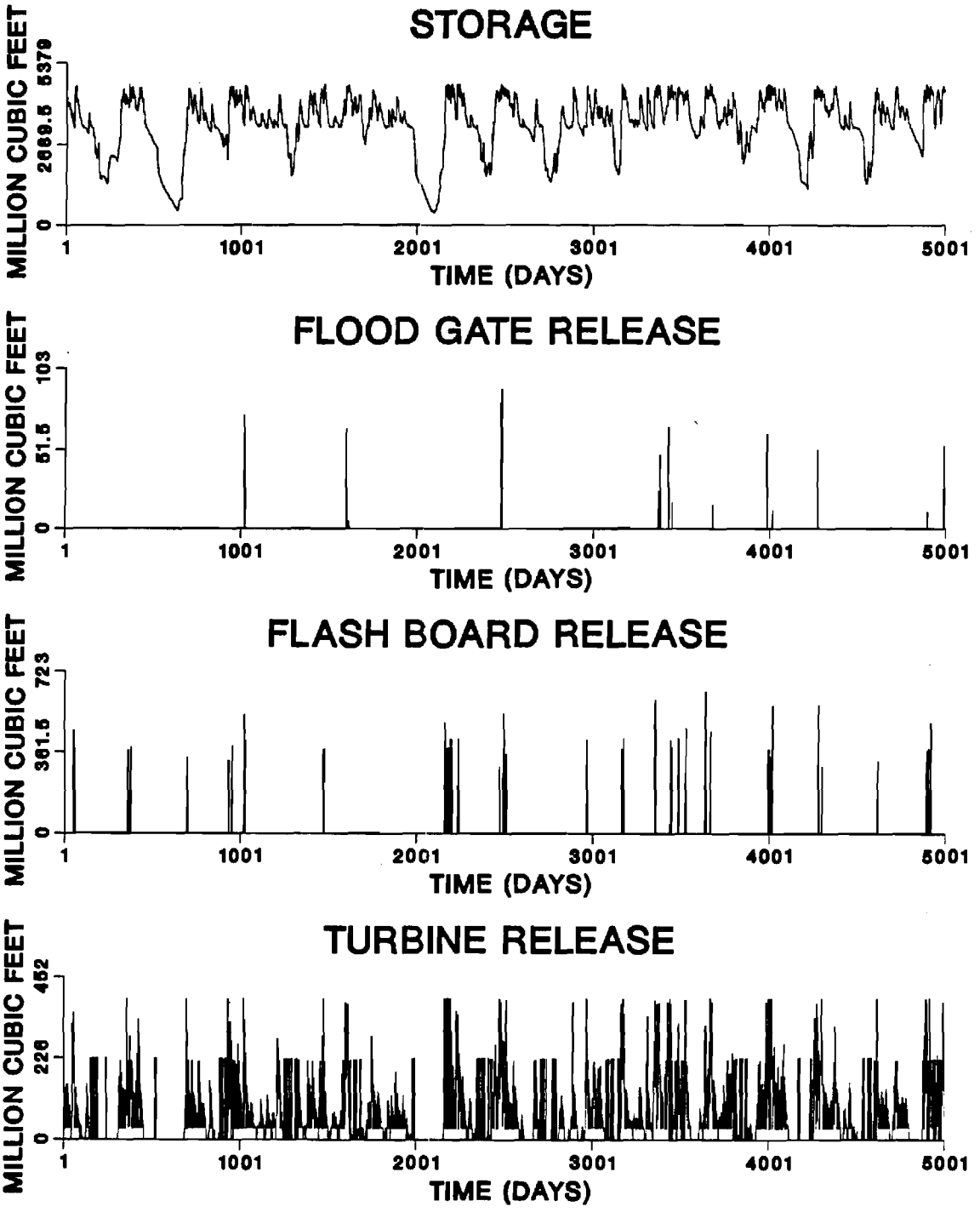

Figure 6.27: Simulation Results — Experiment III

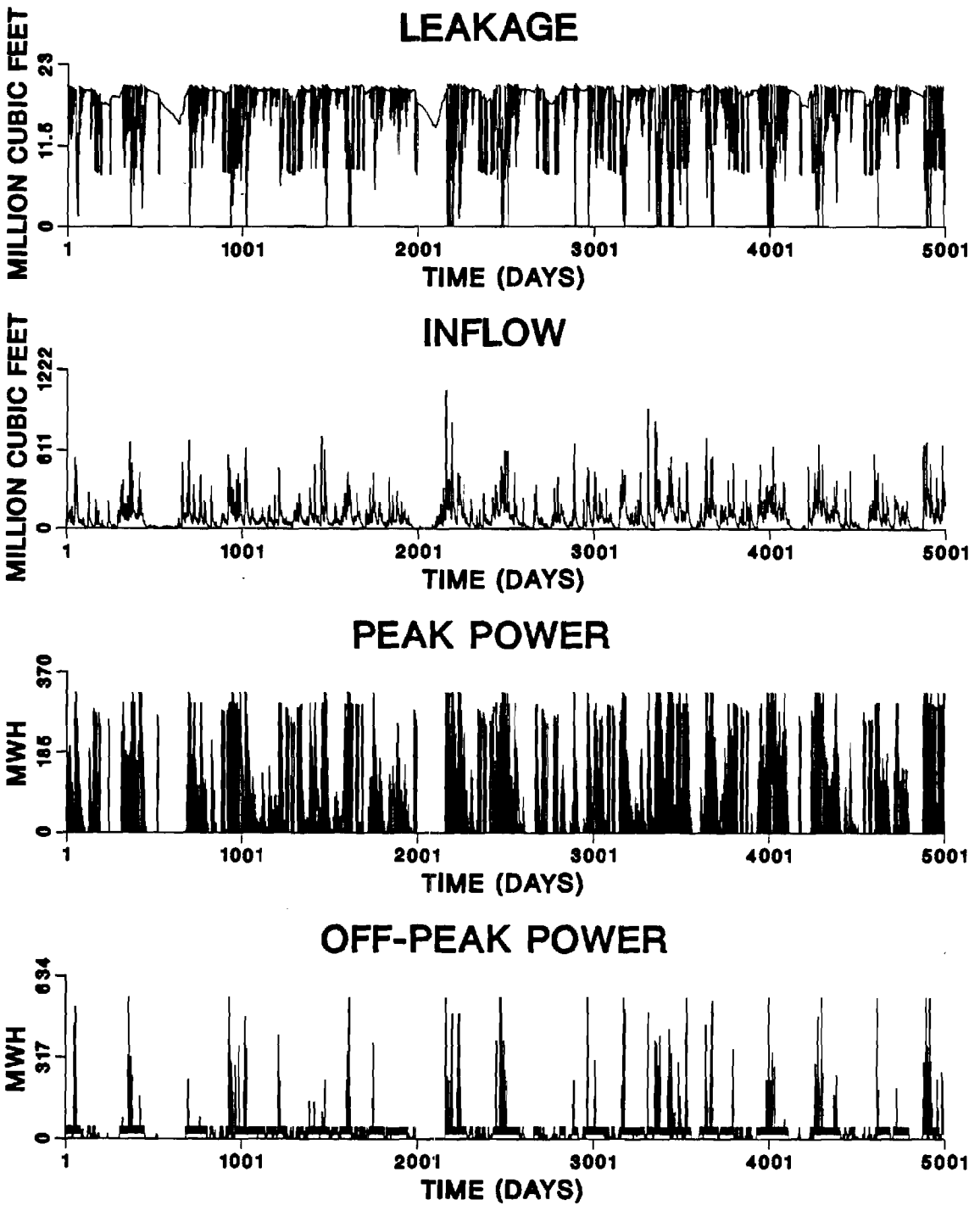

Figure 6.28: Simulation Results — Experiment III

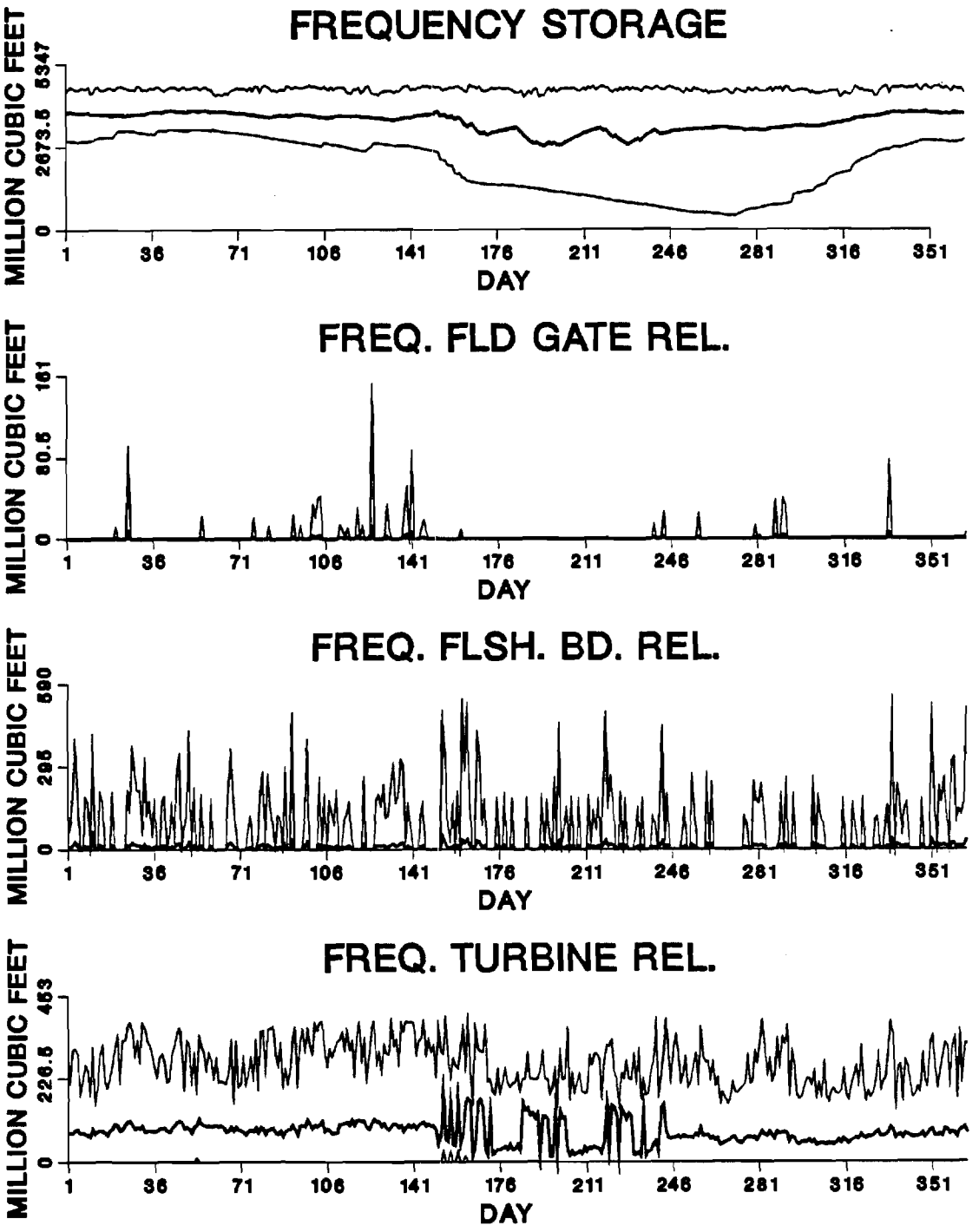

Figure 6.29: Daily Frequencies — Experiment III

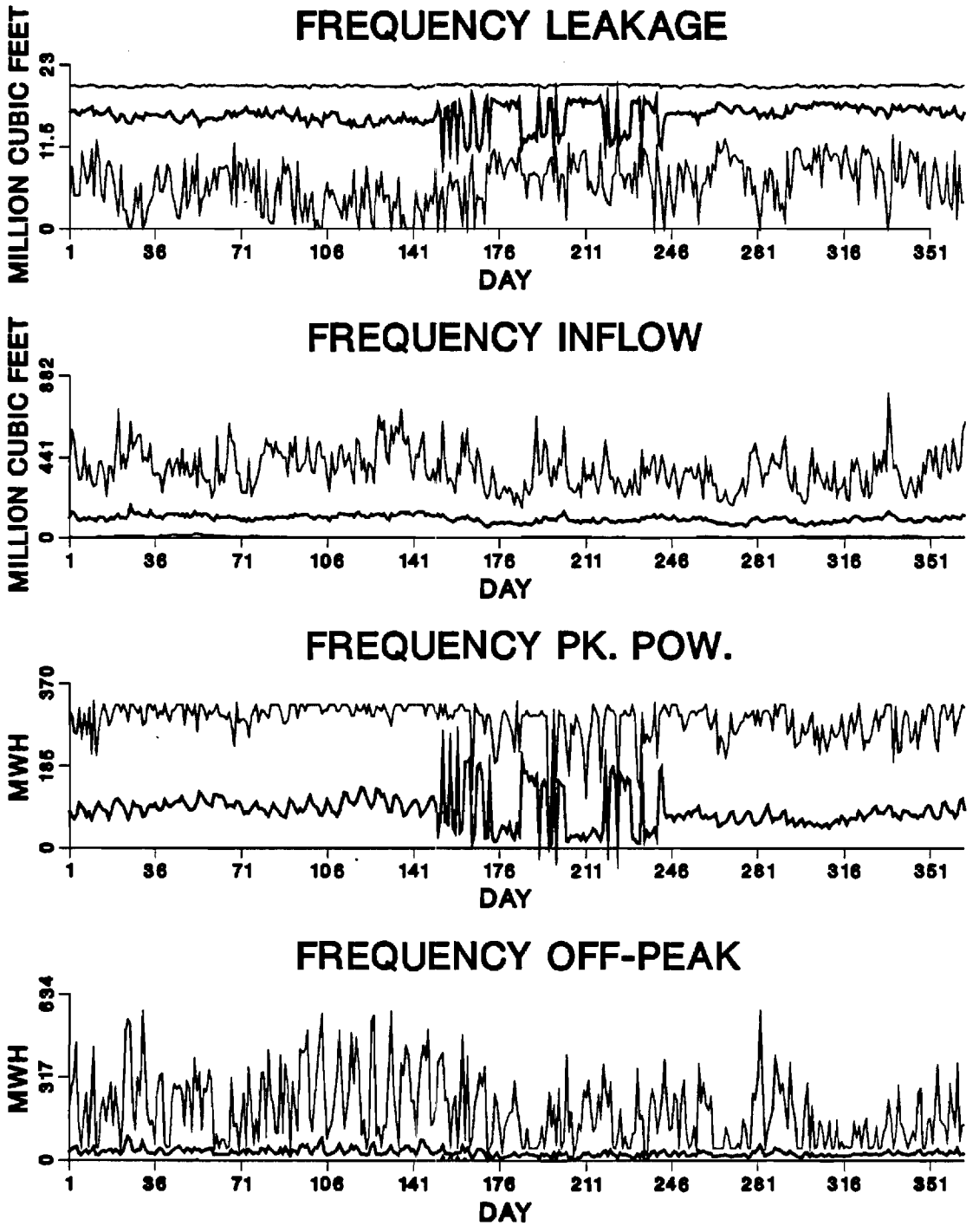

Figure 6.30: Daily Frequencies — Experiment III

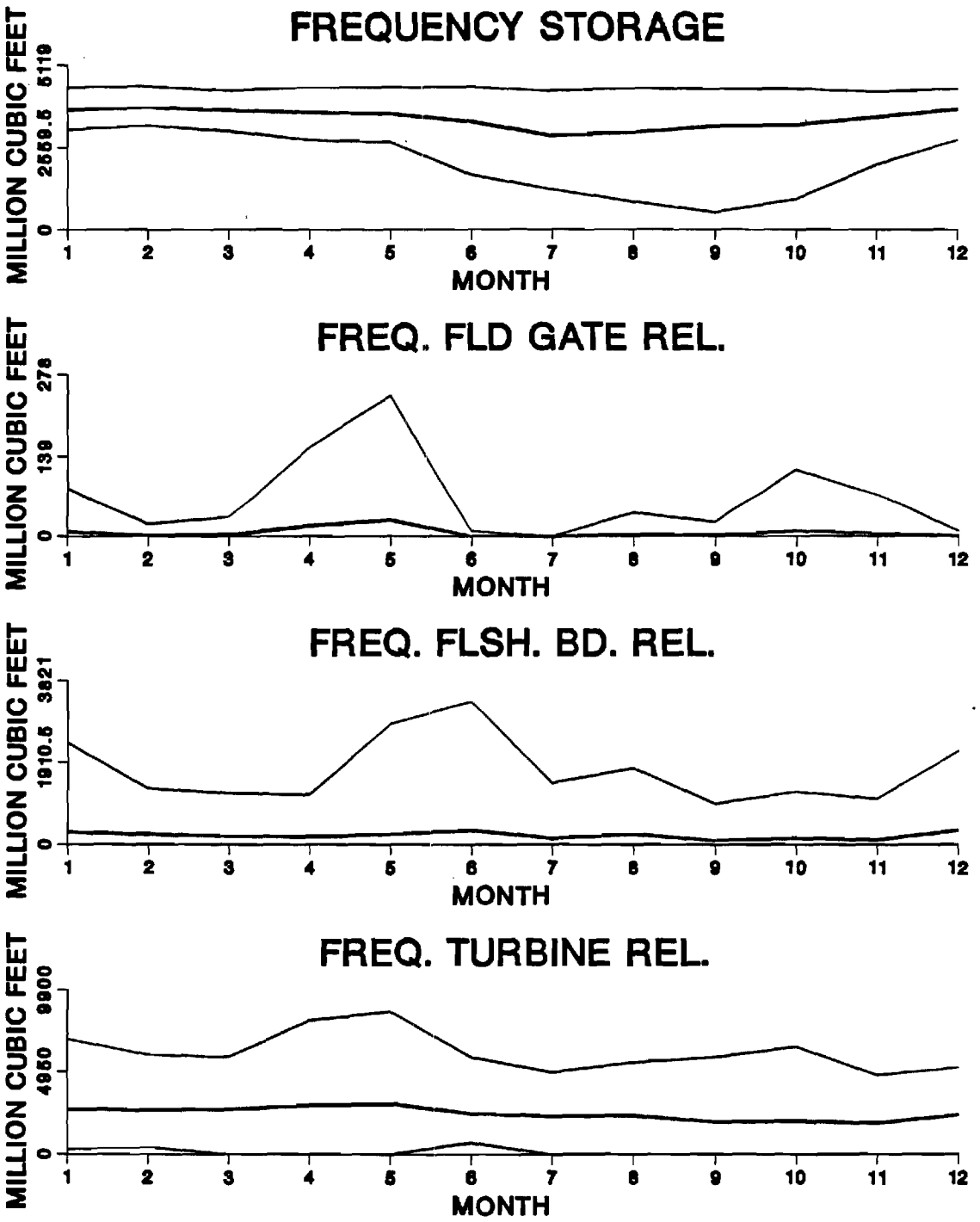

Figure 6.31: Monthly Frequencies — Experiment III

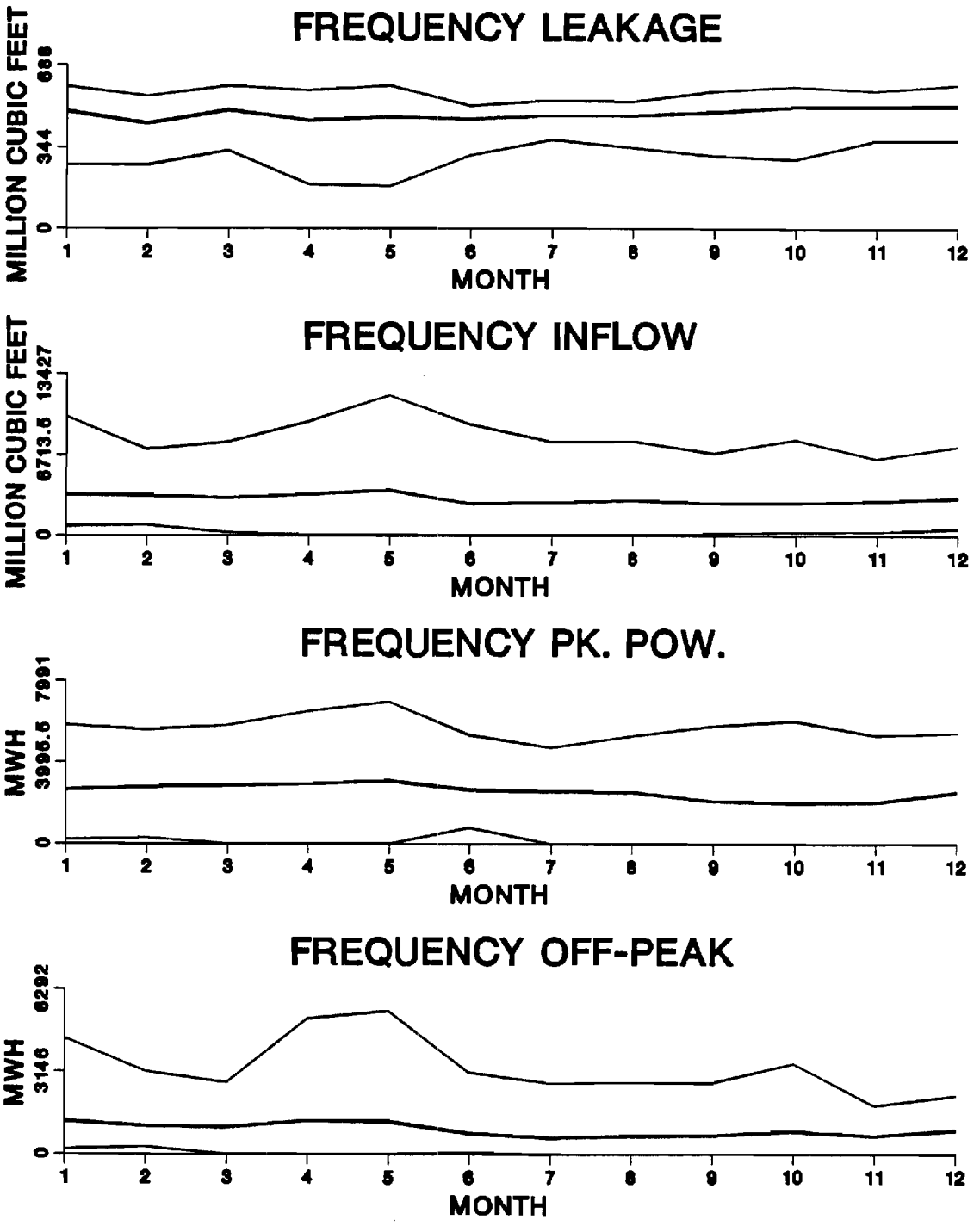

Figure 6.32: Monthly Frequencies — Experiment III

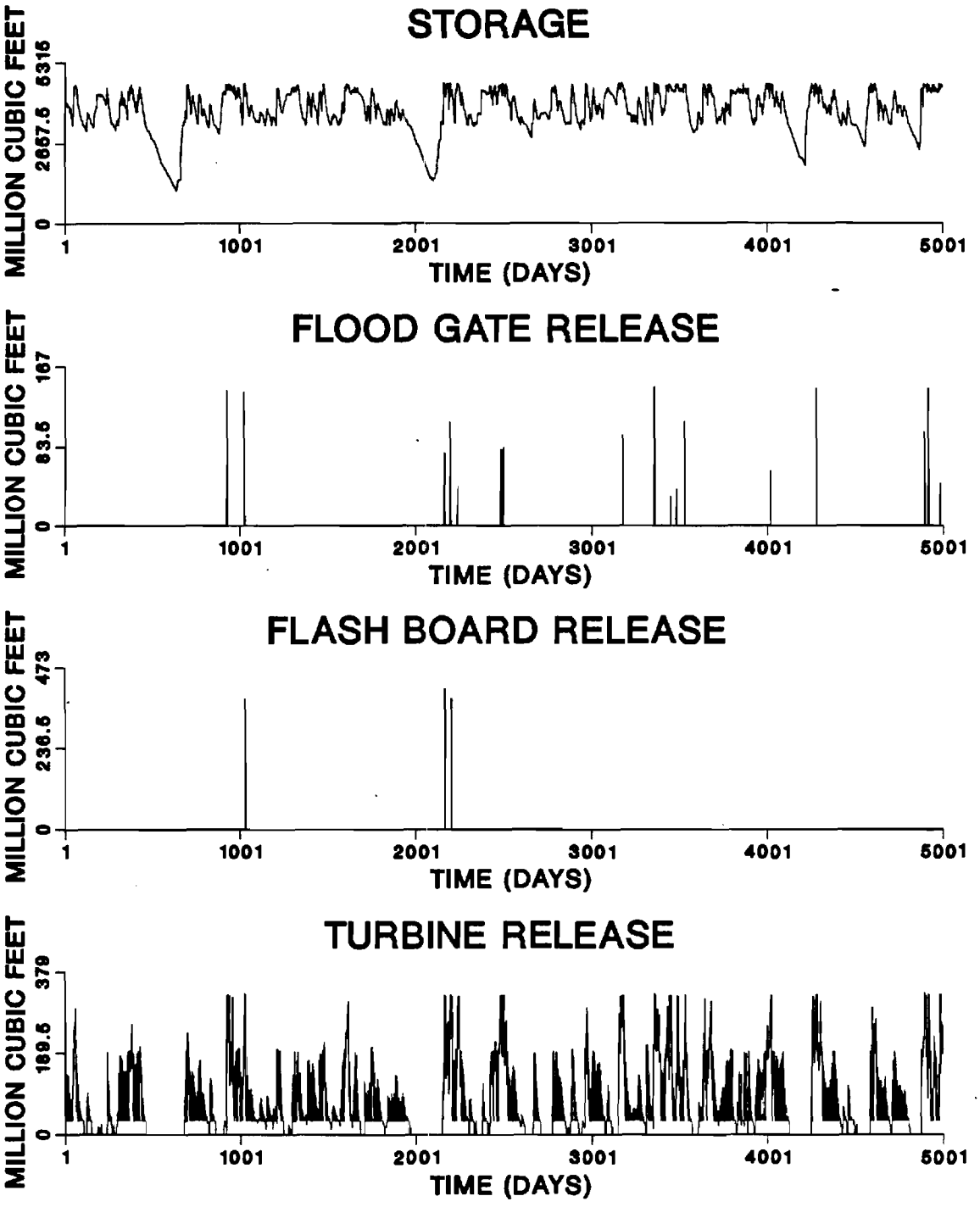

Figure 6.33: Simulation Results — Experiment IV

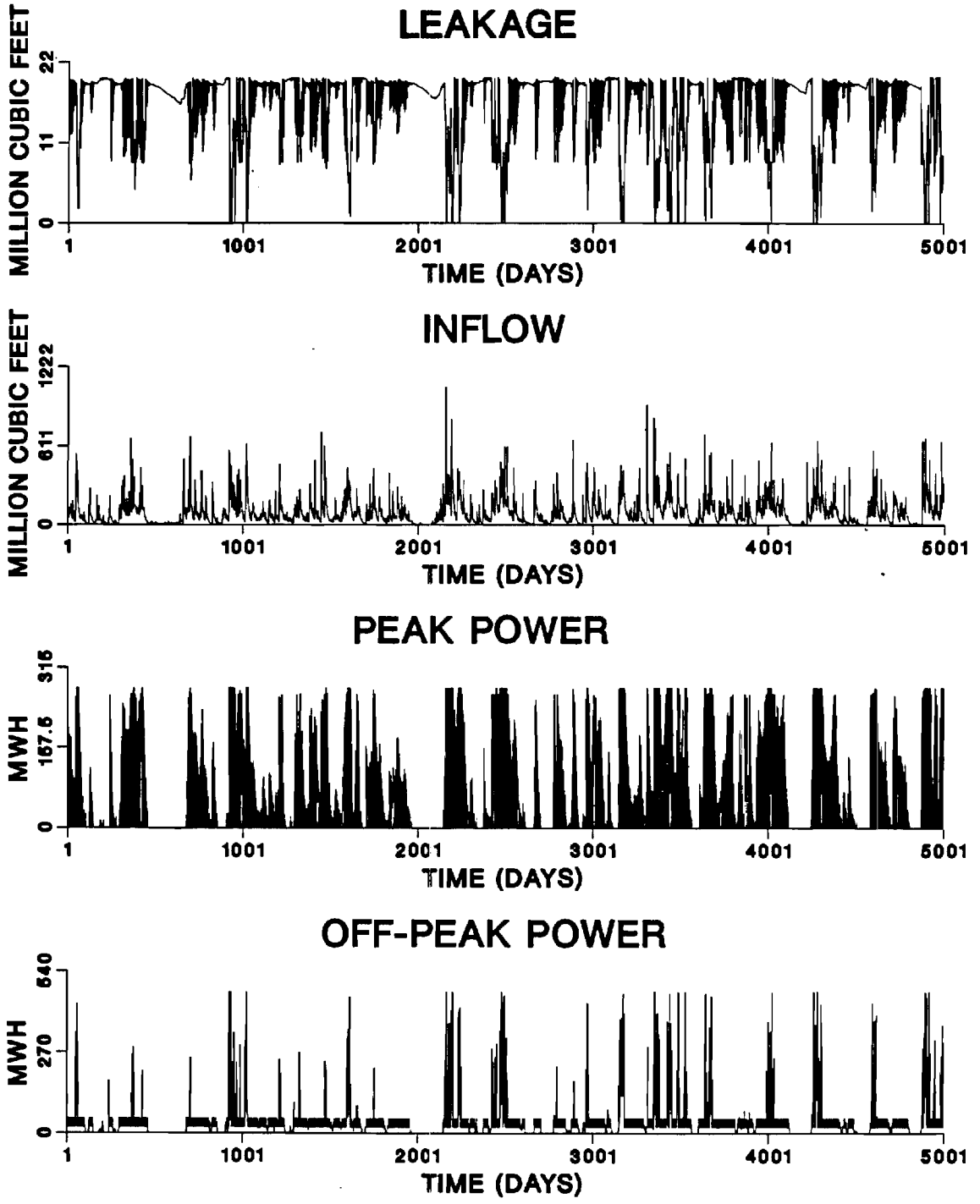

Figure 6.34: Simulation Results — Experiment IV

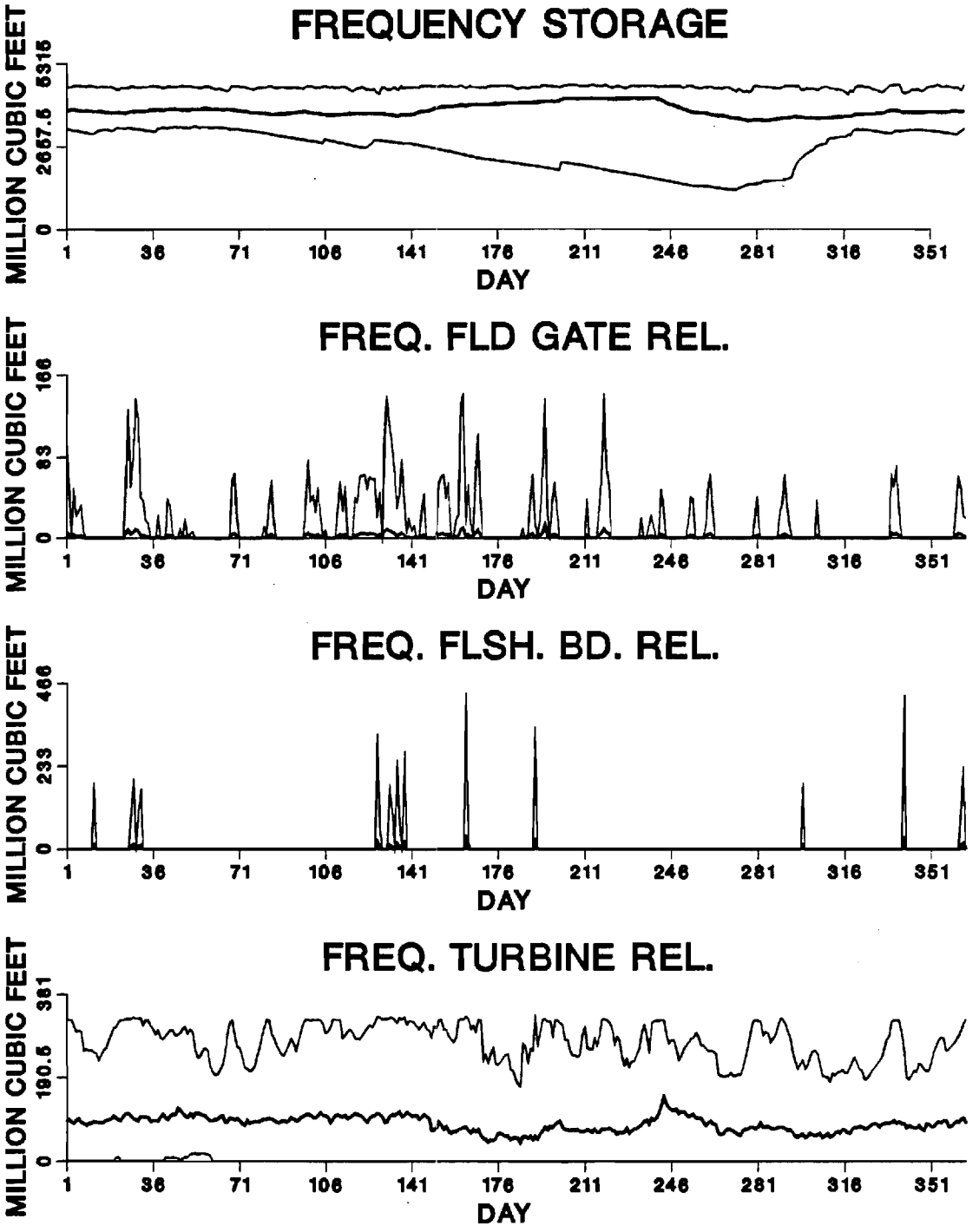

Figure 6.35: Daily Frequencies — Experiment IV

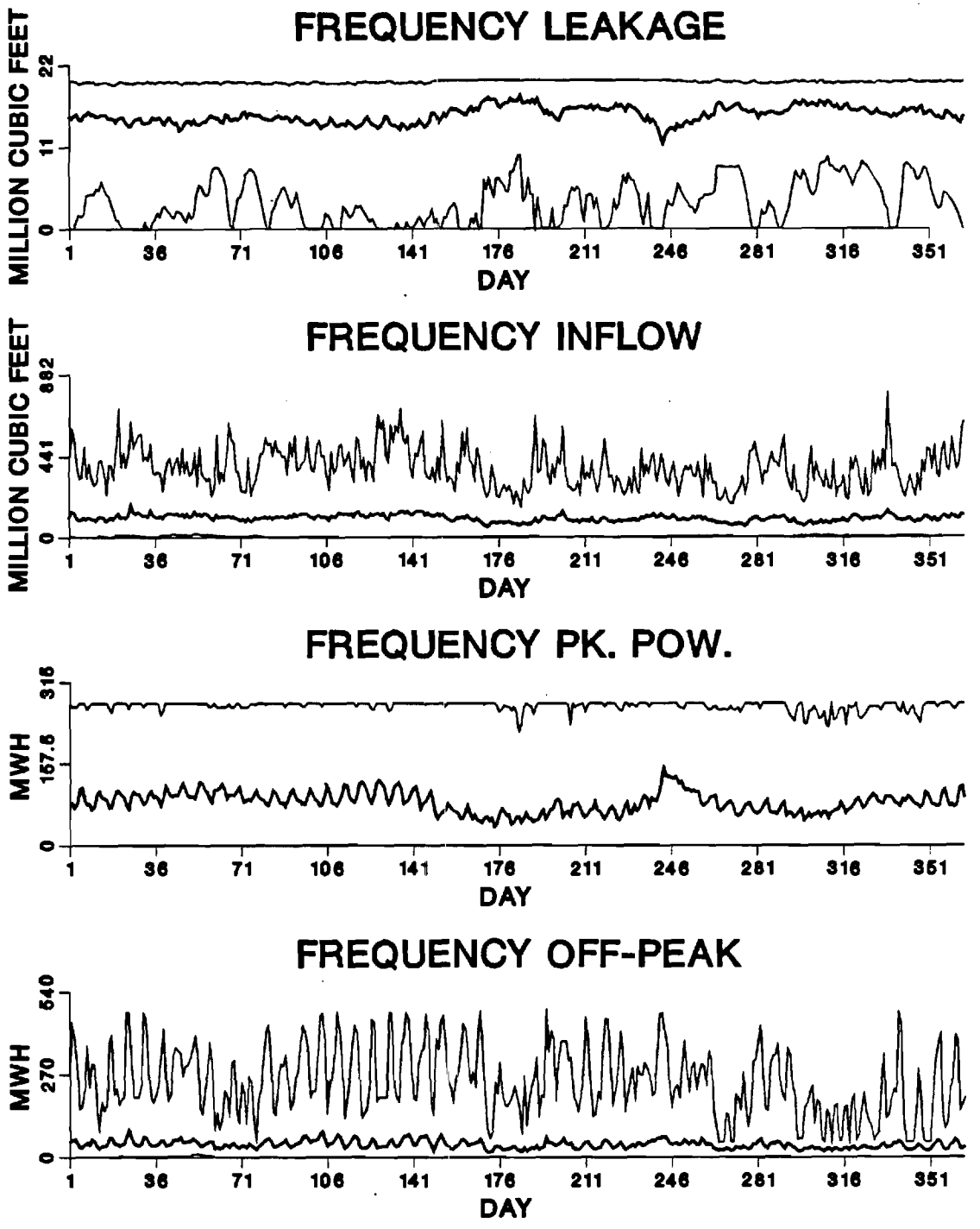

Figure 6.36: Daily Frequencies — Experiment IV

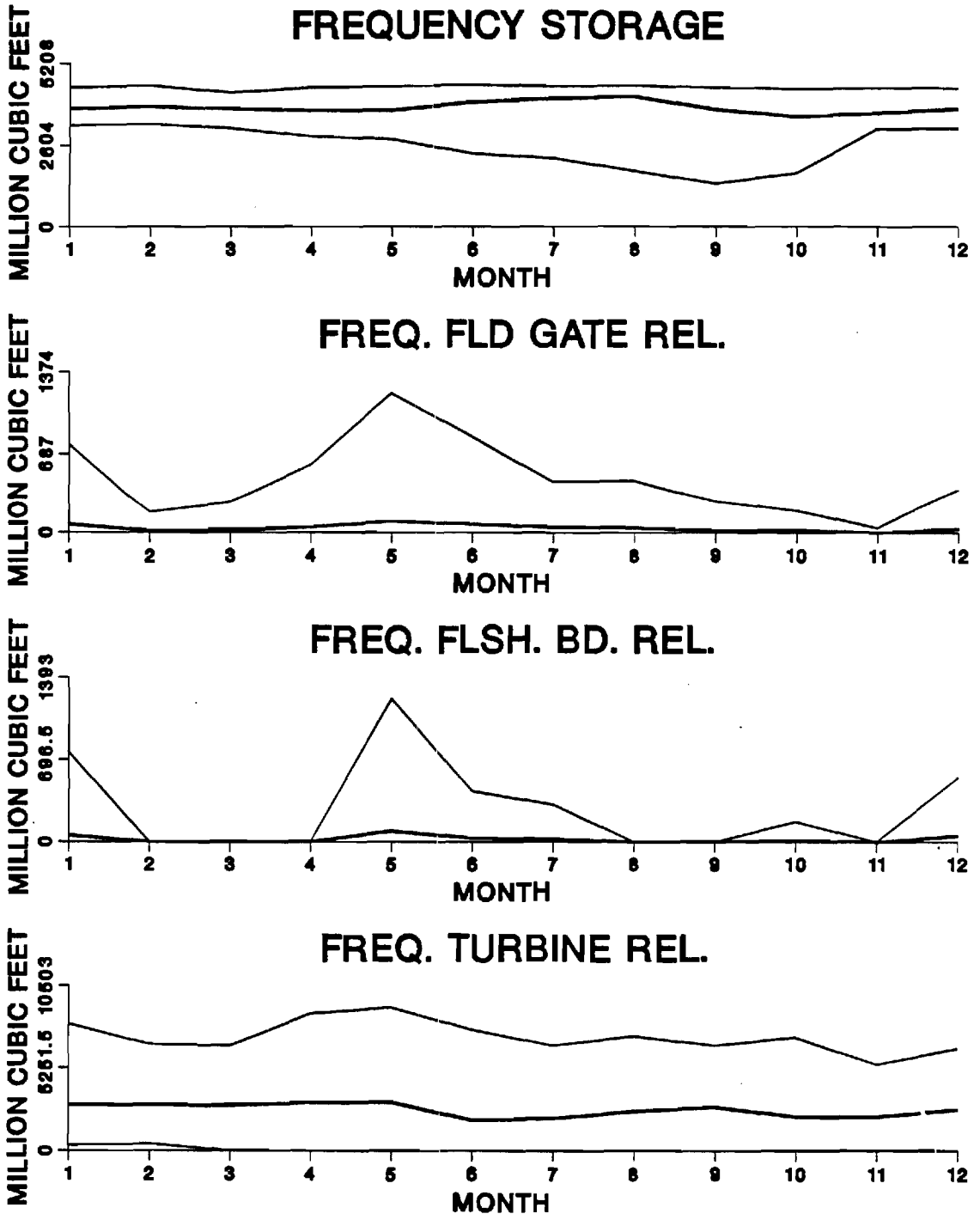

Figure 6.37: Monthly Frequencies — Experiment IV

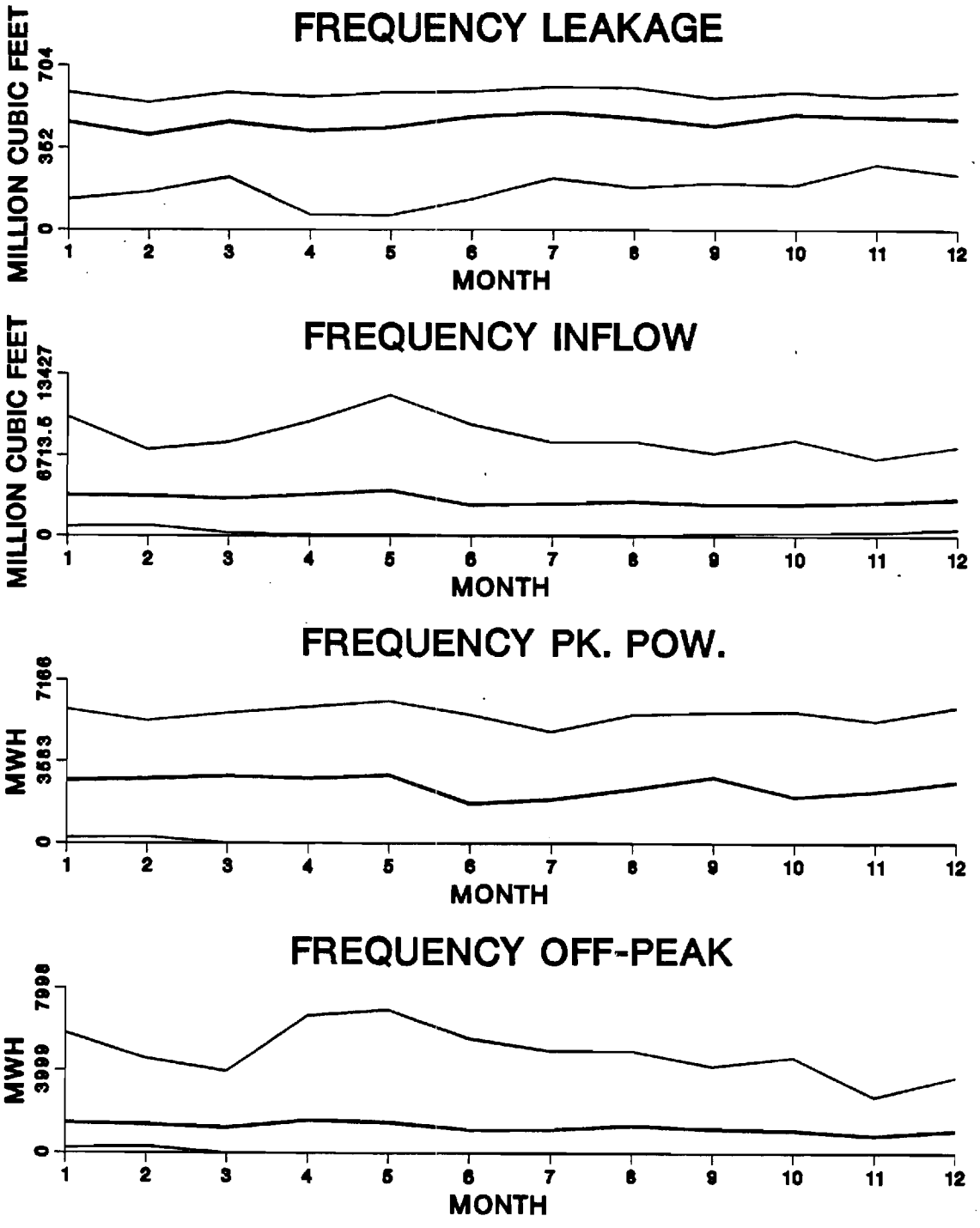

Figure 6.38: Monthly Frequencies — Experiment IV

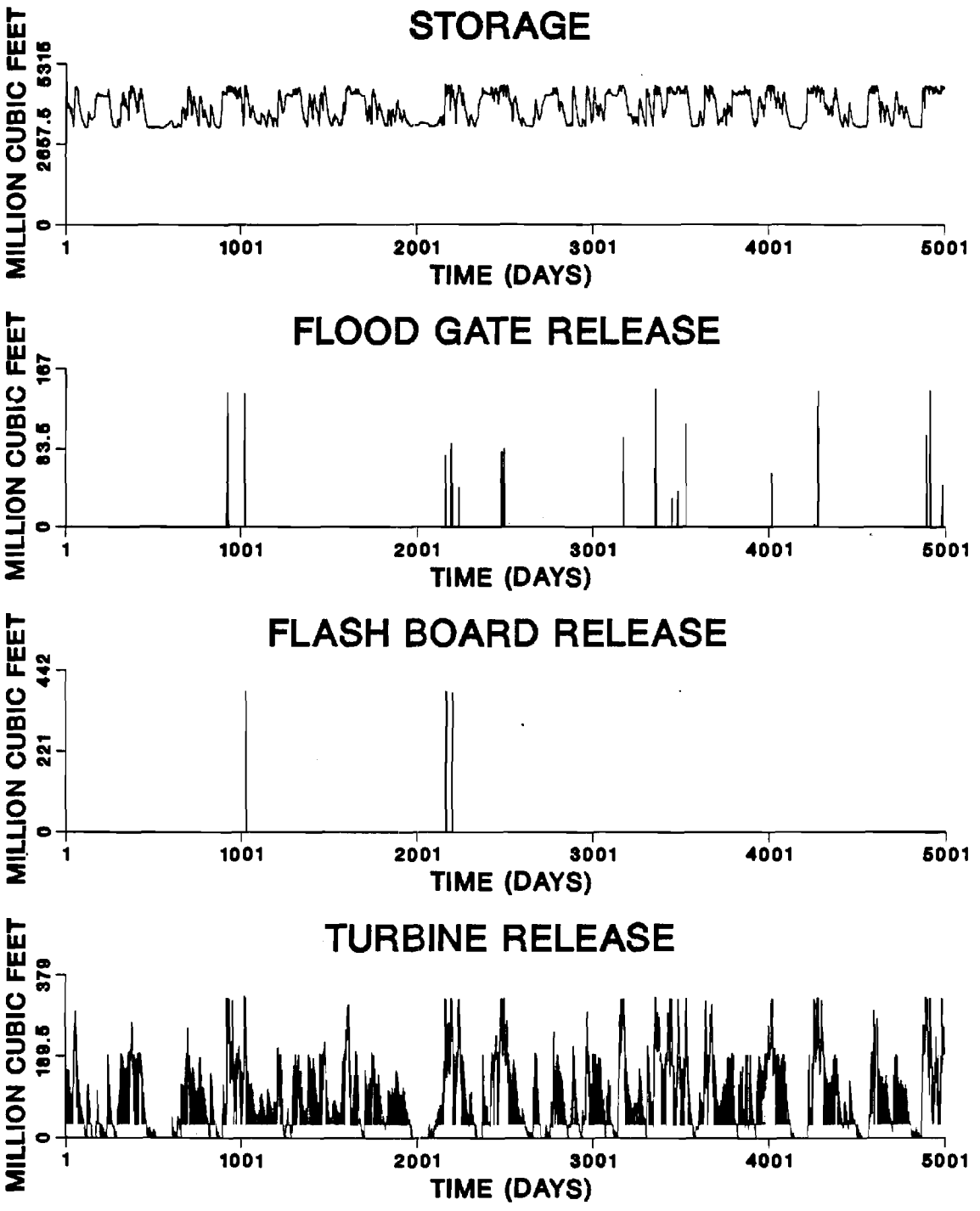

Figure 6.39: Simulation Results — Experiment V

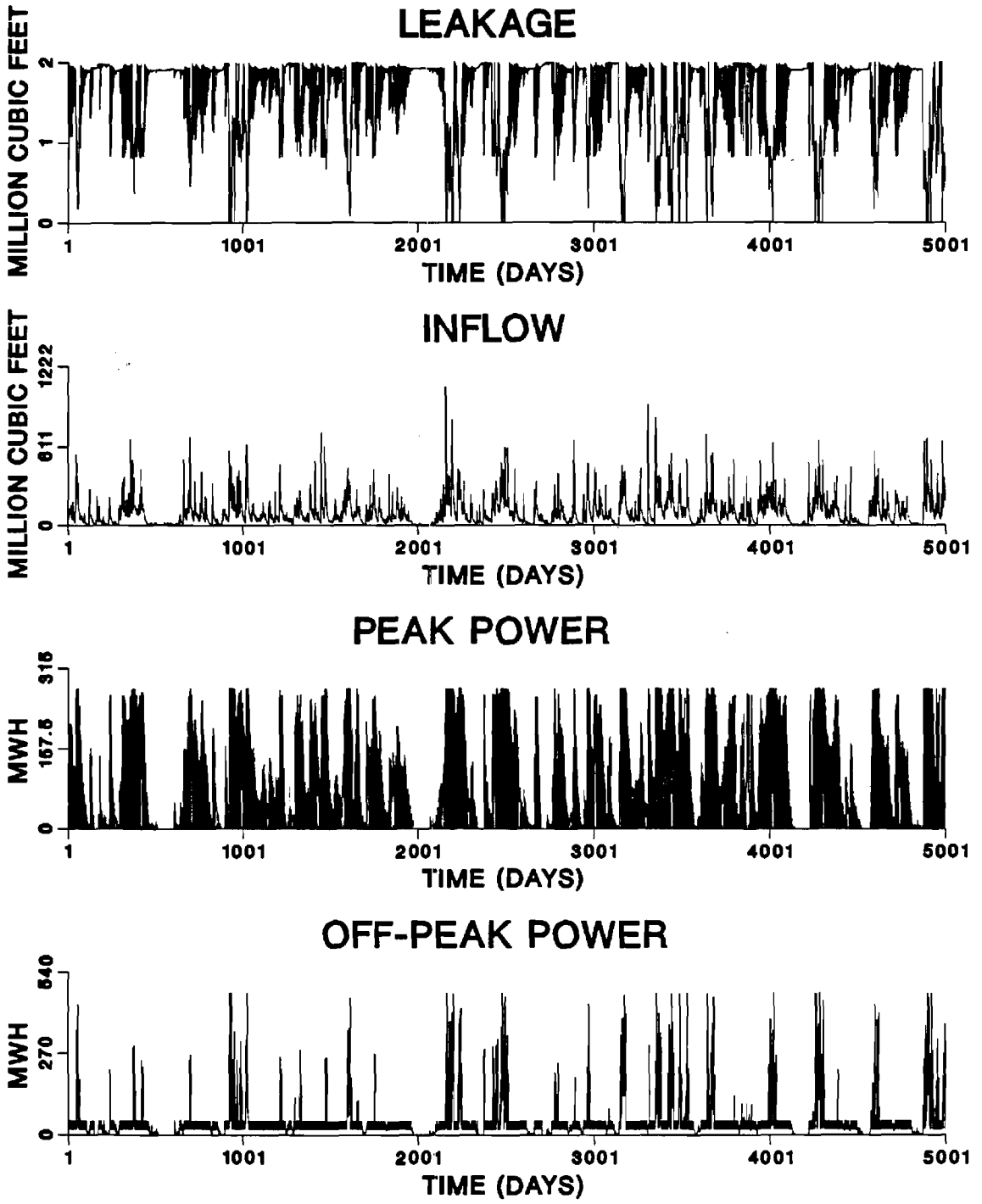

Figure 6.40: Simulation Results — Experiment V

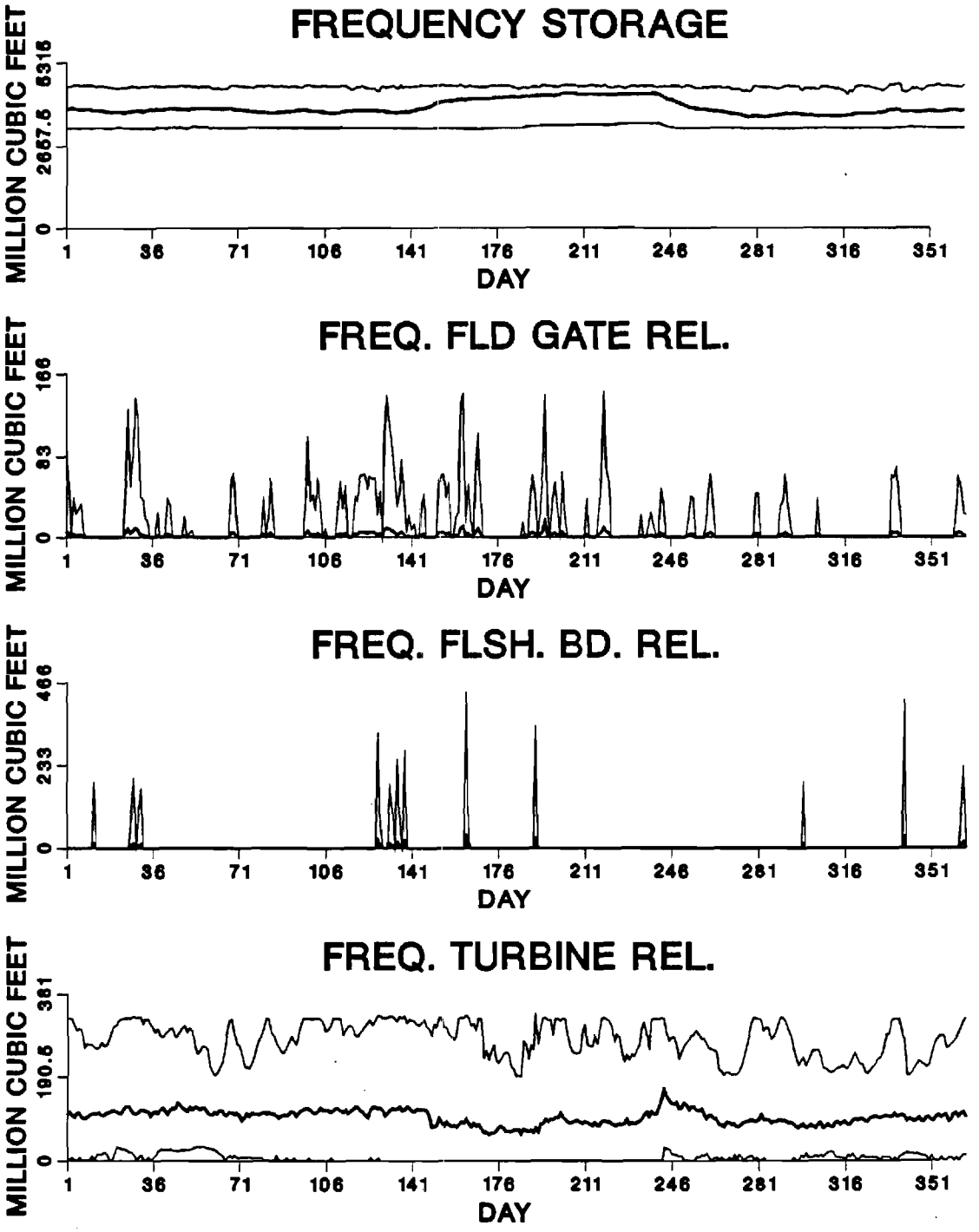

Figure 6.41: Daily Frequencies — Experiment V

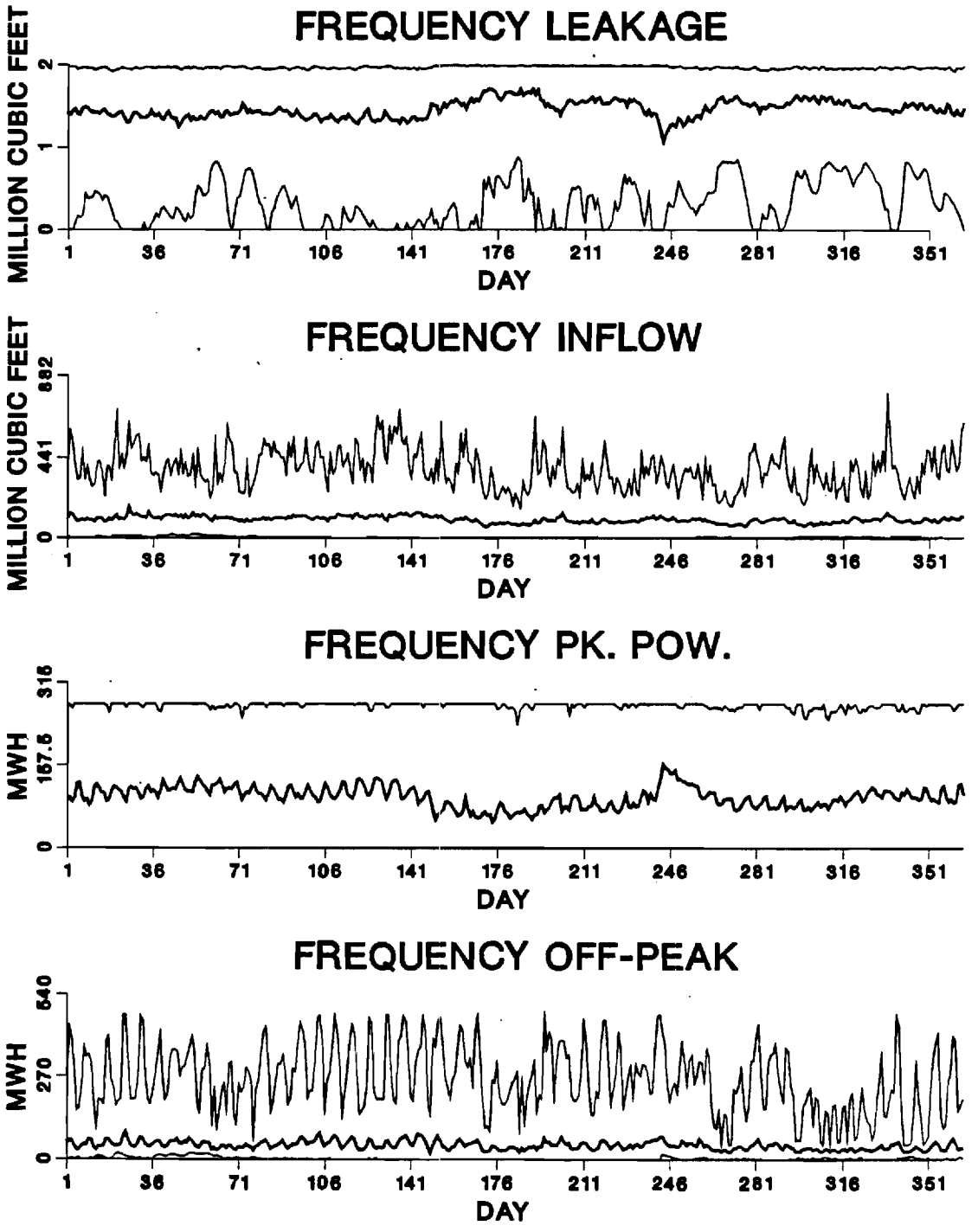

Figure 6.42: Daily Frequencies — Experiment V

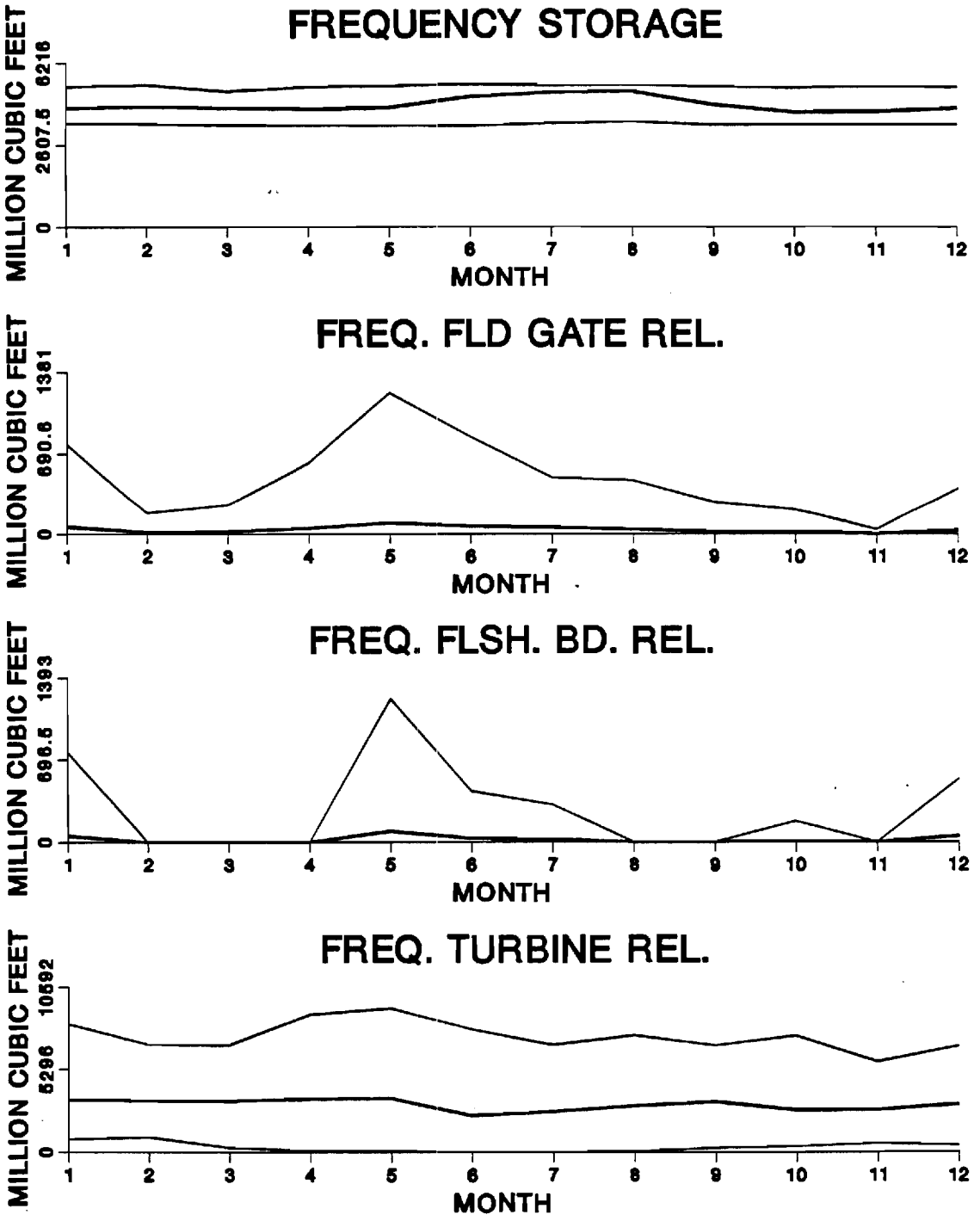

Figure 6.43: Monthly Frequencies — Experiment V

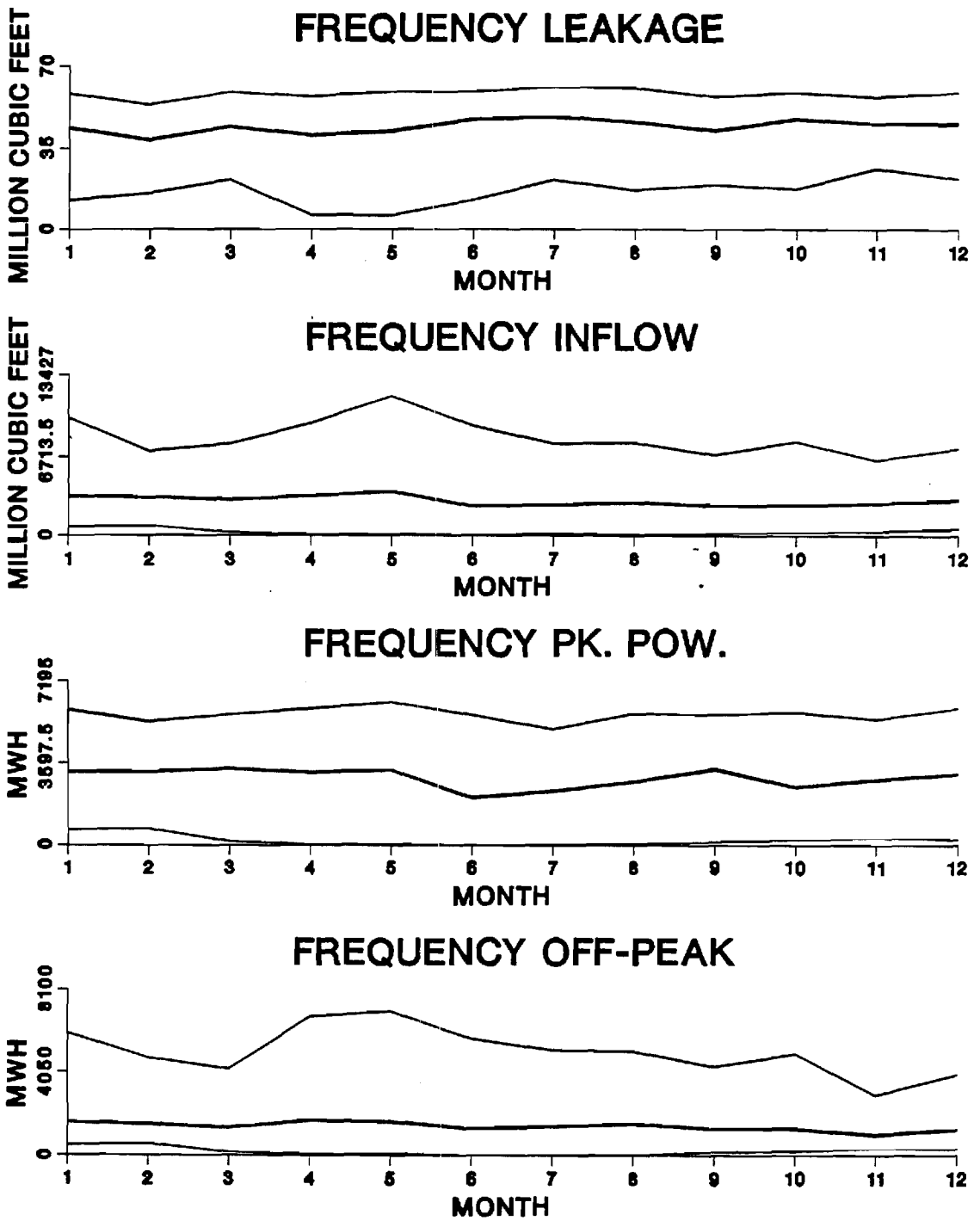

Figure 6.44: Monthly Frequencies — Experiment V

6.6 Closing Remarks

This chapter discusses the theory and application of a new control model for the operation of the Lloyd Shoals hydroelectric facility. This model is based on a state-of-the-art stochastic control approach but also includes new enhancements that make it suitable for hydropower systems. The new model is designed to determine optimal power generation schedules on a daily basis and can also be used in a simulation mode to investigate policy issues. The following discussion summarizes the conclusions from such investigations.

As a general comment, stochastic control methods are expected to outperform deterministic approaches, because they are based on a more pragmatic system model. More specifically, the Lloyd Shoals facility was seen in the previous section to generate on the average 3,500 MWH more energy per year under stochastic control guidance. This gain represents 1,000 MWH of peak and 2,500 MWH of off-peak energy generation, or about $85,000 of yearly saved expenditures.

Streamflow forecasting enhances reservoir management by extending the decision time which is available to the operator. Due to inadequate rainfall and streamflow data records, a reliable streamflow forecasting model for Lloyd Shoals cannot be calibrated. However, the potential gains from improving the instrumentation network and developing such a model were estimated to be substantial. On the average, as much as 4,100 MWH of additional energy may be produced, about 1,300 MWH of which would represent peak and 2,800 MWH off-peak energy generation. These energy gains would translate into an average of $100,000 yearly saved expenditures. In that regard, a telemetry rainfall and streamflow instrumentation network would be the most appropriate real time data collection system.

The addition of a 7th turbine will enhance the plant capacity to accommodate flood volumes without having to resort to flood gate operation. The simulation analysis indicates that approximately 800 MWH of previously off-peak energy generation per year becomes available as peak energy generation. Naturally, the question is whether this improvement outweighs the unit purchasing and installation outlay. On the other hand, any expenditures reconditioning the existing turbines (in the way of leakage reduction) will result in considerable hydropower gains. According to the results of the previous section, such improvements may result in 7,500 MWH of additional energy production, 5,250 MWH of which would represent peak energy generation and the remaining off-peak energy improvements. On the average, these gains would amount to about $300,000 to $350,000 of yearly saved expenditures.

It is noted that all previous estimates represent gains pertaining to individual improvements. Thus, the total expected gain from a stochastic control model with accurate streamflow forecasting and six rehabilitated turbines would be about 15,000 MWH per year, about half of which would represent peak energy generation. On the average, this energy gain would constitute $500,000 of saved expenditures per year.

Furthermore, usage of these techniques in larger hydroelectric projects or systems of hydroelectric projects is expected to generate higher profits.

The control model researched in this work is characterized by high computational efficiency. Thus, although the original computer code has been developed on a main frame computer (CYBER 180/990), it can also be modified for microcomputer implementation. An extensive description of the control and simulation programs and their use is provided in a separate document (Georgakakos, 1989c).

7. OPTIMAL REGULATION OF THE SOUTHEASTERN U.S. RESERVOIR SYSTEM

7.1 Introduction

This chapter briefly discusses an application of the multilevel stochastic control method presented in the previous chapter to an 11-reservoir, 43-turbine system. The goal is to investigate whether the method maintains its efficiency and reliability in large scale system applications.

7.2 The Southeastern U.S. Reservoir System

This application concerns the regulation of 11 Corps-of-Engineers reservoirs located in the Alabama-Coosa, Apalachicola, and Savannah River basins (Figure 7.1). The Alabama-Coosa Rivers drain a small part of Tennessee, northwestern Georgia, and east-central Alabama. The Apalachicola-Flint-Chatahoochee system drains northern and western Georgia, southeastern Alabama, and a part of Florida's western extension (panhandle). The Savannah River system has already been described in previous chapters.

The major projects in these basins are the Carters, Allattoona, Jones Bluff, and Millers Ferry Reservoirs in the Alabama-Coosa basin; Buford, West Point, George, and Woodruff in the Apalachicola; and Hartwell, Russell and Clark Hill reservoirs in the Savannah river basin.

The regulation of the projects in the Apalachicola and Alabama Coosa basins is the responsibility of the Mobile Corps-of-Engineers District office; those of the Savannah river are regulated by the Savannah Corps-of-Engineers District office; the Atlanta office of the Corps oversees the overall system coordination.

Some characteristics of these projects are summarized in Table 7.1; the items reported are the project drainage area, storage allotted to flood control and power generation, installed power capacity, and other purposes such as flood control, recreation, navigation, and water supply. Other hydrologic, operational, or physical project characteristics used in this study can be found in the U. S. Army Corps of Engineers (C.O.E.) reservoir operation manuals provided by the Mobile C.O.E. district office.

Hartwell, Buford, and Clark Hill are the largest reservoirs of this group with storages that exceed or are close to 1.5 million acre-feet, while the others are smaller projects. As a matter of fact, the main function of Jones Bluff, Millers Ferry, George and Woodruff is to maintain channel navigability, and they are operated and thought of as run-on-the-river projects. Also, the crucial role of Buford, Hartwell and Clark Hill during the recent droughts cannot be overemphasized.

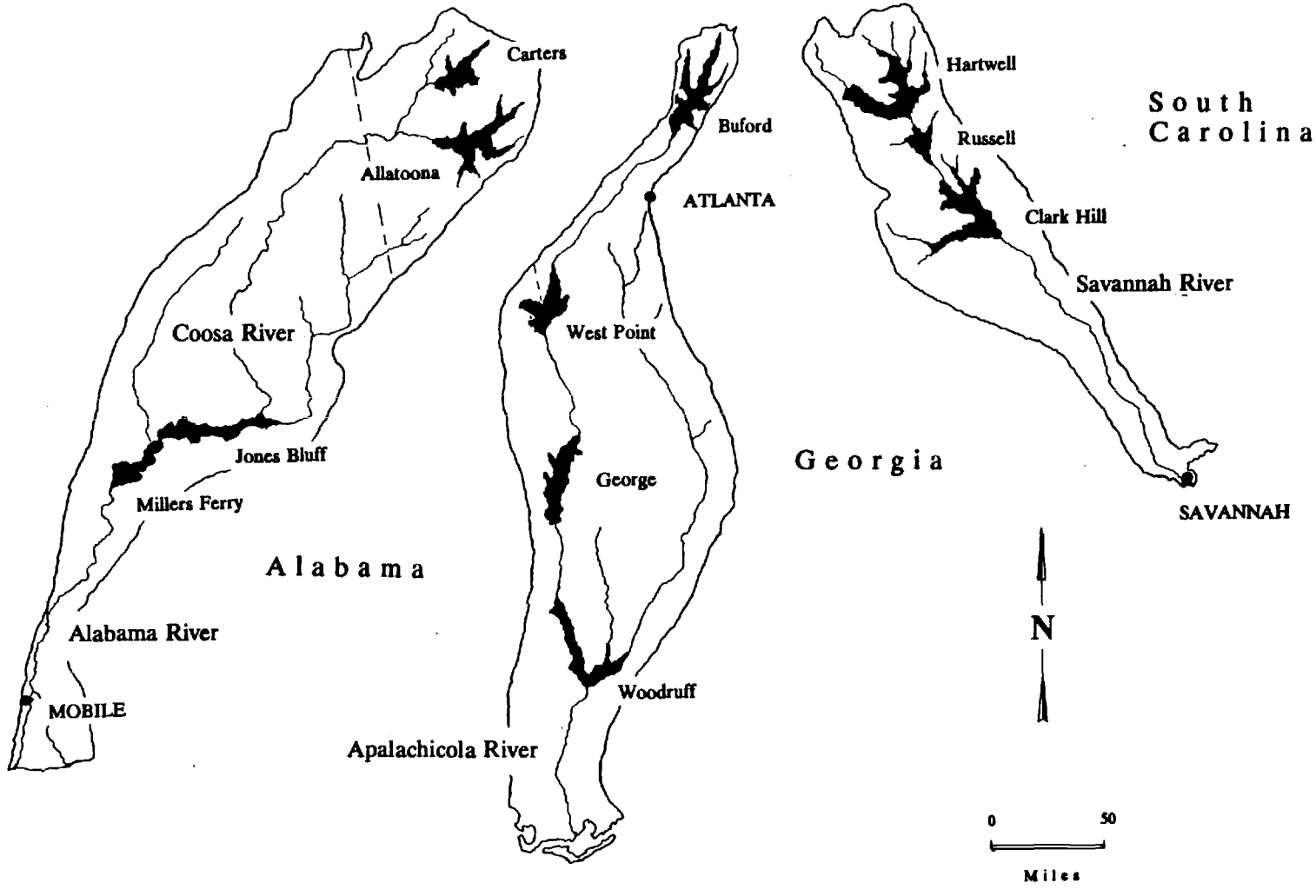

Figure 7.1: The Southeastern U.S. Reservoir System

Table 7.1: Reservoir Characteristics

	Drainage Area mi^2	Usable Storage $Acre-Ft$	Power Capacity MW	Other Purposes
Carters	376	230,276	500	F,R
Allatoona	1,110	587,042	74	F
Jones Bluff	16,307	12,163	68	N
Millers Ferry	20,708	17,027	76	N
Buford	1,041	1,686,530	86	F,WS,R
West Point	3,442	306,494	109	F,WS,R
George	7,463	244,060	130	N
Woodruff	17,237	426,997	30	N
Hartwell	2,088	1,708,678	344	F,N
Russell	2,890	266,759	300	-
Clark Hill	6.144	1,434,803	280	F,N

Objective Function

$$J = E\{\sum_k\{ E^*(k) - \sum_i t_i(k) \sum_j P_{i,j}[h_{i,j,n}(k), u_{i,j}(k)]\}^2\} + terminal\ cost$$

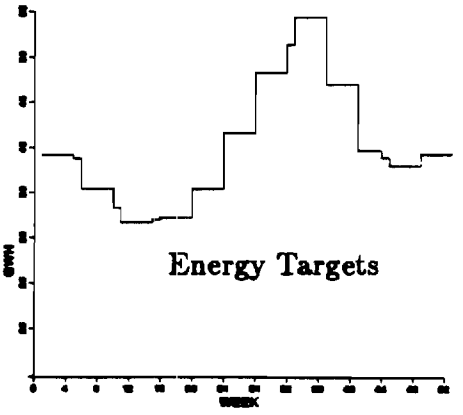

Were it not for these projects, the drought damages would have been much higher.

Although these 11 reservoirs are situated in geographically separate drainage basins, their operation should be coordinated. The energy produced by this system is marketed by the Department of Energy and contracted to a number of power companies (Georgia, Alabama and Duke Power companies and other cooperatives). The energy flow among the power companies integrates all projects into one system and creates the need for coordination.

In terms of an objective function for the control model, this implies that the goal is to satisfy the weekly energy commitment, $E^*(k)$, from the energy produced by each system turbine subject to the other system objectives as constraints on the storages and releases. The system energy production is obtained as the sum total of the power generation from each reservoir turbine times the scheduled generation time. The terminal cost term reflects established system priorities such as which reservoir should be depleted last during droughts or filled-up first during of water surplus.

7.3 High Flow Control Experiments

This control experiment simulates the system regulation during high flows. The priorities are such that the "run-on-the-river" projects produce as much energy as possible at best turbine efficiency during peak and off-peak generation periods. The other reservoirs generate as much as necessary so as to supplement the energy requirement at best turbine efficiency during the peak generation period. As far as the filling process is concerned, priority is given to the most upstream reservoirs.

Figures 7.2, 7.3, and 7.4 depict the optimal generation time and storage trajectories for the reservoirs of each basin. The total energy generation of these trajectories and those of the other basins is about 500 GWh and is equal to the energy target. Also, the filling process is in agreement with the states priority of filling the upstream reservoirs first. The results of the Apalachicola basin indicate that energy is primarily produced by the smaller "run-on-the-river" projects and Buford is allowed to fill-up. Among the three largest reservoirs of this system, Hartwell, Buford and Clark Hill, Buford was assigned the highest priority in filling-up first and depleting last due to its importance as a water supplier for Atlanta.

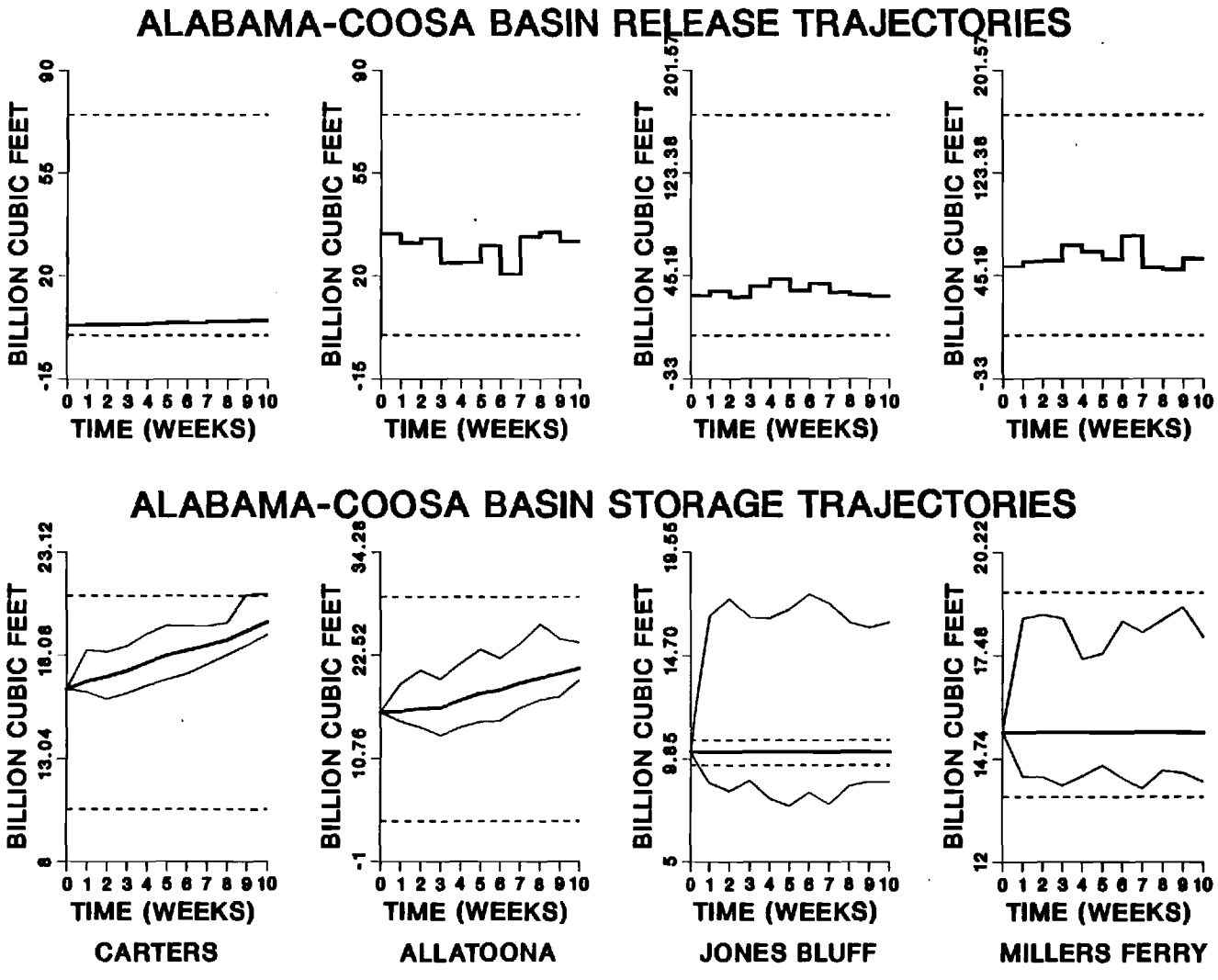

Figure 7.2: Optimal Sequences for High Flow Control Experiment

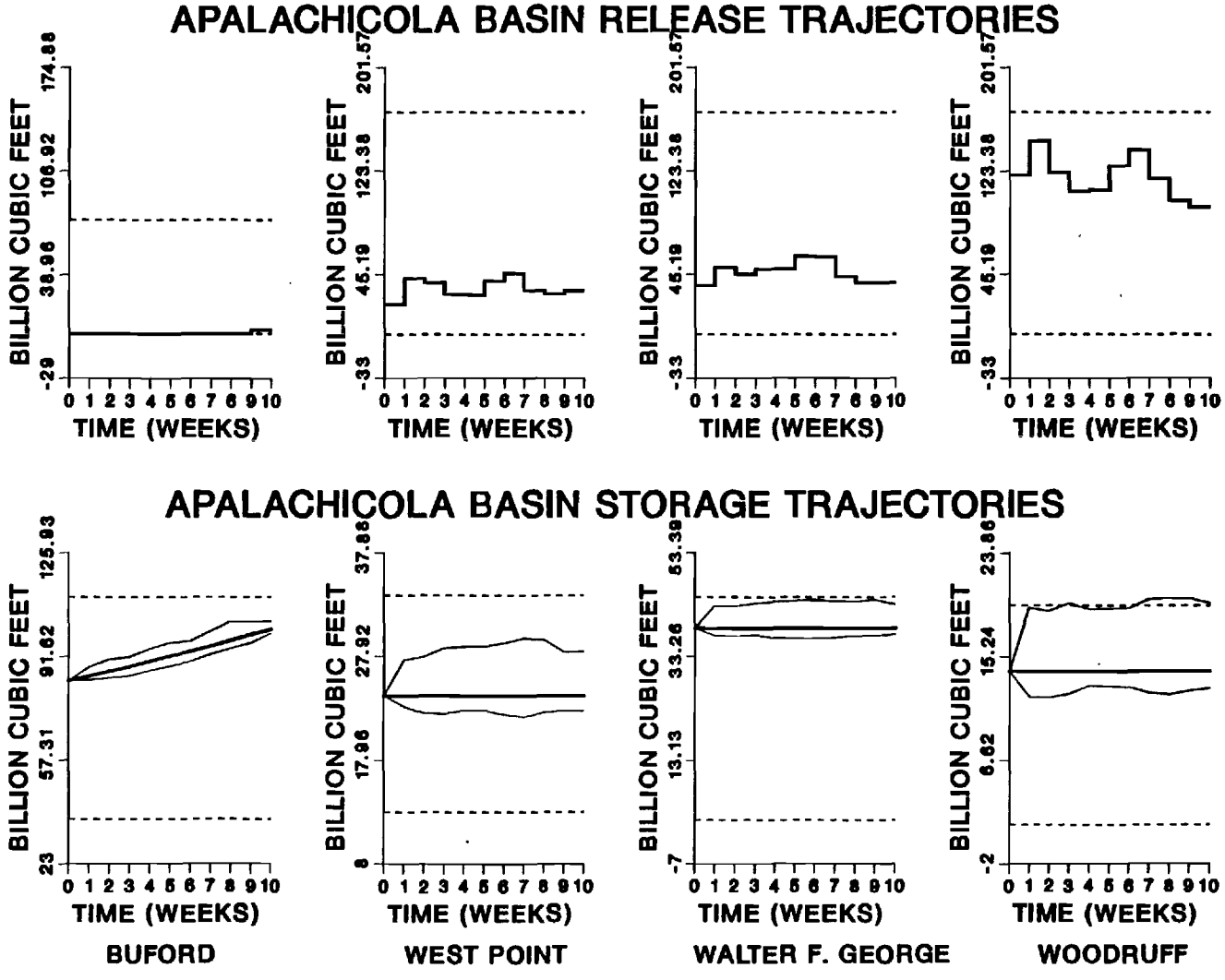

Figure 7.3: Optimal Sequences for High Flow Control Experiment

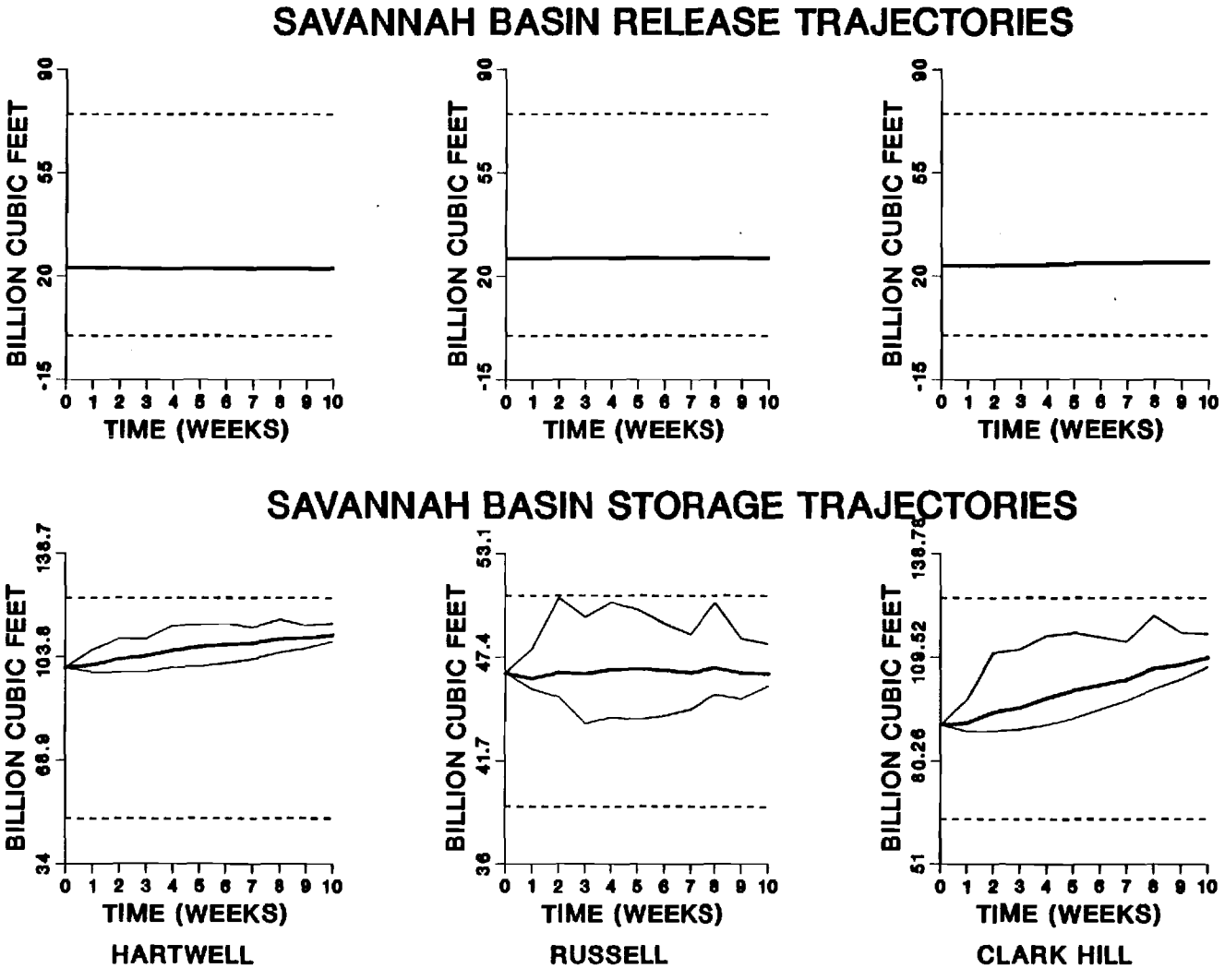

Figure 7.4: Optimal Sequences for High Flow Control Experiment

7.4 Low Flow Control Experiments

The second control run simulates the system operation under low flows, which in this case were taken equal to 10% of the average inflows. The energy commitments were the same as before. The optimal sequences are included in Figures 7.5, 7.6, and 7.7.

The "run-on-the-river" projects produce as much energy as they can, but the burden of satisfying the energy contracts now falls primarily upon the larger reservoirs of the group. Those on the upstream end are depleted last.

In the Alabama-Coosa System, most of the energy is produced at Allattoona, but overall energy generation from these projects is low because the reservoirs are already over-drawn. In the Apalachicola basin, Buford contributes the most, but the energy targets are really met by the Savannah river projects.

These runs take approximately 30 seconds of CPU time on a CYBER 990 main frame computer system; namely, the computer time requirements of the method are minimal as a result of its analytical structure.

7.5 Closing Remarks

With regard to the control method, the previous experiments indicate that high computational efficiency and reliability are distinct method characteristics even in large scale system applications.

The previous control model was developed here for testing purposes. However, it can effectively assist the C.O.E. in the weekly system management. Furthermore, it can be used in a simulation mode to identify trade-offs among the various system objectives and project priorities. Given the recent droughts in the southeast, this appears a timely investigation.

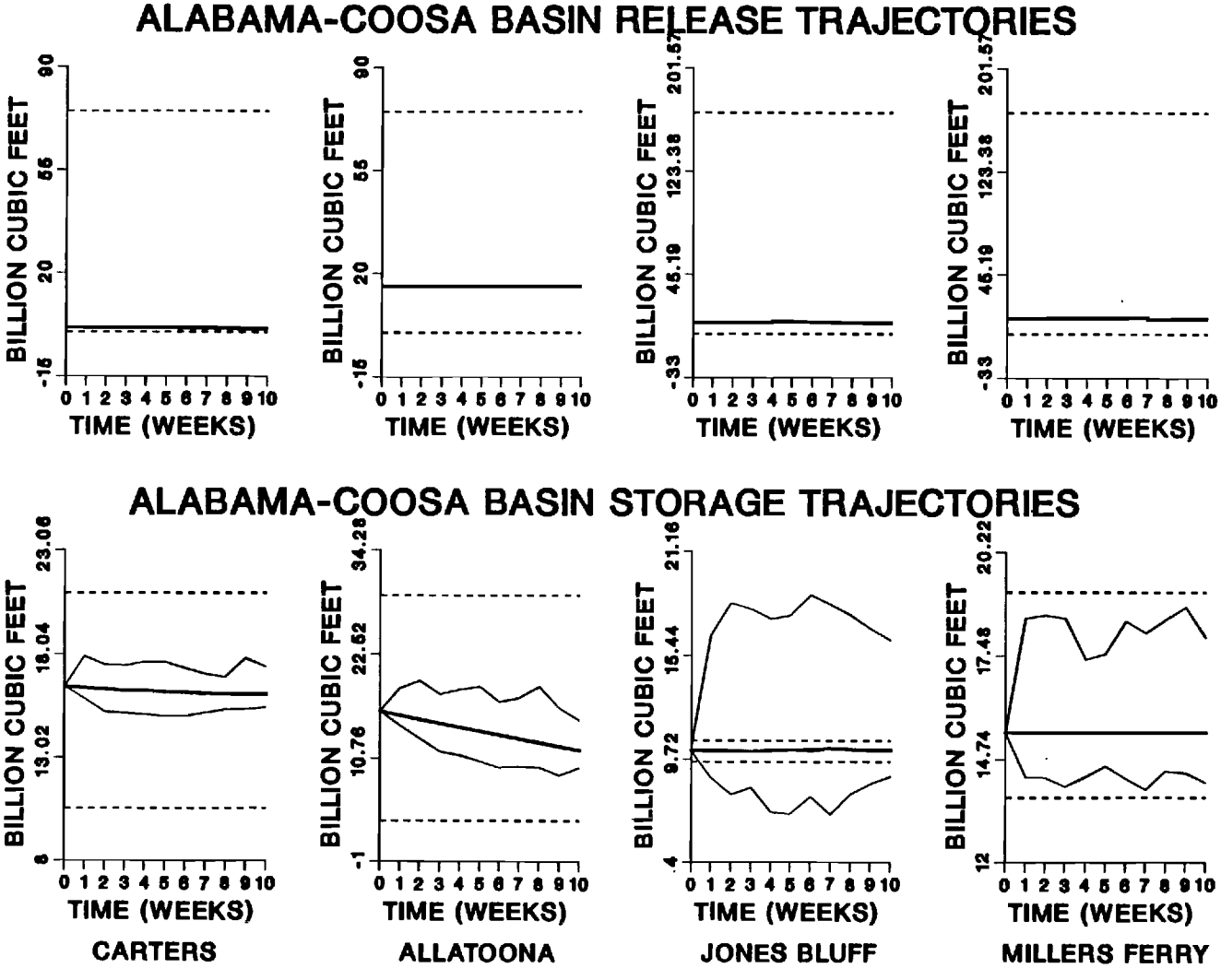

Figure 7.5: Optimal Sequences for Low Flow Control Experiment

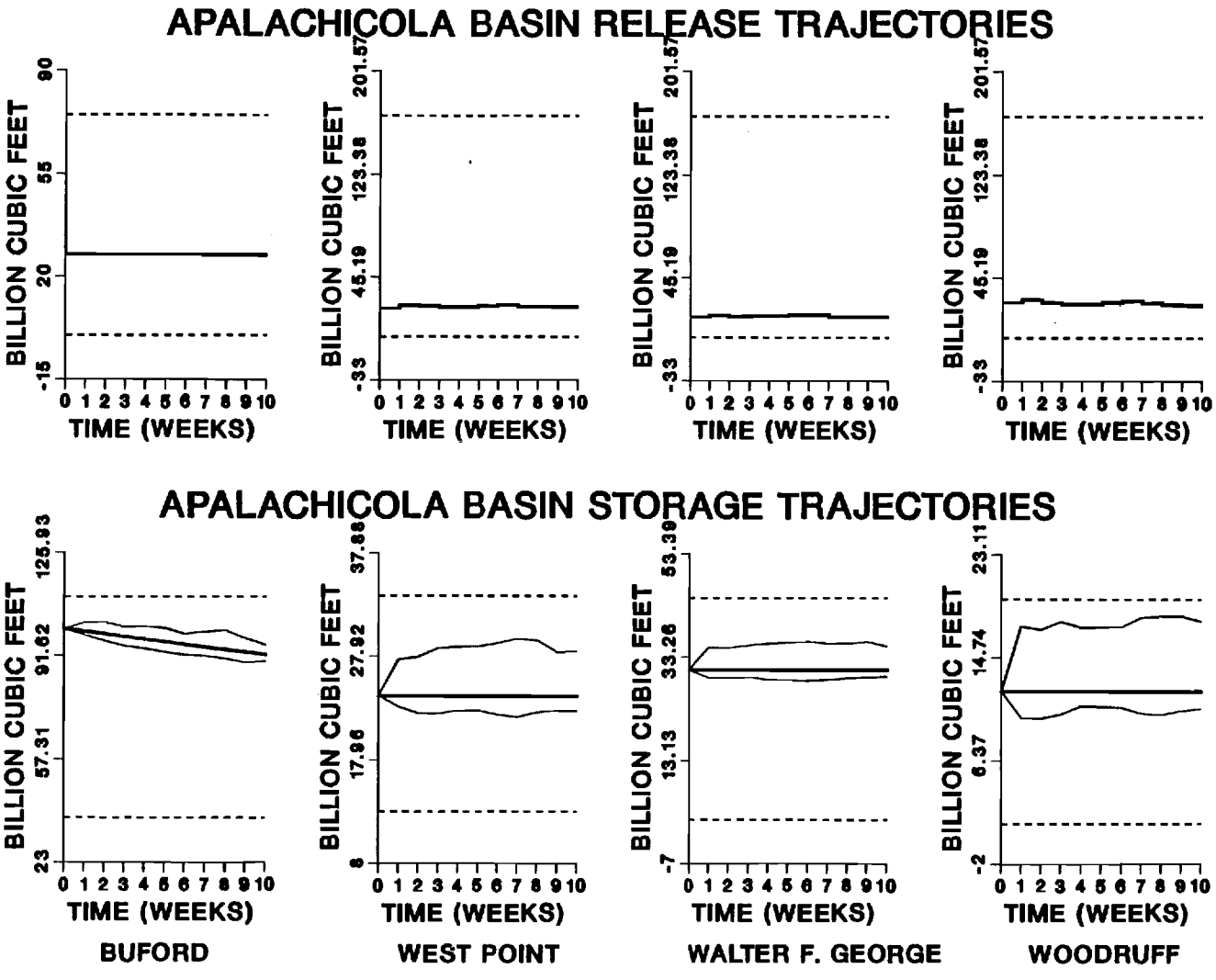

Figure 7.6: Optimal Sequences for Low Flow Control Experiment

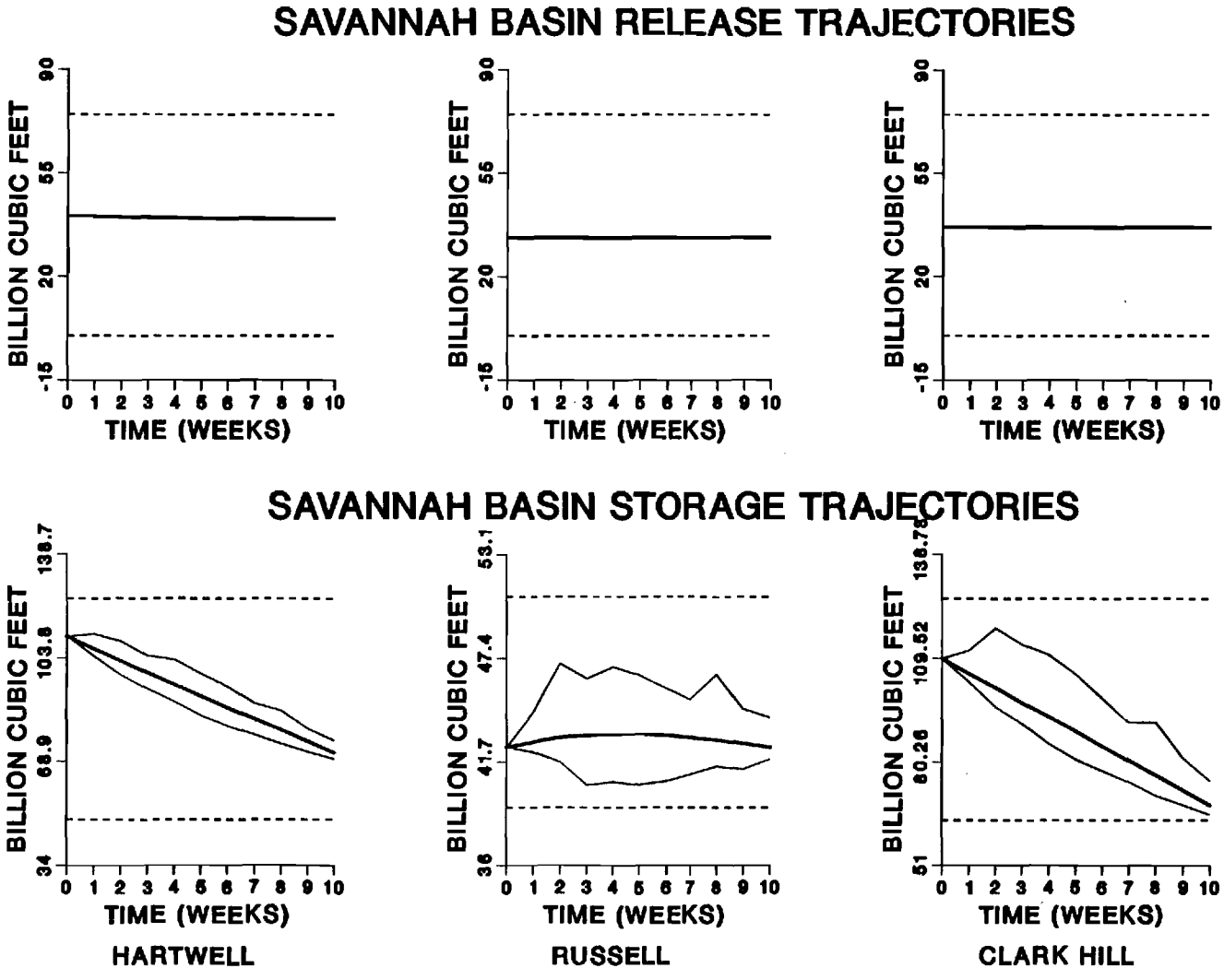

Figure 7.7: Optimal Sequences for Low Flow Control Experiment

8. SUMMARY AND FUTURE RESEARCH RECOMMENDATIONS

8.1 Summary

Optimization models are an integral part of real time reservoir management. Being random, nonlinear, constrained, dimensionally large, and multiobjective, reservoir systems present researchers and practitioners with challenging operational problems. It is a general conclusion of this work that reservoir control advances can meet this challenge effectively. However, the transfer of this experience to the practicing engineers is a process requiring persistent pursuit in a methodological manner.

The principal contribution of this research is the development of an efficient stochastic control method for real time reservoir management. This method is based on the Extended Linear Quadratic Gaussian (ELQG) control approach [Georgakakos, 1984, Georgakakos and Marks, 1987] but includes several original enhancements. These enhancements include (1) the development of new procedures to efficiently account for nongaussian system inputs and probabilistic storage constraints and (2) the development of a multilevel control model for the day–to–day scheduling of hydropower systems. Since reservoir inflows frequently exhibit skewness, the first of the above contributions adds to the accuracy and applicability of the technique, while the second extends their use in a real time operational environment. The most meaningful verification of the developments in (1) was obtained when the control model nominal reliability was shown to be in agreement with the reliability realized during actual operation. The control model in (2) is based on a new formulation of the hydropower scheduling problem and utilizes five control levels and two control modules. The control levels are sequentially activated and are designed to seek solutions using increasingly effective, yet less preferable, operational controls. The control process is completed when an activated level converges to feasible storage and power generation schedules. Each level employs a two–module solution algorithm. The first module uses turbine operational characteristics from the second module and the ELQG control method to determine optimal generation time schedules. The second module optimizes turbine efficiency or power output. This approach facilitates a more realistic representation of hydroelectric project features and was shown to be computationally efficient even in large reservoir systems.

As part of the verification process, the previous method was applied to three different reservoir systems. Extensive simulation experiments indicated that its usage in connection with real time streamflow forecasting techniques may substantially improve hydropower gains even for small scale operations. In particular, the total expected gain from the Lloyd Shoals hydroelectric facility (one relatively small reservoir) would be about 15,000 MWH per year, about half of which would represent

peak energy generation. On the average, this energy gain would constitute $500,000 of saved expenditures. Such gains are expected to increase in larger reservoir systems. Apart from hydropower improvements, modern forecasting and control techniques are expected to enhance flood protection and water supply reliability.

The previous control approach requires that system dynamics be represented in state-space form. In real-time reservoir operation, river routing introduces critical delays and needs to be modelled explicitly. Although river routing has extensively been researched, existing models cannot be combined with the previous control method. An additional contribution of this work is the development of a state-space routing model which can readily be calibrated using physical channel characteristics. This model was shown to perform adequately and to be compatible with the methods developed in both phases of this research.

8.2 Future Research Recommendations

Future research can proceed along several directions. The control structure presented in Chapter 6 could be further augmented by including another control level between Levels 2 and 3. The additional level would seek to maintain peak generation at maximum power output and off-peak generation at best turbine efficiency. The modules of this new level would be similar to those of Level 3, except that the generation time t(k) would be divided into peak and off-peak segments. The peak period release would become part of the system dynamics, while the objective of the first module would be to determine the off-peak generation time meeting the stated constraints. The second module would determine the maximum and best efficiency power output. The addition of this control level would enhance the overall control process; however, given the lesser off-peak energy value, it is not expected to significantly improve system performance.

During the ELQG solution process, the first control module generates a probabilistic storage sequence (see Chapter 4). The second module, however, accounts for storage uncertainty simply through the mean storage value. Instead, a more elaborate scheme can be adopted whereby second module discharge optimization also utilizes the other statistical moments provided by the first control module. Under this scheme, efficiency would be defined by Equation (6.16); however, reservoir storage uncertainty would now be characterized by all available statistics, most likely the mean, variance, and skewness, calculated as in Chapter 4. The problem would be to determine the turbine discharges, u_i, $i=1,\ldots,M$, which maximize expected turbine efficiency, $E\{e_i\}$, $i=1,\ldots,M$, subject to constraints (6.17). The solution could proceed by Taylor expanding e_i, retaining an appropriate number of terms, and formally evaluating the efficiency expectation. The resulting expression would depend on the storage statistics and the optimization

could be carried out as in Algorithm IIα. In fact, the procedure adopted earlier is based on the same principle where only the first two Taylor series terms have been retained. However, second and higher order derivatives of e_i are typically insensitive to changes in u_i, and the simpler procedure suggested earlier will usually suffice.

Rather than maximizing the efficiency of each turbine, the second control module could also seek to maximize the *overall* plant efficiency. For example, one such measure can be defined as follows:

$$e = \frac{\sum_{i=1}^{M} p_i[h_i^n, u_i]}{\eta \sum_{i=1}^{M} u_i h_i^n}, \qquad (8.1)$$

where e is the plant efficiency and p_i, h_i^n, and u_i are the power, net hydraulic head, and discharge rate of the i^{th} turbine. Then, the problem of the second module would be to maximize e subject to constraints (6.17). Algorithm IIα would again be applicable, with Step 5 optimizing expression (8.1). If the plant turbines have similar generation and hydraulic characteristics, then the results will be the same as before. In facilities with dissimilar turbines, this second approach will tend to overload the more efficient turbines.

Another research direction concerns the usage of stochastic control techniques in a more general framework designed to additionally schedule thermal and other types of power plants in a cost-effective manner. This will constitute an improvement over the existing approaches which usually include crude approximations of the hydropower component. As reservoir management agencies and utilities rely more and more on personal computers, this effort should focus on designing efficient control algorithms for microcomputer implementations.

Lastly, the control method developed is not limited to reservoir systems. It is applicable to any stochastic dynamical system in state-space form. Two areas that can also benefit from the aforementioned advances are the management of groundwater systems and wastewater treatment plants. Research by our team has shown that these problems can also be formulated in a format amenable to control methods with one crucial difference: the associated problems are characterized by much larger dimensionality. Here the effort should be to design more efficient control algorithms for such highly dimensional systems. The most promising direction along these lines appears to lead in decomposed (multilevel) implementations. The presence of natural and parameter uncertainties makes this an interesting undertaking. This research effort will extend the applicability of optimal control techniques to a number of other processes and problems of spatial nature.

9. REFERENCES

Alarcon, L., and D.H. Marks, A stochastic dynamic programming model for the operation of the High Aswan Dam, Technical Report No. 246, Ralph M. Parsons Lab. for Water Resour. and Hydrodyn., Dep. of Civ. Eng., M.I.T., Cambridge, Mass., 1979.

Arunkumar, S. and W. W.-G. Yeh, Probabilistic models in the design and operation of a multi-purpose reservoir system, Technical Report, Contribution No. 144, California Water Researches Center, University of California, Davis, December 1973.

Askew, A., Optimum reservoir operating policies and the imposition of a reliability constraint, Water Resources Research, 10(1), 51-56, 1974a.

Askew, A., Chance-constrained dynamic programming and the optimization of water resource systems, Water Resources Research, 10(6), 1099-1106, 1974b.

Athans, M., and P. Falb, Optimal Control: An Introduction to the Theory and Its Applications, McGraw-Hill, New York, 1966.

Bellman, R., Adaptive Control Processes, Princeton University Press, 1961.

Bellman, R., and S. Dreyfus, Applied Dynamic Programming, Princeton University Press, 1962.

Benjamin, J. R., and C. A. Cornell, Probability, statistics, and decision for civil engineers, McGraw-Hill, New York, 1970.

Bertsekas, D., Dynamic programming and stochastic control, Academic Press, Orlando, Fla., 1982.

Blench, T., Regime behaviour of canals and Rivers, Butterworths Scientific Publications, 1957.

Bras R., R. Buchanan, and K. Curry, Real-time adaptive closed-loop control of reservoirs with the High Aswan Dam as a case study, Water Resources Research, 19(1), 33-52, 1983.

Brater, E. F., and H. W. King, Handbook of Hydraulics, McGraw-Hill, New York, 1963.

Buchanan, R., and R. Bras, Study of real-time adaptive closed-loop control for reservoir operation, Ralph M. Parsons Lab. for Hydrology and Water Resources, Dept. of Civil Engineering, M.I.T., Technical Report No. 265, 1981.

Butcher, W., Stochastic dynamic programming for optimum reservoir operation, Water Resources Bulletin, 7(1), 115-123, 1971.

Chen, C.T., Introduction to linear system theory, Holt, Rinehart and Winston, Inc., N.Y., 1970.

Cunge, J.A., On the subject of a flood propagation method (Muskingum method), Journal of Hydraulic Research, International Association for Hydraulic Research, 7(2), 205-230, 1969.

Colorni, A., and G. Fronza, Reservoir management via reliability programming, Water Resources Research, 12(1) 85–88, 1976.

Croley II, T.E., Sequential deterministic optimization in reservoir operation," Journal of the Hydraulics Division ASCE, 100(HY3), 443-459, 1974.

Eagleson, P. S., Climate, Soil, and Vegetation: 2. The Distribution of the Annual Precipitation Derived From Observed Storm Sequences, Water Resources Research, 14(5), 713–721, 1978.

Eisel, L.M., Chance constrained reservoir model, Water Resources Research, 8(2), 339–347, 1972.

Fread, D.L., National Weather Service Operational Dynamic Wave Model, W23, NOAA, Silver Springs, MD, 20910, April 1978.

Fread, D.L., A "Unified" Coefficient Routing Model, January 1983. Presented at invited seminars at: Pennsylvania State University, February 28-March 4, 1983 and Minneapolis RFC, March 7-11, 1983.

Fread, D. L., Channel Routing, in Hydrological Forecasting, Ed. M. G. Anderson and T. P. Burt, John Willey and Sons Ltd., N.Y., 437-503, 1985.

Foufoula–Georgiou, E., and P. K. Kitanidis, Gradient dynamic programming for stochastic control of multidimensional water resources systems, Water Resources Research, 24(8), 1345–1359, 1988.

Georgakakos, A. P., Extended Linear Quadratic Gaussian (ELQG) control: further extensions, Water Resources Research, 25(2), 191–201, 1989a.

Georgakakos, A. P., The Value of Forecasting in Reservoir Control, in press, Water Resources Bulletin, 1989b.

Georgakakos, A. P., A Two–Level Control Method for Hydropower Scheduling, *Computer Program Manual*, sponsored by Georgia Power Company under Research Project POE–06608, 1989c.

Georgakakos, A. P., and J. C. Kabouris, A Streamflow Model Based on Geomorphologic Unit Hydrographs, in press, *Journal of Hydrology*, 1989.

Georgakakos, A.P., and D.H. Marks, Real time control of reservoir systems, Technical Report No. 301, Ralph M. Parsons Lab. for Hydrology and Water Resources, Dept. of Civ. Eng., M.I.T., 363p, May 1985.

Georgakakos, A.P., and D.H. Marks, A new method for the real time operation of reservoir systems, Water Resources Research, 23(7), 1376–1390, 1987.

Georgakakos, K. P., and R. L. Bras, Real-time, statistically linearized, adaptive flood routing, Water Resources Research, 18(3), 513-524, 1982.

Georgakakos, K. P., Real-time flash-flood prediction, Journal of Geophysical Research, 92(D8), 9615-9629, 1987.

Georgia Power Company, Communication with Mr. Marvin Meeks, Section Supervising Engineer, 1988.

Gill, M.A., "Flood routing by the Muskingum Method," Journal of Hydrology, Vol. 36, 353-363, 1978.

Henderson, F.M., Open channel flow, MacMillan & Co., New York, N.Y., 1966.

Jacobson, D., and D. Mayne, Differential Dynamic Programming, Elsevier Science, New York, 1970.

Jamshidi, M., and M. Heidari, Application of dynamic programming to control Khuzestan water resources system, Automatica, 13,287–293, 1977.

Jazwinski, A., Stochastic Processes and Filtering Theory, Academic Press, Orlando, Fla., 1970.

Joeres, E.F., G.J. Liebman, and C.S. ReVelle, Operating rules for a joint opertion of raw water sources, Water Resources Research, 7(2), 225–235, 1971.

Kailath, T., Linear systems, Prentice-Hall, Englewood Cliffs, N.J., 1980.

Kalman, R.E., A New Approach to Linear Filtering and Prediction Problems, ASME, J. of basic engineering, Vol. 82D, pp. 35-45, 1960.

Kushner, H. and F. Schweppe, A maximum principle for stochastic control systems, J. Math. Anal. Appl., 8, 287–302, 1964.

Koussis, A.D., Theoretical estimations of flood routing parameters, Journal of the Hydraulics Division, ASCE, 104(HY1), 109-115, 1978.

Kitanidis, P.K., and R.L. Bras, Real-Time Forecasting of River Flows, Technical Report No 235, Ralph M. Parsons Lab. for Hydrology and Water Resources, Dept. of Civ. Eng., M.I.T., Cambridge, Mass. 1978.

Kitanidis, P.K., and E. Foufoula-Georgiou, Error analysis of conventional discrete and gradient dynamic programming, Water Resour. Res., 23(5), 845-858, 1987.

Larson, R., State Increment Dynamic Programming, American Elsevier, New York, 1970.

Larson, R., and J. Casti, Principles of Dynamic Programming, Parts I and II, Marcel Dekker, New York, 1970.

Larson, R., and W. Keckler, Applications of dynamic programming to the control of water resource systems, Automatica, 5, 15–26, 1969.

Lighthill, M.J. and Whitham, G.B., On kinematic waves I. Flood movement in long rivers, Proc. Roy. Soc. A., Vol. 229, pp. 281-316, 1955.

Loaiciga, H.A., and M.A. Marino, An approach to parameter estimation and stochastic control in water resources with an application to reservoir operation, Water Resources Research, 21(11), 1575–1584, 1985.

Loucks, D.P., Some commentson linear decision rules and chance constraints, Water Resources Research, 6(2), 1970.

Loucks, D.P., and P. Dorfman, An evaluation of some linear decision rules in chance-constrained models for reservoir planning and operation, Water Resources Research, 11(6), 1975.

Luenberger, D.G., Introduction to Linear and Nonlinear Programming, Addison-Wesley, Reading, Mass., 1973.

Marino, M., and B. Mohammadi, Reservoir management: a reliability programming approach, Water Resources Research, 19(3), 613–620, 1983.

Maybeck P.S., Stochastic Models, Estimation and Control, Academic Press, New York, 1982.

Mein, R. J., E. M. Laurenson, and T. A. McMahon, Simple nonlinear model for flood estimation, Journal of Hydraulics Division, ASCE, 100(HY11), 1507-1518, 1974.

Murray, D., and S. Yakowitz, Constrained differential dynamic programming and its applications to multireservoir control, Water Resources Research, 15(5), 1017–1027, 1979.

Nash, J.E., A Note on the Muskingum Method of Flood Routing, Journal of Geophysical Research, Vol. 64, No. 8, Aug. 1959, pp. 1053-1056.

Overton, D.E., Muskingum flood routing of upland streamflow, Journal of Hydrology, Vol. 4, 1966, pp. 185-200.

Papageorgiou, M., Optimal multireservoir network control by the discrete maximum principle, Water Resources Research, 21(12), 1824–1830, 1985.

Ponce, V.M., and Yevjevich, V., Muskingum-cunge method with variable parameters, Journal of the Hydraulics Division, ASCE, Vol. 104, No. HY12, Dec., 1978, pp. 1663-1667.

Ponce, V.M., Simplified muskingum routing equation, Journal of the Hydraulics Division, Vol. 105, No. HY1, January, 1979.

Pontryagin, L.S., V. Boltyanskii, R. Gamkrelidze, E. Mishchenko, The Mathematical Theory of Optimal Processes, Interscience Publishers, Inc., New York, 1962.

ReVelle, C., E. Joeres, and W. Kirby, The linear decision rule in reserovir management and design 1: development of the stochastic model, Water Resources Research, 5(4), 767–777, 1969.

Rockwood, D.M., Columbia basin streamflow routing computer, Transactions, ASCE, vol. 126, Part 4, pp. 32–56, 1958.

Rodriguez-Iturbe, I., J.B. Valdes, and J.M. Velasquez, Keynote Lecture on the Applications of Kalman Filter in Rainfall–Runoff Studies, AGU Chapman Conference on Applications of Kalman Filter to Hydrology, Hydraulics and Water Resources, Pittsburgh, 1978.

Schweig, Z., and J. Cole, Optimal control of linked reservoirs, Water Resources Research, 4(3), 479–497, 1968.

Simonovic, S., and M. Marino, Reliability programming in reservoir management: 1. single multipurpose reservoirs, Water Resources Research, 16(5), 844–848, 1980.

Simonovic, S., and M. Marino, Reliability programming in reservoir management: 3. system of multipurpose reservoirs, Water Resources Research, 18(4), 735–743, 1982.

Simons, D.B., and M.L. Albertson, Uniform water conveyance channels in alluvial material, Proc. Am. Soc. Civil Engrs., vol. 86, no HY5, 1960.

Sniedovich, M., Reliability-constrained reservoir control problems: 1. methodological issues, Water Resources Research, 15(6), 1574-1582, 1979.

Sniedovich, M., A variance-constrained reservoir control problem, Water Resources Research, 16(2), 271-274, 1980a.

Sniedovich, M., Analysis of a chance-constrained reservoir control model, Water Resources Research, 16(5), 894-853, 1980b.

Stedinger, J., B. Sule, D. Loucks, Stochastic dynamic programming models for reservoir operation optimization, Water Resources Research, 20(11), 1499–1505, 1984.

Su, S., and R. Deininger, Generalization of White's method of successive approximations to periodic Markovian decision processes, Operations Research, 20(2), 318–326, 1972.

Su, S., and R. Deininger, Modeling the regulation of Lake Superior under uncertainty of future water supplies, Water Resources Research, 10(1), 11–25, 1974.

Toebes, G.H., and A.A. Sheppard, Ed., Reservoir systems operations, Proceedings of the National Workshop on Reservoir Systems Operations, University of Colorado, Boulder, August 13–17, 1979.

Trezos, T. and W. W–G. Yeh, Use of stochastic dynamic programming for reservoir management, Water Resources Research, 23(6), 983–996, 1987.

Turgeon, A., Optimal short–term hydro scheduling from the principle of progressive optimality, Water Resources Research, 17(3), 481–486, 1981.

Wasimi, S. A., and P. K. Kitanidis, Real–time forecasting and daily operation of a multireservoir system during floods by linear quadratic gaussian control, Water Resources Research, 19(6), 1511–1522, 1983.

Weinmann, P.E. and Laurenson, E.M., Approximate flood routing methods: a review, Journal of the Hydraulics Division, ASCE, 105(HY13), Proc. Paper 15057, pp. 1521-1533, 1979.

Yeh, W. W.–G., State of the art review: theories and applications of systems analysis trechniques to the optimal management and operation of a reservoir system, Technical Report, UCLA–ENG–82–52, 1982.

Yeh, W. W.–G., Reservoir management and operation models: a state–of–the–art review, Water Resources Research, 21(12) 1797–1818, 1985.

Yeh, W. W-G, L. Becker, D. Fults, D. Sparks, and G. Logan, Optimization of real-time daily operation of multiple reservoir system, Engineering Report No 7628, University of California, Los Angeles, April 1976.

Yeh, W. W-G, L. Becker, and W-S Chu, Real-time hourly reservoir operation, Journal of the Water Resources Planning and Management Division, ASCE, 187-203, Sept. 1979.

Young, G.K., Finyding reservoir opertion rules, Journal of the Hydraulics Division, ASCE, 93(HY6), 297-321, 1967.

A P P E N D I X A

This appendix summarizes some information pertinent to the control of the reservoirs in the Savannah system.

A.1 Hartwell

A.1.1 Elevation vs Storage Relationship

$$h = e^{a_3} \; e^{a_1 s} \; s^{a_2}$$

$a_3 = 0.55442029 \times 10^{+1}$

$a_1 = 0.19146204 \times 10^{-8}$

$a_2 = 0.63936589 \times 10^{-1}$

h: elevation (feet), s: storage (acre-ft).

A.1.2 Tailwater curve

$$t = e^{a_5} \; e^{a_1 u} \; u^{a_2} \; e^{a_3 h} \; h^{a_4}$$

$a_5 = 0.53414559 \times 10^{+2}$

$a_1 = 0.10725323 \times 10^{-2}$

$a_2 = -0.24835179 \times 10^{-2}$

$a_3 = 0.37710725$

$a_4 = -0.17473616 \times 10^{+2}$

t: tailwater elevation (feet/10),

u: discharge (cfs/10000),

h: Russell elevation (feet/10).

A.1.3 Power (5 turbines)

$$P = e^{a_5} \; e^{a_1 u} \; u^{a_2} \; e^{a_3 h} \; h^{a_4}$$

$a_5 = -0.61888698 \times 10^{+1}$

$a_1 = -0.11294264 \times 10^{-1}$

$a_2 = 0.16704826 \times 10^{+1}$

$a_3 = -0.58959841 \times 10^{-1}$

$a_4 = 0.19092384 \times 10^{+1}$

P: power (MW),

u: turbine discharge (cfs/100),

h: net head (feet/10).

A.2 Russell

A.2.1 **Elevation vs Storage Relationship:**

$h = e^{a_3} \; e^{a_1 s} \; s^{a_2}$

$a_3 = 0.51836143 \times 10^{+1}$

$a_1 = 0.10965342 \times 10^{-7}$

$a_2 = 0.69968157 \times 10^{-1}$

h: elevation (feet), s: storage (acre-ft).

A.2.2 **Tailwater curve**

$t = e^{a_5} \; e^{a_1 u} \; u^{a_2} \; e^{a_3 h} \; h^{a_4}$

$a_5 = 0.12830082 \times 10^{+2}$

$a_1 = 0.11389940 \times 10^{-2}$

$a_2 = -0.30287137 \times 10^{-2}$

$a_3 = 0.14865647$

$a_4 = -0.40729693 \times 10^{+1}$

t: tailwater elevation (feet/10),

u: discharge (cfs/10000),

h: Clark Hill elevation (feet/10).

A.2.3 **Power** (4 turbines)

$P = e^{a_7} \; e^{(a_1 u + a_2 u^3)} \; u^{a_3} \; u^{a_4 \, \ln u} \; u^{a_5 (\ln u)^2} \; h^{a_6}$

$a_7 = 0.44967871 \times 10^{+3}$

$a_1 = 0.38391504 \times 10^{+1}$

$a_2 = -0.16952332 \times 10^{-4}$

$a_3 = -0.46174283 \times 10^{+3}$

$a_4 = 0.15797048 \times 10^{+3}$

$a_5 = -0.20876873 \times 10^{+2}$

$a_6 = 0.11538901 \times 10^{+1}$

P: power (MW),

u: turbine discharge (cfs/100),

h: net head (feet/10).

A.3 Clark Hill

A.3.1 Elevation vs Storage Relationship

$$h = e^{a_5}\ e^{a_1 s}\ s^{a_2}\ s^{a_3 \ln s}\ s^{a_4 (\ln s)^2}$$

$a_5 = 0.48770600 \times 10^{+2}$

$a_1 = 0.45747061 \times 10^{-3}$

$a_2 = -0.19238983 \times 10^{+2}$

$a_3 = 0.28889917 \times 10^{+1}$

$a_4 = -0.14707181$

h: elevation (feet), s: storage (acre-ft/1000).

A.3.2 Tailwater curve

$$t = e^{a_3}\ e^{a_1 u}\ u^{a_2}$$

$a_3 = 0.29012214 \times 10^{+1}$

$a_1 = 0.12456147 \times 10^{-2}$

$a_2 = 0.46835476 \times 10^{-1}$

t: tailwater elevation (feet/10),

u: discharge (cfs/10000),

A.3.3 Power (7 turbines)

$$P = e^{a_5}\ e^{a_1 u}\ u^{a_2}\ e^{a_3 h}\ h^{a_4}$$

$a_5 = -0.66354710 \times 10^{+1}$

$a_1 = -0.16620056 \times 10^{-1}$

$a_2 = 0.16010340 \times 10^{+1}$

$a_3 = -0.11566747$

$a_4 = 0.25655811 \times 10^{+1}$

P: power (MW),

u: turbine discharge (cfs/100),

h: net head (feet/10).

APPENDIX B

A STATE SPACE MODEL FOR RIVER ROUTING

B.1 Introduction

Efficient flood routing schemes are useful in a variety of engineering applications. Flood warning systems depend on flow predictions from rainfall–runoff and river routing models and, more often than not, are the only defense against life-threatening and costly floods [e.g., Georgakakos and Bras, 1982, Georgakakos, 1987]. Likewise, river routing models are an integral part of operational reservoir management schemes which are concerned with water supply at demand locations in a timely manner. Recent advances in reservoir control [Wasimi and Kitanidis, 1983; Kitanidis and Foufoula–Georgiou, 1987; Georgakakos and Marks, 1987; and Georgakakos, 1989a] favor dynamic, state–space, system formulations due to (1) their efficiency and (2) their ability to account for natural and model uncertainties. However, the most efficient river routing schemes, the "hydraulic" methods [Weinmann and Laurenson, 1979], are not directly compatible and cannot be integrated with these formulations. On the other hand, simpler river routing schemes, collectively known as "hydrologic" routing methods [Fread, 1985], can easily be cast into state–space format and utilized by modern reservoir control techniques. These methods can be kinematic [Mein et al., 1974], ignoring both inertia and gravity terms in the momentum equation, or diffusion type [Cunge, 1969], ignoring only inertia terms. The hydrologic routing methods do not model the exact flow equations and become approximate when inertia effects are important; their performance, however, can be enhanced if flow measurements are taken into account.

The purpose of this study is to design efficient flood routing models which can benefit from the existing research experience and can utilize real-time measurement information. The approach taken is to convert a promising hydrologic routing scheme in state-space form, model its inaccuracies through random error terms, and establish an updating scheme based on modern estimation theory results and discharge measurements. The coefficients of this model can readily be determined by channel characteristics, inflow-outflow measurements, or both, while its updating mechanism allows for more accurate flow predictions.

This appendix includes four additional sections. The Muskingum–Cunge routing scheme and its representation in state–space form is presented in Section 2. In Sections 3 and 4, this model is linked with a stochastic filtering scheme and tested in realistic case studies. The study is concluded with Section 5 which summarizes the research findings.

B.2 State Space Representation of the Muskingum-Cunge Routing Model

Simplified river routing models have drawn the attention of many researchers over the last 50 years. Included among these models are the Muskingum model [Nash, 1959; Overton, 1966; Cunge, 1967; Koussis, 1978; Ponce and Yevjevich, 1978; Ponce, 1978], kinematic models [Mein, 1974, Georgakakos and Bras, 1982], the kinematic wave model [Lighthill and Whitham, 1955], the SSARR model [Rockwood, 1958], and the Muskingum-Cunge model [Cunge, 1969]. Fread (1983) demonstrates that all simplified routing models share a common basis and can be derived from his Unified Coefficient Routing Model. This model has the following form:

$$O(t+\Delta t) = C_1 I(t) + C_2 I(t+\Delta t) + C_3 O(t) + C_4 \qquad (B.1)$$

where $O(t)$ is the outflow value from a channel reach of length (Δx) at time t, $I(t)$ is the inflow to this reach at time t, Δt is the time step, and C_1, C_2, C_3 are routing coefficients which may be empirically derived or evaluated from the hydraulic characteristics of the channel reach. Coefficient C_4 accounts for the effect of lateral inflows along the routing reach.

Equation (B.1) may be rewritten in the following form:

$$Q_{i+1}(t+1) = C_1 Q_i(t) + C_2 Q_i(t+1) + C_3 Q_{i+1}(t) + C_4, \qquad (B.2)$$

where Q denotes discharge, subscript i denotes the upstream end of the routing reach, subscript i+1 denotes the downstream end of the routing reach, and time instants t and t+1 are Δt time units apart. The coefficients C_1, C_2, C_3 and C_4 are given by the following expressions:

$$C_0 = 1 + \psi \tilde{a} - X \qquad (B.3a)$$

$$C_1 = [(1-\psi) \tilde{a} + X]/C_0 \qquad (B.3b)$$

$$C_2 = (\psi \tilde{a} - X)/C_0 \qquad (B.3c)$$

$$C_3 = [1 - (1-\psi) \tilde{a} - X]/C_0 \qquad (B.3d)$$

$$C_4 = \tilde{q} \Delta x \tilde{a}/C_0 \qquad (B.3e)$$

$$\tilde{a} = c \Delta t/\Delta x \qquad (B.3f)$$

$$\tilde{q} = [q_i(t) + q_i(t+1)]/2 \qquad (B.3g)$$

$$0 \le \psi \le 1 , \qquad (B.3h)$$

$$0 \le X \le 1 . \qquad (B.3i)$$

In the above equations, $\tilde{q}$ is the lateral inflow or outflow along the reach Δx during the interval Δt, and c is the wave speed. Fread [1983]

demonstrates how each simplified routing model may result from the previous formulation through appropriate definition of the parameters $(\psi, x, \tilde{a})$. For instance, the Muskingum-Cunge procedure results when

$$\psi = 1/2, \tag{B.4a}$$

$$X = 1/2\ [1 - q_0/(c\ \Delta x\ S_0)], \text{ and} \tag{B.4b}$$

$$\tilde{a} = c\ \Delta t/\Delta x = \Delta t/K, \tag{B.4c}$$

where q_0 is the unit-width discharge, K is the travel time through reach Δx, and S_0 is the channel bottom slope.

Fread [1983] suggests the following procedures for the estimation of these paramaters: The wave speed c can be computed from

$$c = \beta\ V = 1.27\ \beta\ S_0^{0.3}\ \ q_0^{0.4}\ /n^{0.6} \tag{B.5a}$$

where

$$\beta = 1.67 - 0.67\ A_0/B_0^2\ (dB_0/dy), \tag{B.5b}$$

A_0 is the associated cross-sectional area, B_0 is the associated channel top width, (dB_0/dy) is the rate of change of B_0 with depth y, and n is the Manning coefficient.

Parameter K may be computed from $K = \Delta x/c$ where Δx is the routing reach length and c is the wave speed. K may also be estimated from measured inflow-outflow hydrographs as the time interval between the inflow and outflow centroids.

The routing interval Δt can be obtained from

$$\Delta t \leq T_r/M\ , \tag{B.5c}$$

where T_r is the time of rise of the inflow hydrograph and M is an integer in the range of 6 to 20. Large M values imply rapid and nonuniform inflow variation.

The routing reach length Δx must be restricted to the following range for numerical accuracy reasons:

$$\Delta x \leq 0.5\ [c\Delta t + q_0/(cS_0)]. \tag{B.5d}$$

The channel energy slope S_0 may be approximated by the channel bottom slope and estimated as the longitudinal average over the reach Δx. It may also be computed from Manning's equation as follows:

$$S_0\ = Q_0^2\ B_0^{4/3}\ \ n/(2.21\ A_0^{10/3})\ , \tag{B.5e}$$

where Q_0 is the uniform initial flow with associated top width B_0 and cross-sectional area A_0.

In natural channels, the estimated hydraulic characteristics that enter or are computed from the Manning's equation represent spatial and temporal averages. For instance, the appropriate depth-discharge relation is given by

$$\bar{Q} = 1.49\ S_0^{1/2}\ \bar{A}^{5/3}\ /(n\ \bar{B}^{2/3})\ , \qquad \text{(B.5f)}$$

where the notation $\bar{x}$ represents the average of the variable x over the time interval Δt and along the reach Δx. $\bar{A}$ and $\bar{B}$ denote the cross-section area and the top width respectively and are known functions of the average depth $\bar{y}$.

Fread [1983] suggests two routing methods in relation to the previous model. In the linear form of the unified coefficient routing model, parameters q_0, A_0, B_0 and (dB_0/dy) may be assumed constant; they are usually associated with a reference discharge Q_0 such as the mean of the discharge hydrograph, the peak, or the center of mass. Then, coefficients C_1, C_2, C_3, and C_4 are constant for each Δx routing reach and throughout the duration of the routing computations.

In the nonlinear routing form, the coefficients vary with each reach Δx and time step Δt. The computations start by estimating the discharge $Q_{i+1}(t+1)$ using a linearly extrapolated value:

$$\hat{Q}_{i+1}(t+1) = Q_{i+1}(t) + [Q_{i+1}(t) - Q_{i+1}(t-1)] \qquad \text{(B.6)}$$

(where the symbol "^" denotes estimate).

Then, the average discharge $\bar{Q}$ is obtained from

$$\bar{Q} = 0.25\ [Q_i(t) + Q_i(t+1) + \hat{Q}_{i+1}(t) + Q_{i+1}(t+1)], \qquad \text{(B.7)}$$

and $\bar{y}$, $\bar{A}$, and $\bar{B}$ are obtained from Equation (B.5f). Lastly, parameters q_0, c, X, K, C_1, C_2, C_3, and C_4 are specified as described previously, and Equation (B.2) is invoked to compute $Q_{i+1}(t+1)$. The procedure is then advanced to another routing reach or another time step, whenever the difference $|\hat{Q}_{i+1}(t+1) - Q_{i+1}(t+1)|$ is smaller than a prespecified threshold [Fread, 1983]. If this difference does not fulfil this requirement, then $\hat{Q}_{i+1}(t+1)$ is replaced by $Q_{i+1}(t+1)$, and the procedure is repeated.

Generally, all simplified routing models are limited to applications where backwater effects (due to channel restrictions, tributary flows, or other conditions) are insignificant and wave propagation is in the downstream flow direction only. However, diffusion-type models are better approximations of the exact flow dynamics and are potentially more accurate. The Muskingum-Cunge model was selected here because it is a diffusion-type model [Cunge, 1969].

Consider a river segment which requires N routing reaches. Direct application of the routing Equation (B.2) to each reach results in the following set of difference equations:

$$Q_1(t+1) = C_{1,1}\, Q_0(t) + C_{1,2}\, Q_0(t+1) + C_{1,3}\, Q_1(t) + C_{1,4} \qquad \text{(B.8a)}$$

$$Q_2(t+1) = C_{2,1}\, Q_1(t) + C_{2,2}\, Q_1(t+1) + C_{2,3}\, Q_2(t) + C_{2,4} \qquad \text{(B.8b)}$$

$$Q_i(t+1) = C_{i,1}\, Q_{i-1}(t) + C_{i,2}\, Q_{i-1}(t+1) + C_{i,3}\, Q_i(t) + C_{i,4} \qquad \text{(B.8c)}$$

$i = 3,4,\ldots,N.$

A state space formulation requires that quantities at time (t+1) are obtained in terms of their values at time t. The previous equations can be converted into such a recursive scheme if the flow $Q_{i-1}(t+1)$ on the right-hand side of the routing equation for reach i is substituted by its expression from the routing equation for reach i-1. As illustrated in Appendix C, these operations lead to the following vector equation:

$$\mathbf{Q}(t+1) = \mathbf{A}\,\mathbf{Q}(t) + \mathbf{B}\,\mathbf{U}(t) + \mathbf{C}\,\mathbf{q}(t), \qquad \text{(B.9)}$$

where $\mathbf{Q}(t) = [Q_1(t)\ Q_2(t)\ \ldots\ Q_N(t)]^T$,

$\mathbf{U}(t) = [Q_0(t)\ Q_0(t+1)]^T$, and $\mathbf{q}(t) = [\tilde{q}_1(t)\ \tilde{q}_2(t)\ \ldots\ \tilde{q}_N(t)]$

(the superscript "T" denotes transpose).

Equation (B.9) constitutes the state equation of the routing model and describes the change in the state of the system, Q(t), responding to the inputs U(t) and q(t). Matrices A, B, and C are related to the routing coefficients as derived in Appendix C.

The above system will be assumed observable through measurements of the discharge $Q_N(t)$ at the outlet of the last reach Δx_N. Thus, the associated observation equation can be stated as follows:

$$z(t) = \mathbf{H}^T\,\mathbf{Q}(t)\ , \qquad \text{(B.10)}$$

where $\mathbf{H} = [0\ 0\ \ldots\ 1]^T$, and z(t) represents the observation at time t. Equation (B.10) is the output equation and relates observations to the system states. Equations (B.9) and (B.10) summarize the deterministic state space formulation of the routing model. Matrix A represents the proportion of the current system state Q(t) which is contributing to the

state change. This state feedback plays a major role in determining the future system behavior. The elements of the matrices **B** and **C** represent the proportion of each input variable that affects each of the state variables. The outputs z(t) are related to the state through the scaling vector H^T. It is noted that all elements of the coefficient matrices can be determined from the hydraulic characteristics of the channels. These coefficients are constants if the linear philosophy of the previous section is adopted; otherwise, they are time-varying.

B.3 Stochasting Filtering and Prediction

The need to convert a deterministic state-space formulation into a stochastic one arises from the possibility of modeling errors. Errors may stem from inadequate modeling, incorrect parameter values, or discrepancies in the input observation data. Typically, these inaccuracies are accounted for by adding random error terms to the state and observation equations:

$$Q(t+1) = \mathbf{A}\, Q(t) + \mathbf{B}\, U(t) + \mathbf{C}\, q(t) + \mathbf{w}(t) \tag{B.11a}$$

$$z(t) = H^T Q(t) + v(t). \tag{B.11b}$$

The terms $\mathbf{w}(t)$ and $v(t)$ represent two uncorrelated, zero-mean, white-noise sequences with covariance parameters $E\{\mathbf{w}(t)\mathbf{w}(t)^T\} = P_w(t)$ and $E\{v^2(t)\}=R(t)$, respectively. Their covariance functions satisfy

$$E\{\mathbf{w}(t_1)\, \mathbf{w}(t_2)\} = P_w(t)\, \delta(t_1 - t_2) \tag{B.12a}$$

$$E\{v(t_1)\, v(t_2)\} = R(t)\, \delta(t_1 - t_2), \tag{B.12b}$$

where $\delta(t)$ is the Kronecker delta and $E\{\cdot\}$ denotes expectation. It is assumed that the initial state Q(0) is statistically known by its mean vector and covariance matrix. Q(0), $\mathbf{w}(t)$ and $v(t)$ are mutually uncorrelated.

The goal of the stochastic model is to combine the system dynamics with the measurement information to "optimally" estimate the state vector. Two desirable properties of these "optimal" estimates are to be (1) unbiased and (2) have the smallest error variance among all other unbiased estimators. In the case of linear systems with white Gaussian statistics, such estimates are obtained from the Kalman Filter (Kalman, 1960).

Let $\hat{Q}(t/t)$ and $\Sigma(t/t)$ denote the best estimate and error covariance matrix of the state at time t given observations up to and including time t, and let $\hat{Q}(t+1/t)$ and $\Sigma(t+1/t)$ be the corresponding quantities at time t+1 given the same observation data. The time update portion of the Kalman filter algorithm provides a prediction Q(t+1/t) of the state at time t+1 along with the associated error covariance $\Sigma(t+1/t)$. The measurement update corrects the previous estimates based on the

measurement $z(t+1)$ at time $t+1$ to yield the aposteriori estimate $\hat{Q}(t+1/t+1)$ and its error covariance $\Sigma(t+1/t+1)$. For these reasons the following discrete-time Kalman filter equations are also called predictor-corrector equations:

(i) *Prediction:* (effect of system dynamics)

$$\text{state estimate:} \quad \hat{Q}(t+1/t) = A\,\hat{Q}(t/t) + B\,\hat{U}(t) + C\,\hat{q}(t) \tag{B.13a}$$

$$\text{error covariance:} \quad \Sigma(t+1/t) = A\,\Sigma(t/t)\,A^T + B\,P_u B^T + C\,P_q C^T + P_w \tag{B.13b}$$

$t = 0,1,2\ldots$

(ii) *Correction:* (effect of measurement $z(t)$)

$$\text{state estimate:} \quad \hat{Q}(t+1/t+1) = \hat{Q}(t+1/t) + K(t+1)\,\nu(t+1) \tag{B.14a}$$

$$\text{error covariance:} \quad \Sigma(t+1/t+1) = [I - K(t+1)\,H^T]\,\Sigma(t+1/t), \tag{B.14b}$$

$$K(t+1) = \Sigma(t+1/t)\,H\,[H^T\,\Sigma(t+1/t)\,H + R]^{-1}, \tag{B.14c}$$

$$\nu(t+1) = z(t+1) - H^T\,\hat{Q}(t+1/t)\,, \tag{B.14d}$$

$t = 0,1,2\ldots$

P_u and P_q are the covariance matrices of the vectors U and q which are assumed to be independent white noise sequences. It is noted that Eq. (B.13b) yields a suboptimal estimate of the predicted state covariance in that the autocorrelation function of U is not identically equal to zero (see definition following Eq. (C.4)). The vector $K(\cdot)$ is the Kalman gain and $\nu(\cdot)$ the Kalman innovations variable. For the system under consideration the measurement update step simplifies as follows:

$$\hat{Q}_i(t+1/t+1) = \hat{Q}_i(t+1/t) + \frac{\Sigma_{iN}(t+1/t)}{\Sigma_{NN}(t+1/t)+R}\,[z(t+1) - \hat{Q}_N(t+1/t)] \tag{B.15a}$$

$$\Sigma_{ij}(t+1/t+1) = \Sigma_{ij}(t+1/t) - \frac{\Sigma_{iN}(t+1/t)\,\Sigma_{Nj}(t+1/t)}{\Sigma_{NN}(t+1/t) + R} \tag{B.15b}$$

where $\hat{Q}_i(t/s)$ and $\Sigma_{ij}(t/s)$ represent respectively the i^{th} and the ij^{th} elements of the vector $\hat{Q}(t/s)$ and the matrix $\Sigma(t/s)$.

The performance of a stochastic filtering scheme is enhanced if the system is observable, controllable, or both. Systems which are both controllable and observable have the following two desirable properties: (1) their stochastic filtering design is stable, and (2) their state-space formulation is irreducible (see Kailath, 1980 and Chen, 1970).

The first implies that, in the state estimator, the observation errors do not accumulate, while the second guarantees that there does not exist any other state-space model of smaller than N dimension. The controllability and observability study of the present system is taken up in Appendix D. It is there shown that this state-space model has both of these properties and, therefore, it is theoretically expected to display optimal performance.

B.4 Case Studies

The performance of the state-space routing model previously presented is tested here in a series of case studies with various geomorphologic characteristics. These characteristics include channel slope, cross-section, roughness, length, and bed and banks material. For consistency and realism, the characteristics of each case study were determined using the "regime" theory of channel morphology [Blench, 1957; Simons and Albertson, 1960; Henderson, 1966]. In each case, both the linear and the nonlinear state-space routing models were implemented and the results were compared to those from the Dynamic Wave OPERational (DWOPER) model developed by Fread [1978].

The regime theory [Henderson, 1966, Section 10.6] is an empirical theory which is based on field studies of man-made channels. Given the nature of the bed and bank material and an estimate of the dominant flow, the Regime theory equations describe the geotechnical conditions (cross-sectional characteristics and bottom slope) which are eventually expected to develop in the channel. In this study, we consider two material types: (1) sand bed and banks and (2) coarse non-cohesive material. The same dominant discharge of 100,000 cfs is assumed for both types. The calculated values for these two cases are shown on Table B.1. It can be seen that the sandy material is associated with a mild slope (about 0.002%) and a wide cross-section (of 996 feet average width); the coarse noncohesive material is expected to form a channel with a steeper slope (0.18%) and narrower cross-section (of 498 feet average width). To investigate the effect of multiple reaches and various channel lengths, we consider three different channel cases for each material type. These channels consist of one, three, and five 100-mile reaches respectively, and their cross-sections are trapezoidal with the characteristics shown on Table B.1. For the simulation runs reported, the routing model used the true parameter values (see Table B.2). The inflow hydrograph varies from 16,667 to 102,500 cubic feet per second and is shown on Figure B.1. Lateral inflows were not included in this analysis. The time step Δt used in all cases is 6 hours, and the routing duration is 84 time steps. The length of each reach and the routing interval were chosen so as to comply with (B.5c) and (B.5d). Both the linear and the nonlinear routing schemes were implemented for each channel case along with the DWOPER routing model. The DWOPER results were considered to be the true river response.

B.4.1 Linear Case

In the linear model, the routing coefficients C_1, C_2, C_3, and C_4 are constant for each Δx routing reach and throughout the duration of the routing computations; therefore, the coefficient matrices in the state equation are not time-varying. All hydrologic parameters are the same for each routing reach Δx and are summarized on Table B.2. For realism,

Table B.1: Case Study Channel Characteristics

	Sand Bed and Banks (1st case)	Coarse Noncohesive Material (2nd case)
Dominant Discharge (cfs)	100,000	100,000
Wetted Perimeter (ft)	1106.80	553.39
Bottom Width (ft)	907.325	452.57
Average Width (ft)	996.117	498.05
Surface Width (ft)	1084.91	543.54
Hydraulic Radius (ft)	32.809	14.51
Water Depth (ft)	32.51	15.49
Cross-section Area (ft^2)	32386.9	7718.01
Velocity (ft/sec)	3.087	12.95
Bottom Slope	0.00002	0.00178
Bank Angle (degrees)	20.11	18.81
Manning n	0.022	0.0288

Table B.2: Muskingum-Cunge Parameter Values for the Linear Case

Parameter	Sand bed and Banks (1st case)	Coarse Noncohesive Material (2nd case)
Manning n	0.022	0.0288
Bottom Slope S_0	0.00002	0.00178
dB_0/dy	5.46	5.87
Area A_0 (ft^2)	32386.9	7718.01
Top width B_0 (ft)	1084.91	543.54
Unit-width discharge q_0 (cfs/ft)	92.1735	183.978
Routing interval Δt (sec)	21600	21600
Coefficient β	1.569	1.567
Wave speed c (ft/sec)	4.67	20.156

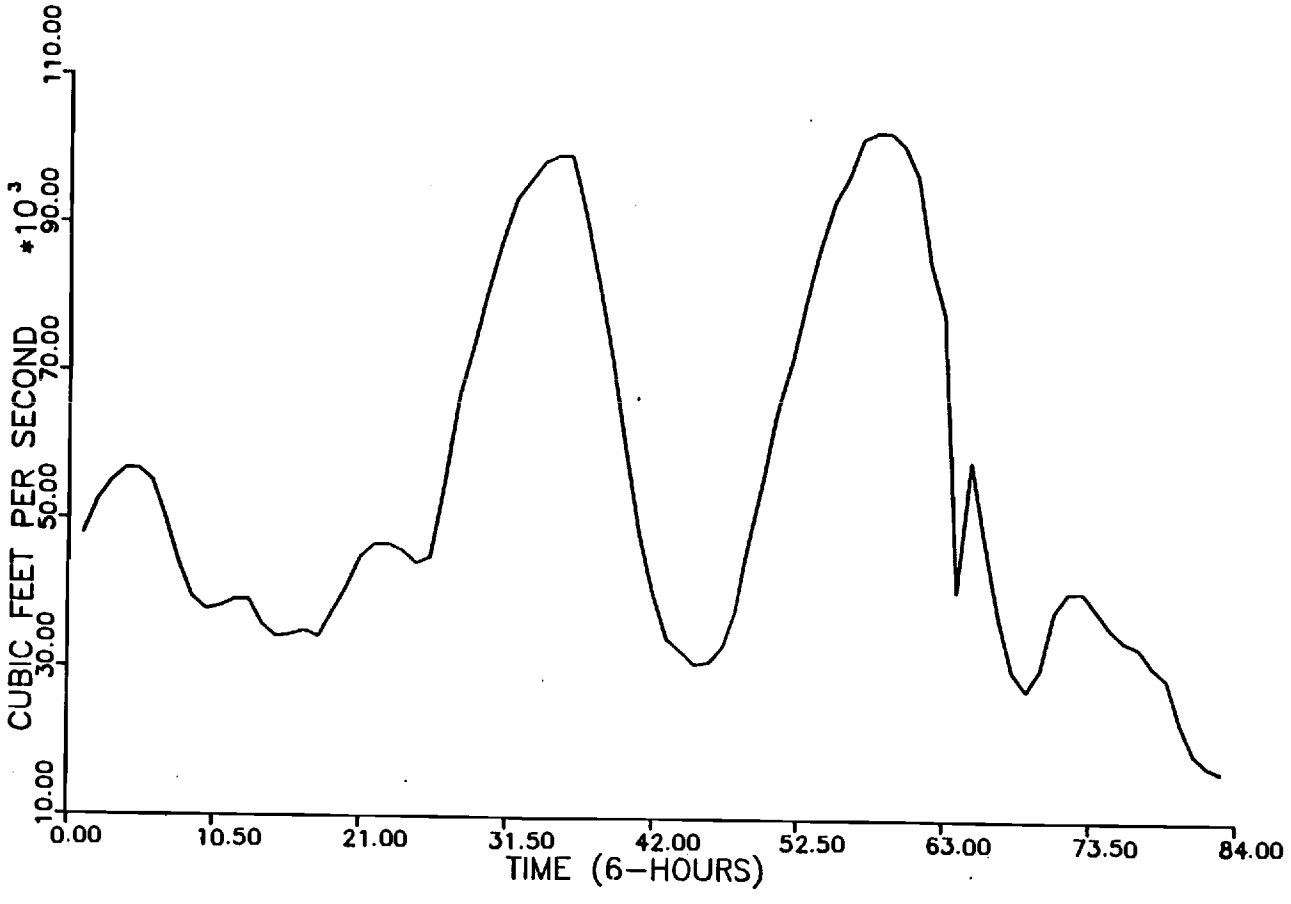

Figure B.1: Input Hydrograph

the observed values (DWOPER results) and the input to the state space model were interjected with randomly generated errors with standard deviation equal to 5% of the actual values. The covariance of the state equation error, w(t), was assumed to have the form $\sigma^2 I$, where I is the unit matrix and σ is a scalar.

Figure B.2 shows the results for the sand bed and bank channel cases with one, three, and five reaches respectively. In these runs, a small σ-value has been intentionally assumed to simulate the situation where model predictions do not consider observations but strictly rely on the system (Muskingum-Cunge) dynamics. The line with the designation "actual" represents the outflow discharge from each channel as predicted by the DWOPER model with input the hydrograph shown on Figure B.1; the one designated "observed" is the "actual" distorted by random errors; lastly, the line labelled "predicted" portrays the 6-hr predicted outflow from the state space model whose input (hydrograph on Figure B.1) was also contaminated by random errors. In all cases, the Muskingum-Cunge predicted outflows are seen to diverge from the actual DWOPER results, with the discrepancy becoming more apparent in the longer channels. This indicates an inadequacy of the Muskingum-Cunge model in channels with very mild slopes and suggests that utilizing real-time discharge measurements may improve model predictions.

Figure B.3 shows the results from the sand bed and bank channel case with one, three, and five reaches respectively when outflow observations are taken into consideration. In these runs, the parameter σ was estimated according to the least squares estimation criterion. Several runs were performed using various σ-values and the ones that produced the minimum quadratic error were selected as optimal. The optimal σ-values along with the associated least squares estimation error are reported on Table B.3 for both this and the coarse noncohesive channel cases. These results indicate that the predictive power of the state space routing model has clearly improved. The one-reach channel case exhibits the highest least squares value. This can be explained by the fact that as the river segment under consideration becomes longer, the outflow hydrograph is attenuated further. As a result, the measurement error (5% of the observed outflow) decreases and the measurement quality increases. Therefore, the model's ability to estimate the state variables improves and the forecasts become more accurate.

A necessary step in any model building attempt is model verification by validating the underlying modeling assumptions. If the state-space model has the correct structure and parameters, the innovation sequence $\nu(t)$ should be a white noise process. To test the whiteness properties of the innovation sequence, we computed its autocorrelation function. This function appears on Figure B.4 for each of the three channel cases. As can be seen by these graphs, the autocorrelation values are contained within the 95% confidence band reasonably well and can be considered statistically negligible.

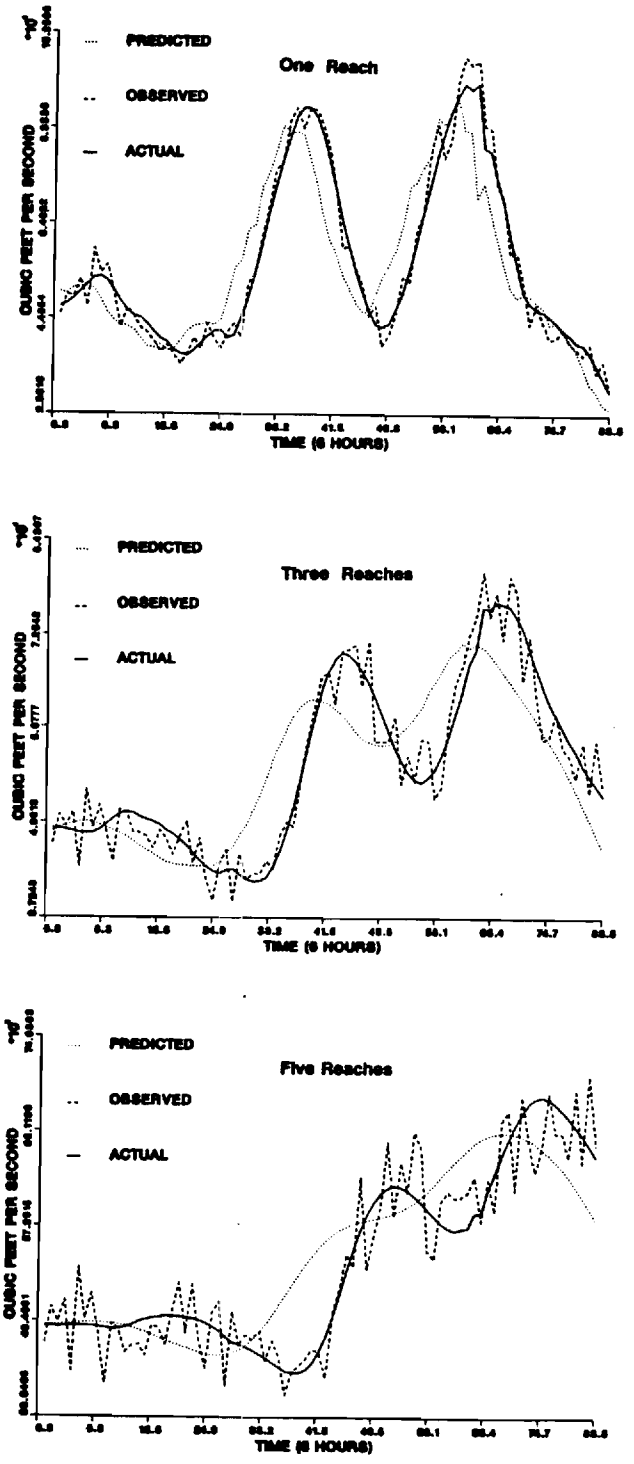

Figure B.2: Linear Model; Sandy Material; No Account of Observations

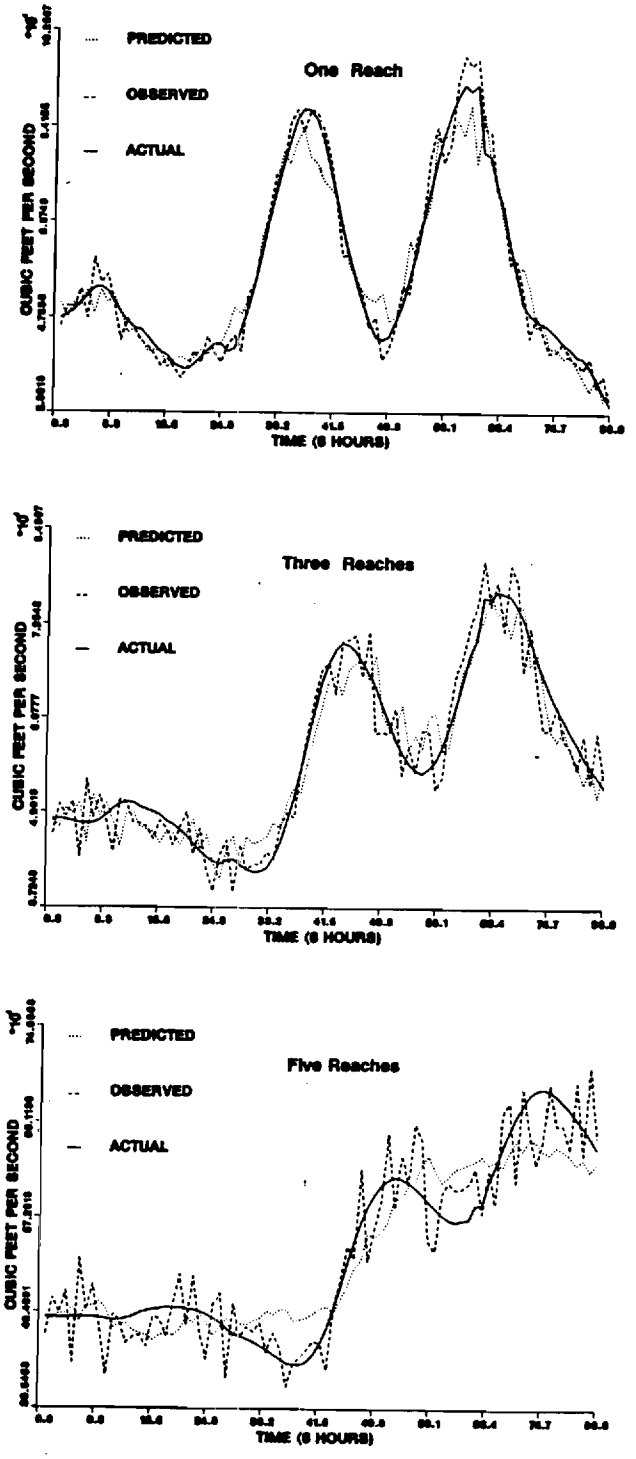

Figure B.3: Linear Model; Sandy Material; Optimal Observation Account

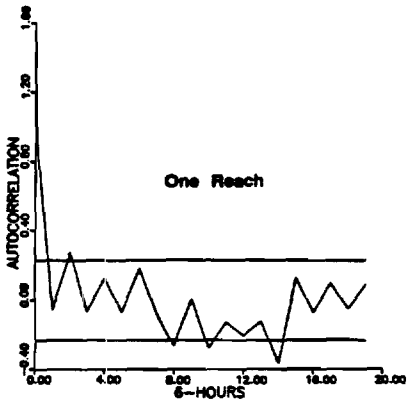

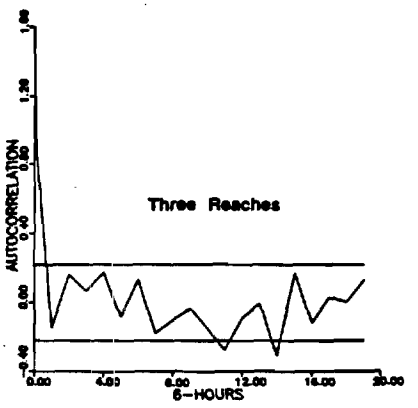

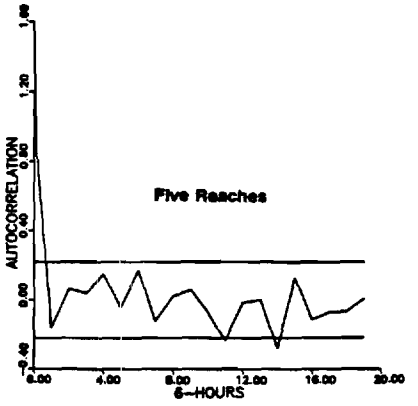

Figure B.4: Linear Model; Sandy Material; Innovations Autocorrelation

Table B.3: Least Squares Estimation for the Linear Models

	Sand Bed and Bank Case		Coarse Non-cohesive Case	
	σ [ft^3/sec]	Least Squares Error [ft^3/sec]^2	σ [ft^3/sec]	Least Squares Error [ft^3/sec]^2
1 Reach	5,475	2.17×10^9	2,250	2.10×10^9
3 Reaches	3,150	1.58×10^9	2,250	2.37×10^9
5 Reaches	2,250	1.39×10^9	3,875	3.94×10^9

Figure B.5 shows the results for the coarse noncohesive material with one, three, and five reaches respectively. In these runs, all versions follow the DWOPER results very closely. By comparison, the optimal σ-values are now smaller than the ones in the sand bed and bank channel case. This is a result of the improved model performance in channels with steep slopes and negligible inertia effects. As can be observed from Table B.3, the one-reach case study exhibits the smallest least squares estimation error. This behavior can be explained by the fact that more reaches introduce more uncertainty and corrupt the model's predictive power. The wave attenuation effect, which was seen to be dominant in the first case study (where the slope was mild), is now minimal and does not revert this trend.

The correlograms for the innovations in this case are shown on Figure B.6. The innovation sequences can be assumed to be white.

B.4.2 Nonlinear Case

In the nonlinear model, the river routing and state space model coefficients are changing with each reach Δx and time step Δt.

For comparative purposes with the linear case, the weighting coefficient and the measurement error variance were as in the previous section. Figure B.7 includes the results from the sand bed and banks using one, three, and five reaches respectively. As expected, model predictions follow the DWOPER actual results at least as well as the respective linear cases.

Remarks similar to the ones in the linear model case apply here as well; that is, as the number of reaches increases from one to five the least square values relatively decrease, while, absolutely, they are

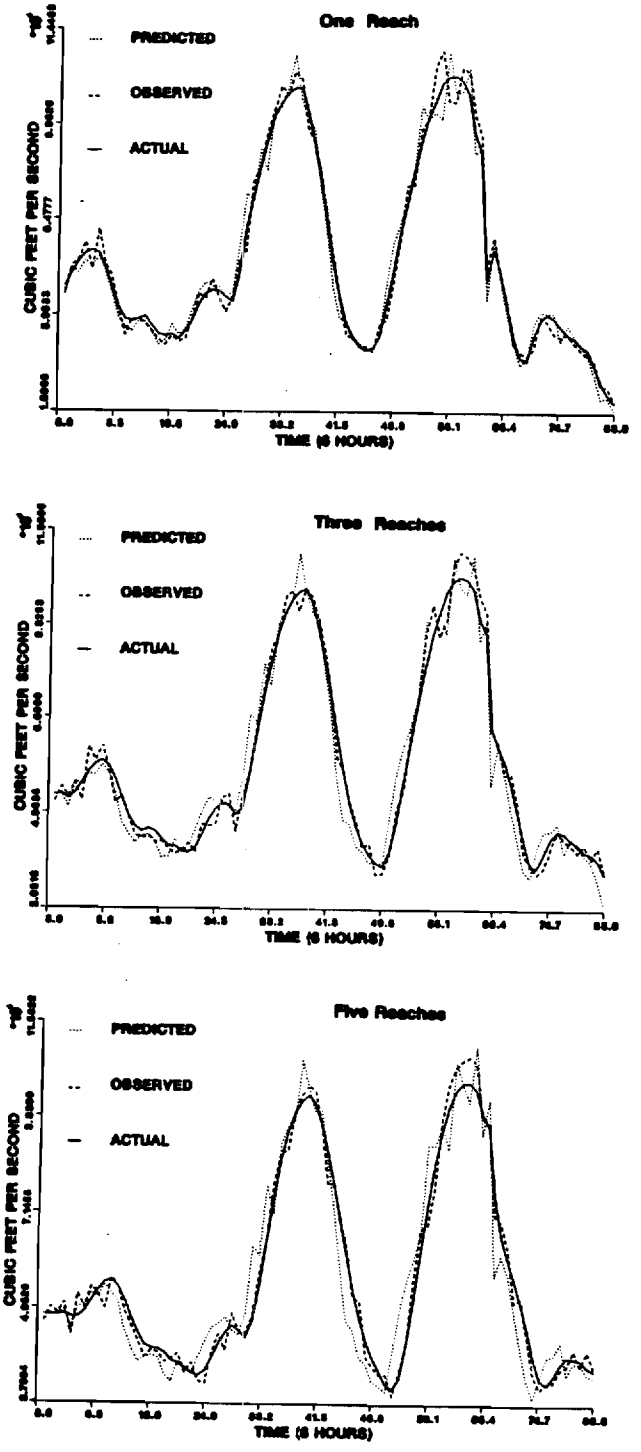

Figure B.5: Linear Model; Coarse Material; Optimal Observation Account

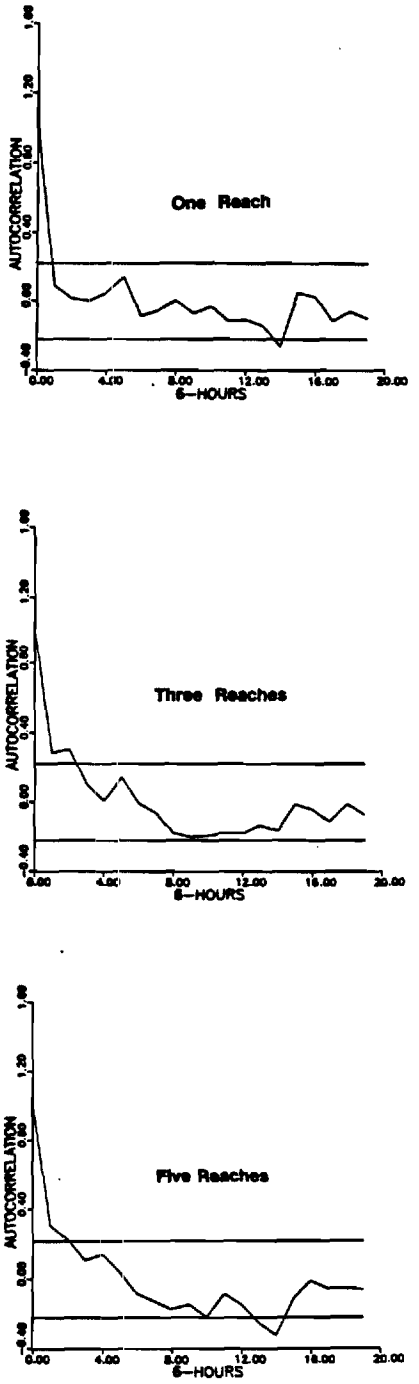

Figure B.6: Linear Model; Coarse Material; Innovations Autocorrelation

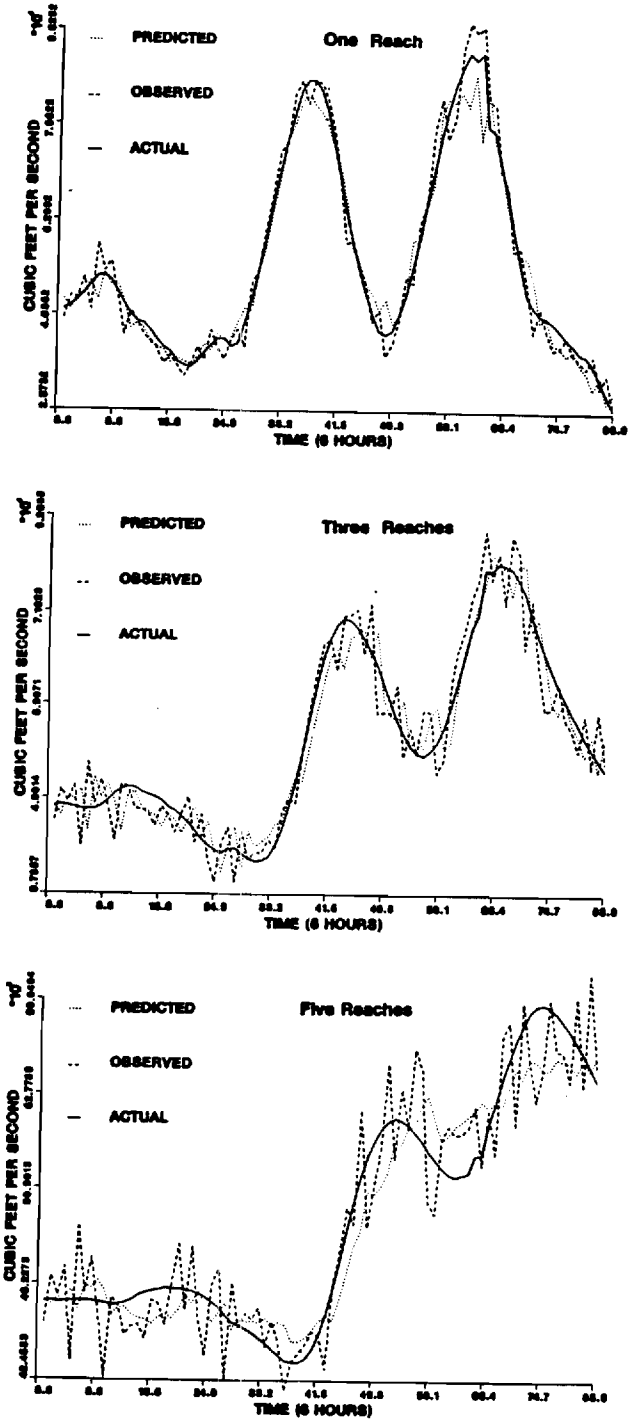

Figure B.7: Nonlinear Model; Sandy Material; Optimal Observation Account

much smaller than those of the corresponding linear cases. The results are shown on Table B.4. The respective correlograms are shown on Figure B.8 and also validate this model.

Table B.4: Least Squares Estimation for the Non-linear Models

	Sand Bed and Bank Case		Coarse Non-cohesive Case	
	σ [ft^3/sec]	Least Squares Error [ft^3/sec]^2	σ [ft^3/sec]	Least Squares Error [ft^3/sec]^2
1 Reach	5,475	1.81×10^9	315	1.95×10^9
3 Reaches	3,150	1.27×10^9	710	2.78×10^9
5 Reaches	1,000	0.88×10^9	1,725	2.33×10^9

Figure B.9 includes runs using small σ-values and emphasize the need of utilizing the observations. By comparison with the linear case, the nonlinear Muskingum-Cunge model is more successful in predicting peak timing.

Figure B.10 show the results for the coarse noncohesive material for one, three, and five reaches respectively. In this case, the values of the covariance matrices are much smaller than those required by the linear models. This happens because the estimation procedure has more confidence on the system dynamics. The results are shown on Table 4. The corresponding correlograms in this case are shown on Figure B.11 and verify the whiteness of the innovation sequences.

B.5 Closing Remarks

This work investigated the utility of state-space formulations in river routing. Two state-space models were suggested based on the linear and nonlinear forms of the Muskingum-Cunge routing procedure and were coupled with a Kalman Filter estimator. The method was tested in two case studies to forecast six-hour discharge values for various river reaches. The case studies involved sand bed and banks material with very mild bottom slope (0.00002) and a coarse noncohesive material with a steeper bottom slope (0.00178). The model results indicate that utilizing flow measurements improves the predictive ability of the Muskingum-Cunge routing scheme, especially in channels with mild slopes and backwater effects.

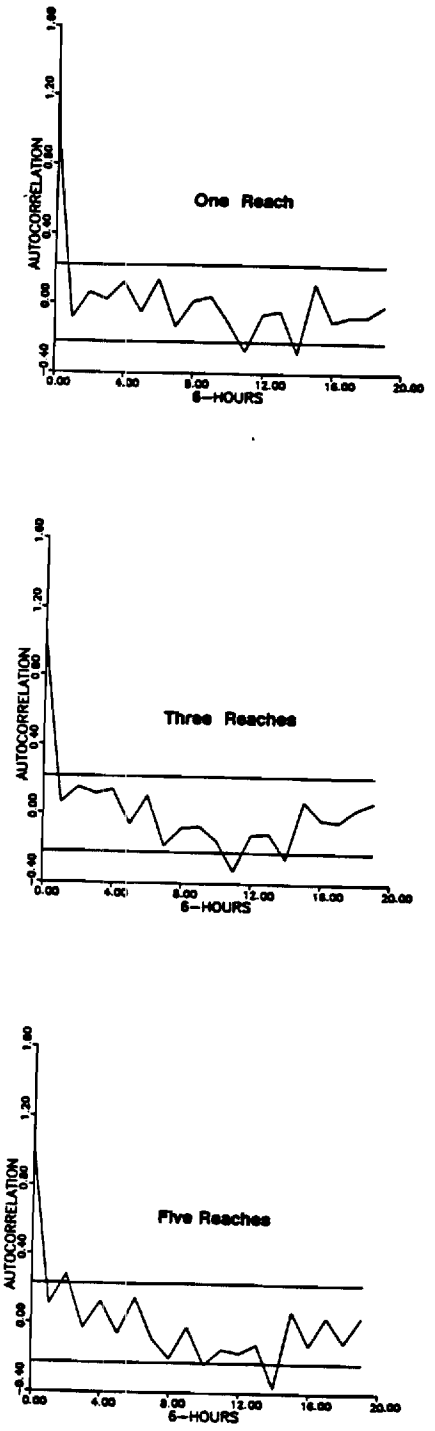

Figure B.8: Nonlinear Model; Sandy Material; Innovations Autocorrelation

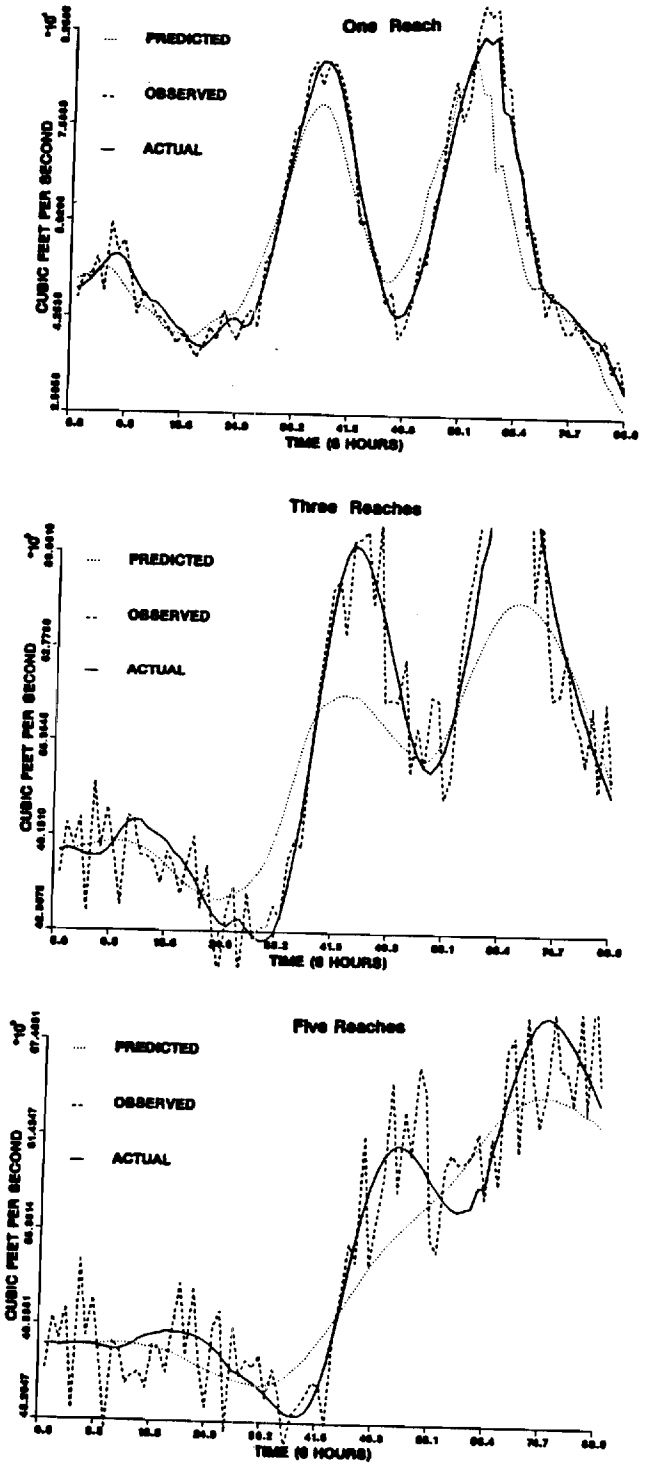

Figure B.9: Nonlinear Model; Sandy Material; No Account of Observations

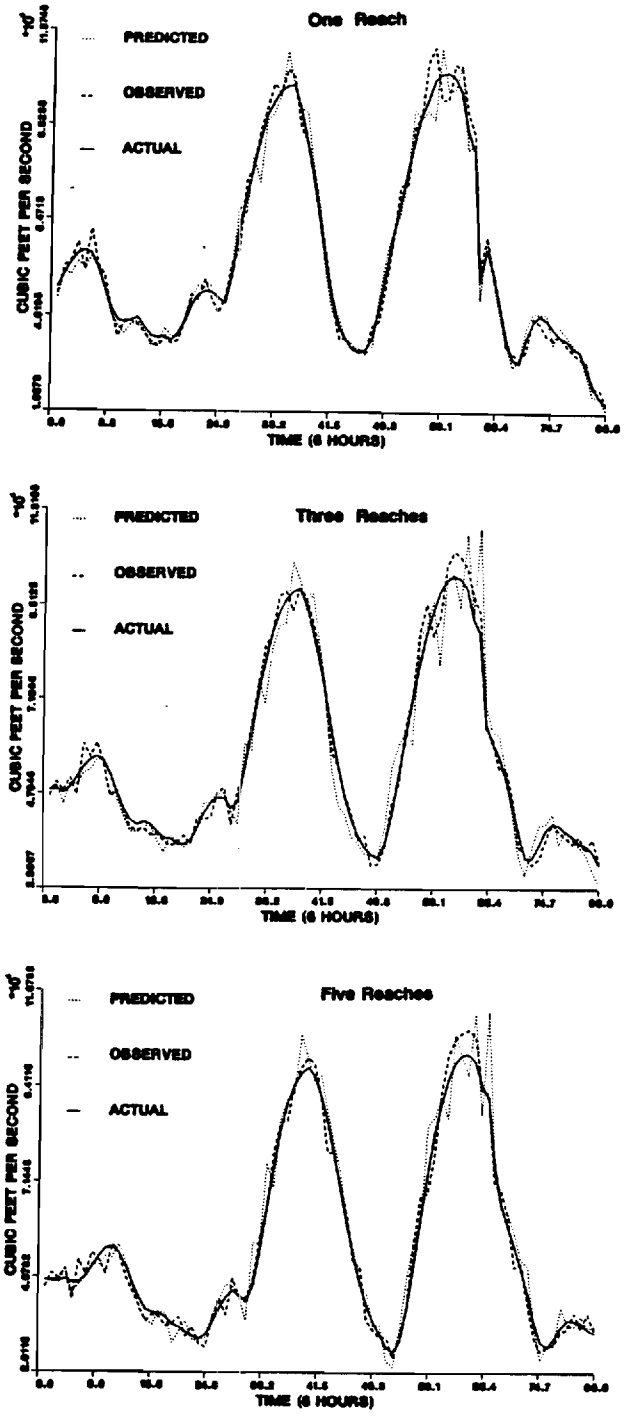

Figure B.10: Nonlinear Model; Coarse Material; Optimal Observ. Account

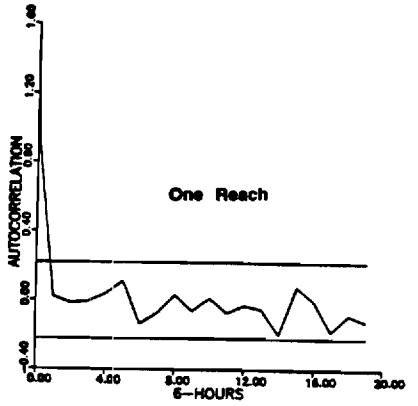

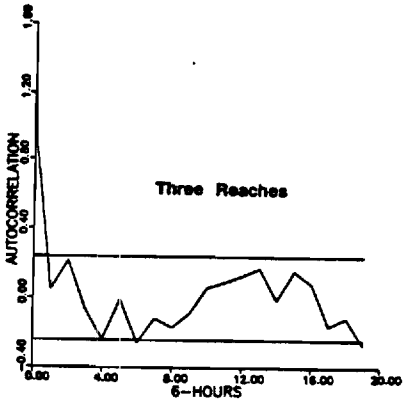

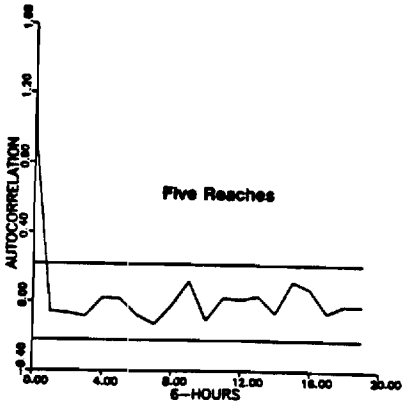

Figure B.11: Nonlinear Model; Coarse Material; Innovations Autocor/tion

APPENDIX C

STATE SPACE REPRESENTATION OF THE ROUTING EQUATIONS

Substituting Equation (B.8a) into Equation (B.8b) and rearranging yields

$$Q_2(t+1) = C_{2,3}\, Q_2(t) + (C_{2,1} + C_{2,2}\, C_{1,3})\, Q_1(t) + C_{2,2}\, C_{1,1}\, Q_0(t) + C_{2,2}\, C_{1,2}\, Q_0(t+1) + C_{2,2}\, C_{1,4} + C_{2,4} \qquad (C.1)$$

Similarly, substitution of this equation into the routing expression for the 3rd reach gives the following result:

$$\begin{aligned} Q_3(t+1) = {} & C_{3,3}\, Q_3(t) + (C_{3,1} + C_{3,2}\, C_{2,3})\, Q_2(t) + \\ & + (C_{3,2}\, C_{2,1} + C_{3,2}\, C_{2,2}\, C_{1,3})\, Q_1(t) + C_{3,2}\, C_{2,2}\, C_{1,1}\, Q_0(t) \\ & + C_{3,2}\, C_{2,2}\, C_{1,2}\, Q_0(t+1) + C_{3,2}\, C_{2,2}\, C_{1,4} + C_{3,2}\, C_{2,4} \\ & + C_{3,4} \end{aligned} \qquad (C.2)$$

In general, there holds that

$$\begin{aligned} Q_i(t+1) = {} & C_{i,3}\, Q_i(t) + (C_{i,1} + C_{i,2}\, C_{i-1,3})\, Q_{i-1}(t) \\ & + C_{i,2}\, (C_{i-1,1} + C_{i-1,2}\, C_{i-2,3})\, Q_{i-2}(t) \\ & + C_{i,2}\, C_{i-1,2}\, (C_{i-2,1} + C_{i-2,2}\, C_{i-3,3})\, Q_{i-3}(t) + \cdots \\ & + C_{i,2}\, C_{i-1,2} \cdots C_{3,2}\, (C_{2,1} + C_{2,2}\, C_{1,3})\, Q_1(t) \\ & + C_{i,2}\, C_{i-1,2} \cdots C_{2,2}\, C_{1,2}\, Q_0(t+1) \\ & + C_{i,2}\, C_{i-1,2} \cdots C_{2,2}\, C_{1,1}\, Q_0(t) + C_{i,4} + C_{i,2}\, C_{i-1,4} \\ & + C_{i,2}\, C_{i-1,2}\, C_{i-2,4} + \cdots + C_{i,2}\, C_{i-1,2} \cdots C_{3,2}\, C_{2,4} \\ & + C_{i,2}\, C_{i-1,2} \cdots C_{2,2}\, C_{1,4} \end{aligned} \qquad (C.3)$$

where $i = 3,4,\ldots,N$.

Using matrix notation, these equations can be expressed in the following equivalent form:

$$Q(t+1) = A\, Q(t) + B\, U(t) + c \qquad (C.4)$$

where $Q(t) = [Q_1(t)\ Q_2(t)\ \ldots\ Q_N(t)]^T$, $U(t) = [Q_0(t)\ Q_0(t+1)]^T$,

$$\mathbf{A} = \underset{(NxN)}{\begin{bmatrix} C_{1,3} & 0 & \cdots & 0 \\ C_{2,1} + C_{2,2}\,C_{1,3} & C_{2,3} & \cdots & 0 \\ \vdots & & & \vdots \\ \prod_{i=3}^{N-1} C_{i,2}(C_{2,1} + C_{2,2}\,C_{1,3}) & \cdots & C_{N-1,3} & 0 \\ \prod_{i=2}^{N} C_{i,2}(C_{2,1} + C_{2,2}\,C_{1,3}) & \cdots & & C_{N,3} \end{bmatrix}}$$

$$\mathbf{B} = \underset{(Nx2)}{\begin{bmatrix} C_{1,1} & C_{1,2} \\ C_{2,2}C_{1,1} & C_{2,2}C_{1,2} \\ \vdots & \vdots \\ \prod_{i=2}^{N} C_{i,2}\,C_{1,1} & \prod_{i=2}^{N} C_{i,2}\,C_{1,2} \end{bmatrix}}$$

$$\text{and } \mathbf{c} = \underset{(Nx1)}{\begin{bmatrix} C_{1,4} \\ C_{2,4} + C_{2,2}\,C_{1,4} \\ \vdots \\ C_{N,4} + C_{N,2}\,C_{N-1,4} + \cdots + \prod_{i=2}^{N} C_{i,2}\,C_{1,4} \end{bmatrix}}$$

Vector **c** is related to the lateral inflow (or outflow), and, in certain cases, may not be present. However, when this model is used as a part of a rainfall-runoff forecasting scheme, the lateral inflow will also be an input, and Equation (B.4) must be considered as follows:

$$Q(t+1) = A\,Q(t) + B\,U(t) + C\,q(t)\ , \qquad (C.5)$$

where $q(t) = [\bar{q}_1(t)\ \bar{q}_2(t)\ \ldots\ \bar{q}_N(t)]^T$ and

$$C_{(NxN)} = \begin{bmatrix} d_{1,4} & 0 & \cdots & 0 \\ C_{2,2}\,d_{1,4} & d_{2,4} & \cdots & 0 \\ \vdots & \vdots & & \vdots \\ \prod_{i=2}^{N} C_{i,2}\,d_{1,4} & \prod_{i=3}^{N} C_{i,2}\,d_{2,4} & \cdots & d_{N,4} \end{bmatrix}$$

with $d_{i,4} = \Delta x_i\ \tilde{a}_i / C_{i,0}$ (see Equation B.3e).

For the segments originating from reservoirs, the input U(t) will represent reservoir releases, while for those emerging from watersheds, it will represent predicted runoff rates.

APPENDIX D

OBSERVABILITY AND CONTROLLABILITY STUDY

A system is observable if and only if a finite series of observations $\{z(t_0), z(t_1), \ldots, z(t_M)\}$ is enough to uniquely determine the initial value of the state vector at time t_0. Equivalently, the previous system is observable (Kailath, 1980, Chapter 2) if and only if the matrix

$$\mathbf{O} = \begin{bmatrix} \mathbf{H}^T \\ - - - - - \\ s\,\mathbf{I} - \mathbf{A} \end{bmatrix} \tag{D.1}$$

has rank N for all s. Substituting $\mathbf{H}^T$ and A from Section B.2 results in

$$\underset{[(N+1)xN]}{\mathbf{O}} = \begin{bmatrix} 0 & 0 & & 1 \\ - - - - - & - - - - - & & - - - \\ s - A_{1,1} & 0 & \ldots & 0 \\ -A_{2,1} & s - A_{2,2} & \ldots & 0 \\ \vdots & \vdots & & \vdots \\ -A_{N,1} & -A_{N,2} & \ldots & s - A_{N,N} \end{bmatrix} \tag{D.2}$$

where the elements $A_{i,j}$ represent the corresponding entries of the matrix A defined following Equation (C.5). The critical values of s for which this matrix may not fulfil the observability requirement are the eigenvalues of A. (If s is not an eigenvalue, the determinant det(sI-A) will be nonzero and thereby matrix O will have rank N.) Given the structure of matrix O, the system is observable if we cannot find an (NxN) submatrix with at least one zero column or row for any value of s. The critical values of s are now restricted to $A_{1,1}$ and $A_{N,N}$, but one can easily verify that in either case no (NxN) submatrix with at least one zero row or column can be found. Thus, the system is observable.

A system is controllable if and only if, given any initial state vector $Q_I(t_0)$ and any terminal state vector Q_T, there exists a finite time t_M and an input sequence $\{U(t_0), U(t_1), \ldots, U(t_M)\}$ which "drives" the system from $Q_I(t_0)$ to Q_T. Alternatively, the system is controllable if and only if the matrix $(sI - A \mid B)$ has rank N for all s. (The following proof refers to the system represented by Equation (A.4);

however, controllability of the system in Equation (C.5) can also be proved in a similar manner.)

Substituting **A** and **B** from Appendix C yields

$$\mathbf{C} = [Nx(N+2)] \left[\begin{array}{cccc|cc} s-A_{1,1} & 0 & \cdots & 0 & C_{1,1} & C_{1,2} \\ -A_{2,1} & s-A_{2,2} & \cdots & 0 & C_{2,2}C_{1,1} & C_{2,2}C_{1,2} \\ \vdots & \vdots & & \vdots & \vdots & \vdots \\ -A_{N-1} & -A_{N,2} & \ddots & S-A_{N,N} & \prod_{i=2}^{N} C_{i,2}C_{1,1} & \prod_{i=2}^{N} C_{i,2}C_{1,2} \end{array}\right]$$

Using arguments similar to those of the observability proof we can easily show that we cannot find an (NxN) submatrix with at least one zero column or row for any value of s. Thus the system is also controllable.